

Durham E-Theses

Late Jurassic Sedimentation in the Boreal-Tethyan Seaway: climate modelling, geochemistry, and petrography of the Kimmeridge Clay Formation

ATAR, ELIZABETH,FILIZ,LINDSAY

How to cite:

ATAR, ELIZABETH,FILIZ,LINDSAY (2019) *Late Jurassic Sedimentation in the Boreal-Tethyan Seaway: climate modelling, geochemistry, and petrography of the Kimmeridge Clay Formation*, Durham theses, Durham University. Available at Durham E-Theses Online: <http://etheses.dur.ac.uk/13132/>

Use policy

The full-text may be used and/or reproduced, and given to third parties in any format or medium, without prior permission or charge, for personal research or study, educational, or not-for-profit purposes provided that:

- a full bibliographic reference is made to the original source
- a [link](#) is made to the metadata record in Durham E-Theses
- the full-text is not changed in any way

The full-text must not be sold in any format or medium without the formal permission of the copyright holders.

Please consult the [full Durham E-Theses policy](#) for further details.

**Late Jurassic Sedimentation in the Boreal-
Tethyan Seaway: climate modelling,
geochemistry, and petrography of the
Kimmeridge Clay Formation**

Elizabeth Filiz Lindsay Atar

Thesis submitted in partial fulfilment for the requirements for the degree
of Doctor of Philosophy

Department of Earth Sciences

Durham University

2019

Abstract

Climate exerts a strong influence on sedimentation. Understanding the processes behind the spatial and temporal heterogeneities in sedimentary successions can, therefore, be used to reconstruct climate processes in the geological past. Deposited across >1000 km in northwest Europe in the shallow (< 200 m), epicontinental Lurasian Seaway, the Kimmeridge Clay Formation provides an exceptional opportunity to study climate processes and their effect on sedimentation at different latitudes through the Late Jurassic (Kimmeridgian–Tithonian). This thesis presents independent climate modelling, sedimentological, and geochemical datasets from three time-equivalent sections, spanning 1 million years, in the northern and southern extents of the Lurasian Seaway (30–60°N palaeo-latitude) in order to investigate climate dynamics and controls on sedimentation at different northern hemisphere latitudes in the Late Jurassic.

The climate modelling results yield two different hypotheses: 1) HadCM3L indicates that an expanded Hadley Cell and migrated intertropical convergence zone resulted in tropical conditions over the Lurasian Seaway, whereby organic carbon-enrichment in sediments was promoted through enhanced nutrient supply resulting from continental weathering and erosion, and 2) FOAM suggests subtropical-temperate conditions prevailed and that organic carbon enrichment was driven by wind-driven upwelling of nutrient-rich water.

Sedimentological and geochemical analyses for the Ebberston 87 Core, drilled in the Cleveland Basin (Yorkshire, UK), indicates depositional conditions fluctuated between three distinct states and that alternations of organic carbon-rich, carbonate-rich, and clay-rich mudstone and redox conditions were driven by the expansion/migration of the intertropical convergence zone. Analysis of the Swanworth Quarry 1 Core, drilled in the Wessex Basin (Dorset, UK), reveals that although depositional energy differed between the Cleveland and Wessex Basins, sedimentation in both basins was driven by the same, over-arching tropical climate control. Analysis of a third core, drilled in Adventdalen (Svalbard), demonstrates that organic carbon-rich sedimentation occurred in a deltaic setting, which had a markedly higher depositional energy. While the depositional environments in the northern and southern sectors of the Lurasian Seaway differed substantially, similarities between the three studied sections, namely cyclical deposition of terrestrial organic carbon-rich and detrital-rich sedimentation, integrated with published data from throughout the seaway, suggest a low-latitude, tropical influence on sedimentation and organic carbon enrichment across the entire Lurasian Seaway. Furthermore, the palaeogeographic setting of the Lurasian Seaway made the sedimentary system sensitive to subtle changes in weathering and water depths, resulting in distinct modes of sedimentation and biogeochemical cycling.

Contents

Contents.....	IV
Acknowledgements.....	X
1 Introduction and background.....	13
1.1 Project rationale and research aims	14
1.2 Organic carbon rich mudstones	15
1.3 Modern day atmospheric dynamics	18
1.4 Late Jurassic climate reconstructions	20
1.5 The Kimmeridge Clay Formation	22
1.6 Thesis outline.....	24
2 Methods and materials	27
2.1 Approach.....	28
2.2 Justification of methods.....	28
2.3 Sample locations and materials and sampling strategy	30
2.3.1 Ebberston 87 Core	30
2.3.2 Swanworth Quarry Core.....	30
2.3.3 DH4 Core	32
2.4 Petrographic methods.....	34
2.4.1 Optical light petrography	34
2.4.2 Scanning electron microscopy	34
2.5 Geochemical methods	34
2.5.1 Crushing and grinding	34
2.5.2 LECO	34
2.5.3 Carbon isotopes.....	34
2.5.4 X-ray fluorescence.....	35
2.6 ICP-MS analysis	36
2.7 Mercury (Hg) analysis	36
2.8 Lithological nomenclature	36
3 Climate modelling in the Late Jurassic.....	39
3.1 Introduction.....	40
3.2 Model description	41

3.2.1	HadCM3L model.....	42
3.2.2	Fast ocean atmosphere model (FOAM)	42
3.3	Experimental design and methods	43
3.3.1	HadCM3L initial and boundary conditions	43
3.3.2	FOAM initial and boundary conditions	44
3.3.3	Notable differences in boundary conditions between HadCM3L and FOAM	45
3.3.4	Model interpolation.....	46
3.3.5	Preindustrial simulations	46
3.3.6	Identification of the intertropical convergence zone (ITCZ), subtropics, and monsoon regions.....	48
3.4	Results and discussion	48
3.4.1	Surface temperature from HadCM3L and FOAM in the Jurassic.....	48
3.4.2	Precipitation from HadCM3L and FOAM.....	50
3.4.3	Predictions for the ITCZ and proposed influence on sedimentation in the Laurasian Seaway	51
3.4.4	Reasons for inter-model variability	53
3.5	Conclusions.....	55
4	Sedimentology of the Ebberston 87 Core	57
4.1	Introduction.....	58
4.2	Geological Setting.....	59
4.3	Methods and materials	62
4.4	Facies descriptions	64
4.4.1	Clastic-detritus-rich medium-grained mudstone.....	65
4.4.2	Organic material and calcareous pellet-rich, laminated mudstone.....	67
4.4.3	Coccolith-dominated medium-grained mudstone	69
4.4.4	Agglutinated foraminifera bearing, medium to coarse- grained, carbonaceous mudstone.....	71
4.4.5	Biogenic detritus dominated, fine to medium-grained mudstone	73
4.4.6	Carbonate cemented, coarse-grained mudstone	74
4.5	Discussion.....	76
4.6	Conclusion	79

5	Dynamic climate-driven controls on the deposition of the Kimmeridge Clay Formation in the Cleveland Basin, Yorkshire, UK.....	81
5.1	Abstract	82
5.2	Introduction.....	83
5.3	Geological setting.....	84
5.4	Materials and methods	85
5.5	Results.....	87
5.5.1	Petrographic characterization	88
5.5.2	Lower variability mudstone interval (LVMI) petrography	88
5.5.3	Higher variability mudstone interval (HVMI) petrography.....	88
5.5.4	Geochemistry	90
5.6	Discussion.....	94
5.6.1	Depositional environment: sediment source, depositional energy, dispersal mechanisms, and climatic context.....	94
5.6.2	Productivity and organic matter composition.....	97
5.6.3	Redox conditions	98
5.7	Conclusions and conceptual model	106
6	Local to global controls on the deposition of organic-rich muds across the Late Jurassic Lurasian Seaway	109
6.1	Abstract	110
6.2	Introduction.....	110
6.3	Material and methods	113
6.4	Results.....	113
6.5	Discussion.....	116
6.5.1	Depositional controls in the UK Wessex and Cleveland Basins	116
6.5.2	Chemostratigraphic cross-seaway correlation.....	122
6.6	Conclusions and implications	124
7	Organic carbon enrichments in the northern Lurasian Seaway (Svalbard) during the Late Jurassic	125
7.1	Introduction.....	126
7.2	Geological setting	127

7.3	Methods and materials	130
7.4	Results.....	133
7.4.1	Petrography	133
7.4.2	Geochemistry	134
7.5	Discussion.....	136
7.5.1	Depositional environment.....	136
7.5.2	Carbon isotopes.....	138
7.6	Conclusions.....	140
8	Synthesis, conclusions, and further ...work	143
8.1	Synthesis	144
8.2	Conclusions.....	149
8.3	Future work.....	150
9	Bibliography.....	151
10	Appendix A - Climate modelling figures.....	166
11	Appendix B – EB87 Core petrographic images	170
	Please see the USB stick attached to the hard copy for this dataset.....	170
12	Appendix C – EB87 Core SEM images	173
	Please see the USB stick attached to the hard copy for this dataset.....	173
13	Appendix D – EB 87 SEM-EDX	175
	Please see the USB stick attached to the hard copy for this dataset.....	175
14	Appendix E – EB87 Core geochemical data	177
	Please see the USB stick attached to the hard copy for this dataset.....	177
15	Appendix F – SQ1 Core geochemical data	179
	Please see the USB stick attached to the hard copy for this dataset.....	179
16	Appendix G – DH4 Core petrographic images	181
	Please see the USB stick attached to the hard copy for this dataset.....	181
17	Appendix H – DH4 Core SEM images.....	183
	Please see the USB stick attached to the hard copy for this dataset.....	183
18	Appendix I – DH4 SEM-EDX.....	185
	Please see the USB stick attached to the hard copy for this dataset.	185

19	Appendix J – DH4 Core geochemical data.....	187
	Please see the USB stick attached to the hard copy for this dataset.....	187

Declaration

I declare that this thesis, which I submit for the degree of Doctor of Philosophy at Durham University, is my own work and not substantially the same as any which has previously been submitted at this or any other university.

Elizabeth F. L. Atar

Department of Earth Sciences, Durham University, March 2019

© The copyright of this thesis rests with the author. No quotation from it should be published without the author's prior written consent and information derived from it should be acknowledged.

Acknowledgements

First and foremost, I thank my supervisory team for their support and guidance over the course of this project. I am grateful to Andy Aplin for his unwavering commitment, endless patience and kindness, and for always having an open door. Thank you to Christian März for always believing in me, inspiring and motivating me, and for sharing his seemingly endless enthusiasm for geochemical data. Thank you to Tom Wagner, for his continued enthusiasm and interest in my work, and for teaching me the value of taking a step back to view the bigger picture.

In addition to my formal supervisors, I have benefitted from a wealth of guidance from others in informal supervisory roles. Firstly, thanks go to Bernhard Schnetger and Olaf Dellwig, whose passion for all things geochemistry has motivated me throughout this project and taught me a great deal about interpretation. Dan Lunt and Alex Farnsworth opened my eyes to the world of climate modelling; I am very grateful for their continued patience during my brief stint in Bristol and for help with all things coding. Les Leith is thanked for interesting and helpful discussions on Jurassic climate and climate modelling and I thank my master's supervisor João Trabucho-Alexandre for believing in me right from the very beginning, and for instilling the importance of ground truthing geochemical data with petrographic observations!

This project was funded by the Natural Environment Research Council (NERC) Centre for Doctoral Training (CDT) in Oil and Gas, whose support is gratefully acknowledged. I owe a great deal of thanks to the CDT; through the training academy I learnt a huge amount about the global energy industry, but perhaps more importantly, I gained an invaluable support network and friendships that will last a lifetime. Special thanks go to John Underhill, Lorna Morrow, and Anna Clark for establishing, maintaining, and facilitating the CDT.

The research benefitted from further financial support in the form of a postgraduate grant award from the International Association of Sedimentologists used for the preparation of specialist thin sections and a NIGL grant-in-kind for the carbon isotope analyses. The modelling components of this thesis were provided by the Bristol Research Initiative for the Dynamic Global Environment (BRIDGE) and Equinor ASA. I gratefully acknowledge IFP Energies nouvelles, specifically Violaine Lamoureux-var, and the University Centre in Svalbard, particularly Snorre Olaussen, for access to core and assistance in sampling. I thank Liam Herringshaw for assistance in sampling. I gratefully acknowledge the Scottish Universities Environment Research Centre for use of their rock crushing facilities and staff at Newcastle University for help and training for LECO analyses. I thank Professor Arek Derkowski for teaching me the ways of quantitative clay mineralogy at the Institute of

Geological Sciences Polish Academy of Sciences, and Paweł Gentry, Tomasz Topór, and Marta Mietelska- Topór for being wonderful guides during my time in Krakow.

Closer to home, Ian Chaplin and Sophie Edwards are thanked for the preparation of thin sections and for never failing to make me smile. I thank Jo Peterkin and Chris Ottley for help and training in the lab. I am grateful to Mathieu Dellinger for teaching me about clean labs and preparation of samples for Li isotope analyses, and to Kevin Burton for facilitating this side project. I thank Leon Bowen and Buddhika Mendis for training on the SEM, and Gary Oswald for help with XRD. I must also thank the admin team in the Earth Sciences Department, who have helped me in numerous ways over the years. Special thanks go to Karen Atkinson, who has always been on hand to provide advice, both professional and personal.

I thank Chris Greenwell and Gillian Foulger for always listening to me. I also thank Chris along with Claire Horwell for their support and feedback as my internal reviewers Chris Saville has taught me a lot about teaching and has inspired me to be the best demonstrator I could be, and has always had time for me.

I am surrounded by wonderful friends, to mention a few; the 214 Family helped me through the darkest of times, without them I doubt I would have gotten this far. Thanks go to Sean, Kate H, Eloïse, Kate G., Erin, Emma, Juliet, Rich, Christian, and Mateja for your continued friendship, love, and support over the last few years and to Tom Snell for always encouraging me to be myself. I thank my office neighbours for the years of entertainment, coffee-drinking, and support, and Olly, Chris W., and Simon, for sharing the ‘joys’ of writing up. I also thank the postdoc community for the endless help and many friendships particularly Tom Phillips and Jason Coumans for making a special effort to look out for me while I was writing this thesis.

Further afield, I thank Becca Neely, who continues to be my biggest champion from the other side of the world, Racheal Hunter for inspiration and support on a daily basis, and Lizzie Lawrenson, who is always at the end of a phone and often knows what I’m thinking before even I do.

Special thanks go to my mum, who taught me from an early age that anything is possible and to Julie and Adam for their unconditional love. We are lucky to be surrounded by a wonderful family; Nigel and John, Christine, Janette and Philip, Robert and Claire, Tony, and the Gunduz Clan are all thanked for believing in me from the very beginning, and Elly and Shaun are thanked for encouraging my inquisitiveness from an early age through the gifting of numerous books. The Cooper Family are thanked for supporting me throughout this project and for providing excellent bracelet-making and dinosaur-wrestling distractions.

Finally, I thank George, who has been with me every step of the way, who never stopped believing in me, gave me endless encouragement, praise, love, and support, and Kilian, for being the best feline companion anyone could ask for.

June 2019.

I thank my examiners Kevin Taylor and James Baldini for thoroughly enjoyable examination.

1 | Introduction and background

Chapter Summary

This chapter outlines the project rationale, aims and key hypotheses, and provides a brief introduction to the key concepts discussed in this thesis. Included but not limited to are (a) the processes associated with the production and preservation of organic carbon, (b) modern atmospheric dynamics, (c) Late Jurassic climate reconstructions, (d) the geological setting of the Kimmeridge Clay Formation, and (e) existing depositional models for the Kimmeridge Clay Formation.

1.1 Project rationale and research aims

Mudstones are the most abundant sedimentary rocks on the Earth comprising more than 60 % of the sedimentary record (Potter et al., 2005). Predominantly composed of fine-grained sediment and deposited under relatively low sedimentation rates and energy levels, they provide the most complete record from the geological past, both marine and terrestrial. The deposition of mudstones is affected by local and global processes, the signals of which are often preserved (Lazar et al., 2015b). Mudstones, therefore, provide a unique insight into past environments and can be used to explore changes in environmental conditions at the highest possible resolution and consistently over extended periods of time. Organic-rich mudstones in particular record extreme climate events (Meyer and Kump, 2008) and help our understanding of how the atmosphere, biosphere, and the hydrosphere reacted under past greenhouse conditions, pertinent to constraining future climate predictions (Crowley, 1996). In addition, organic carbon-rich mudstones have long been recognised as a source rock for both conventional and unconventional hydrocarbon plays (Palacas, 1870). In the context of rising exploration costs and increasing difficulty to find and extract new reserves, there is a need for better understanding of the controls on source rock formation and their spatiotemporal distribution to meet the world's ever-growing energy demands. Understanding the nature and distribution of black shales is therefore of great interest and importance to the petroleum industry, (palaeo)climatologists, and (palaeo)environmentalists.

The Kimmeridge Clay Formation (KCF) is an organic carbon-rich succession deposited in the shallow, epicontinental Lurasian Seaway, across northwest Europe in the Late Jurassic. Its vast lateral extent (> 1000 km) and expanded nature make it an ideal succession to use in investigating spatial and temporal controls on sedimentation, and its latitudinal extent (*ca.* 30-60°N) enables exploration of depositional controls across different climate belts. Furthermore, the Kimmeridge Clay Formation has been extensively studied, meaning there is a well-established chronostratigraphy to aid correlation between different areas in the seaway. In this thesis, I present two opposing climate model simulations, and then use geochemical and sedimentological data from the northern and southern limits of the Lurasian Seaway, to explore which of the two modelling simulations is more likely.

Project aims:

- To compare and contrast two independent climate model simulations for the Late Jurassic, specifically regarding the location and dynamics of the intertropical convergence zone (ITCZ) in relation to the Lurasian Seaway, a shallow seaway connecting the low latitude western Tethys Ocean with the proto-Arctic Ocean, and to develop conceptual ideas that can be tested and validated using detailed study wells.
- To use integrated sediment geochemistry and petrography to constrain the depositional processes of three laterally-equivalent sections in the Lurasian Seaway.
- To use the knowledge of the depositional processes obtained from the well records to constrain the local and global scale controls on sedimentation across the Lurasian Seaway.
- To integrate geochemical, sedimentological, and climate modelling results to determine the main drivers of Late Jurassic sedimentation in northwest Europe.

1.2 Organic carbon rich mudstones

Organic-rich mudstones are a recurrent feature in Earth history and record perturbations in the global carbon cycle (Meyer and Kump, 2008, Negri et al., 2009, Pancost et al., 2004, Parrish and Curtis, 1982). At the present day, organic carbon (OC)-rich sediments, comparable to ancient OC-rich mudstones, are limited in extent and restricted to specific local conditions (e.g. Namibia Shelf or Northern Indian Ocean). This is in marked contrast to the extensive deposits of OC-rich mudstones found in epicontinental basins and continental margins in the past. The challenge for understanding marine OC-rich mudstone distribution, thickness, and internal variations in deep time is to better constrain large-scale/basin-wide processes that controlled OC production and burial (Wagner et al., 2013). Elevated OC burial resulted from a complex interplay between primary organic productivity, preservation, and sediment dilution (Figure 1.1)(Wignall and Hallam, 1991). The relative contribution of each of these factors is debated and varies between depositional settings (Bohacs et al., 2005, Meyers, 2006, Pedersen and Calvert, 1990a, Stein et al., 1986, Tyson, 2005a, Trabuchio-Alexandre, 2015b). Traditionally, these factors have been grouped into three distinct depositional models, outlined below. The causes, consequences, and caveats of these models have, however, been extensively debated in the literature and reviewed several times (e.g.(Katz, 2005, Tyson, 2005a, Potter et al., 2005).

In the organic-productivity driven models, prolific organic productivity, stimulated by enhanced nutrient supply, either through elevated continental weathering and runoff or

oceanic upwelling, generates an increased mass of organic matter that sinks to the sediment surface (Pedersen and Calvert, 1990a, Parrish, 1995, Hay, 1995). Much of this material is oxidised, but the sheer volume means that a substantial quantity of the OC flux still makes it to the sediment surface, thus into the sedimentary record (Pedersen and Calvert, 1990a). High oxidation rates can lead to oxygen depletion in the sediment pore and bottom waters, promoting redox stratification of the water column (Katz, 2005). This process is important and necessary for strong organic carbon enrichment because under normal marine conditions, only 1% of organic carbon is incorporated into the sedimentary record (Bralower and Thierstein, 1987, Katz, 2005). Therefore, redox stratification, driven by primary productivity, promotes organic carbon burial through increasing the preservation conditions at the sediment water interface (Bertrand and Lallier-Verges, 1993). Preservation potential is further enhanced by increased OC export efficiency through elevated sedimentation rates (Bertrand et al., 1994). In these models, variations in primary productivity are the causal mechanism behind observed differences in OC enrichment.

A contrasting view is presented by preservation models which are centred on preserving OC in anoxic settings, where the consumption of oxygen far exceeds supply and productivity may not be elevated (Katz, 2005, Demaison et al., 1991). Examples of settings where this occurs include silled basins and density stratified water columns (Trabucho-Alexandre, 2015b, Arthur and Sageman, 1994). Limitation of exposure to oxidants is achieved through several mechanisms; hydrographic restriction prevents oxygen supply renewal leading to density and redox stratification (Tyson, 2005a, Algeo et al., 2008); sediment dispersal mechanisms, such as flocculation and pelletisation of OC and clay minerals, aid OC preservation by increasing the sedimentation rate thus reducing exposure time (Ittekkot et al., 1992); and an absence of benthic organisms is thought to enhance preservation in anoxic environments due to the reduction of scavenging, OC remineralisation, and irrigation of the sediment during bioturbation (Demaison et al., 1991, Aller, 1994). OC type also affects its preservation potential (Boussafir et al., 1995, Tribovillard et al., 1996); marine kerogen type II OC comprises algae, which is more vulnerable to oxidative destruction than its terrestrial type III counterpart (Katz, 2005). Furthermore, amorphous algal material has a larger surface area to volume ratio than other OC particles making it more susceptible to oxidative degradation (Waples, 1983). In the OC-preservation models, variations in OC content are attributed to differences in redox state of the water column (Demaison and Moore, 1980a) as it is commonly observed that highest OC enrichments occur in the absence of oxygen (Katz, 2005, Katz, 1995, Curiale and Gibling, 1994). However, Canfield et al. (1993) notes that under high sedimentation rate, bottom water oxygen concentrations exert no or minimal effect on the OC destruction because degradation of OC can occur predominantly through anaerobic pathways.

The third group of models relate to the relative dilution of OC in the sediment (Katz, 2005). In environments where sedimentation rates are low, OC is concentrated and forms a higher proportion of the sediment (Tyson, 2001). When sedimentation rate is high, OC can be diluted by other sediment, e.g. detrital material or marine carbonate, and anaerobic degradation of OC can still take place (Canfield et al., 1993). However, there is a fine balance between sedimentation rates and dilution because a higher sedimentation rate reduces the exposure to oxidants by burying the OC relatively quickly, therefore they can act to enhance OC preservation and enrichment; this is the rapid burial model (Katz, 2005). The condensed section model instead focusses on the lack of detrital material as an OC diluent (Katz, 2005, Wignall, 1991, Loutit et al., 1988).

Numerous studies have demonstrated that in the modern world, there are sites and systems that agree with or discredit each of the aforementioned mechanisms. Enrichment of organic carbon in sediments results from a combination of these three variables which are strongly influenced by tectonic, climatic, and hydrographic settings. However, a major caveat in applying modern day processes to the geological record is the lack of an analogous tectonic, climatic, and hydrographic setting. Therefore, we must consider the underlying principles, strengths, and weaknesses of each of the proposed models for OC enrichment, and apply them to the geological record.

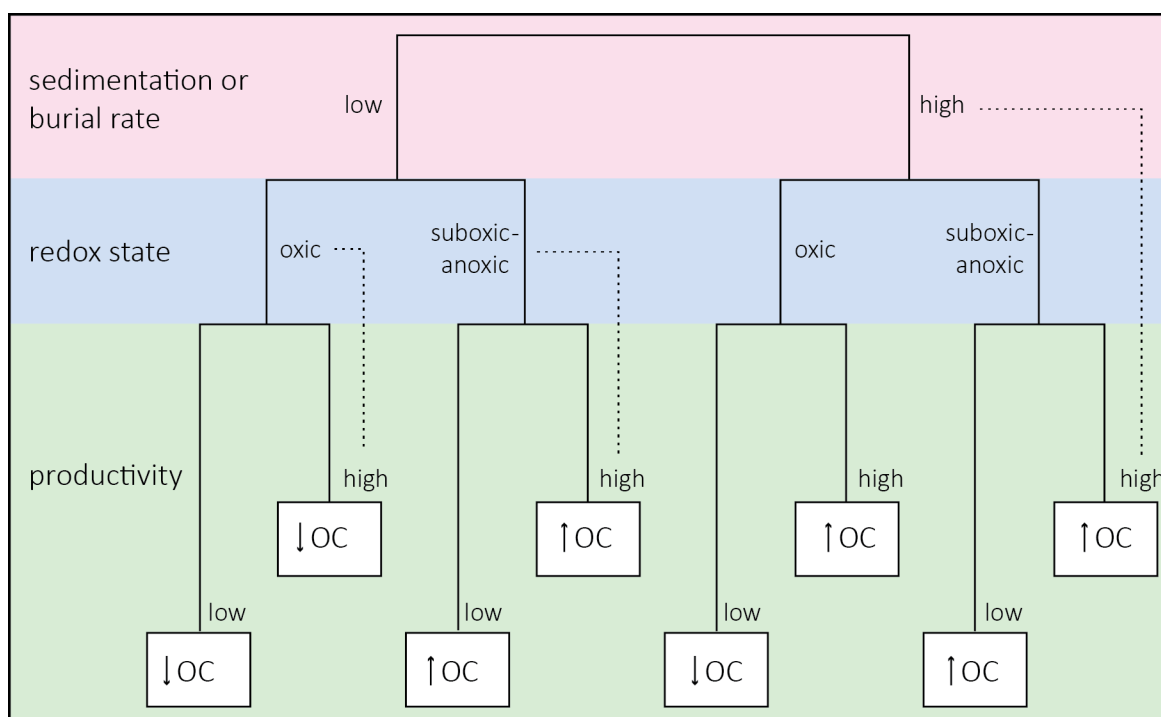


Figure 1.1. Schematic diagram illustrating the combination of sedimentation rate, redox state, and productivity level and resulting enrichment of organic carbon; upwards pointing arrows indicate relatively high levels. Adapted from Katz (2005).

1.3 Modern day atmospheric dynamics

An understanding of modern-day atmospheric dynamics and how they influence OC enrichment is fundamental to reconstructing atmospheric conditions and controls on sedimentation in the geological past. In the present day, the northern hemisphere has three atmospheric circulation cells; the equatorward Hadley Cell, the Ferrel Cell, and the northernmost Polar Cell (Figure 1.2)(Waliser et al., 1999, Kjellsson and Döös, 2012). This configuration is mirrored in the southern hemisphere. Under present day conditions, the Hadley Cells of the northern and southern hemispheres are broadly symmetrical. The ascending limb, where both Hadley Cells converge, is located at the thermal equator. Here, warm moist air rises, and adiabatic cooling and condensation results in a zone of very high precipitation ($6\text{--}8\text{ m yr}^{-1}$) throughout the year, defining the core tropics; this prominent atmospheric feature is called the Intertropical Convergence Zone (ITCZ; Figure 1.3). Very high precipitation rates, associated with the ITCZ, enhance continental weathering and runoff, which increases the supply of nutrients to the oceans. In optimal oceanic conditions, high nutrient supply increases OC production, which is then incorporated into the sedimentary record.

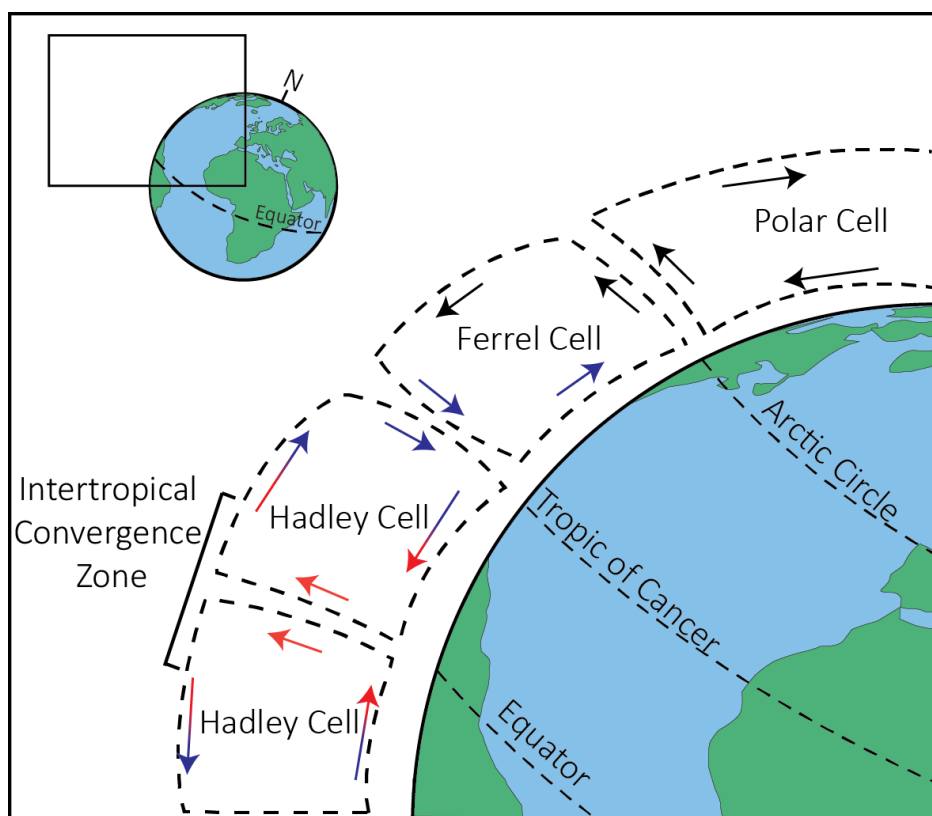


Figure 1.2. Schematic diagram showing the northern hemisphere atmospheric circulation cells and the position of the intertropical convergence zone (ITCZ).

Dry and cooling air spreads and descends towards the outer boundaries of the Hadley Cells, which under modern conditions is at around 30° north and south. The poleward extent of the Hadley Cell depends on palaeogeography, $p\text{CO}_2$, and latitudinal temperature gradient; therefore it has fluctuated in the past and is likely to change in a warmer future (Hu et al.,

2013). Dry air that meets the land surface in the subtropics forms the trade winds that define the arid desert regions; these winds and Ekman transport displace coastal surface waters and promote oceanic upwelling, which, as discussed in the previous section, also promotes OC production and preservation under the right oceanic conditions. The ascending and descending limbs of the Hadley Cell define markedly different climate regimes that stimulate contrasting processes relevant to marine organic matter production and burial. Further information on the principles of Hadley Cell dynamics for the present day can be found in (Frierson, 2007, Johanson and Fu, 2009, Lu et al., 2007, Yin, 2005, Hu et al., 2013).

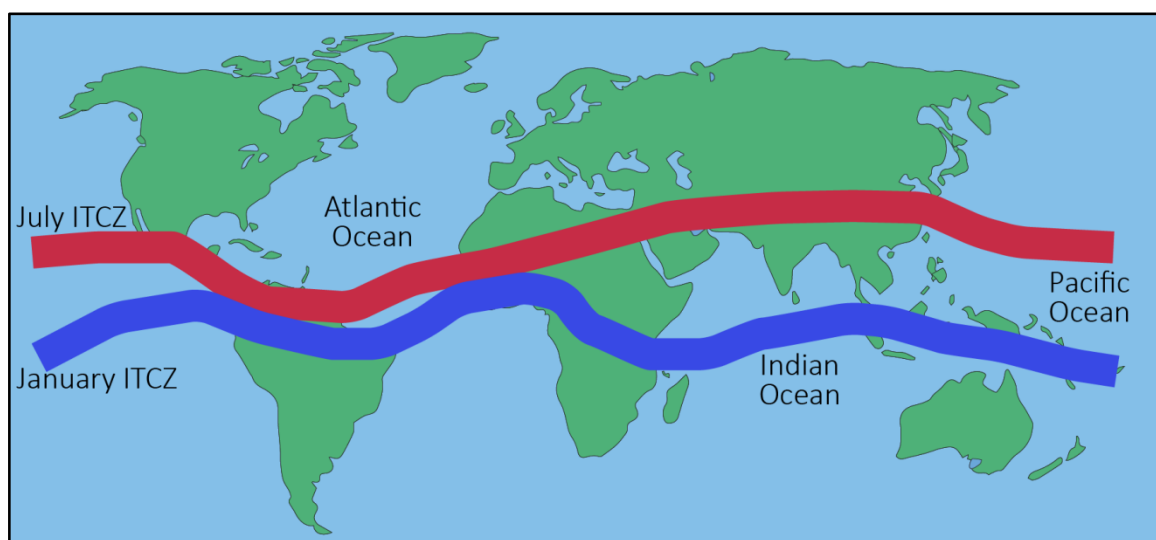


Figure 1.3. Schematic diagram showing the position of the intertropical convergence zone (ITCZ) in the northern hemisphere summer (red line) and winter (blue line)(Schneider et al., 2014b).

The position of the ITCZ, and hence the Hadley Cell, responds to solar insolation. Changes in solar radiation in tropical latitudes affect changes in temperature, which alters atmospheric pressure heat export to higher latitudes via the Hadley atmospheric circulation and wind-driven, ocean surface currents. Increasing (decreasing) heat flux results in an intensification (weakening) of the Hadley circulation, reflected most notably in low latitudes by a strengthening (weakening) of the monsoonal climate system. The position of the ITCZ tracks the solar zenith and peak sea surface temperature, leading to seasonal fluctuations in the location of the ITCZ (Armstrong et al., 2009). On longer Milankovitch and geological timescales the location of the ITCZ is controlled by latitudinal temperature gradient, the balance between tropical and polar temperatures, climate modes, and palaeogeography (Hastenrath, 1991). These factors are strongly influenced by orbital forcing (Milankovitch cycles), which systematically modulates the amount of solar insolation received by the Earth, resulting in regular/cyclical fluctuations in the position of the ITCZ as part of the Hadley Cells.

Under the ascending limb of the Hadley Cell, precipitation is intensified so nutrient input into the oceans via continental runoff is the primary driver of marine productivity. In the arid subtropics, trade winds drive coastal upwelling systems, particularly along the western margins of the continents. Hadley Cell dynamics can be directly linked to the mechanisms of

high OC production and burial, and thus black shale formation in the geological past. Conversely, deciphering these mechanisms in deep time allows reconstructions of the palaeo-Hadley Cell, independent of climate models, and hence key features of atmospheric circulation. As discussed below, preliminary work indicates that deposition of the sediments across northwest Europe in the Late Jurassic was strongly influenced by Hadley Cell dynamics. In this thesis, I will use climate modelling, which combines knowledge of modern day atmospheric dynamics and Jurassic palaeogeography, to investigate Hadley Cell dynamics in the Late Jurassic. This will then be tested with geochemical and petrographic observations of the sedimentary rock record.

1.4 Late Jurassic climate reconstructions

General circulation models (GCMs) use the laws of physics, derived from the modern day, along with palaeogeographical configurations, to simulate atmospheric and oceanic processes at different intervals in the geological past (e.g. (Sellwood and Valdes, 2006, Lunt et al., 2012)). GCMs can be atmospheric, oceanic or atmosphere-ocean coupled models and have varying resolutions. The resulting climate predictions are routinely ground-truthed with proxy datasets (Armstrong et al., 2016). By definition GCMs are global in nature therefore yield a more complete overview than sparse proxy data alone; they reveal insights into variables such as precipitation and temperature, and can match well with climatically sensitive facies (Sellwood and Valdes, 2008). A big challenge of truthing climate model predictions with the stratigraphic record is the lack of wells in strategic positions. Furthermore, they generate predictions of climatically important factors that cannot be observed in the rock record, such as cloud cover (Sellwood and Valdes, 2008). A caveat of using GCMs to investigate paleoclimate is their apparent lack of calibration variables of boundary conditions (e.g. atmospheric $p\text{CO}_2$, paleo-bathymetry, ocean current systems) and sensitivity to localised phenomena, which results from a commonly coarse (c. $2^\circ \times 2^\circ$) grid cell size and the parameterisation of processes across this resolution (Price et al., 1995). Despite these limitations, GCMs are powerful tools which provide essential information about past climate conditions and prominent processes.

The Late Jurassic is widely referred to as a 'greenhouse world' (Price et al., 1995), meaning that it was warmer than the present day (Sellwood and Valdes, 2008), despite receiving up to 2% less solar insolation than the present day (Kump et al., 2004). Atmospheric $p\text{CO}_2$ levels are determined to be four times greater in the Late Jurassic than the present day by model simulations (Sellwood and Valdes, 2006). Elevated $p\text{CO}_2$ accounts for the higher global temperatures, consistent with proxy data from other studies (Valdes et al., 1999). The consequences of greenhouse conditions are predicted to include an enhanced hydrological cycle and a reduction in oceanic oxygen and carbon dioxide solubility (Sellwood and Valdes, 2006), both of which represent very different boundary conditions to today with

consequences for processes connecting the atmosphere, biosphere and hydrosphere, some of which translate in to the rock record as fluctuations in sedimentary geochemistry and composition.

Simulated Late Jurassic terrestrial biomass production indicates patchy forest and predominantly xeromorphic vegetation at low latitudes, maximum productivity and terrestrial plant diversity at mid-latitudes, and dense, deciduous forest across high latitude continents (Rees et al., 2004, Sellwood and Valdes, 2006). Climatically-sensitive sedimentary facies (evaporites and coals) are distributed symmetrically around the equator, consistent with modelled latitude-dependant precipitation and evaporation rates (Sellwood and Valdes, 2006, Valdes et al., 1999). These conditions are markedly different to modern day observations (Hallam, 1985). Whether or not climate conditions changed across the Late Jurassic, and if so at what timescales and affecting what regions, has proven difficult to elucidate. Rees et al. (2000) suggested that the climate zones they defined remained constant but that the continents migrated across climate zones due to plate tectonics. Sellwood and Valdes (2006) indicate the requirement for, as yet to be generated, palaeomagnetic data to demonstrate this relationship. Conversely, Hallam (1985) attributed modelled southern Eurasian precipitation/evaporation patterns to a tectonic induced rain shadow effect (Sellwood and Valdes, 2006). The effects of orbital forcing on local/sub-regional environmental conditions are largely unknown, making it difficult to match (local) field and well observations to coarse-scale simulations.

Early modelling simulations (Moore et al., 1992a, Moore et al., 1992b, Valdes and Sellwood, 1992, Valdes et al., 1995, Price et al., 1995) for the Kimmeridgian and Tithonian have been reviewed by Rees et al. (2000) and Valdes et al. (1999). Sellwood and Valdes (2006) recognise these reviews to be significant progressions on Jurassic palaeoclimate simulations, in part owing to the technological advancements made in climate modelling in the intervening years. Sellwood and Valdes (2008) present simulations for the Kimmeridgian from an atmosphere-only GCM and preliminary sea surface temperatures from a fully coupled GCM. The authors report significantly warmer oceans (*c.* 8°C) than present day, greenhouse conditions, an enhanced convective hydrological cycle, strong seasonality at mid to high latitudes, and a predominance of subtropical conditions over the British sector of the Lurasian Seaway.

In a study of the Cretaceous Atlantic Ocean, Wagner et al. (2013) combined geochemical datasets and climate model simulations to suggest that an expanded Hadley Cell, forced by elevated $p\text{CO}_2$ levels, promoted OC production and burial across marine basins through elevated nutrient supply from either enhanced precipitation or wind-driven upwelling. Armstrong et al. (2016) applied this hypothesis to the Late Jurassic; they combined Late Jurassic climate simulations with sedimentological and geochemical data from the Wessex

(Dorset, UK) and Cleveland (Yorkshire, UK) Basins and concluded that tropical climate conditions prevailed over the southern Laurasian Seaway and promoted OC burial in the KCF. The aims of this thesis are intended to further validate and refine this hypothesis.

1.5 The Kimmeridge Clay Formation

The Late Jurassic spans 163.5–145.0 Ma (Gradstein et al., 2012). During this interval, atmospheric $p\text{CO}_2$ levels were around 4 times those of today, and global temperatures were much warmer than today (Sellwood and Valdes, 2008).

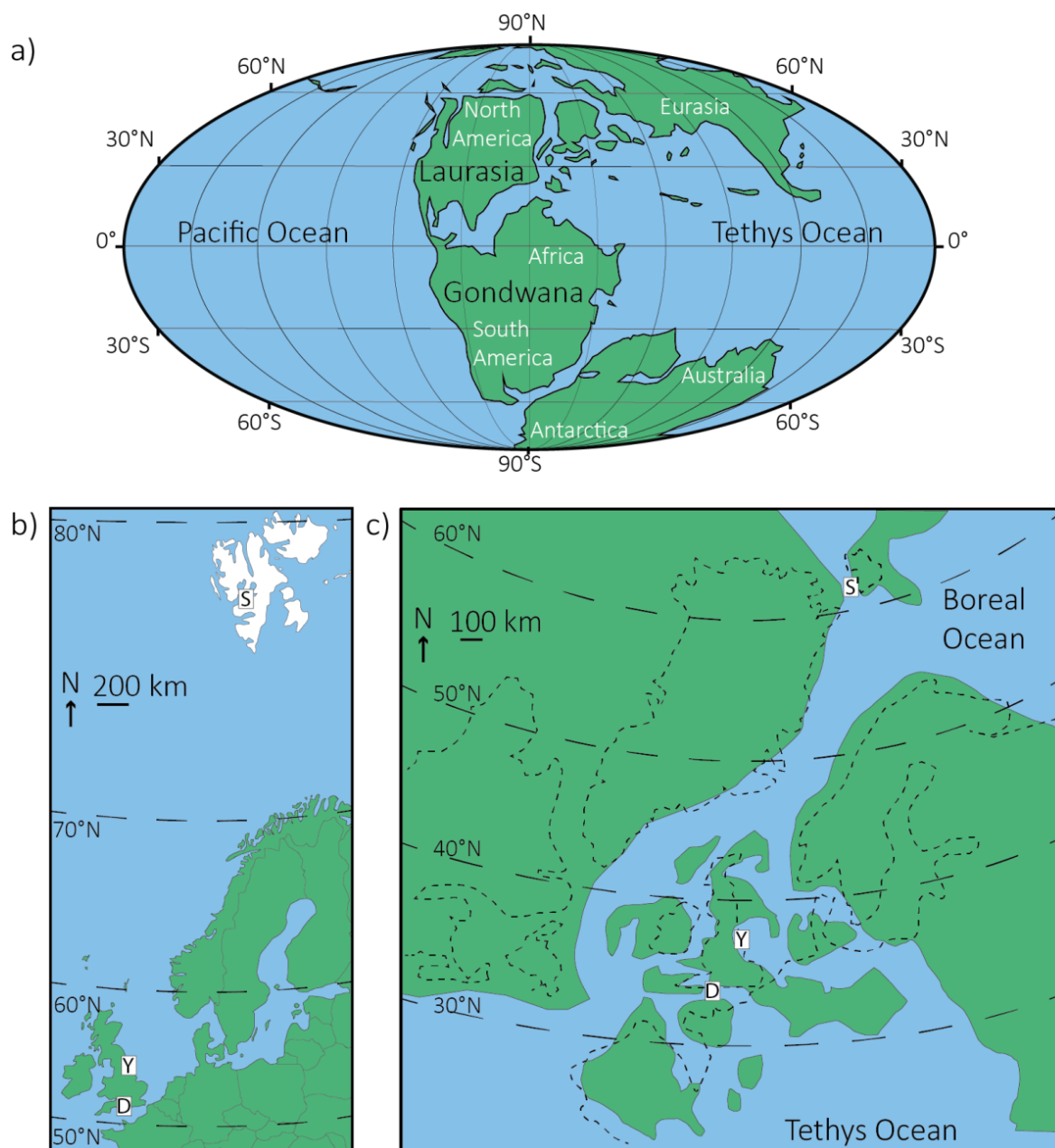


Figure 1.4. a) Palaeogeographic map from the Late Jurassic adapted from Armstrong et al. (2016). Black and white lettering denotes palaeo-features and modern day geography, respectively. b) Map of modern day Northwest Europe. c) Palaeogeographic map of northwest Europe in the Late Jurassic (Miller, 1990). Dashed lines denote positions of the modern-day landmasses. Sample sites in this study are marked by D=Dorset, Y=Yorkshire, and S=for Svalbard.

Rifting, related to the breakup of Pangea (Figure 1.4a), formed the Laurusian Seaway in northwest Europe and caused a major global transgression throughout the Late Jurassic. The KCF is an OC-rich, laterally extensive, stratigraphically thick (up to 500 m; Cox and Gallois, 1981) succession deposited across the UK sector of the North Sea (Figure 1.4b) in the Laurusian Seaway (Figure 1.4c).

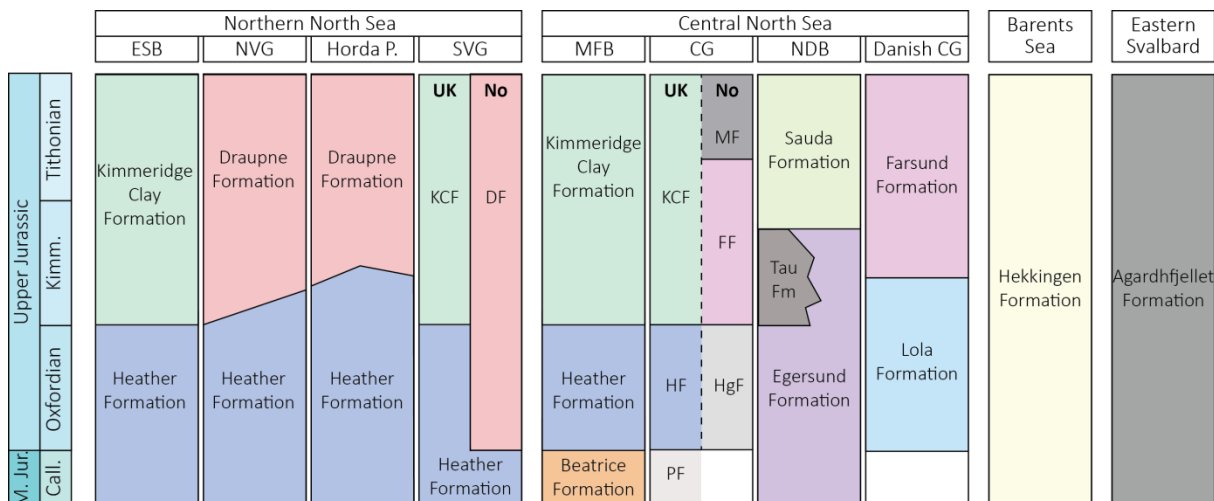


Figure 1.5. Panel showing the lithostratigraphic names across the North Sea up to the Arctic section (adapted from the Millennium Atlas). UK = United Kingdom. NO = Norway.

The Laurusian Seaway was a shallow (<200 m), epicontinental seaway comprised of numerous interconnected sub-basins and many low-lying islands (Figure 1.4c) that connected the Boreal and Tethys Oceans via the Viking Corridor (Figure 1.4c).

The KCF is lithologically heterogeneous, comprising intercalated mudstones, sandstones, and limestones, and its lateral equivalents (Figure 1.5) (spread over >1000 km) are commonly also enriched in OC and comprise similar lithologies. OC enrichment in the KCF is prolific, so much so that it is Europe's best source rock, and it has been the subject of intense research throughout the last century (Cooper et al., 1995, Cope, 2015, Gallois, 2004, Schwarzkopf, 1992, Arkell, 1933, Aigner, 1980, Fox-Strangways, 1892). Its fine grained nature and vast extent lends itself well to palaeoclimate reconstructions; palaeontologists (Lees et al., 2004, Lees et al., 2006), stratigraphers (Morgans-Bell et al., 2001, Cope, 2015, Cox and Gallois, 1981, Gallois, 2000, Gallois and Etches, 2001), sedimentologists (Macquaker and Gawthorpe, 1993, Macquaker et al., 2010b, Lazar et al., 2015b), geochemists (Pearce et al., 2008), and climate modellers (Sellwood and Valdes, 2008) have all studied the KCF in great detail, aiming to elucidate the main drivers of sedimentation and to reconstruct Late Jurassic climate conditions. Many depositional models have been proposed for the KCF, for example Hallam and Bradshaw (1979) proposed the 'Irregular Bottom Topography Model' in which localised stagnant conditions results from differential subsidence across the seaway floor, enhancing OC preservation; Oschmann (1988) proposed the 'North Atlantic Passage Model' in which seasonal upwelling from the deep Atlantic promoted density and temperature stratification

in the seaway, also promoting OC preservation; and Miller (1990) proposed the 'Warm Saline Bottom Water Model' which invokes a sluggish circulation resulting from a Boreal to Tethyan flow of water, Coriolis effect, and bottleneck palaeogeography, as the key driver of enhanced OC preservation; however, we are still lacking a consensus.

In this thesis, I will use sedimentological and geochemical data from a 1000 km transect of the Kimmeridge Clay Formation, to a) look at the variations in oceanographic conditions in space and time, and b) provide constraints on the atmospheric processes that may have resulted in these conditions.

1.6 Thesis outline

Descriptions of individual chapters are outlined below. Chapters 3–7 have been written as standalone pieces of work, which have/will be submitted for publication, I have noted the relevant co-authors where relevant. Each chapter contains a standalone introduction, geological background, methods (detailed in full in chapter 2), results, discussion, and conclusions. The thesis is synthesised as a whole, and overarching conclusions and suggestions for further work are presented in chapter 8.

Chapter 2: Methods and materials

The approach of the study and a brief justification of methods is presented. Information pertaining to sample material, locations, and sampling resolution is outlined, before detailed methods are described for each of the implemented analyses.

Chapter 3: Climate models of the Late Jurassic

A comparison between the HadCM3L climate model (Armstrong et al., 2016) and the independent Fast Ocean Atmosphere Model (FOAM) simulations for the Kimmeridgian/Tithonian is presented. The simulations are compared and contrasted in terms of surface temperature and precipitation rates, and seasonal calculations of the position of the Intertropical Convergence Zone from each model. Implications for sedimentation in the Laurasian Seaway are also discussed.

Chapter 4: Sedimentology of the Kimmeridge Clay Formation in the Cleveland Basin (Yorkshire, UK)

A six-member facies model for the Ebberston 87 Core from the Cleveland Basin (Yorkshire, UK) is presented and discussed with reference to sediment composition, sediment transport and dispersal mechanisms, and a palaeo-depositional environment reconstruction.

Chapter 5: Dynamic climate-driven controls on the deposition of the Kimmeridge Clay Formation in the Cleveland Basin (Yorkshire, UK)

Major and trace element contents, total organic carbon and carbonate contents, and organic carbon isotopes are discussed, with reference to the petrography (Chapter 4), to construct a

palaeo-depositional model for the Kimmeridge Clay Formation in the Cleveland Basin (Yorkshire, UK).

Chapter 6: Local to global controls on the deposition of organic-rich muds across the Late Jurassic Laurasian Seaway

Major and trace element contents, total organic carbon and carbonate contents, and organic carbon isotope data for the Swanworth Quarry 1 Core from the Wessex Basin (Dorset, UK) is compared to equivalent datasets from the Cleveland Basin (Chapters 4 and 5). The comparison is discussed in the context of chemostratigraphic correlation and overarching controls on sedimentation.

Chapter 7: Organic carbon enrichments in the northern Laurasian Seaway (Svalbard) during the Late Jurassic

Petrographic and geochemical data, namely major and trace element contents, total organic carbon and carbonate contents, and organic carbon isotopes, are presented from the DH4 Core, drilled in Advendalen (Svalbard, Spitsbergen) from a time-equivalent section to the Ebberston 87 and Swanworth Quarry 1 Cores (Chapters 4, 5, and 6).

Chapter 8: Synthesis, conclusions, and further work

Chapters 3–7 are synthesised together with reference to the project aims and hypotheses presented in Chapter 1. Overall conclusions of the study and recommendations for future work are also presented.

2 | Methods and materials

Chapter Summary

This chapter outlines the approach taken in this study and a justification of methods. Details of sample material, locations, and sampling strategy are presented. Detailed methodologies, including sample preparation, storage, analytical procedures, and accuracy/precision, where relevant, are outlined. The lithological nomenclature utilised throughout this study is also summarised.

2.1 Approach

As discussed in Chapter 1, global climate models are a powerful tool with which we can investigate atmospheric processes at different geological intervals. However, these models have inherent uncertainties and detailed truthing with environmental proxy data is required to ensure predictions are robust (e.g. Tabor et al., 2016). In Chapter 3, two independent model simulations are presented to explore climate conditions across the Lurasian Seaway in the Late Jurassic. Methods pertaining to each of these simulations are presented in Chapter 3 as they are relevant to the discussion of the resulting predictions.

In order to investigate global and local controls on spatial and temporal variations in sedimentation and organic carbon (OC) enrichment across the Lurasian Seaway, three time-equivalent sections, spanning approximately 1 million years, have been characterised using an array of techniques, which are detailed in this chapter. These data are interpreted to discern the local and global processes influencing sedimentation and OC enrichment and are then discussed in the context of the two climate model simulations.

2.2 Justification of methods

Sedimentary rocks can be interrogated in a number of ways, each having their own merits and drawbacks (Lazar et al., 2015b). While the fine-grained nature of mudstones lends itself well to detailed environmental reconstruction, it can also pose challenges for observations (Lazar et al., 2015a). This is particularly true for petrographic characterisation of mudstones; the fine and soft nature of several mudstone components, for example clay minerals, can lead to smearing during preparation of thin sections. It also makes light penetration difficult so thin sections have to be prepared to a <30 µm thickness (Lazar et al., 2015b, Macquaker et al., 2007), which poses technical challenges. Detailed investigation of mudstones, in hand specimen, under optical light, and under scanning electron microscope, provides information on sediment composition, sediment transport and dispersal mechanisms, post depositional history (diagenesis) and, importantly, provides a tool with which to ground truth geochemical observations (Ghadeer and Macquaker, 2012, Lazar et al., 2015a, Lazar et al., 2015b, Macquaker et al., 2010a, Macquaker and Adams, 2003, Macquaker and Bohacs, 2007, Macquaker and Howell, 1999, Macquaker et al., 2010b, Macquaker et al., 2007, Macquaker et al., 2014, Newport et al., 2017, Taylor, 1998, Bohacs et al., 2014, Aplin and Macquaker, 2011, Trabucho-Alexandre, 2015a, Trabucho-Alexandre, 2015b, Trabucho-Alexandre et al., 2012, Kranck, 1975, Li and Schieber, 2018, Schieber, 1989).

Geochemical characterisation provides a wealth of information on mudstones that can be used to interpret factors affecting mudstones from continental weathering rates through to post depositional history (Sageman et al., 2013). There are too many to consider in one study, so in this thesis, I use major and trace element contents to glean information on sediment

composition and provenance, grain size variations, continental weathering rates, redox state of the sediment pore and bottom waters (Sageman et al., 2003, Brumsack, 2006, Tribovillard et al., 2006); total organic carbon and carbonate contents to indicate OC enrichment and sediment composition; and stable carbon isotopes to provide insight in to OC type and carbon cycling (Gröcke et al., 2003). When preparing samples for geochemical analyses, a 'slice' of sediment must be ground and homogenised, thus each geochemical data point represents a time averaged signal, which must always be remembered during interpretation. Combining sediment thickness with age constraints, however derived, gives an indication of sedimentation rate that can be used to approximate the time interval covered (Algeo et al., 2011). Petrographic results are invaluable in ground-truthing geochemical observations in light of this.

A third technique consists of using the laws of physics, observations of modern day, and palaeogeographic reconstructions, to simulate climatic processes with global climate models (Sellwood et al., 2000, Lunt et al., 2017, Lunt et al., 2016). There are numerous different climate models available, all with their own limitations (Lunt et al., 2012). However, global climate simulations provide a 'big picture' insight in to global scale processes at varying degrees of resolution. The validity of each simulation must be tested with observational data derived from the rock records to ensure a logical agreement (Price et al., 1995, Price et al., 1997). Large uncertainties are inherent in climate modelling due to uncertainty related to input and often sparsity of proxy data with which we can test the data. However, they have been demonstrated to be an invaluable tool in global scale palaeoenvironmental conditions (Sellwood and Valdes, 2008).

It is for this reason, that I have used an integrated petrographic, geochemical and climate modelling approach in this thesis. Integrating datasets recording microscale heterogeneity to global scale climate simulations is one of the big challenges of this project, but consideration of the different aspects of sedimentation that each method reveals is a strength of this unique, well-rounded approach.

2.3 Sample locations and materials and sampling strategy

During the first year of the project (2014-2015), samples were collected from cores from three locations in North West Europe. Sampling location was chosen according to lithology, geological timespan and latitude in order to meet the aims of the project, and for more practical reasons such as material availability and accessibility of the core.

2.3.1 Ebberston 87 Core

The Ebberston 87 Core is one of four cores drilled in the Cleveland Basin, Yorkshire, as part of a joint venture between IFPEN and BGS in the 1980s. The original project aim was to investigate how source rock characteristics changed from a proximal (the Flixton Core) to a relatively deep marine (Marton Core) setting (Herbin et al., 1991). 116 samples were collected from the Ebberston 87 Core from the upper *Pectinatus wheatleyensis* ammonite subzone to the lower *Pectinatus pectinatus* ammonite subzone at a 50-cm resolution. Samples of 1 cm thickness were collected at 50 cm intervals through a 40-metre-thick section of the core. Sampling resolution was increased to 10 cm in darker, organic carbon-rich intervals. Using established chronology of the Ebberston 87 Core (Herbin et al., 1993), and assuming a linear sedimentation rate, the studied interval spans approximately 800 kyr.

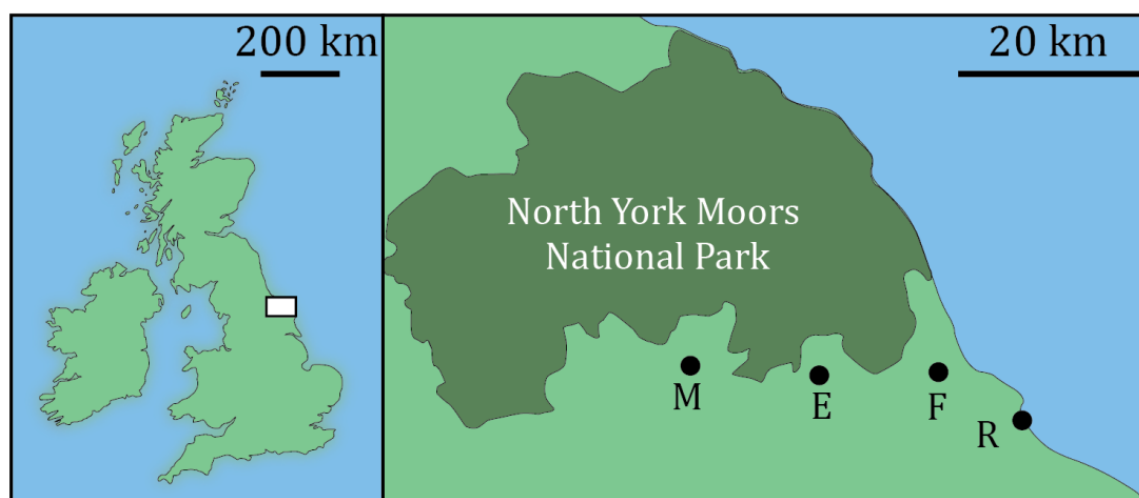


Figure 2.1 Present day map showing drilling sites of the cores sampled in the IFPEN/BGS project. M = Marton, E = Ebberston, F = Flixton, and R = Reighton. After Herbin *et al.* (1991).

2.3.2 Swanworth Quarry Core

The type section of the Kimmeridge Clay Formation is exposed along the southern coast of England, UK. In order to conduct a high resolution multidisciplinary study of the section on unweathered samples from a stratigraphically complete section, three cores were drilled as part of the Natural Environment Research Council's (NERC) Rapid Global Geological Events (RGGE) project special topic 'Anatomy of a Source Rock' in 1996-97. The project was set up to investigate the dominant sedimentological and environmental controls the Kimmeridge Clay Formation (Morgans-Bell et al., 2001, Pearson, 2000). The Swanworth Quarry 1 (SQ1) Core is studied in this thesis. The core location coordinates are SY 9675 7823. The core is stored in

the British Geological Society (BGS) core store in Keyworth, Nottinghamshire. 172 samples were collected from the SQ1 Core between the *Pectinatus wheatleyensis* and the

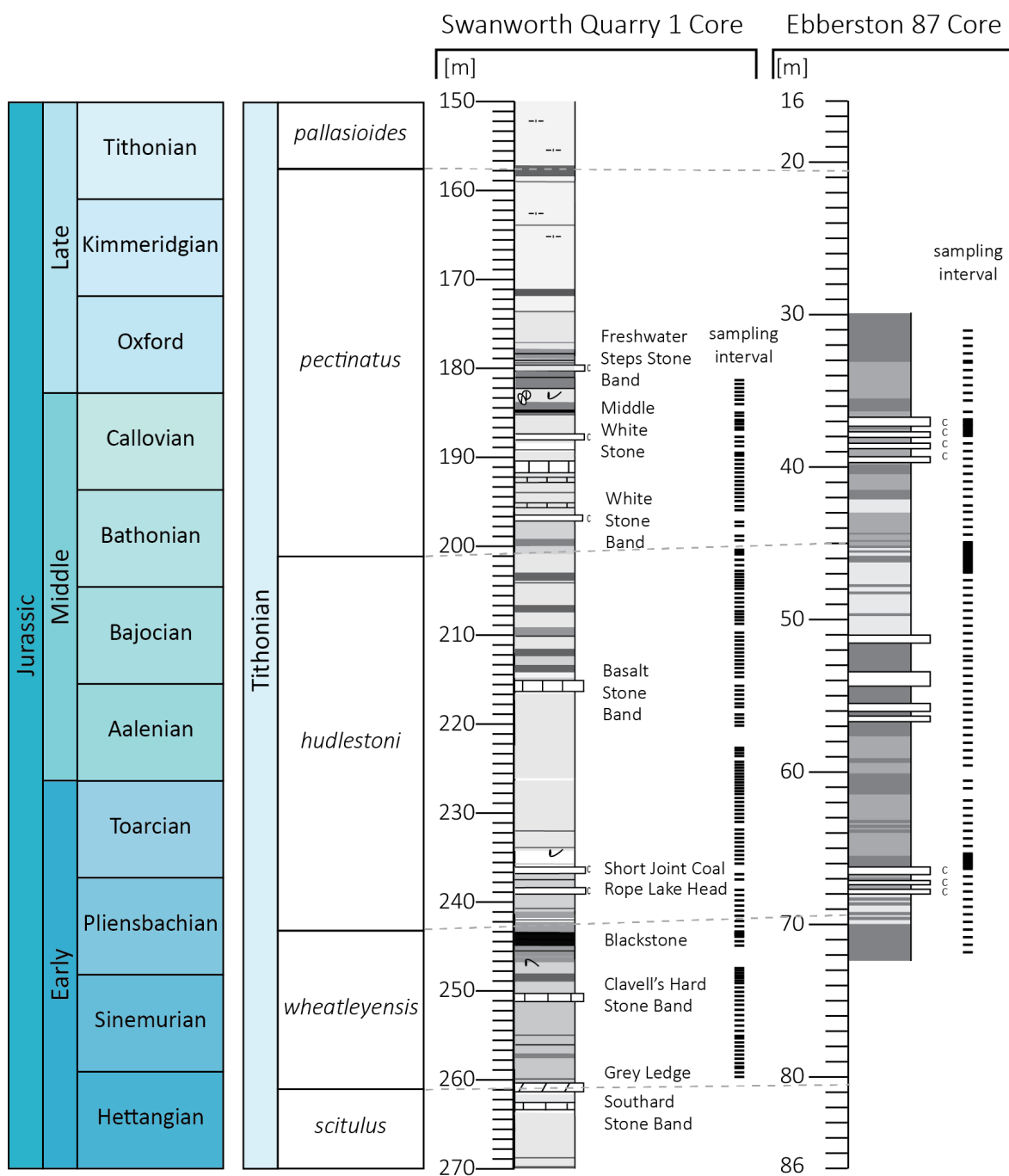


Figure 2.2 Stratigraphy of the studied interval in the Cleveland (Yorkshire, UK) and Wessex (Dorset, UK) Basins. Swanworth Quarry 1 Core after Morgans-Bell et al. (2001). Chronostratigraphic divisions after Gradstein et al. (2012). Sampling intervals are marked for both cores. Grey dashed horizontal lines denote biostratigraphical ties.

Pectinatus pectinatus ammonite subzones at a resolution of 50 cm. Approximately 30 g of sample was taken and prepared for analyses. Given the extensive research already carried out on core and equivalent coastal outcrop (Lazar et al., 2015b, Macquaker and Gawthorpe, 1993, Macquaker and Bohacs, 2007), thin sections were not prepared so petrographic analyses was not carried out on this core.

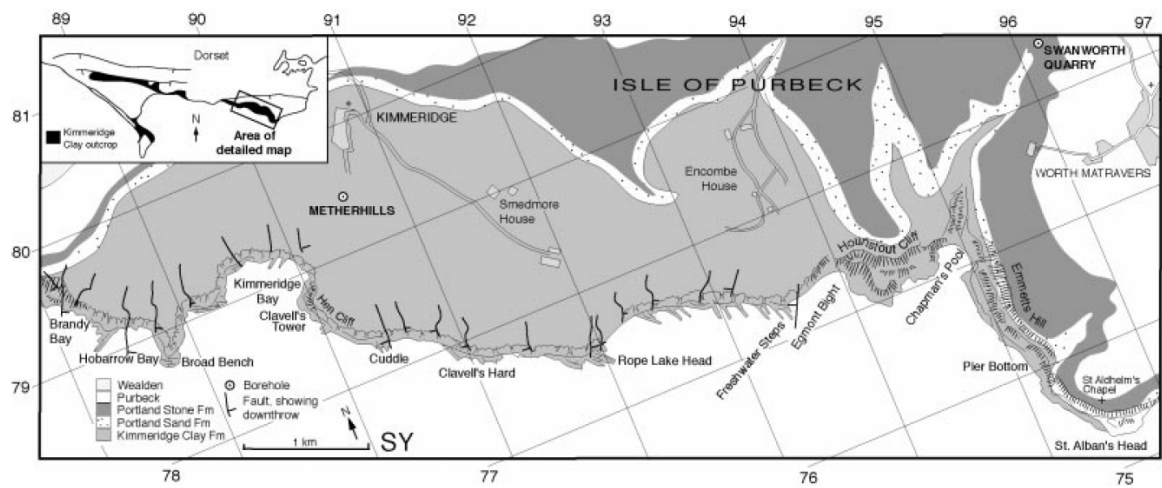


Figure 2.3 Map showing the outcrop of the Kimmeridge Clay Formation in Dorset and the cores referred to in the text. After Morgans-Bell et al. (2001)

2.3.3 DH4 Core

The northern and southern sectors of the Lurasian Seaway are correlated using different ammonite zones and a slightly different timescale (Figure 2.4); however, ongoing work is improving correlation across this area (Turner et al., 2019, Koevoets et al., 2016, Koevoets et al., 2018). The DH4 Core is one of four cores drilled as part of the Longyearbyen CO₂ Lab's project to investigate whether or not the local geological conditions are appropriate for subsurface storage of CO₂ (Braathen et al., 2012).

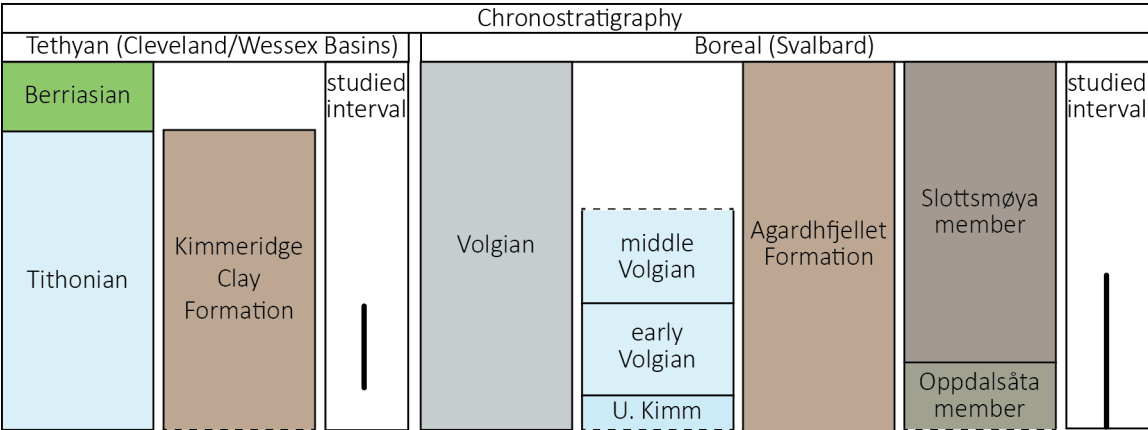


Figure 2.4. Summary diagram of the relevant Boreal and Tethyan chronostratigraphy from the Lurasian Seaway. Chronostratigraphic divisions after Gradstein et al. (2012). Studied intervals are marked by vertical black lines.

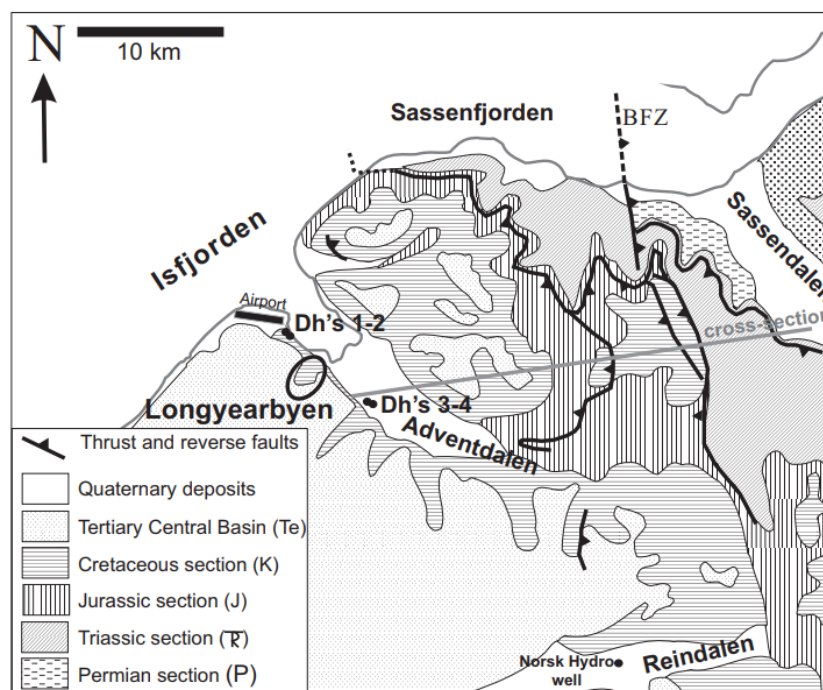
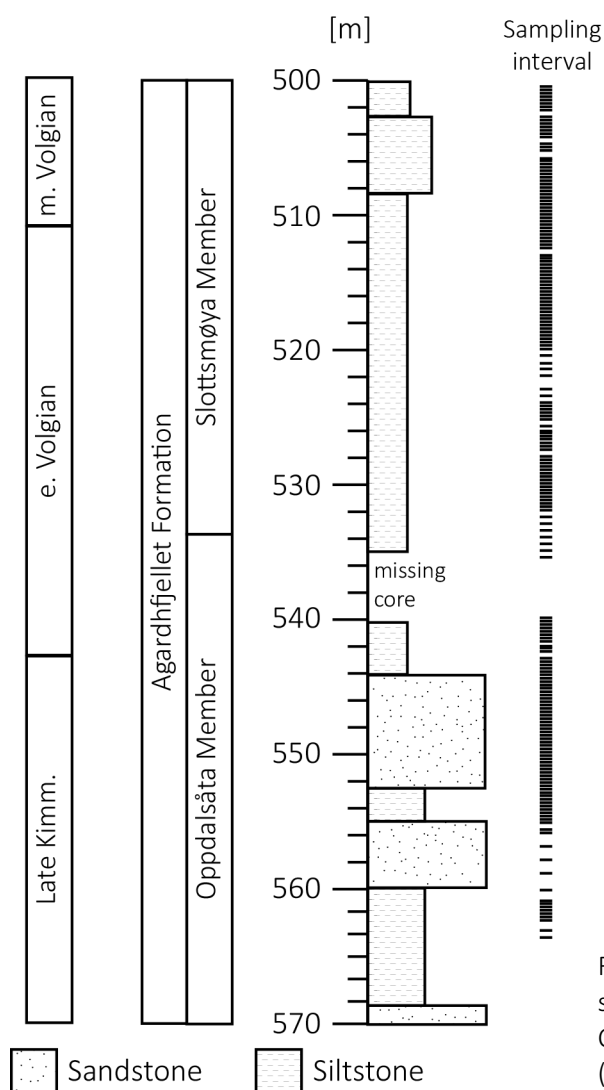


Figure 2.5. Geological map showing the location of the DH4 map. After Braathen et al. (2012)



The DH4 Core is located in Adventdalen, Svalbard (Figure 2.5). 195 samples were collected at a resolution of 25 cm from 500.00m to 563.00 metres below surface (Figure 2.6). Approximately 20 g of sample was collected and prepared for analysis.

Figure 2.6. Litholog, chronostratigraphy, and sampling interval for the DH4 Core. Chronostratigraphic divisions after Koevoets et al. (2016).

2.4 Petrographic methods

2.4.1 Optical light petrography

A representative subset of samples was selected and prepared for petrography. Glass-mounted thin sections were prepared to a thickness of 30 μm and examined under optical light using a Leica DM750P. Thin sections were imaged under plain polarised light and cross polarised light using a Leica ICC50 HD camera microscope.

2.4.2 Scanning electron microscopy

Thin sections selected for investigation under the scanning electron microscope (SEM) were polished with 1 μm diamond paste and coated with 30 μm of carbon before being examined with a Hitachi SE-70 High Resolution Analytical SEM. The SEM was used to image and acquire chemical maps of the samples.

The samples were imaged in the backscattered electron (BSE) setting at a range of magnifications. The microscope was operated at 15 kV, 2 nA, and approximately 15 mm working distance.

Element maps were collected for specific fields of samples with the main aim of calibrating the bulk-rock geochemical proxies. The chemical map data was processed in to phase maps using the Aztec software. Unprocessed data is presented in Appendices D and I.

2.5 Geochemical methods

2.5.1 Crushing and grinding

Approximately 30 g of each sample was crushed to c. 10 μm using an agate Retsch, RS200, Vibratory Disc Mill at the Scottish Universities Environmental Research Centre. The powders were stored in air tight glass jars in preparation for the further analyses. It is worth noting that due to average sample thicknesses of 1 cm, the geochemical compositions of individual samples might represent mixed signals that would not resolve any sub-cm scale geochemical variability.

2.5.2 LECO

Samples were prepared for total organic carbon (TOC) measurements by decalcification in hot (60-70°C) 12.5 ml HCl. Then they were rinsed and dried before being analysed. Total carbon (TC) and total sulphur (TS) measurements were carried out on bulk powders. TOC, TC, and TS were measured using a LECO CS230 Carbon-Sulphur analyser at Newcastle University. Total carbonate was calculated from $(\text{TC}-\text{TOC}) \times 8.33$.

2.5.3 Carbon isotopes

Prior to the analysis for $\delta^{13}\text{C}$ of the organic fraction, the inorganic fraction must be removed. To do this, samples were mixed with 5% hydrochloric acid and left overnight. Samples were

then rinsed in deionised water until a neutral pH was measured and then dried overnight at 40°C. Powders were homogenised with an agate pestle and mortar and weighed in to vials ready for analysis.

$^{13}\text{C}/^{12}\text{C}$ analyses were performed by combustion in a Costech ECS4010 Elemental Analyser on-line to a VG TripleTrap and Optima dual-inlet mass spectrometer, with $\delta^{13}\text{C}$ values calculated to the VPDB scale using a within-run laboratory standards calibrated against NBS18, NBS-19 and NBS 22. Replicate analysis of well-mixed samples indicated a precision of $+ <0.1\text{‰}$ (1 SD). C/N ratios can also be measured if required, and these are calibrated against an Acetanilide standard. Replicate analysis of well-mixed samples indicated a precision of $+ <0.1$. Samples were analysed for $\delta^{13}\text{C}_{\text{org}}$ values, calculated to the VPDB standard, at the BGS NERC Isotope Facility.

2.5.4 X-ray fluorescence

Wavelength-Dispersive X-Ray Fluorescence (XRF) analyses were conducted at the Institute for Chemistry and Biology of the Marine Environment (ICBM, University of Oldenburg). In preparation for determination of selected major (Si, Ti, Al, Fe, Mn, Mg, Ca, Na, K, P and S) and trace elements (As, Ba, Ce, Co, Cr, Cu, Ga, Mo, Ni, Nb, Pb, Rb, Sr, Th, Y, V, U, Zn, and Zr), 0.7 g of sediment was mixed with 4.2 g of $\text{Li}_2\text{B}_4\text{O}_7$ and 1.0 g of $(\text{NH}_4)_2\text{NO}_3$ (oxidising agent) and fused to a borate glass bead at 1350°C in a platinum crucible. The composition of the beads was measured using a Philips PW-2400 WD-XRF spectrometer. Precision was measured at $<0.5\%$ for major elements and $<7\%$ for trace elements, excluding U for which precision was measured at 16 %. Major and trace elements are expressed as wt % and ppm, respectively.

All elements were normalised to Al to allow for assessment of relative concentration changes irrespective of variable dilution by organic matter or carbonate. Aluminium is chosen as representative of the siliciclastic fine grained sediment fraction due to its generally high contents in the samples and its limited involvement in biological, redox and diagenetic processes (Tribovillard et al., 2006). Element/Al ratios are expressed as wt %/wt % or ppm/wt % as appropriate.

Enrichment factors of selected trace elements are calculated as:

$$\text{EF} = (\text{element}/\text{Al}) / (\text{element}/\text{Al})$$

Adapted from Brumsack (2006), with $\text{EF} > 1$ indicating relative enrichment compared to the background sediment, while $\text{EF} < 1$ indicates relative depletion. In chapter 5, EF's are calculated relative to Upper Continental Crust (Rudnick and Gao, 2003) rather than the frequently applied average shale (Wedepohl, 1991) due to clear and systematic deviations of both conservative and redox-related elements and derived element/Al ratios from the average shale composition, which would result in misleading EF patterns.

2.6 ICP-MS analysis

Selected trace elements (Mo, Cd, U, V, Re, Tl, W, As, and Sb) concentrations were obtained of a subset of 50 samples from the Ebberston 87 Core. Trace metals were measured in acid digestions by Quadrupole Inductively Coupled Plasma Mass Spectrometry (Q-ICP-MS; iCAP Q, Thermo Fisher Scientific) coupled to a PrepFast automated dilution device (ESI) at the Leibniz Institute for Baltic Sea Research (IOW). About 50 mg of ground sediment powder was digested in closed Teflon vessels at 180°C for 12 h using a mixture of HNO₃, HF, and HClO₄. After digestion, the acids were evaporated at max. 200°C on a heated block, fumed-off three-times with semi-concentrated HCl, and finally diluted to 50 mL with 2 Vol% HNO₃. All acids used were of suprapure quality. ICP-MS measurements were performed by using He as collision gas, an external calibration, and with Be, Ga, In, Rh, and Ir as internal standards. The final dilution factor of the measured acid digestions was 5,000. Precision and trueness were checked by replicate measurements (n=14) of the international reference material SGR-1b (USGS) and were better than 3.6 % and 11.3 %, respectively. For informative or missing reference values of SGR-1b, the GeoReM database (Jochum et al., 2005) was used.

The ICP-MS derived element data were processed analogous to the XRF derived element data regarding the normalisation to Al and the calculation of enrichment factors. Data are reported as ppm/wt % or ppb/wt % as appropriate.

2.7 Mercury (Hg) analysis

Hg contents analysis was conducted at the Leibniz Institute for Baltic Sea Research (IOW). The contents of Hg were determined from ~100 mg of sediment material by a direct mercury analyser (DMA80, Milestone). Precision and trueness were checked with the certified reference materials BCR-142R (Community Bureau of Reference) and TH-2 (National Water Research Institute, Canada) and were better than 3% and -1.0%, respectively.

2.8 Lithological nomenclature

Fine grained sedimentary rocks have been recognised and recorded for centuries but limited investigative techniques meant that it was not possible to fully explore the heterogeneous nature of these sediments until recent decades. Terms such as mudstone, siltstone, claystone, shale and variations between them are entrenched within the literature often with ambiguous definitions (Lazar et al., 2015b). Sedimentary rocks have been traditionally categorised based on their grain size, composition and textures. However, this principle breaks down at the fine grain size end of the scale where it becomes impossible to distinguish individual grains with the naked eye.

Recent advances in optical and electron microscopy, as well as improvements in the digital imaging of the techniques, have vastly improved the resolution, speed and ease at which we

can investigate fine-grained sedimentary rocks and share and learn from each other. In light of recent technological advances and the recognition that fine-grained sedimentary rocks record intricate and diverse processes, a revision of nomenclature and description of fine grained sedimentary rocks was necessary in order to streamline and ease comparison between studies in a rapidly expanding discipline. Lazar et al. (2015a) did just that through an extensive nomenclature review addressing textural, bedding, and composition definitions; furthermore, Lazar et al. (2015b) propose a methodology for the systematic investigation of fine-grained sedimentary rocks.

To negate the challenges outlined above and to maintain consistency between studies, all original work in this thesis will use the nomenclature scheme devised by Lazar et al. (2015a), and although it is summarised below, Lazar et al. (2015a, b and references therein) should be consulted for further discussion and detailed comparison between fine-grained sedimentary rock nomenclature and description classifications.

Lazar et al. (2015a) present a nomenclature scheme devised with the intention of fitting its purpose as a tool for sedimentologists to describe, name and compare successions with ease, repeatability and in an efficient time manner and maximise continuity between the published record. The conventional all-encompassing ternary diagram for siliciclastic rocks is improved through the defining of size fractions and splitting of the mud fraction (figure 2.5), that is to say that sand is defined as any grain between 62.5 μm and 2000 μm , coarse mud is between 62.5 μm and 32 μm , medium mud is between 32 μm and 8 μm , and fine mud is anything less than 8 μm . In this scheme the name of the rock is determined by the relative proportions of grain size within the succession.

It is important to be specific with terminology regarding sedimentary bedding as this characteristic can provide information of sediment accumulation rates, input and transport, benthic energy and fauna, and sediment pore and bottom water chemical conditions (Lazar et al., 2015a). A lamina is the smallest megascopic layer and is defined as sediment between two erosional or non-deposition surfaces with no internal structure. Laminae can be described with respect to their shape, continuity and geometry. A laminaset is a series of genetically, compositionally and texturally similar laminae. The largest megascopic layer is a bed, which is usually comprised of a series of lamina and/or laminasets, is bound by erosional or non-depositional surfaces, may or may not contain internal structure and may vary in composition (Lazar et al., 2015a). The composition of mudstones can be very diverse with common sedimentary components including quartz, biotic or abiotic carbonate grains, feldspars, clay minerals, biological ooze, phosphate minerals, and marine and terrestrial organic material. Mudstones are often varied in composition and this can reveal a lot about the formation of the succession. Figure 2.6 shows the classification of mudstones based on composition as determined by Lazar et al. (2015a).



Figure 2.7 Nomenclature guidelines for fine-grained sedimentary rocks (Lazar et al., 2015a). See original text for discussion of limitations of this representation

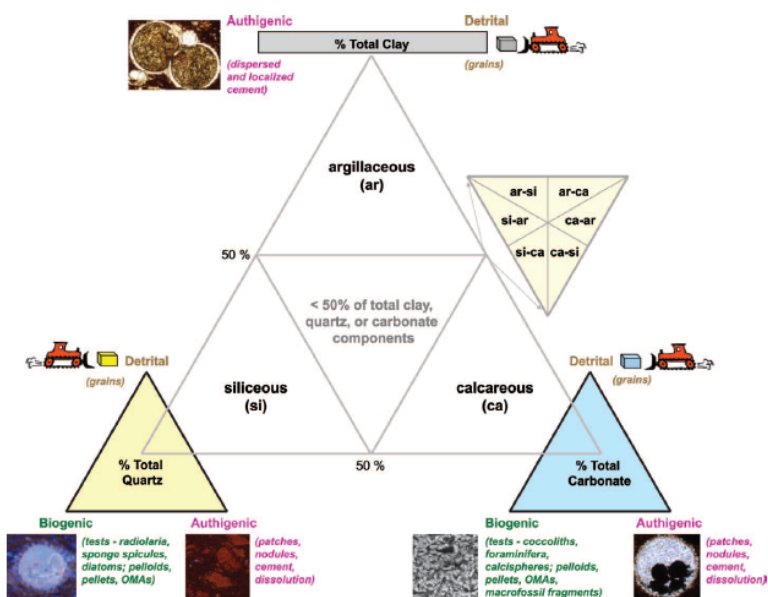


Figure 2.8 Composition classification of mudstones from Lazar et al. (2015a).

3 | Climate modelling in the Late Jurassic

Chapter Summary

Two independent climate modelling experiments are presented, compared, and discussed in the context of tropical climate belts, the intertropical convergence zone, and the implications of both simulations on the depositional conditions in the Lurasian Seaway in the Late Jurassic. The HadCM3L simulation implies a northward migration of the intertropical convergence zone that results in tropical conditions across the Lurasian Seaway. Conversely and in agreement with previous studies, the FOAM simulation indicates subtropical – temperate conditions across the Lurasian Seaway in the Late Jurassic. Agreement of independent modelling results would indicate a robust outcome and corroborate predictions of a northward migration of the Late Jurassic Hadley Cell compared to present day, but differing predictions raises questions over the validity and reliability of the model simulations presented by Armstrong et al. 2016, and requires further testing.

3.1 Introduction

Elevated global temperatures are posited to exert a large effect on the atmosphere, biosphere, and hydrosphere (IPCC, 2014). Changes in atmospheric dynamics can be on a global scale, occur over a range of timescales, and have direct but spatially diverse consequences for marine sedimentation and carbon burial. All of these processes can be simulated using global climate models and validated with data from the sedimentary rock record (Markwick and Valdes, 2004). Modelling climate processes during different periods in the Earth's history is pertinent to understanding how the Earth evolves over time and responds to different factors, such as elevated atmospheric $p\text{CO}_2$ levels (Lunt et al., 2016), it is therefore important to improving future climate predictions (Lunt et al., 2013). In addition to this, understanding how global atmospheric processes affected marine sedimentation in the past, in particular organic carbon (OC) enrichment, can improve cross-basin correlation and the characterisation and prediction of petroleum source rocks. Thus, understanding the influence that atmospheric processes exert upon marine sedimentation is of central interest to both climatologists and the petroleum industry.

In the present day, the corridor where the tropical limbs of the northern and southern hemisphere Hadley Cells converge is called the intertropical convergence zone (ITCZ). Here, warm, wet air ascends cooling as it does so, when the moisture condenses, it returns to the Earth's surface as precipitation (Schneider et al., 2014a). Thus, the ITCZ is characterised by wet, tropical conditions with high precipitation rates. In meteorology there is no formal, agreed method of defining the ITCZ (Berry and Reeder, 2014); it can be defined several ways using variables such as precipitation, sea-level pressure, air mass velocity, and low cloud-top temperature. The outer limbs of the Hadley Cells mark the boundary between the subtropical and temperate climate zones; these regions are characterised by persistent trade winds that promote oceanic upwelling along the western sides of continents (e.g. Namibia, NW Africa) and disperse dust export (Zhang et al., 2015). The position of the ITCZ migrates seasonally, however, it is also sensitive to changes in the intensity and latitudinal distribution of solar insolation, so the ITCZ also migrates due to orbital forcing on decadal to millennial timescales (Zhang et al., 2015, Meyers and Malinverno, 2018).

Understanding of Hadley Cell dynamics under greenhouse conditions is poorly constrained but a poleward Hadley Cell expansion under elevated $p\text{CO}_2$ is supported by climate modelling of the Cretaceous (Fluteau et al., 2007, Zhou et al., 2012) and geological evidence (Wagner et al., 2013). It is suggested that elevated $p\text{CO}_2$ levels intensifies the hydrological cycle leading to higher precipitation, continental weathering and run off (Flögel et al., 2011), associated with large latitudinal changes in net moisture transport (Poulsen et al., 2003). Based on detailed geochemical data from shelf and deep sea sections from the Atlantic basins, Wagner et al. (2013) identified that the Hadley Cell strongly affects OC burial at the inner and the outer

limbs. Under the ITCZ, hot, humid, tropical conditions prevail, which maintain intense continental weathering, erosion and runoff. In contrast, at the outer limb of the Hadley Cell, vigorous trade winds promote oceanic upwelling and dry hinterlands (commonly deserts). In both settings, elevated nutrient supply, whether from continental runoff or upwelling, promotes the production and preservation of organic carbon. Migration, modulation, and expansion of the Hadley Cells lead to varying OC richness in the sedimentary record (Wagner et al., 2013).

Armstrong et al. (2016) took this conceptual framework from the Cretaceous Atlantic forward and, by integrating geochemistry, sedimentology and modelling, concluded that the Jurassic (Kimmeridgian) ITCZ was situated around 30°N during the boreal summer, which is significantly further north than in the present day (23°N), and it migrated south during the boreal winter. In addition to the seasonal migration of the ITCZ, orbitally-driven migration of the ITCZ has significant consequences for sedimentation across the NW European seaway, which at the time of the Kimmeridgian (150 Ma) was a shallow epicontinental seaway (Bradshaw et al., 1992a). Based on sedimentology and geochemistry, the authors proposed that these tropical, stormy conditions promoted OC-rich production and burial and attributed the deposition of the Kimmeridge Clay Formation to atmospheric conditions. Further research is required to model the affect that orbital variations exert on Late Jurassic sedimentation.

There are large, inherent uncertainties with all modelling, particularly when extending back into the geological record, but the predictions made by Armstrong et al. (2016) have significant implications for global climate, source rock prediction and characterisation, and sedimentation at high sub-polar latitudes, warranting further investigation. In this chapter, I compare and contrast two independent modelling results for the Kimmeridgian to validate the predictions made by Armstrong et al. (2016). Agreement of independent modelling results will indicate a robust outcome and corroborate predictions of a northward migration of the Late Jurassic Hadley Cell compared to present day, but differing predictions raises questions over the validity and reliability of the model simulations presented by Armstrong et al. 2016, and will require further testing.

3.2 Model description

Two independent simulations are presented for the Late Jurassic Kimmeridgian. The simulations were run with two models: the Hadley Centre Coupled Model, version 3 low resolution (HadCM3L) and the Fast Ocean Atmosphere Model (FOAM). The models have different resolutions and were run with different initial states and boundary conditions, meaning that a direct comparison cannot be made. However, the differences in model setups can be advantageous as it accounts for the uncertainties associated with the palaeoenvironmental reconstructions (Lunt et al., 2012).

3.2.1 HadCM3L model

HadCM3L is a coupled atmosphere ocean global climate model that was developed in 1999 by the UK Meteorological Office in the Hadley Centre for Climate Prediction and Research. The model was the first of its kind to simulate present day climate without requiring flux adjustments to prevent drifting in to unrealistic climate states (Reichler and Kim, 2008). The model comprises an atmosphere component and an ocean component. Both components have a horizontal resolution of 2.5 degrees of latitude and 3.6 degrees of longitude, and the atmosphere has 19 vertical levels and the ocean has 20 levels. The HadCM3L utilises an interactive vegetation model, TRIFFID (Top-down Representation of Interactive and Flora Including Dynamics; (Cox, 2001)), which has been shown to warm global climate through the feedbacks involving water vapour and albedo (Loftson et al., 2014); however, this is not considered in the present study.

The original model, HadCM3, had an ocean resolution of 1.25 x 1.25 degrees which enabled simulation of intricate ocean structures; however, the lower resolution model was used in the study where the ocean and atmosphere resolutions are the same. Further information can be found in Valdes et al. (2017).

3.2.2 Fast ocean atmosphere model (FOAM)

FOAM is a coupled atmosphere-ocean climate model that was developed by the Space Science and Engineering Centre at the University of Wisconsin-Madison and the Mathematics and Computer Science Division of Argonne National Laboratory. It comprises a low resolution parallelised atmosphere component that is founded on the NCAR community climate model (CCM3) and a medium resolution parallelised ocean component, which is similar to the Modular Ocean Model created by the Geophysical Fluid Dynamics Laboratory in the US National Oceanic and Atmospheric Administration. FOAM also comprises a land model, a sea model, and a coupler. The coupler is a 50 m mixed-layer ocean that facilitates heat transport through diffusion in a computational efficient manner (Donnadieu et al., 2009). It also links the other four components by allowing flux flow through it, while allowing for each component to run independently at differing timescales and resolutions. The FOAM atmosphere component has a resolution of $4.5^{\circ} \times 7.5^{\circ}$ which gives a 40 latitude x 48 longitude grid and has 18 vertical levels. The FOAM ocean and coupler components have a resolution of $1.4^{\circ} \times 2.8^{\circ}$ which gives a 128 latitude x 128 longitude grid. The ocean component has 24 vertical levels. Further information can be found in Jacob et al. (2001).

FOAM has been used to investigate Neoproterozoic and Cretaceous climate (Donnadieu et al., 2009, Donnadieu et al., 2006, Poulsen et al., 2003, Poulsen et al., 2002, Poulsen et al., 2001) and is reported to simulate aspects of the present day climate, such as surface temperature

and precipitation, well considering its low resolution and fast computing time (Donnadieu et al., 2009).

3.3 Experimental design and methods

3.3.1 HadCM3L initial and boundary conditions

The HadCM3L simulation has a spin up time of 1422 model years and results are averaged across the final 30 model years to produce climatologies; this is the same model presented in Armstrong et al. (2016). At model initiation, the atmosphere is set at an arbitrary state that is derived from a previous pre-industrial simulation, zonal mean ocean temperature is given as a cosine function of latitude, the ocean is stationary, ocean salinity is 30 ppm, and land surface conditions are homogenous.

	HadCM3L	FOAM
Initial Conditions		
Total spin up time	1422 years	1000 years
Temperature structure	zonal mean temperature structure given by an idealised cosine function of latitude	zonal mean temperature structure given by an idealised cosine function of latitude
Salinity	30 ppt	Levitus reference annual mean
Ocean velocity	0	0
Atmosphere	arbitrary atmospheric state from a previous preindustrial simulation	arbitrary atmospheric state from a previous preindustrial simulation
Boundary Conditions		
CO ₂	1120 ppm	2100 ppm
CH ₄ and NO ₂	preindustrial levels	preindustrial levels
Palaeogeography	modified from Getech	modified from Merlin
Solar constant	1347 W/m ²	1347 W/m ²
Obliquity	present day	present day
Eccentricity	present day	present day
Precession	present day	present day

Table 3.1. Summary of initial and boundary conditions for the HadCM3L and FOAM simulations.

The digital elevation model (palaeogeography) used in this study was produced by GeTECH Ltd using the methods of Markwick and Valdes (2004). The original palaeogeography was produced at a resolution of 0.5° x 0.5°, and then interpolated to native model resolution (3.75° x 2.5°) (Figure 3.1a). The land-sea mask (Figure 3.1), bathymetry, topography, and orography (Figure 3.2) are derived from the palaeogeography reconstruction and are all requisite for the model simulation (Lunt et al., 2016). A summary of the initial and boundary

conditions including atmosphere composition, solar constant, and orbital parameters is presented in Table 3.1.

3.3.2 FOAM initial and boundary conditions

The FOAM simulation has a spin up time of 1000 model years, and like in HadCM3L, the climatologies are calculated as a mean over the last 30 model years. At model initiation, atmosphere conditions are residual from a previous pre-industrial simulation, zonal mean temperature is a cosine function of latitude, the ocean is stationary, ocean temperature and salinity are set at Levitus reference values, and land surface conditions are homogenous. The digital elevation model (palaeogeography) used in this study was produced by CGG as part of the Robertson Predictions package (formerly Merlin+) and subsequently modified by Equinor ASA. The land-sea mask (Figure 3.1), bathymetry, topography, and orography (Figure 3.2) are derived from the palaeogeography reconstruction at FOAM resolution ($4.5^\circ \times 7.5^\circ$). Initial conditions including atmosphere composition, solar constant, and orbital parameters were kept at default; these are summarised along with boundary condition in Table 3.1

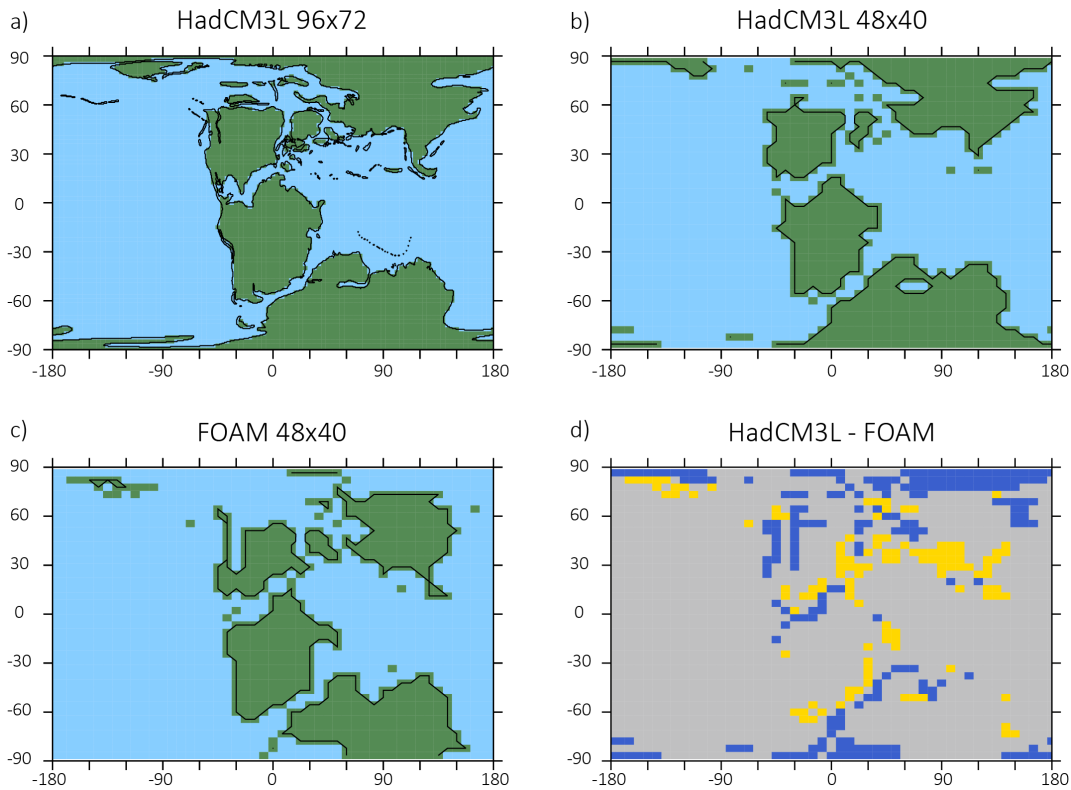


Figure 3.1. Land sea masks, where green denotes land and blue denote sea, for the a) HadCM3L at model resolution (96×72) and continental outline at a resolution of $0.5^\circ \times 0.5^\circ$, b) HadCM3L at a lower resolution (48×40), c) FOAM at model resolution (48×40), and d) the difference between b and c, where grey indicates the same grid square definition, yellow is where the grid square is land in FOAM but ocean in HadCM3L, and blue is where the grid square ocean in FOAM but land in HadCM3L.

3.3.3 Notable differences in boundary conditions between HadCM3L and FOAM

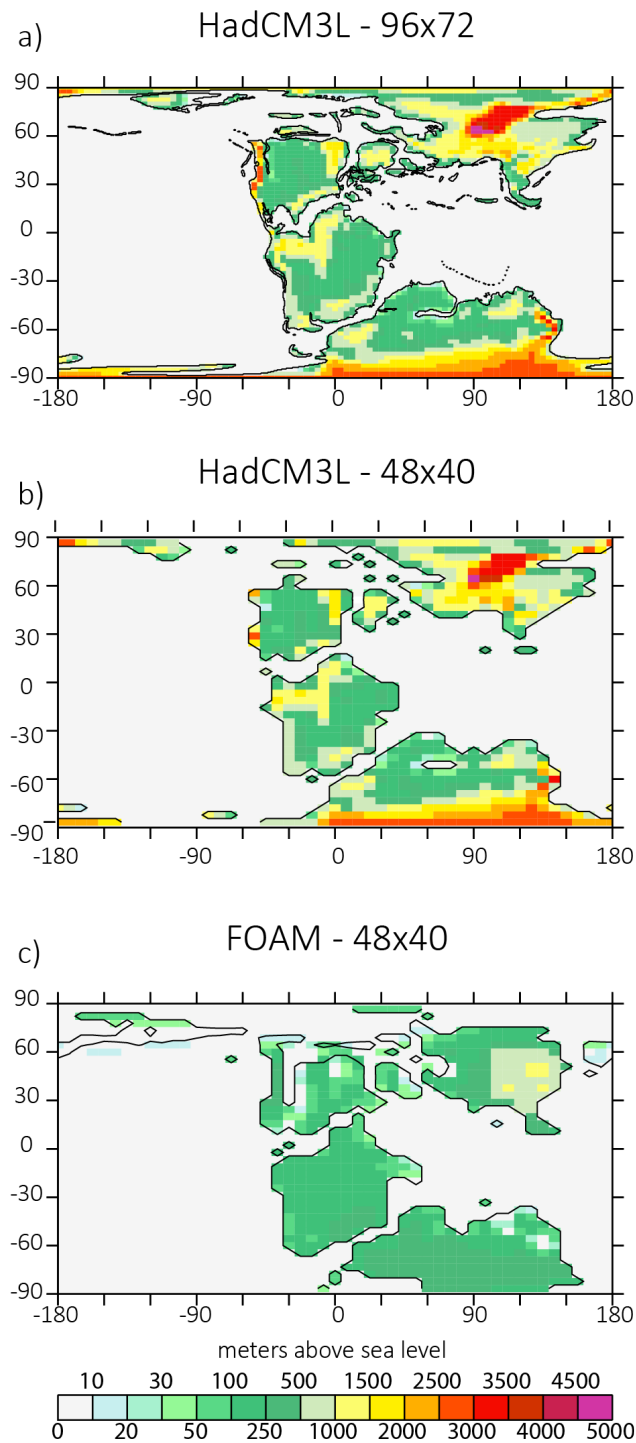


Figure 3.2. Orography maps for a) HadCM3L at model resolution (96 x 72), b) HadCM3L at a lower resolution (48 x 40), and c) FOAM at model resolution (48 x 40).

The majority of boundary conditions remain consistent between the models; however, notable differences occur in the atmospheric $p\text{CO}_2$ levels and the palaeogeographies between the HadCM3L and FOAM simulations. At 2400 ppm, the FOAM level is six times greater than the preindustrial level and more than two times greater than the HadCM3L level, which was 1120 ppm. The difference in shape and positioning of the continents is illustrated in Figure 3.1. The HadCM3L palaeogeography has land at both poles whereas the FOAM palaeogeography does not have land at the poles. The northernmost continents in the FOAM palaeogeography are positioned at slightly lower latitude than the equivalent continents in the HadCM3L palaeogeography.

Perhaps the most notable differences between the two simulations resides in the orography maps (Figure 3.2). While both palaeogeographies have key orographic features related to the Eurasian mountain ranges, albeit of differing magnitude, the palaeogeography used for the FOAM simulation does not have the North African or proto-Appalachian mountain ranges that are present in the palaeogeography used for the HadCM3L simulation (Figure 3.2). On the whole, the orography used in FOAM is much smoother and lower than the one used in HadCM3L.

3.3.4 Model interpolation

Model simulations need to be at the same resolution in order for them to be compared quantitatively. To do this, the HadCM3L atmospheric variables (surface temperature, precipitation, and zonal winds) at native model resolution (96 x 72) were regridded to FOAM resolution (48 x 40) using a bilinear interpolation. The HadCM3L land sea mask was regridded to FOAM resolution using a nearest neighbour interpolation.

3.3.5 Preindustrial simulations

Prior to comparing the model simulations of the Jurassic, it is important to evaluate the ability of the models to simulate a known atmospheric circulation. To this end, we can compare a preindustrial simulation to observed modern-day data. Armstrong et al., (2016) compared their preindustrial simulations to the CPC Merged Analysis of Precipitation (CMAP), averaged over 1979–2011, and reported that the HadCM3L simulations reproduced the main features of mean surface precipitation patterns well. Figure 3.3 shows the CMAP observational data for the annual, winter, and summer mean precipitation at the Earth's surface, along with surface precipitation from the HadCM3L and FOAM preindustrial simulations over the same time intervals.

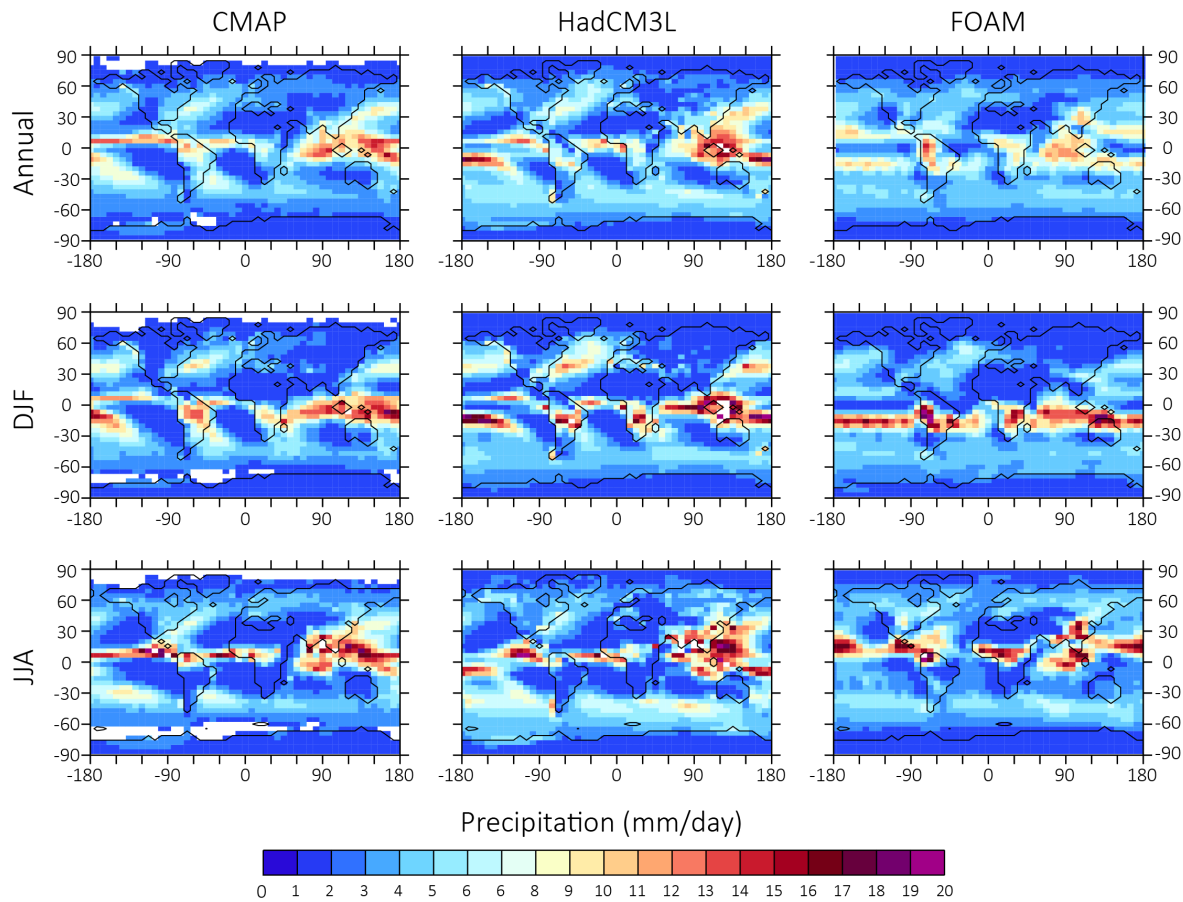


Figure 3.3. All at 48x40 resolution. (a, d, and g) Observed annual, winter (DJF), and summer (JJA) CMAP precipitation 1979–2009, (b, e, h) Annual, winter (DJF), and summer (JJA) precipitation from HadCM3L, (c, f, and i) Annual, winter (DJF), and summer (JJA) precipitation from FOAM.

Figure 3.4 shows the difference between the CMAP data and model simulations. Both models over predict precipitation relative to the CMAP data. The main differences occur at low latitudes and the FOAM simulation deviates further away from the CMAP data than HadCM3L does, which is indicated by stronger colours. This suggests that HadCM3L is a more robust model for simulating atmospheric dynamics. Given that the simulations had the same $p\text{CO}_2$ levels; it is likely that differences in climate sensitivity between the models are a large factor in this.

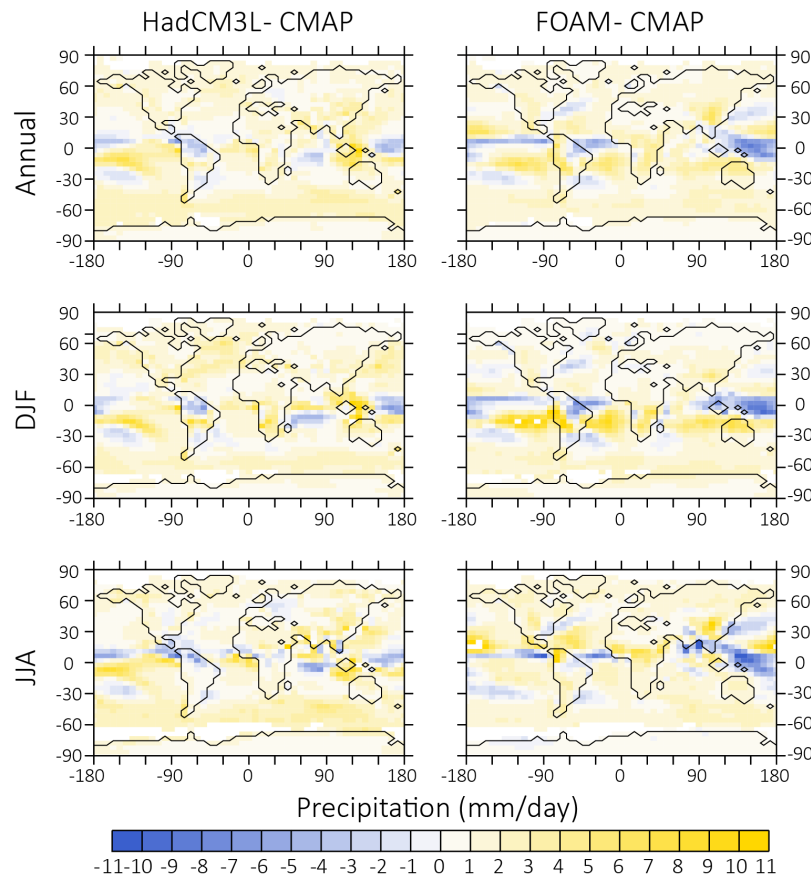


Figure 3.4. Annual, summer, and winter HadCM3L (left) and FOAM (right) simulations minus the CMAP data averaged across 1979–2009.

Figures A1 and A2 (an Appendix A) compare the HadCM3L and FOAM preindustrial simulations to one another; the annual, summer, and winter near surface temperatures and surface precipitation are plotted and Table A1 contains annual and season mean surface temperatures. The FOAM preindustrial simulation is significantly cooler than HadCM3L (Fig. A1). Precipitation is concentrated around the equator in both models (Fig. A2) and in general HadCM3L has higher precipitation rates. In the boreal summer, precipitation in HadCM3L exceeds that in FOAM in the southern hemisphere low latitudes but is lower than FOAM in the northern hemisphere low latitudes. This trend is reversed in the boreal winter. This may relate to surface temperature distributions (Fig. A1) but it is not possible to say with certainty with the present dataset. Nevertheless, these differences are important to keep in mind when interpreting the Late Jurassic simulations.

3.3.6 Identification of the intertropical convergence zone (ITCZ), subtropics, and monsoon regions

The ITCZ is defined automatically using two different methods that are adapted from Berry and Reeder (2014). The first uses the surface expression of precipitation (maximum tropical precipitation) to define position of the ITCZ, while the second uses maximum velocity of the ascending air masses in the mid-troposphere (500 mbr). Subtropical conditions, marking the outer limit of the Hadley Cell, were defined using a similar methodology. Maps of seasonal precipitation with depictions of local maximum precipitation, dry regions and regions of mid-atmosphere descent, which were used to identify the ITCZ and subtropical limits, are shown in Figure A1.

Global monsoon regions were defined, where local summer precipitation is greater than 55% of the total annual precipitation and the summer minus winter precipitation exceeds 2mm/day, after Wang et al. (2011) (see below).

3.4 Results and discussion

3.4.1 Surface temperature from HadCM3L and FOAM in the Jurassic

The HadCM3L simulation exhibits a higher global mean annual near surface temperature (~ 1.5 m; SAT) than the FOAM simulation (Table 3.2). Figure 3.5 shows the mean annual, winter (DJF), and summer (JJA) SAT for each of the simulations and the difference between them. Over the oceans, SATs are broadly similar between the two models; however, SATs over land in HadCM3L are consistently greater than in FOAM, with the exception of the high latitude land masses (Figure 3.5 a, b, c).

Global mean near-surface temperature (°C)	HadCM3L 48x40	FOAM 48x40	Difference (°C)
Annual	22.6	19.3	3.3
JJA	22.3	19.0	3.3
DJF	23.5	19.7	3.8

Table 3.2. Annual, winter (DJF), and summer (JJA) global mean surface temperatures for the HadCM3L and FOAM and the difference between the two models.

Given that the FOAM experiment had a predetermined atmospheric $p\text{CO}_2$ concentration of 2100 ppm, significantly higher than the 1120 ppm for HadCM3L, we would expect the simulated SAT from FOAM to be higher than those of HadCM3L. It is possible but unlikely that this difference relates to the shape and positioning of the high latitude landmasses in the HadCM3L experiment (Figure 3.1) that would become cooler than the equivalent oceans in FOAM. In a study of the Cretaceous, using the FOAM model, where palaeogeography changed

but a constant $p\text{CO}_2$ concentration was maintained, Donnadieu et al. (2006) report significant temperature differences resulting from the changes in palaeogeography. However, the probable cause of this is that HadCM3L has higher climate sensitivity (i.e. response to CO_2) than FOAM.

SATs from the FOAM preindustrial simulation are also unexpectedly low so differences inherent to the models may also explain the observed temperatures. Further experiments are required to test the sensitivity of the model to the opening and closing of ocean gateways and positioning of continents, both of which affect heat flow and distribution, to constrain whether palaeogeography, atmospheric CO_2 , or climate sensitivity is responsible for the observed differences. In both models, the boreal winter global mean SATs are higher than in summer (

Table 3.2), possibly owing to the distribution of landmasses. A greater difference between summer and winter global mean SATs in HadCM3L demonstrates stronger seasonality, which is shown by the SAT difference maps (Figure 3.5 c, f, i).

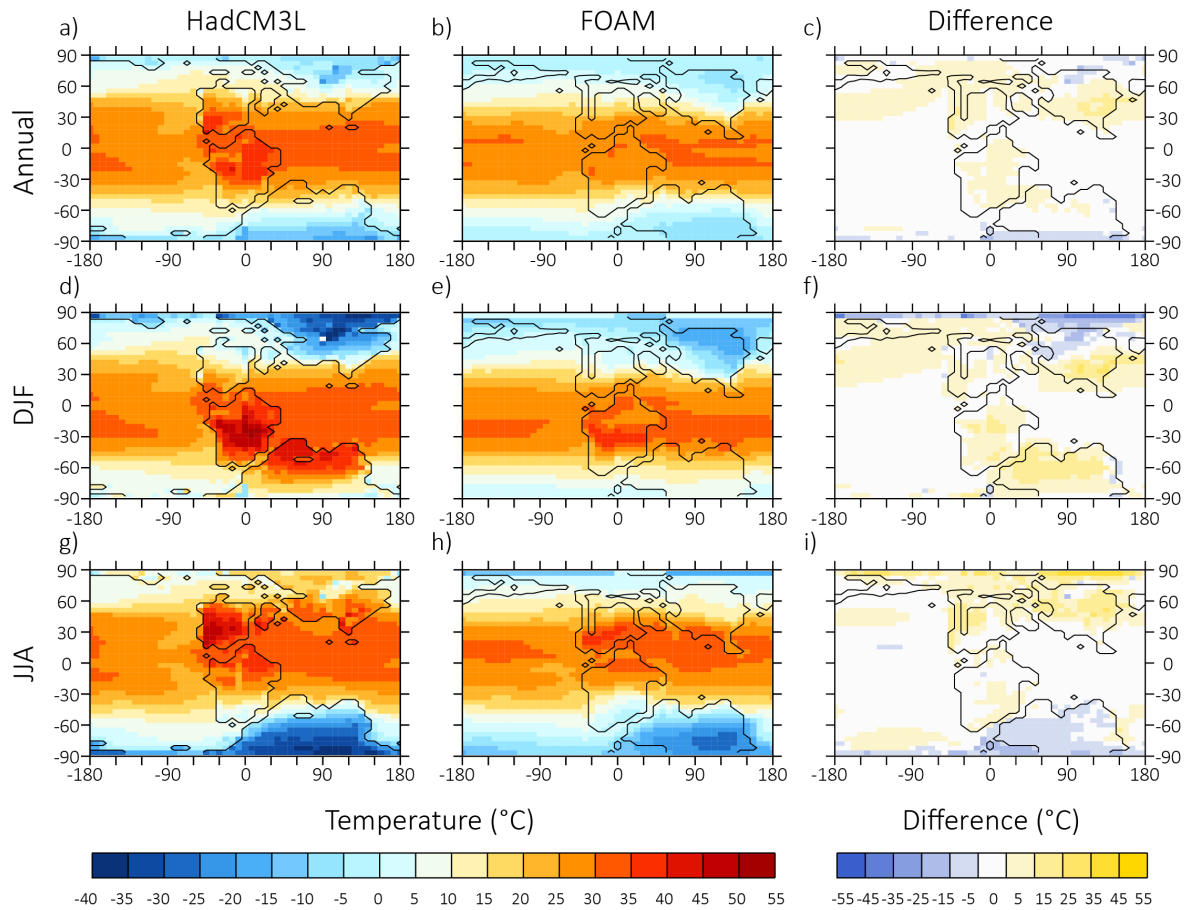


Figure 3.5. (a, d, and g) Annual, winter (DJF), and summer (JJA) surface temperature maps from HadCM3L at 48 x 40 resolution, (b, e, h) Annual, winter (DJF), and summer (JJA) surface temperature maps from FOAM at 48 x 40 resolution, (c, f, and i) Annual, winter (DJF), and summer (JJA) temperature differences between HadCM3L and FOAM.

3.4.2 Precipitation from HadCM3L and FOAM

Figure 3.6 shows annual, winter, and summer surface precipitation derived from each model. The large-scale spatial trends within each model are reasonably consistent; the annual precipitation map shows maximum global precipitation occurs across the Tethys and Pacific Oceans within 20° of the equator; this is also reflected in the defined positioning of monsoonal regions (Figure 3.7). The precipitation is shown to be seasonal alternating between slightly higher across the southern hemisphere in the boreal winter and a slightly higher across the northern hemisphere in the boreal summer. However, the absolute rate of precipitation is different between the models. HadCM3L is consistently drier across the Pacific Ocean compared to FOAM; the opposite is true for the Tethys Ocean where HadCM3L is consistently wetter than FOAM. Precipitation across the Laurasian Seaway and adjacent landmasses does not change much, with FOAM being slightly wetter than HadCM3L.

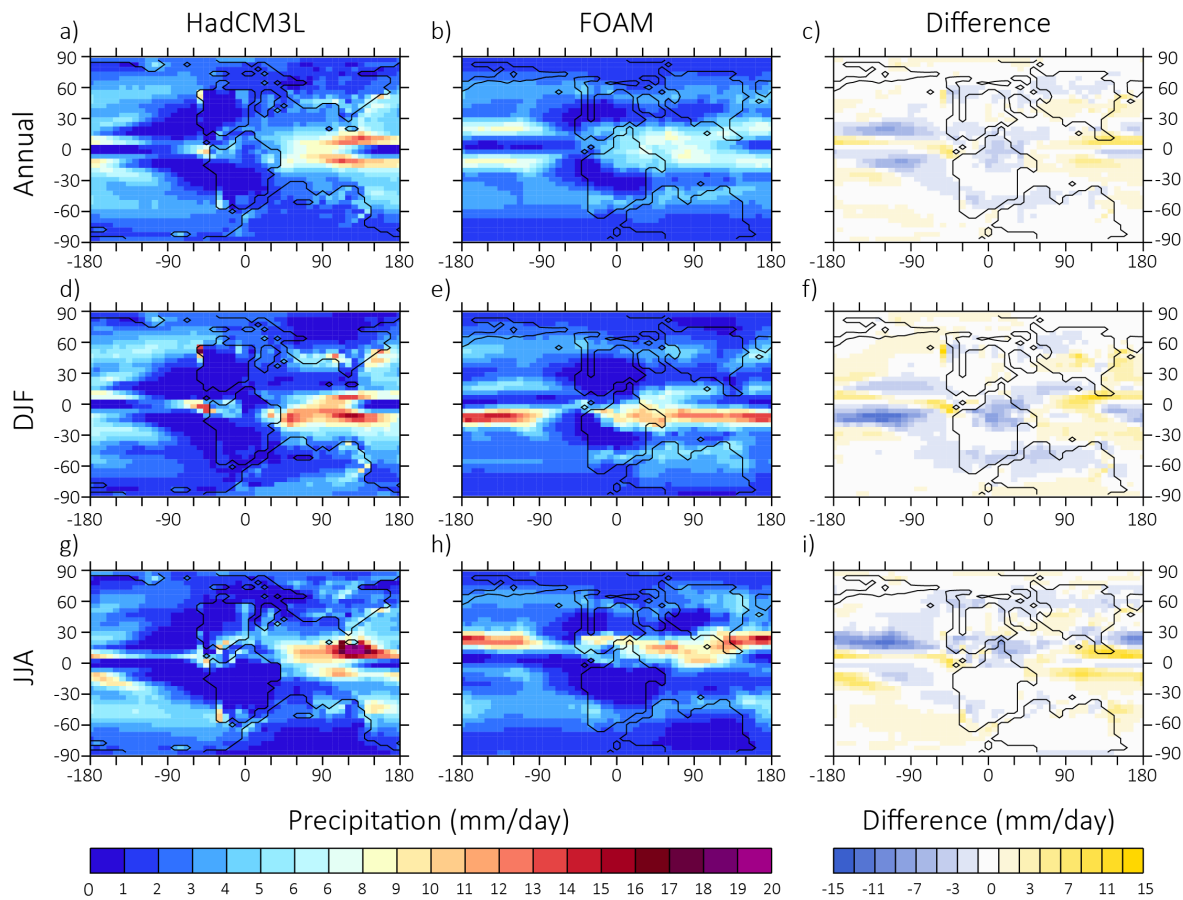


Figure 3.6. (a, d, and g) Annual, winter (DJF), and summer (JJA) precipitation from HadCM3L at 48 x 40 resolution. (b, e, h) Annual, winter (DJF), and summer (JJA) precipitation from FOAM at 48 x 40 resolution. (c, f, and i) Annual, winter (DJF), and summer (JJA) precipitation differences between HadCM3L and FOAM.

The location of monsoon regions at the southern limit of the seaway in both models supports the interpretation the climate in these areas was highly seasonal, likely with intense bursts of rainfall followed by dryer periods. Sellwood and Valdes (2008) attributed the symmetrical distribution of Late Jurassic evaporites and coals around the equator to a zone where

precipitation significantly exceeded evaporation, i.e. under wet and tropical conditions, which is consistent with both the FOAM and HadCM3L simulations from this study.

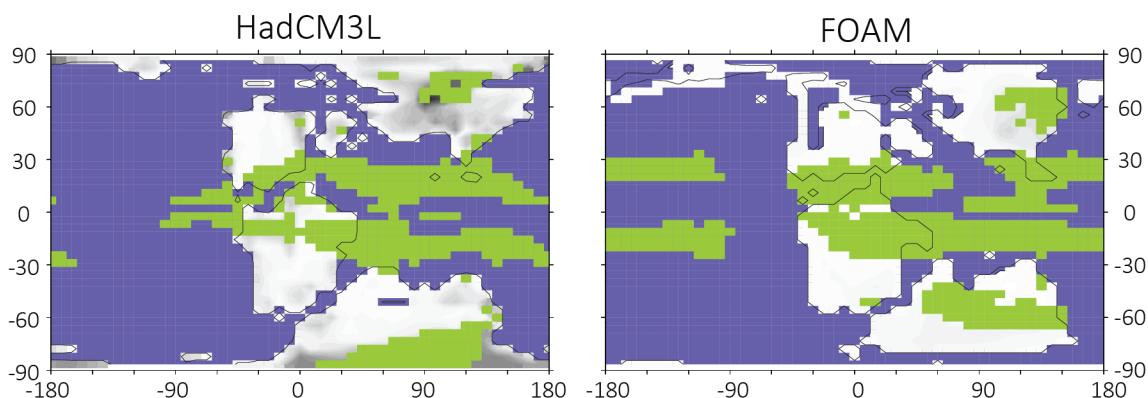


Figure 3.7. Simulated monsoon regions from the HadCM3L (left) and FOAM (right) models. Monsoon regions are defined as where summer minus winter precipitation exceeds 2 mm/day and where summer precipitation is greater than 55% of total annual precipitation (after Wang et al., 2011).

3.4.3 Predictions for the ITCZ and proposed influence on sedimentation in the Laurasian Seaway

As discussed in Armstrong et al. (2016), HadCM3L simulations show a more southerly positioning of the ITCZ in the winter month (DJF) and a northerly position in the summer (JJA), with both seasons having a northwards deflection of the ITCZ over the Laurentian landmass (Figure 3.8). The outer limb of the Hadley Cells show lateral fluctuations between the seasons; the poleward extent of the northern hemisphere Hadley Cell is around 40°N during boreal winter and expands to nearer 70°N in boreal summer (Figure 3.8), covering main parts of the seaway. The opposite is true for the southern hemisphere Hadley Cell, which has an outer positioning of -40°N in summer that extends to around -70°S in winter. The HadCM3L simulation places the southern part of the Laurasian Seaway under the direct influence of the tropics in the summer. In this scenario, sedimentation would be strongly influenced by precipitation and associated continental weathering and runoff (Armstrong et al., 2016). OC production would proliferate under an excessive nutrient supply, which would establish a redox stratification of the water mass thus facilitate OC preservation. OC preservation would be further enhanced due to the shallow water depths associated with the Late Jurassic Laurasian Seaway (Bradshaw et al., 1992a). However, storm tracks, commonly associated with hot, humid, tropical conditions, may have hindered preservation, by mixing of the water column and remobilising the sediment. Late Jurassic geological sections from the Wessex (Dorset, UK) and Cleveland (Yorkshire, UK) Basins have been correlated using biostratigraphy and total organic carbon contents (Cox and Gallois, 1981, Herbin and Geyssant, 1993). Armstrong et al. (2016) used the coeval cyclical occurrence of OC enrichment across a distance of ~400 km, to support the HadCM3L simulations. This study paired the geochemical correlation with sedimentological evidence from the Wessex Basin

and attributed the observed storm deposition to the simulated tropical/monsoonal conditions.

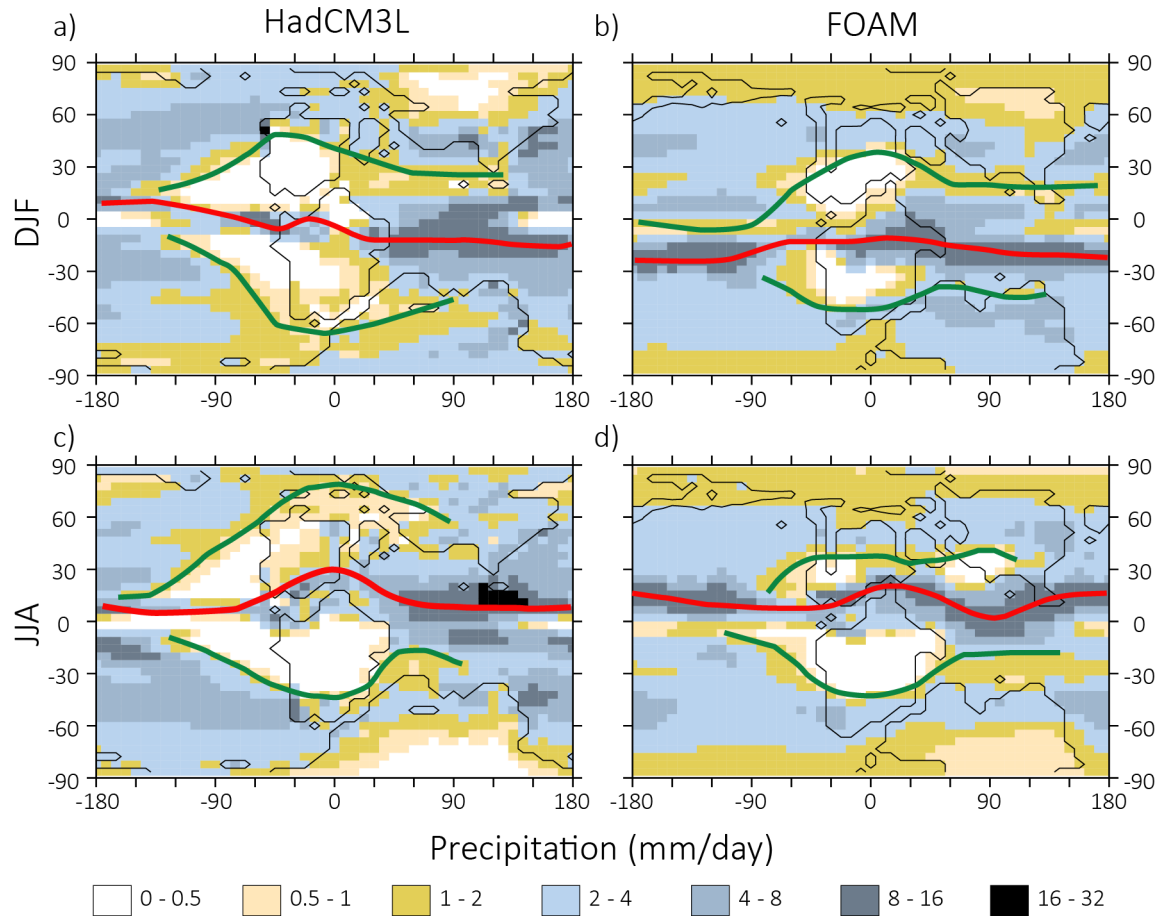


Figure 3.8. a and b) simulated precipitation in winter (DJF) from HadCM3L and FOAM. c and d) simulated precipitation in summer (JJA). Red lines denote positions of the intertropical convergence zone and green lines denote descending limbs of the Hadley Cells (or outer extent of subtropical conditions) as interpreted from the automated processes outlined in the methods section. Figure A3 in Appendix A shows the automatically identified zones.

In this scenario, under the ITCZ, it is expected that the sediment would comprise marine Type II OC, from elevated levels of primary productivity, and clastic detrital sediment and terrestrial Type III OC that was washed in during wet conditions. Sedimentary textures would exhibit evidence of storms and grain size indicators would coincide with storm events and redox proxies would indicate OC accumulated under oxygen deficient conditions. Relatively quiescent and dry intervals would be characterised by oligotrophic organisms such as coccoliths. Providing the palaeoceanographical setting was similar, i.e. no dramatic changes in water depth or ocean currents, if externally forced by a tropical climate belt, sedimentation should be similar across the Lurasian Seaway. Furthermore, the expanded/migrated ITCZ would exert a low latitude (precessional) signal at higher palaeolatitudes.

Conversely, the FOAM simulation positions the ITCZ between 25 and 30°S in the boreal winter and between 0 and 28° N in the corresponding summer. Unlike the HadCM3L

simulation, only the summer season has a northwards deflection of the ITCZ towards the Laurentian landmass but the ITCZ does not extend beyond 30°N into the southern part of the seaway. Despite the ca. 60° shift in the ITCZ, the subtropical boundaries in each hemisphere shift much less; the northernmost descending limb of the Hadley Cell flattens out along latitude in the summer compared to the winter but the maximum northerly extent remains the same (Figure 3.8). The southernmost descending limb of the Hadley Cell flattens out in the winter compared to the summer and shifts ca. 15° in a southerly direction. This is in stark contrast to the major swings inferred from HadCM3L (Figure 3.8) and is likely to result from the differences in orography. It is likely that the proto-Appalachian and North African mountain ranges exert a large effect on the distribution of heat, as seen by the surface temperature maps (Figure 3.5), which will have consequences for surface precipitation. Orography also influences the positioning of the ITCZ by affecting zonal winds. The FOAM simulations place the southern extent of the Lurasian Seaway under the tropical-subtropical boundary in the summer and close to the subtropical-temperate boundary in winter, suggesting that subtropical conditions prevailed throughout the year. In this scenario, OC enrichment and sedimentation are likely to be driven by upwelling of nutrient-rich waters. In an upwelling dominated scenario, the sedimentary rock will bear similarities to modern-day deep water sedimentation in that it will comprise a large proportion of biogenic sediment, e.g. chert or diatomaceous ooze (Böning et al., 2004, Meilijson et al., 2018).

This comparison raises questions about the validity of the modelling approaches used and which of the two simulations is the most appropriate to use for investigating palaeoclimate. On one hand, the FOAM simulations agree with previous climate modelling studies that placed the UK sector of the Lurasian Seaway under the subtropical-temperate climate transition zone, however, the HadCM3L yields more dynamic results, agrees with modern day observations, and uses a more resolved palaeogeography. These two scenarios provide us with two differing hypotheses that can be tested with geological data.

3.4.4 Reasons for inter-model variability

As discussed above, simulations from HadCM3L and FOAM result in different predictions of the climate zones, which have strong implications for the main controls on sedimentation and OC burial across the Lurasian Seaway. Further modelling studies, iteratively changing a single boundary condition in one or both of the models, are required to ascertain the differences behind the predictions. Further modelling is beyond the scope of this project but the possible causes of the observed differences are briefly discussed below.

Changes in global temperatures, particularly ocean temperatures as they act to distribute heat globally, are thought to have significant effects on atmospheric and climatological processes. The primary causes of elevated global temperatures in periods of the geological past (e.g. Cretaceous) are widely attributed to elevated greenhouse gases, when Earth was in

a 'greenhouse state' (Donnadieu et al., 2006). Enhanced global temperatures and the resulting changes in atmospheric dynamics have been shown to result from the interplay between elevated atmospheric greenhouse gases (mainly CO₂), palaeogeographical configurations, and a varying solar constant (Lunt et al., 2016).

In the geological past, atmospheric CO₂ levels fluctuated due to changes in carbon dioxide sources and sinks; volcanic outgassing was the predominant source of CO₂ to the atmosphere, silicate weathering countered this by removing CO₂ from the atmosphere, and the oceans acted as CO₂ sinks (Lunt et al., 2016). Volcanic activity is a product of plate tectonics, silicate weathering proliferated with high orography and wet climate (e.g. Cohen et al., 2004), and ocean storage capacity is influenced by changes in ocean circulation and bathymetry that resulted from tectonic activity (Lauderdale et al., 2013); therefore, atmospheric CO₂ is tectonically forced through geological time. While reconstruction of CO₂ concentrations through the geological past is an active area of research, there are still massive challenges associated with the proxy methods that increase large uncertainty on the results (Jenkins et al., 2015). The use of different predetermined CO₂ levels in the present model simulations may account for some of the observed near surface temperature differences, however, climate sensitivity of the respective model is likely to exert a strong influence on near surface temperature but this cannot be constrained in the present experiment due to unknown carbon cycle responses and feedback in the respective models. Climate modelling studies that have maintained a constant CO₂ level have shown that palaeogeography and solar constants exert a large effect on the resulting simulations (Lunt et al., 2016, Donnadieu et al., 2006) and it is thought that CO₂ levels alone are not enough to explain the elevated global temperatures observed in geological periods (e.g. the Cretaceous) (Markwick and Valdes, 2004). The amount of energy the Earth receives from the sun exerts an effect on climate through time; however, the solar constant and orbital cycles were the same in both of these experiments so these are not considered a factor in the present study.

Palaeogeography exerts a fundamental control on atmospheric dynamics; the size and positioning of the landmasses determines the distribution of heat across the Earth, with consequences for atmospheric, oceanic, and hydrological cycle dynamics (Barron and Washington, 1982). Landmasses in the Getech and Merlin+ palaeogeographies are situated in similar latitudinal positions indicating that this does not exert a large control. Of particular relevance to this study is the control that orography exerts on temperature and precipitation; uplands are commonly colder affecting zonal winds and precipitation patterns thus differences in orography can affect the positioning of the tropical and subtropical belts (Markwick and Valdes, 2004). Armstrong et al. (2016) attribute the expanded position of the ITCZ in HadCM3L to the positioning of the proto-Appalachian and North African mountain ranges, which is supported by this model comparison. The absence of these mountain ranges in the Merlin+ orography may account for the more southerly position and significantly

narrower extent of the Hadley Cell in the FOAM simulations. This observation hints towards a strong orographic control on the positioning of the ITCZ in the Late Jurassic. Furthermore, Lunt et al. (2016) showed continental area and global orography exert a control on global mean temperature, which may also account for the temperature differences between the HadCM3L and FOAM simulations.

3.5 Conclusions

- Two independent climate model simulations were compared to investigate the climate conditions across the Lurasian Seaway in the Late Jurassic.
- The HadCM3L simulation places the intertropical convergence zone over the southern section of the Lurasian Seaway, at least seasonally. In this scenario, enhanced continental weathering and run off, associated with tropical climate conditions, promotes primary productivity and subsequent redox and temperature stratification of the water column and organic carbon enrichment.
- Conversely, the FOAM simulations place the southern extent of the Lurasian Seaway under prevailing outer subtropical conditions. In this scenario, OC-rich sedimentation is controlled by wind-driven upwelling. The FOAM results agree with previously published climate modelling results that simulate temperate climate conditions of the southern Lurasian Seaway (Sellwood and Valdes, 2008).
- Inter-model variability may result from differences in palaeogeography, orography, pCO_2 , or differences between the models; however, further modelling is required to explain these differences, which is beyond the scope of this thesis.
- HadCM3L more closely simulates preindustrial precipitation, and has a more detailed orography, therefore those results are likely more robust. With this in mind, subsequent modelling should aim to use the best models, and best topography, otherwise results may be misleading.

4 | Sedimentology of the Ebberston 87 Core

Chapter Summary

Optical light microscopy and scanning electron microscopy were used to construct a facies model for the Ebberston 87 Core, drilled in the Cleveland Basin, (Yorkshire, UK). Six facies were defined as 1) clastic-detritus-rich medium-grained mudstone, 2) organic material and calcareous pellet-rich laminated mudstone, 3) coccolith-dominated medium-grained mudstone, 4) agglutinated foraminifera bearing medium to coarse-grained carbonaceous mudstone, 5) biogenic detritus-dominated fine to medium-grained mudstone, and 6) carbonate-cemented coarse-grained mudstone. Synthesis of this data indicated sedimentation was very similar to the coeval section in the Wessex Basin (Dorset, UK).

4.1 Introduction

Mudstones comprise fine-grained (<62.5 μm) sediment (Lazar et al., 2015a, Potter et al., 2005) and make up *c.* 66 % of the sedimentary record (Stow, 1981, Picard, 1971, Aplin et al., 1999). The mechanisms of mudstone deposition are relatively unexplored, compared to its coarser-grained counterparts (Schieber et al., 2013, Macquaker et al., 2007), due to the difficult, time consuming and expensive nature of its investigation. Technological advances have drastically improved thin section preparation and analysis of fine-grained sediment, and have revealed intricate compositional, textural, and structural heterogeneities, thus it is much more practical and possible to investigate these deposits than in previous times. Conventional models hypothesise that mudstone results from continual settling of sediment in low energy environments (Potter et al., 2005, Aplin and Macquaker, 2011, Macquaker and Bohacs, 2007). However, detailed investigation of ancient mudstones (Macquaker and Gawthorpe, 1993, Macquaker, 1994, Macquaker et al., 2010b, Aplin and Macquaker, 2011, Lazar et al., 2015b, Trabucho-Alexandre et al., 2011, Trabucho-Alexandre et al., 2012, Trabucho-Alexandre, 2015a, Trabucho-Alexandre, 2015b, Schieber, 1999), experimental sedimentology (Schieber, 2011, Wilson and Schieber, 2014, Schieber, 2016a), and observations of modern shelf settings (Macquaker et al., 2010a, Bohacs et al., 2014) have demonstrated that mudstones are often heterogeneous on millimetre to decimetre scale and that petrographic investigation of fine-grained sedimentary rocks can yield unique insight into dynamic and complex depositional processes (Macquaker et al., 2007, Schieber et al., 2007, Trabucho-Alexandre et al., 2012, Lazar et al., 2015a, Lazar et al., 2015b, O'Brien and Slatt, 2012). Much of the world's petroleum and mineral reserves reside in fine grained sedimentary rocks so understanding processes related to the formation has huge significance for the world's petroleum and mining industries (Mackenzie et al., 1983). Additionally, mudstones record key environmental conditions so can be used to reconstruct global geochemical cycles throughout geological history (Brumsack, 2006, Tribovillard et al., 2006, Martinez-Ruiz et al., 2015, Pietras and Spiegel, 2018, März et al., 2009, März et al., 2016).

The Kimmeridge Clay Formation (KCF) is Europe's most prolific petroleum source rock, having been the source of hydrocarbons for the majority of the North Sea oil fields. As such, there is a wealth of material available from coastal outcrops and drill cores, and of geochemical and wireline data. Several depositional models have been posited for the KCF and include discussions on the various roles that sediment supply and production, orbital forcing, oceanography, climate, and tectonics played of the production and preservation of organic material in the KCF (Oschmann, 1988, Wignall, 1989, Macquaker and Gawthorpe, 1993, Morgans-Bell et al., 2001, Raiswell et al., 2001, Hesselbo et al., 2009) but these models are often founded on geochemical data alone. Components of lateral sediment transport and potentially multiple episodes of sediment remobilisation prior to deposition mean that

mudstones may record palaeoenvironmental conditions from other areas of the ocean with little or no evidence of doing so (Schieber et al., 2007). It is for this reason, we need a thorough understanding of the physical processes and sources of the sediment before any conclusions are drawn from geochemical, palaeontological, or electromagnetic analyses (Macquaker and Bohacs, 2007).

Geochemical and wireline datasets are common for the KCF, while sedimentological and petrographic data for the KCF is comparatively low (Macquaker and Gawthorpe, 1993, Macquaker et al., 1997, Macquaker et al., 2010b, Herbin et al., 1991). The most detailed-to-date analysis of the KCF was conducted on a ten metre section from Clavell's Hard, Dorset, Southern England (Lazar et al., 2015b). Twelve lithofacies were described and defined with reference to composition, texture, bedding, and grain origin, and interpreted in the context of a dynamic depositional environment. Several different sedimentary sources were identified, including siliciclastic detritus, organic and inorganic marine products, and relict lithic grains, which are dispersed through several different mechanisms, namely suspension settling, aggregate and pellet formation, sediment transport, and bioturbation. The study concluded that a complex interaction of multiple processes is responsible for the deposition of the Kimmeridge Clay Formation in Dorset, UK (Lazar et al., 2015b).

Petrographic analysis conducted on the KCF of Yorkshire (UK) data recognised similar sedimentary components to those found in Dorset but concluded that the KCF exhibited 'extreme' homogeneity (Herbin and Geyssant, 1993). In light of recent advances in understanding of mudstone deposition and preparation of thin sections, the KCF of Yorkshire needs to be revisited to investigate the sedimentology of the formation. The aim of the present study is to conduct a detailed lithofacies analyses study of a section of the Kimmeridge Clay Formation deposited in the Cleveland Basin (Yorkshire, UK) to investigate the sedimentology of the KCF in Yorkshire and to compare it to that of Dorset. The material used for this study is from the Ebberston 87 Core, which was drilled in the 1980s by the Institut Français du Pétrole (IFPEN). The studied interval is time-equivalent to the study presented by (Lazar et al., 2015b) so provides an ideal opportunity to compare and contrast geographically-separated contemporaneous deposits and revisit petrographic work in the context of modern understanding.

4.2 Geological Setting

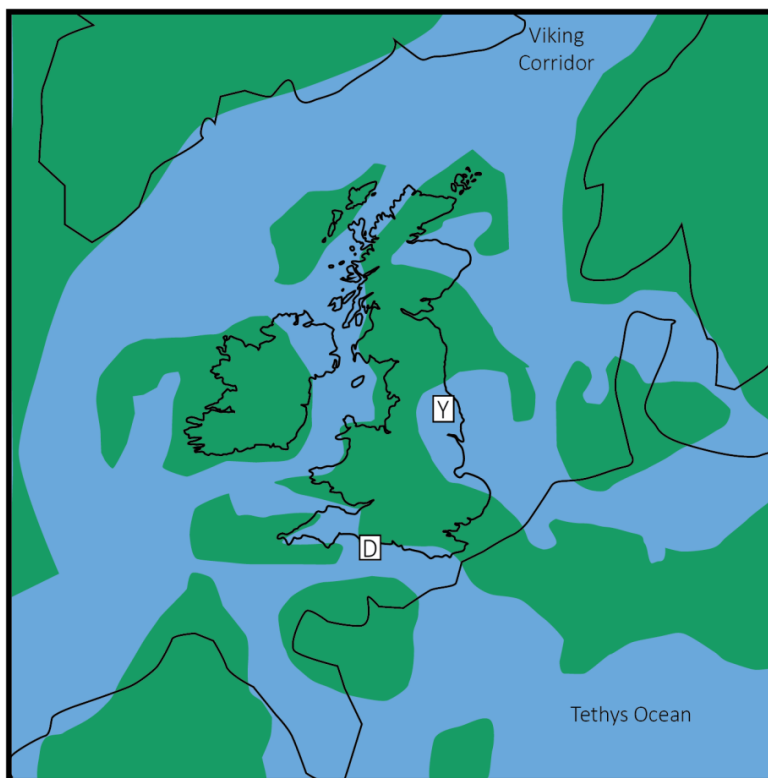
The Kimmeridge Clay Formation is a laterally extensive deposit that has been studied extensively over the past century (Fox-Strangways, 1892, Arkell, 1933, Gallois, 1976, Wignall, 1989, Herbin et al., 1991, Morgans-Bell et al., 2001, Cope, 2015). Relevant literature pertaining to the geological background of the Cleveland Basin and the previous work on the Ebberston 87 Core is summarised here.

Chapter 4

(a)

Key

- D Dorset
- Y Yorkshire
- Land
- Sea
- 100 km



(b)

Key

- Chalk
- Speeton Clay
- Ampthill Clay and Kimmeridge Clay
- Corallian Group
- Osgodby Fm- Oxford Clay
- Ravenscar Group Dogger
- Middle and Upper Lias
- Lower Lias

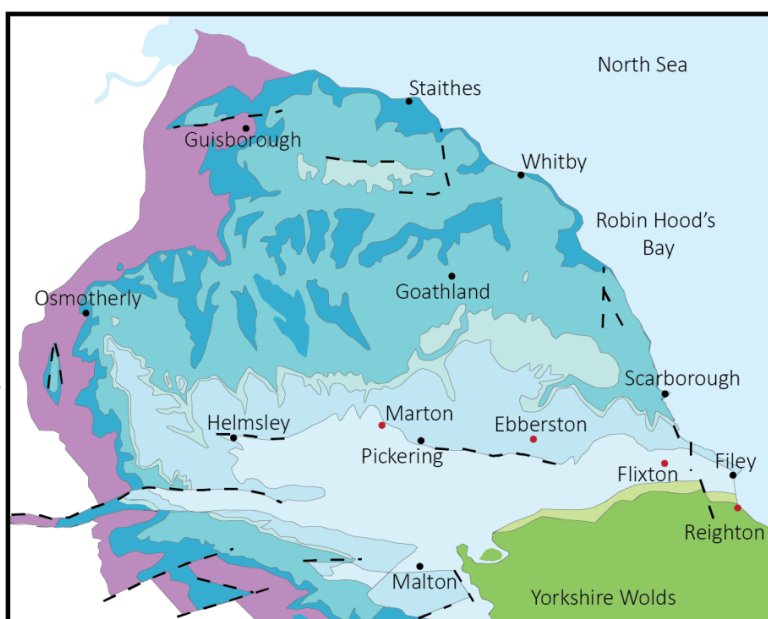


Figure 4.1 a) Palaeogeographic map of North West Europe during the Kimmeridgian stage after Miller (1990). b) Geological map of the Cleveland Basin (Powell, 2010).

Throughout the Late Jurassic, atmospheric carbon dioxide concentrations were up to four times higher than that of today (Sellwood and Valdes, 2008) and there is no evidence for ice at the poles (Dera et al., 2011), indicating elevated global temperatures. During this time, much of North West Europe was submerged under a shallow epicontinental sea, the Laurasian Seaway. The Laurasian Seaway was composed of a series of interconnected basins that formed as a result of differential subsidence that started in the Triassic and continued through the Jurassic and into the Cretaceous (Rawson et al., 2000). The seaway connected the

Boreal ocean to the Tethys Ocean through the Viking Corridor and was situated between 35–40° N (Korte et al., 2015). It is postulated that the climate was hot and humid across this area and that weather patterns were similar to that of modern day tropical monsoons (Armstrong et al., 2016).

The Cleveland Basin is a small extensional basin bound to the north by the Mid North Sea High, to the west by the Pennine Hills, to the East by the Sole Pit Basin and to the south by the Market Weighton High (Figure 4.1b)(Powell, 2010). In the Early to Mid-Jurassic, basin inversion associated with the Central North Sea Forties-piper Volcanic Centre caused south-westward tilting of the Cleveland Basin and rapid subsidence (Bradshaw et al., 1992b). Continued regional uplift of the Mid North Sea High and the Market Weighton High, also associated with the volcanic activity, caused shallowing of seaways across the North Sea and led to fluvial progradation through the Middle Jurassic. As the rate of regional uplift slowed down, subsidence and sea level rise continued, fully marine conditions were re-established in the Cleveland Basin by the mid-Oxfordian and continued into the Cretaceous. Late Jurassic intermittent east-west trending faulting of the Basin defined the Vale of Pickering, the site of thick marine sedimentation (Powell, 2010). The Kimmeridge Clay Formation was deposited in the Cleveland Basin throughout the Kimmeridgian and Tithonian stages of the Late Jurassic.

The Kimmeridge Clay Formation has been drilled and cored in Dorset (Swanworth Quarry core; (Morgans-Bell et al., 2001)) and Yorkshire (Ebberston 87 Core; (Herbin et al., 1991)). Coeval organic carbon-rich intervals have been identified in the Dorset (Gallois and Medd, 1979) and Yorkshire sections (Herbin et al., 1991). A stratigraphic cross plot of the Ebberston 87 Core and the Swanworth Quarry 1 Core demonstrates high resolution correlation of organic carbon peaks between the two sections across 400 kilometres (Armstrong et al., 2016). Herbin et al. (1991) reported the Kimmeridge Clay Formation to be geographically and stratigraphically homogenous. Herbin and Geyssant (1993) note the Kimmeridge Clay Formation exhibits 'extreme uniformity' and that, other than slight changes in colour, sedimentological variation cannot be recognised with macroscopic observations. Herbin et al (1991) report x-ray diffraction (XRD) and scanning electron microscope (SEM) data analyses that reveal the major sedimentary constituents of the Ebberston 87 Core are clay minerals, quartz, planktonic organic material and biogenic calcite. The authors conclude that the KCF of the Cleveland Basin was deposited below the storm wave base (Herbin and Geyssant, 1993).

Water depths of the Laurasian Seaway are contentious and depend upon the preferred depositional model, some authors favour a model where water depth is on the scale of tens of metres (Aigner, 1980, Oschmann, 1988, Hallam, 1975, Bradshaw et al., 1992b), while others suggest a Late Jurassic major global transgression led to much greater depths on the order of

hundreds of metres (Gallois, 1976, Haq et al., 1988, Herbin et al., 1991). Initial interpretations from the Vale of Pickering cores were that sea level was a dominant control on organic carbon enrichment throughout North West Europe through an apparent correlation between organic maxima and transgressions (Herbin et al., 1991). The coeval Boulonnais section was deposited in a setting that was more proximal than the Yorkshire and Dorset sections. An interdisciplinary approach established a sequence stratigraphic framework for the Boulonnais section which was then extrapolated across the region (Proust et al., 1995). After this study, it was concluded that transgressions do not appear to control sea level fluctuations but that they act to reveal climatic variations (Herbin et al., 1995). This reiterated the earlier view that fluctuations across Basins (between Yorkshire and Dorset) must be related to climatic fluctuation and periods of high stand revealing the cyclicity by exaggerating the effects of the underlying phenomena, such as changes in continental weathering and run off and associated nutrient supply and water column stratification (Herbin et al., 1991, Herbin et al., 1995). However, it is important to note the relative sea level change in the Cleveland Basin cannot be perfectly matched to global sea level reconstructions due to local tectonic events (Powell, 2010).

4.3 Methods and materials

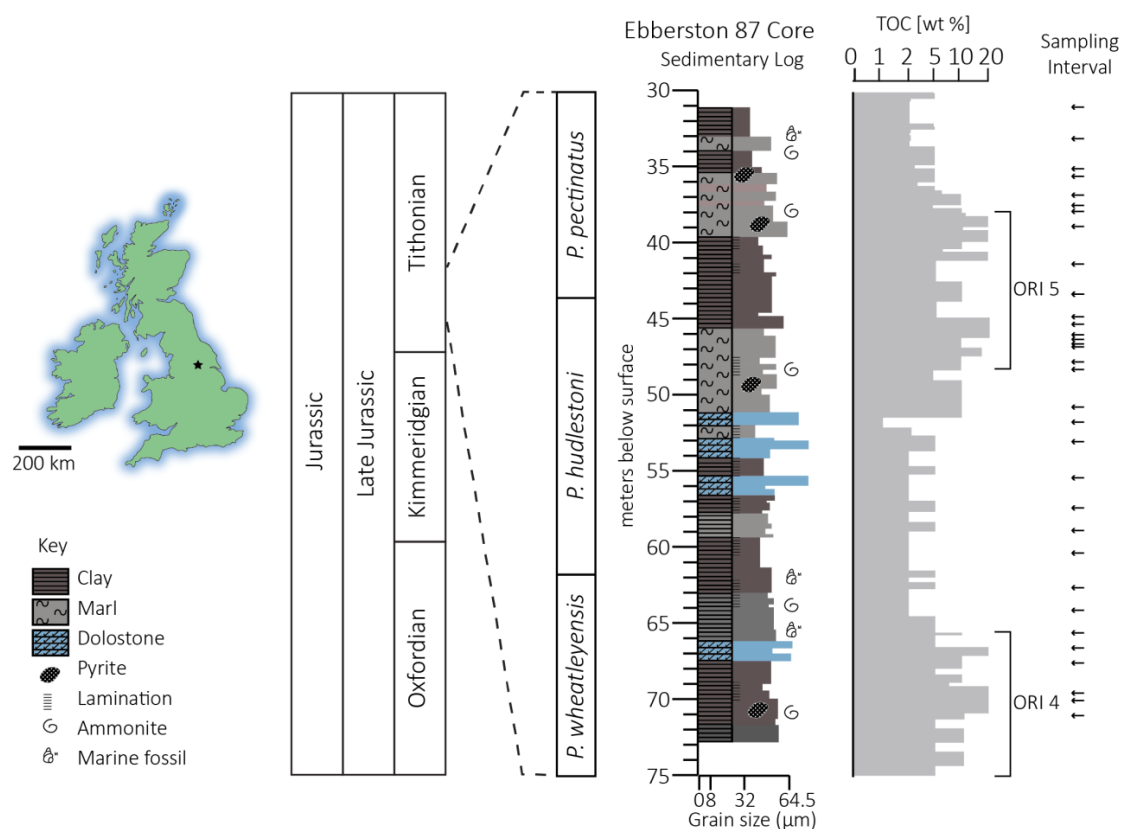


Figure 4.2 Map of the UK. The black star marks the location of the Ebberston 87 Core. Lithographic log, after IFPEN, and total organic carbon concentration (TOC) in wt % after Herbin et al. (1991). Organic rich intervals (ORI) 4 and 5 (Cox and Gallois, 1981) and denoted by brackets. The arrows mark the sampling intervals for the petrographic study.

This study was conducted upon the Ebberston 87 Core stored in the IFPEN core repository (Chatres, France). Samples were collected at an interval of 20—50 cm to cover a < 40 kyr temporal resolution (based on a linear sedimentation rate) from the uppermost *Pectinatus wheatleyensis* ammonite zone to the lowermost *Pectinatus pectinatus* ammonite zone. A subset of samples was selected based on lithological variability and sampling interval and prepared as thin sections. Data used in this chapter is located in Appendices B, C, and D.

4.4 Facies descriptions

Name	Brief Description	Samples
1 Clastic-detritus-rich medium-grained mudstone	Heavily bioturbated, argillaceous matrix with abundant medium to coarse mud sized detrital clasts. Calcareous nannofossils are present and often infilled with authigenic kaolinite.	31.07, 33.17, 35.17, 41.50, 48.00, 57.70, 63.00, 64.50, 67.00, 71.50
2 Organic material and calcareous pellet-rich, laminated mudstone	Lenticular, discontinuous wavy laminated, algal maceral dominated mudstone. Calcareous faecal pellets float within an argillaceous and carbonaceous matrix.	36.92, 45.44, 45.50, 45.59, 46.20, 46.50, 66.00, 68.00
3 Coccolith-dominated medium mud-grained mudstone	Fine to medium normally-graded calcareous mudstone beds. Dominated by coccolith plates and coccolith-rich faecal pellets. Matrix comprises coccoliths, clay minerals and quartz grains.	38.00, 39.00, 45.00, 47.00
4 Agglutinated foraminifera bearing, medium to coarse-grained, carbonaceous mudstone	Heavily bioturbated with no remaining sedimentary structures. Argillaceous and carbonaceous matrix with detrital components and abundant agglutinated foraminifera.	43.50, 46.60 37.00, 37.60,
5 Biogenic detritus dominated, fine to medium-grained mudstone	Disarticulated shell fragments dominate this facies. Shells and very abundant fine to coarse mud-sized quartz grains are set within an argillaceous matrix.	70.00, 70.50
6 Carbonate cemented, coarse-grained mudstone	Medium to coarse, angular, diagenetic carbonate grain-dominated sediment with an argillaceous matrix.	51.00, 53.30, 55.70

Table 4.1. Summary table of the facies descriptions.

4.4.1 Clastic-detritus-rich medium-grained mudstone

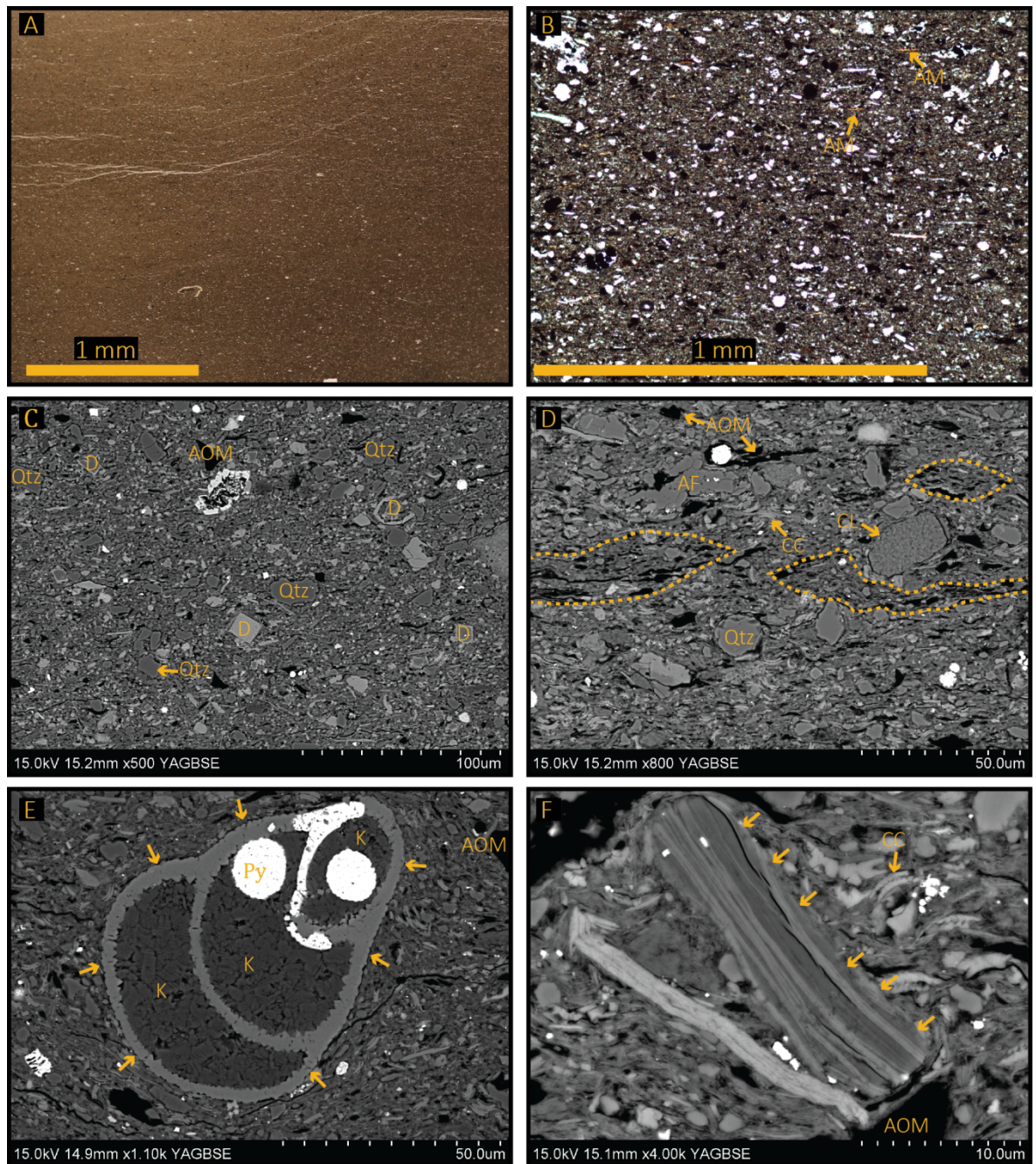


Figure 4.3 A) Low power optical photomicrograph of EB 33.17 m showing the homogenous nature of the facies. B) Optical micrograph of sample EB 33.17 m showing homogeneous nature of the sample. Note the argillaceous matrix. C) Backscattered electron photomicrograph of sample EB 57.70 m. Note the dolomite rhombs (D) and the amorphous organic material (AOM). D) Backscattered electron photomicrograph of sample EB 64.50 m. Yellow dashed lines mark the boundary of organo-minerallic aggregates. Note the presence of single collapsed agglutinated foraminifera (AF), clay mineral grain (CL) and coccolith debris (CC) in the matrix. E) Backscattered electron photomicrograph of sample EB 35.17 m showing a multi-chambered foraminifera (yellow arrows) infilled with authigenic kaolinite (K). Note the presence of pyrite (high η) as framboids and as a replacement mineral in the foraminifera test. E) Backscattered electron photomicrograph of sample EB 35.17 m showing a chlorite grain (indicated by the yellow arrows).

4.4.1.1 Description

The clastic-detritus-rich medium-grained mudstone is composed of fine mud-sized matrix with medium to coarse mud-sized framework grains within it. All of the samples are homogenized to such an extent that primary lamination and bedding features are completely destroyed (Figure 4.3). Occasional mottling caused by burrowing can be seen on the flatbed scans of the thin sections.

The matrix is predominantly K-rich clay minerals with minor amounts of organic material (occurring as equant particles), coccolith plates, and scarce pyrite framboids dispersed throughout the matrix. In addition to the equant organic material, occasional organo-mineralic aggregates, comprising algal material and clay minerals, were observed in some samples (Figure 4.3 D). Element maps show fine mud-size grains of titanium dioxide (e.g. Rutile) dispersed throughout the matrix. Framework grains consist of abundant, fine to coarse mud-sized subrounded quartz grains, occasional medium mud-sized chlorite grains (Figure 4.3 F), fine mud-sized titanium oxide grains, and medium mud-sized lithic clasts. Some samples contain very occasional phosphatic clasts. Framboidal pyrite occurs occasionally throughout the facies (Figure 4.3 C-F).

Foraminifera are the most commonly occurring fossil within the facies (Figure 4.3 E). Occasional, collapsed, agglutinated foraminifera are observed. Fragments of disarticulated calcitic shells are commonly observed throughout the facies. As is the case with all of the observed fossils, the matrix is compacted around the shell fragments.

There are several diagenetic features in this facies. Hollow foraminifera and some pieces of amorphous organic material are infilled with authigenic kaolinite (Figure 4.3 E) or calcite. Pyrite occurs as a replacement mineral in some of the tests of the calcitic foraminifera (Figure 4.3 E) and shell fragments. Occasional dolomite rhombs are observed in the matrix. Microcrystalline calcitic strands, approximately 10 μm thick and 100 μm in length, are aligned to the bedding plane.

4.4.1.2 Interpretation

The dominant sedimentary components are detrital grains, e.g. clay minerals, quartz grains and lithic clasts, suggesting this facies was deposited in a system that received a regular supply of terrigenous material. This is further supported by the ubiquitous presence of titanium oxide which is likely to reside in the resistant refractory mineral rutile. Total organic carbon concentrations throughout this facies range between 2-5 wt % (Herbin et al., 1991). Petrographic observations of equant particles of organic material suggest that the majority of this is from terrigenous organic material with a minor component of marine-derived algal material. Extensive bioturbation indicates a well-oxygenated water column that allowed burrowing fauna to colonise the sediment surface. The sparsity of algal macerals in the matrix is supporting evidence for an oxygenated water column as algal macerals are easily destroyed

through oxidation. Sub-oxic benthic conditions are evident in light of the presence of agglutinated foraminifer. The presence of organo-mineralic aggregates offers a plausible explanation for the delivery of algal maceral material to the seafloor; forming of physical and chemical attractions between the aggregate components constitutes a protective barrier to oxidative destruction of the algal macerals, thus facilitated the preservation of this fraction of the marine section.

The homogenous nature of the sediment, resulting from bioturbation and physical mixing processes, makes discerning sediment transport, dispersal and reworking very difficult. However, we can infer a moderate sedimentation rate because sedimentation rate must have been slow enough to accommodate faunal colonisation but quick enough to preserve organic material delivered to the sea floor.

The fine-grained nature of the formation suggests it was either deposited on the distal part of a shelf or was starved of coarser sediment through its deposition. The presence of calcitic fossils and algal maceral-bearing organo-mineralic aggregates suggests that primary productivity was low to moderate at the time of deposition, and that preservation of the marine organic material was not favourable.

4.4.2 Organic material and calcareous pellet-rich, laminated mudstone

4.4.2.1 Description

The major sedimentary components of this facies are organic material, clay minerals, quartz, and biogenic material (e.g. coccolith plates and foraminifera). It is comprised of a fine mud matrix with medium to coarse mud-sized framework grains and pellets. Discontinuous wavy laminae are organised into normally graded beds with erosional bases (Figure 4.4 A). Some samples exhibit compositional alternations between carbonate pellet-rich and clay-rich beds (Figure 4.4 B and C).

There are two forms of organic material in this facies. A facies-defining feature is the presence and high abundance of algal macerals, which appear red and wispy under plain polarised light and wraps around other sedimentary components. Commonly, algal macerals are deposited as organo-mineralic aggregates (Figure 4.4 E and F). Additionally, particles of equant organic material float within the matrix.

The framework components are medium to coarse mud-sized quartz grains, lithic clasts, and calcareous nanofossil tests that float within the organic carbon-rich argillaceous matrix. The lithic clasts are sub-rounded, up to 20 μm in length, and are composed of clay and fine quartz. The nanofossil tests are generally still intact and filled with either authigenic calcite or kaolinite. Occasional, collapsed agglutinated foraminifera tests are comprised of quartz, clay minerals, coccolith plates, and pyrite. Coccolith material is generally organised in to pellets but also floats in the matrix. Some of the pellets are comprised of finer, disarticulated

coccolith material and others contain pristinely preserved coccolith plates and coccospheres. Framboidal pyrite is abundant throughout the facies and pyrite is also present as euhedral crystals and as a replacement mineral.

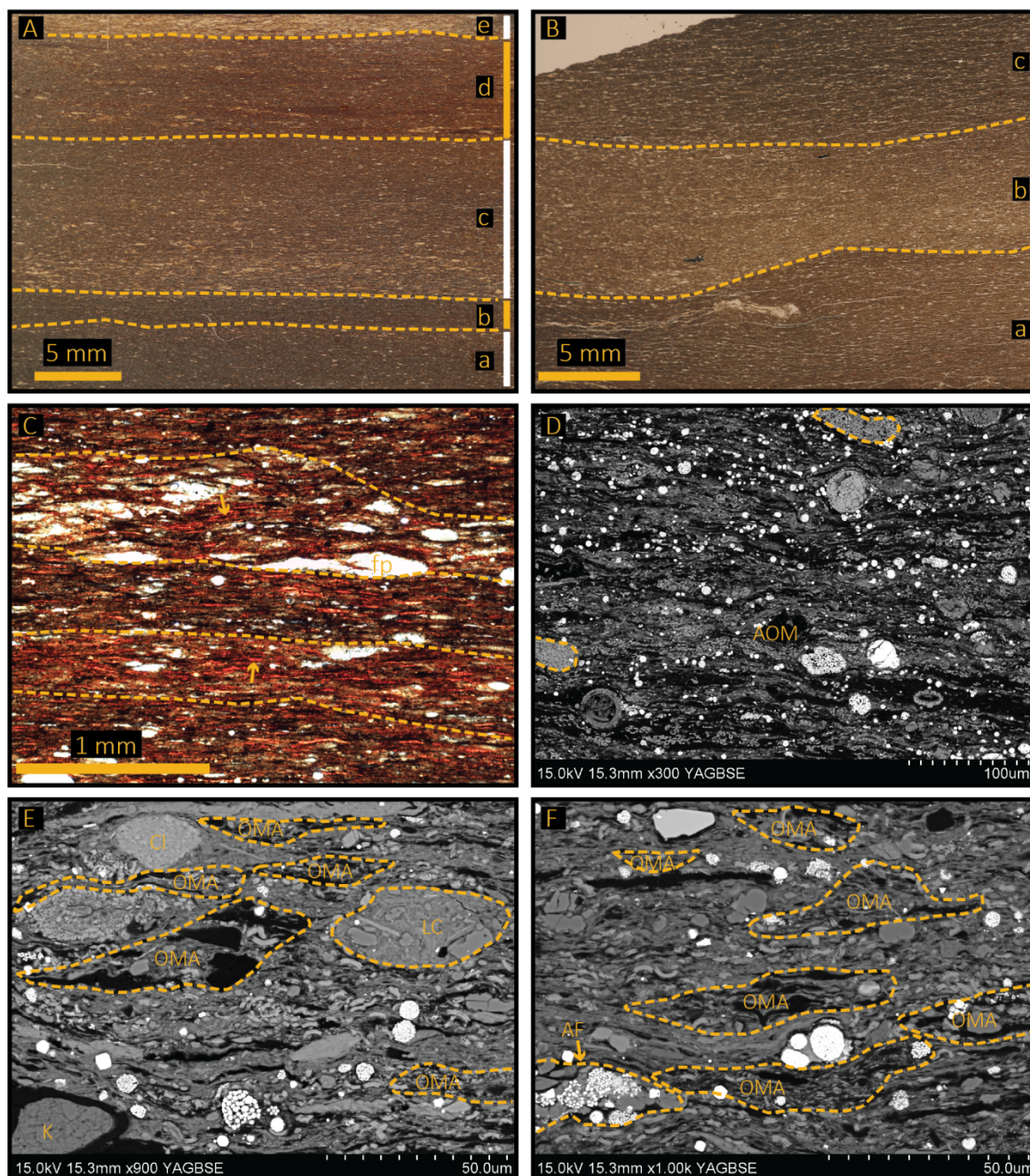


Figure 4.4 A) Low powered optical micrograph of sample EB 46.20 m showing normally graded beds that have erosional bases (a to d). B) Low powered optical micrograph of sample EB 45.50 m showing apparent compositional banding between the lamina. C) Optical micrograph of sample EB 46.50 m. Note the apparent compositional banding between the lamina (outlined by yellow dashed lines). Calcareous faecal pellets are labelled as fp and red algal macerals are marked by yellow arrows. D) Backscattered electron photomicrograph of sample EB 36.92 m. Faecal pellets (fp), amorphous organic matter (AOM) float in a clay and organic rich matrix. Pyrite is present as framboids, microcrystals and as a replacement mineral (high η). E and F) Backscattered electron photomicrographs of sample EB 46.50 m. Lithic clasts (LC), organo-minerallic aggregates (OMA) and clay minerals (Cl), and agglutinated foraminifer (AF) sit within a clay and coccolith-rich matrix. F) Backscattered electron photomicrograph of sample EB 46.50 m.

4.4.2.2 Interpretation

This facies is interpreted to represent the highest level of primary productivity due to the high abundance of algal organic material and coccolith plates. Normally-graded beds with erosional bases are interpreted to represent local reworking of the sediment, however long distance sediment transport is ruled out due to the abundance of algal macerals and organo-mineralic clasts which would be destroyed if transported over long distances.

The discontinuous wavy laminae structure within this facies may be explained through the deposition of organic material as algal mat structures and their subsequent disruption through bioturbation. Alternatively, it may represent the compaction of discrete aggregates.

The calcareous pellets are interpreted to be faecal pellets because they comprise coccolith plates that were likely eaten by higher trophic organisms. The shape, size and composition of the pellets suggest that they were produced by zooplankton that selectively fed upon coccolith material (Macquaker et al., 2010b). Frequent occurrence of quartz grains, clay minerals and terrestrial organic material indicates that the depocentre still received detrital material throughout the deposition of the facies. Compositional alternations between beds dominated by clay minerals and beds dominated by algal macerals and calcareous faecal pellets are interpreted to reflect the dynamic interaction between detrital sediment supply and primary productivity.

4.4.3 Coccolith-dominated medium-grained mudstone

4.4.3.1 Description

The coccolith-dominated medium mudstone facies is sorted in to normally-graded laminae that have erosional bases (Figures 4.4 A and C). It comprises coccolith material, clay minerals and organic material. Coccoliths are ubiquitous in the matrix and are also arranged into pellets (Figure 4.5 A-F). The pellets range in size from tens of micrometres to several millimetres and can be categorised into three distinct groups based on composition. The most commonly occurring pellets comprise solely very fine, disarticulated coccolith plates. The remaining two groups occur much more occasionally; one comprises the coccolith plates and coccospheres and the other exhibits a sparry calcitic texture. The coccosphere-rich pellets appear darker in colour in SEM-BSE due to the hollow centres of the coccospheres (Figure 4.5 F).

The matrix is predominately pristinely preserved coccolith plates and coccospheres (Figure 4.5 E and F) but also contains clay minerals, amorphous lumps of organic material and wispy algal macerals, calcispheres (Figure 4.5 D), chlorite grains, coarse mud-sized sub-rounded quartz grains (Figure 4.5 E), pyrite framboids, and euhedral pyrite crystals (Figure 4.5 F).

In addition to prolific coccolith material, compacted calcareous foraminifera are present throughout this facies, along with very occasional agglutinated foraminifera and rare undifferentiated shell fragments (Figure 4.5 A and B).

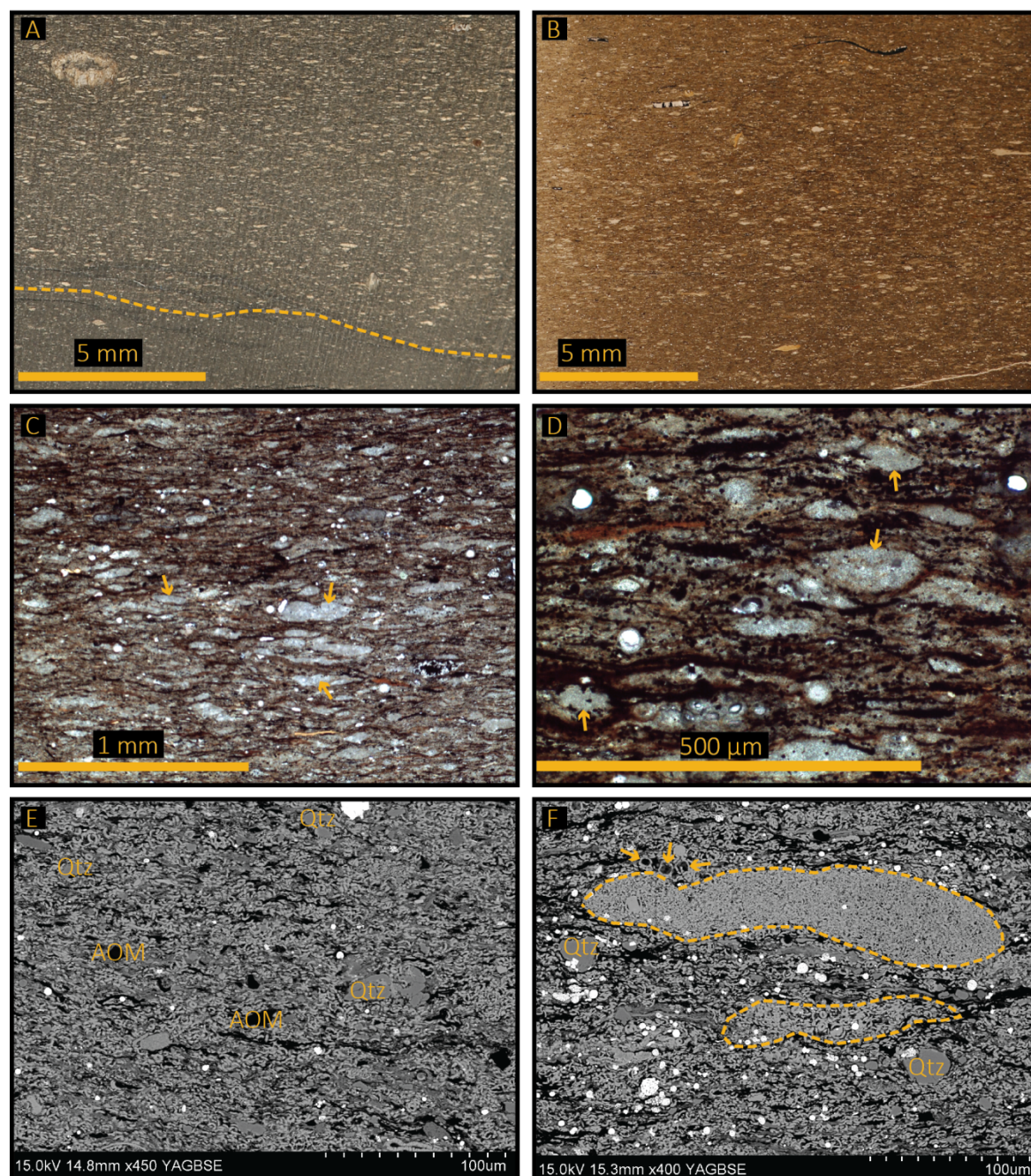


Figure 4.5 Sample EB 39.00 m. A) Low power optical micrograph of a slab. Yellow dashed line shows erosional base. B) Low power optical micrograph of a polished thin section. C) Optical micrograph showing the calcareous pellet-rich (yellow arrows) nature of this sample. D) Optical micrograph showing the calcareous pellets in an argillaceous and carbonaceous matrix. Note the presence of organic macerals (red horizontal lines) and pyrite framboids (high η). E and F) Backscattered electron photomicrographs showing the coccolith rich nature of the pellets (dashed yellow lines) and surrounding matrix. Note the presence of quartz grains (Qtz), amorphous organic material (AOM), and pyrite framboids (high η) and the exceptional preservation of coccospheres (yellow arrows in F).

4.4.3.2 Interpretation

The dominance of coccolith material coupled with the preservation of organic material suggests that this facies was deposited under a highly productive water column. The presence of detrital quartz and clay indicates a continued terrigenous supply of sediment and the gradational nature of the beds along with their erosional bases suggests sediment has been locally reworked.

The coccolith-rich faecal pellets are likely to be the product of selective-feeding zooplankton in the water column, indicating the water column was oxygenated. Modelling and experimental investigation has demonstrated that export of carbon and sediment flux to the seafloor is significantly greater when it is facilitated by scavenging zooplankton (e.g. Turner, 2015) owing to the larger grain size and denser nature of the faecal pellet.

The presence of abundant foraminifera supports the interpretation that the facies was deposited during a time of high primary productivity. The calcispheres have unknown origins but may be remnants of dinoflagellates thus may point towards a productive water column.

4.4.4 Agglutinated foraminifera bearing, medium to coarse-grained, carbonaceous mudstone

4.4.4.1 Description

The agglutinated foraminifera bearing, medium to coarse-grained, carbonaceous mudstone facies is composed of an argillaceous, calcareous, and carbonaceous matrix with medium to coarse framework grains (Figure 4.6 A and B). It is heavily bioturbated in most parts but some relict lamination may be observed in one of the samples (not shown).

Framework grains are predominantly composed of agglutinated foraminifera, lithic clasts, algal macerals, and clay and quartz grains (Figure 4.6 C). Agglutinated foraminifera are comprised of quartz grains, coccolith debris, and clay minerals (Figure 4.6 D and E). Some of them have post-depositional replacement by pyrite. Organic material is in the matrix and in organo-mineralic aggregates (Figure 4.6 D). Occasional coccolith-rich pellets are observed floating in the matrix.

4.4.4.2 Interpretation

During the deposition of this facies, the basin received sediment from a terrigenous source as indicated by the presence of detrital clays, quartz, and lithic clasts. In addition to this, marine-derived algal material is a large constituent of this facies.

High abundance of agglutinated foraminifera and heavily bioturbated nature of this facies indicates the presence of oxygen at the sediment-water interface. However, the carbonaceous nature of the matrix implies at least periodic sediment pore anoxia.

This facies represents periods where the basin experienced constantly fluctuating conditions brought about through interplay of allochthonous terrestrial and autochthonous biogenic sediment supply.

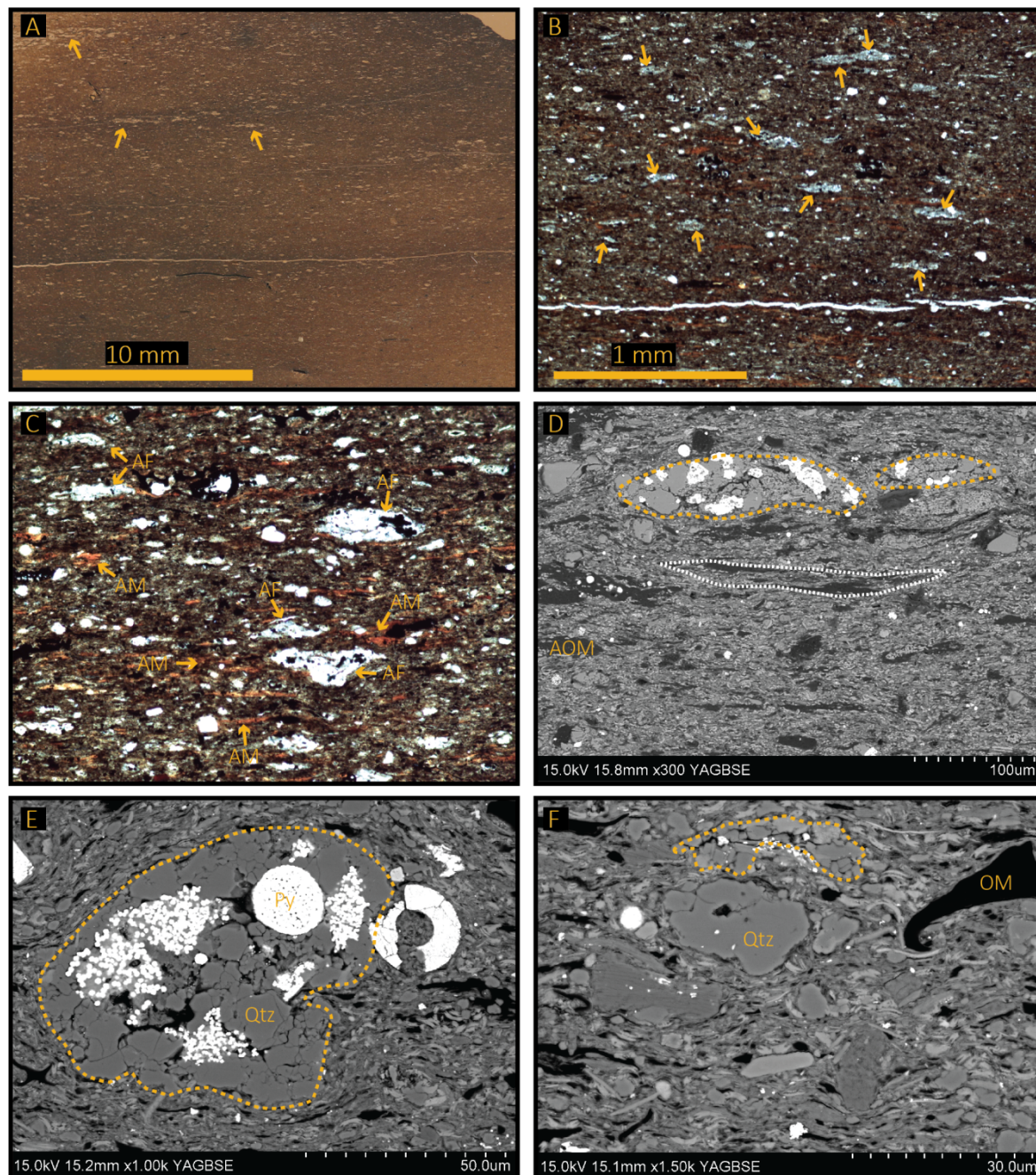


Figure 4.6 Sample EB 46.60 m. A) Low power optical micrograph of a thin section. Yellow arrows point to collapsed agglutinated foraminifera. B) Optical micrograph. Yellow arrows indicate abundant agglutinated foraminifera. C) Optical micrograph showing agglutinated foraminifera (AF) amongst algal macerals (AM). D) Backscattered electron photomicrographs showing amorphous organic material (AOM), agglutinated foraminifera (yellow dashed line) and organo-mineralic aggregate (white dotted line) in an argillaceous matrix. E) Backscattered electron photomicrographs showing an agglutinated foraminifer (dashed yellow lines) comprised of quartz and pyrite and surrounding matrix. F) Sample EB 43.50 m. Backscattered electron photomicrographs quartz (e.g. Qtz), clay grains, organic material (OM), agglutinated foraminifera (yellow dashed line) in an argillaceous matrix.

4.4.5 Biogenic detritus dominated, fine to medium-grained mudstone

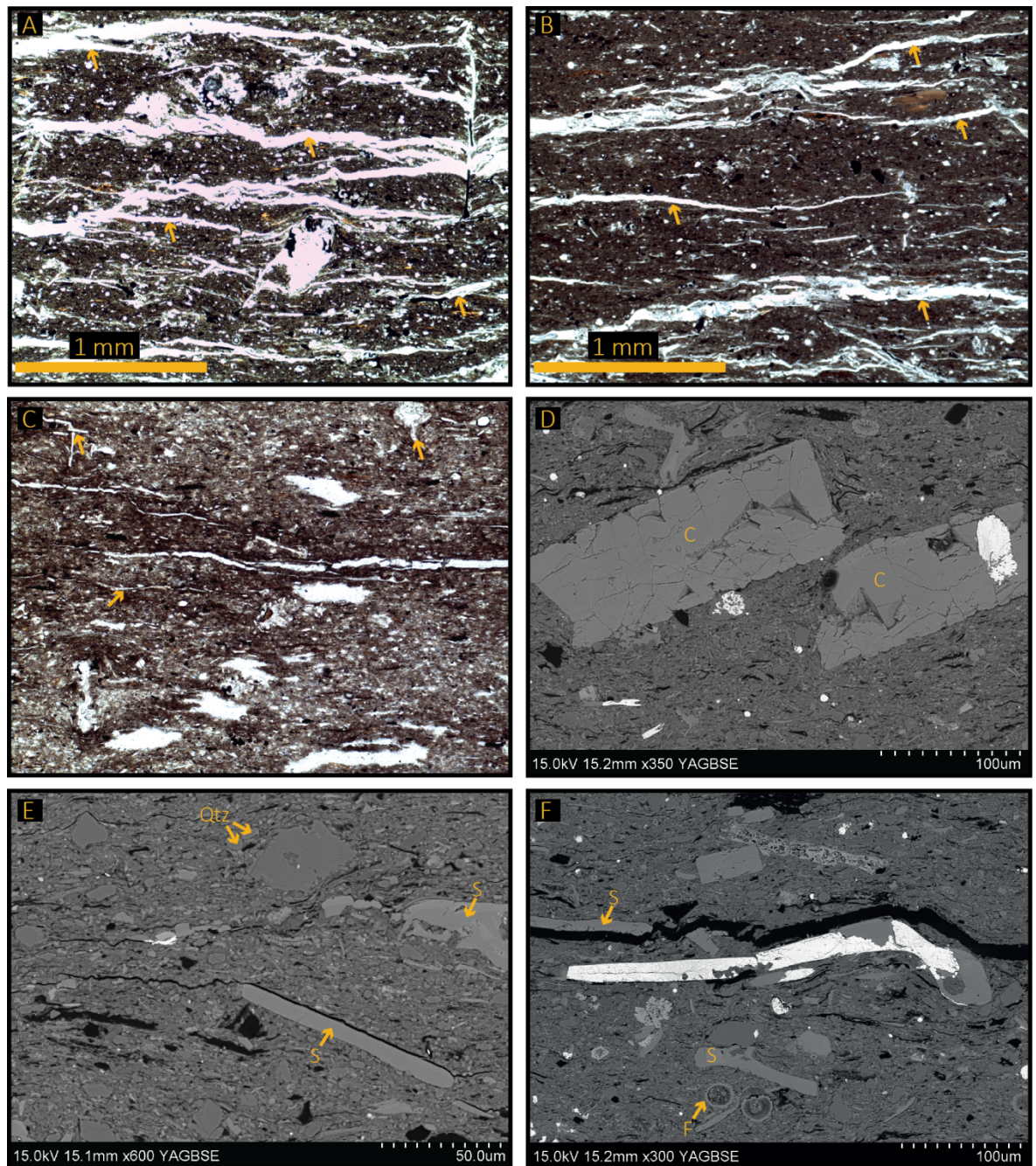


Figure 4.7 A and B) Sample EB 71.00 m. Optical micrograph showing a network of discontinuous calcareous structures (pointed to by the yellow arrows) through an argillaceous matrix. C) Sample EB 70.50 m. Optical micrograph showing discontinuous calcareous structure and shell fragments (yellow arrows) in an argillaceous matrix. D) Backscattered electron photomicrograph showing precipitated calcite crystals (C) in an argillaceous matrix. E) Backscattered electron photomicrograph showing calcareous shell fragments (S) and abundant quartz grains (Qtz) in an argillaceous matrix. F) Backscattered electron photomicrograph showing a calcitic shell that has been partially replaced by pyrite. Note the presence of foraminifera tests (F).

Description

Disarticulated calcitic shells dominate the biogenic detritus dominated, fine to medium-grained mudstone facies. They are wholly or partially replaced by pyrite (Figure 4.7 D). Locally, a network of discontinuous calcareous structures overprints this facies. The network

'filaments' are generally sub-parallel to the bedding and have a calcitic composition (Figure 4.7 A and B).

Other framework grains include abundant medium mud to sand-size quartz and clay mineral grains, e.g. chlorite, calcareous rhombs, foraminifera shells, amorphous organic material and framboidal pyrite. The grains sit within a quartz-rich argillaceous matrix.

4.4.5.1 Interpretation

This facies is interpreted to represent a time when depositional energy was relatively high compared to the rest of the section. The shell fragments were likely transported to the site of deposition by unusual storm and/or current activity and disarticulated in the process.

There is a moderate diagenetic overprint to this facies in the whole and partial replacement of shells by pyrite. Furthermore, it is likely that the carbonate strands formed due to the partial dissolution of the shells and re-precipitation along sedimentary planes or weaknesses.

4.4.6 Carbonate cemented, coarse-grained mudstone

4.4.6.1 Description

In hand specimen, this facies is yellow to white, hard and resistant to weathering. Optical light petrography shows this is a medium to coarse mud-sized, angular, diagenetic carbonate grain-dominated sediment with an argillaceous matrix (Figure 4.8 A and B). Scanning electron microscopy investigation shows that the carbonate grains are microcrystalline zoned non-ferroan calcite and non-ferroan dolomite crystals. Relict matrix, comprising of coccolith debris, illitic clay and fine quartz grains, can be seen between the diagenetic components. Minor pyrite is present as small ($>10\ \mu\text{m}$) framboids throughout the matrix and within carbonate crystals (Figure 4.8 A-F).

4.4.6.2 Interpretation

The dolomite in this facies is interpreted to be very early diagenetic authigenic crystals given their rhombohedral shape, and therefore low temperature formation. Dolomite is a calcium magnesium carbonate that is formed through the alteration of calcite on contact magnesium rich water. The easiest way for this to occur is the concentration of magnesium in sea water, either through increased discharge of meteoric water in to a marine setting, or through restriction of an oceanic setting leads to net evaporation of the water column. However, both of these mechanisms are difficult reconcile in the present setting due to an absence of sedimentological evidence for enhanced fluvial input or marine restriction. This is supported by oxygen isotope data that indicate the water column was not restricted at the time of deposition (Herbin et al., 1991). Instead, a third mechanism put forward for the Yorkshire section by Herbin et al. (1991) and for the Dorset section by Irwin et al. (1977), involving microbial mediation of dolomite precipitation is favoured. Microbial mediation of dolomite

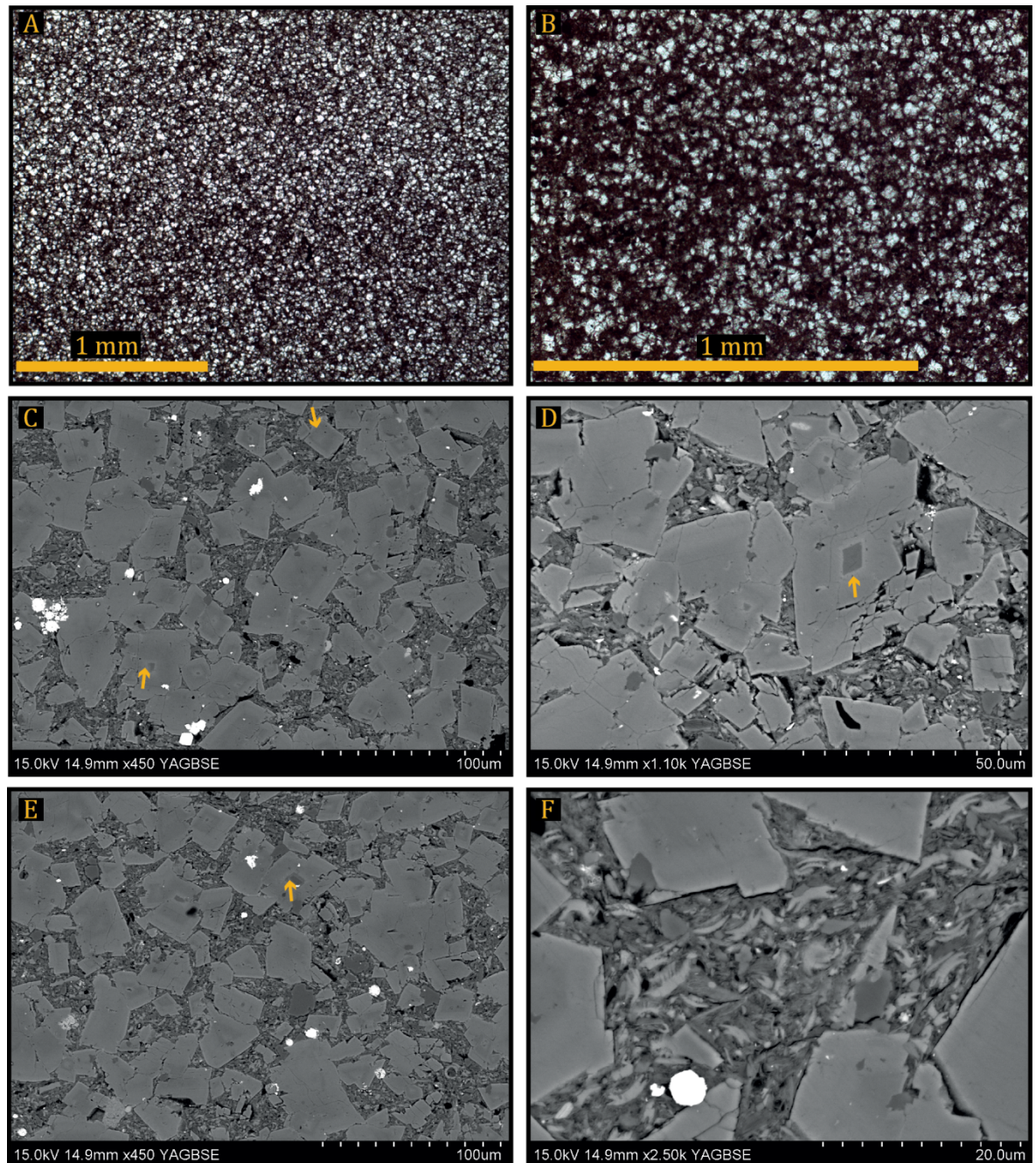


Figure 4.8 A and B). Optical micrographs of carbonate cemented, coarse grained mudstone. C-F). Backscattered electron photomicrographs. Yellow arrows point to zonation within dolomite crystals. Note the relict matrix composed of clay minerals and coccolith debris. Note the presence of pyrite within both the matrix and crystals.

is not yet fully understood, however, it is thought that increased alkalinity and pH associated with bacterial sulphate reduction may overcome the kinetic barrier to dolomite precipitation. Furthermore, the removal of sulphate from sediment pore waters provides a source of magnesium once liberated from magnesium sulphate ion complexes. Thus, sulphate reducing bacteria create the required conditions for the precipitation of calcium magnesium dolomite (Vasconcelos et al., 1995, Van Lith et al., 2003).

This facies is ignored in the context of palaeoenvironmental discussion because the main component, authigenic dolomite, is not a primary depositional feature.

4.5 Discussion

The studied succession is made up of differing proportions of detrital clay minerals, quartz, lithic clasts, organic material, biological components and authigenic minerals; this is in agreement with initial studies on the core (Herbin et al., 1991, Herbin and Geyssant, 1993). Sedimentary composition, textures and bedding characteristics have been used to divide the section up in to 6 facies. The fine-grained nature of the succession indicates that the depocentre was situated in relatively distal setting away from a major river system.

Quartz may enter the marine realm as aeolian dust, volcanic ash or detrital sediment. An aeolian source is difficult to reconcile in a time where sea levels were high and much of the continent was submerged under water given the inevitable reduction in aerial extent of desert (Schieber, 2016b). Volcanic ash is ruled out as a source of quartz in the studied succession due to the absence of fragmented volcanic rock, glass and minerals observed in the petrography. Epicontinental seaways are often on the order of 1000 km wide and rarely exceed 200 m water depth leading to 'shelf slopes' around 0.03° (Schieber, 2016b). Given this setting, it is not unreasonable to assume that detrital clay and quartz entered the basin through riverine input and was transported by wind-driven, Coriolis forces, and Ekman transport-influenced bottom currents (Schieber, 2016b). Riverine input of detrital quartz is the most likely source and mechanism through which quartz entered the Cleveland Basin. Rivers feeding an epicontinental seaway are likely to be smaller than those of today given the relatively large portion of flooded continent (Schieber, 2016b). The fine mud-sized clay matrix is likely to be the product of weathering and erosion of sub aerally exposed siliciclastic rocks. Late Oxfordian age sediments in the Cleveland Basin point towards the Market Weighton High as a sediment origin but Kimmeridgian and Tithonian sediment is much more likely to be hemipelagic (Powell, 2010).

The composition of the detrital fraction does not change throughout the section. Each sample has a component of consistently sized quartz and lithic clasts within it. The variation is in the proportion of detrital and organic components that each sample contains. For example, a defining feature of the clastic detritus-rich medium grained mudstone is its notable proportion of detrital material (quartz, lithic clasts, and fine-grained clay matrix). In contrast, the organic material and calcareous pellet-rich laminated mudstone is distinguished based on its high carbon content and large component of biological pellets, but quartz and clay grains are still identified within this facies. These results indicate that the supply of detrital components was relatively constant throughout the interval of deposition, through processes such as wind-driven bottom currents along an almost flat seafloor, and that the dominant control on the change in facies is the nature of the biological components and the proportion of the sediment they make up.

In the context of a compositionally uniform detrital material, it is necessary to explore the controls on the highly variable volume and nature of biological material in the studied section. The introduction of the concept of productivity-driven organic enrichment, opposed to a scenario where bottom water anoxia provided the ideal organic carbon preservation conditions, was considered a paradigm shift in the productivity versus preservation debate of organic enriched rocks (Pedersen and Calvert, 1990a). Ocean-atmosphere modelling results concluded that ocean overturn through thermohaline and surface circulation may have been key drivers in the well-known oceanic anoxic events (OAEs) e.g. Cretaceous Atlantic (Pedersen and Calvert, 1990a). The deposition of the Kimmeridge Clay Formation is not considered an oceanic anoxic event due to the absence of a widespread negative carbon isotope excursion but the processes behind organic enrichment can still be compared to well-established OAEs. Ocean overturn stimulates primary productivity in the surface waters, which translates to an increased carbon flux to the sea floor. In a depositional setting where water depth is likely to have ranged between 100 to 150 m deep (Schieber, 2016b), it is conceivable to imagine a change in water column productivity affecting the entire water column, given the photic zone likely extended to the sea floor. The result of this would be an elevated flux of organic carbon to the sea floor. Alternatively, an increased nutrient supply through weathering and erosion may drive primary productivity. This is difficult to constrain with petrography alone, however evidence of sediment transport (normally graded beds with erosional bases) may indicate storm-driven mixing of the water column.

The preservation of prolific quantities of organic carbon in the KCF (up to 50 wt %) has been the subject of scientific research for many years (e.g. Boussafir et al., 1995, Tyson et al., 1979). Traditional models favour a strongly stratified water column with widespread anoxia in the sediment pore and bottom water to inhibit degradation of organic material (Demailson et al., 1991). Organic material is oxidised and remobilised into the water column on contact with oxygen and so oxygen depletion is necessary for the preservation of organic material. However, it is difficult to maintain complete stratification and bottom water anoxia in an open setting such as an epicontinental seaway. Furthermore, petrographic evidence of oxygenation (bioturbation, agglutinated foraminifera) and energetic depositional environment indicate a dynamic, oxygenated depositional environment during the deposition of most of the section. Macquaker et al. (2010b) discuss the role of algal mats, algal blooms, and marine snow in hyper-organic enrichments from other sections. Due to the nature of an algal mat, pockets of anoxia can occur within the structure. This enhances preservation potential of the surrounding organic material. Clearly there was oxygen in the bottom waters, for at least some of the time, as evidenced by faunal colonisation and bioturbation of sediment. This, and the fact that the likely sediment delivery process was through organo-mineralic aggregate settling and pellets, suggests that a relatively high sedimentation rate

coupled with pockets of anoxia are the dominant controls on the intervals of hyper organic enrichment in the section.

However, the background levels of 2-5 % TOC (Herbin et al., 1991) (Figure 4.2) cannot be explained through this. Macquaker et al. (2010b) recognised organo-minerallic aggregates in a number of mudstone successions, including the type section of the KCF, and compared them to modern day marine snow. They conclude that a combination of planktonic mucus secretions acting as glue, electrochemical attractions and physical interlocking of individual grains are the key processes involved in the formation of these aggregates. The relative robustness of the terrestrial organic material and the incorporation in to aggregates may explain the presence of relatively high background TOC.

Given the fluctuating conditions between deposition of predominantly detrital components and the deposition of facies comprising mainly biological components, the sedimentation rate through this succession was very variable. Pelleted material would have a much quicker sedimentation rate than if the components were separate and unbound to anything else. This has been demonstrated in lab experiments where phytoplankton organised into pellets falls through the water column at a five times the rate than individual components (e.g. Shanks, 2002). Given the palaeogeographical setting, where water depth exceeded no more than 200 metres, it is likely that settling of pellets took less than a day to reach the seafloor. It has been posited that turbulent surface waters can promote phytoplankton settling. The implication of this is that higher energy environments promote sedimentation of organic material; where a higher energy, well mixed, and productive surface water, may lead to a sedimentation rate that promotes organic carbon preservation. We have a scenario where background sedimentation was dominated by bottom water currents moving detrital sediments along a faunal colonised sea floor, under a well-oxygenated water column. These conditions are punctuated by intervals of hyper TOC enrichment and primary carbonate production resulting from either a water column nutrient, temperature, or salinity change and the associated productivity blooms or from enhanced nutrient supply cause by increased continental weathering.

This interpretation is in agreement with previous work on the Kimmeridge Clay Formation of Yorkshire and other areas. The close relationship between coccolith plates and organic material led Gallois (1976) to suggest that the wider Kimmeridge Clay Formation was deposited in a semi-open ocean setting whereby marine blooms led to short term 'poisoning' of the lower water column and thus temporary preservation conditions. Herbin and Geyssant (1993) invoked a similar mechanism for the Vale of Pickering cores; they attribute the algal blooms to ocean overturn. The interpretation from the present study is broadly similar to that of the coeval section in Dorset (Lazar et al., 2015b). Although the Dorset section was deposited in an environment with higher energy than the Yorkshire section, biological

activity was a key driver in the deposition of both successions, and sediment dispersal mechanisms were diverse in both settings. The similarities between both successions (approximately 400 km apart) is remarkable. Armstrong et al. (2016) invoke a global-scale climate belt shift and consequential enhanced hydrological runoff for this. However, detailed geochemical analyses and climate modelling is required to further investigate this.

4.6 Conclusion

A detailed lithofacies analyses study of a section of the Kimmeridge Clay Formation deposited in the Cleveland Basin was conducted in order to investigate the sedimentology of the KCF in Yorkshire. Six facies were identified based on the sedimentary texture, bedding and composition. The facies are defined as 1) clastic-detritus-rich medium mudstone, 2) organic material and calcareous pellet-rich laminated mudstone, 3) coccolith-dominated medium mudstone, 4) agglutinated foraminifera bearing medium to coarse carbonaceous mudstone, 5) biogenic detritus-dominated fine to medium mudstone, and 6) carbonate-cemented coarse grained mudstone.

The succession was deposited in a dynamic environment that fluctuated between a detrital-rich sedimentation to biogenic component-dominated sedimentation. Background sedimentation was in a well-oxygenated setting beneath a moderately productive water column. During this time, algal material was produced, as seen in organo-mineralic aggregates, but was poorly preserved. More resistant, terrestrial organic material is the background contributor to the total organic content of this facies. The composition of detrital material was consistent throughout the studied interval but the abundance and nature of biological components changed significantly at two intervals in the succession. These intervals are dominated by organic carbon and primary carbonate (i.e. coccoliths) and were deposited at a time of high primary productivity.

There is no petrographic evidence of enhanced detrital input associated with enhanced continental weathering and runoff. Therefore, the results of this study agree with previous work that oceanographic change led to the productivity blooms responsible for the hyper organic enrichment observed in occasional intervals in the Kimmeridge Clay Formation.

The results of this study demonstrate that contemporaneous KCF deposits in Yorkshire and Dorset are comparable in terms of lithofacies and depositional processes. Further work involves geochemical comparison and atmosphere-ocean modelling of the period to investigate the dynamic depositional controls responsible for the deposition of the KCF.

5 | Dynamic climate-driven controls on the deposition of the Kimmeridge Clay Formation in the Cleveland Basin, Yorkshire, UK

This chapter is based on a manuscript that is under open review in the journal *Climate of the Past* at the time of submission. The manuscript is online as a preprint:

Atar, E., März, C., Aplin, A., Dellwig, O., Herringshaw, L., Lamoureux-Var, V., Leng, M.J., Schmetger, B. and Wagner, T., 2019. Dynamic climate-driven controls on the deposition of the Kimmeridge Clay Formation in the Cleveland Basin, Yorkshire, UK. *Climate of the Past Discussions*, pp.1-34.

5.1 Abstract

The Kimmeridge Clay Formation (KCF) is a laterally extensive, total organic carbon-rich succession deposited throughout Northwest Europe during the Kimmeridgian–Tithonian (Late Jurassic). Here we present a petrographic and geochemical dataset for a 40 metre-thick section of a well-preserved drill core recovering thermally-immature deposits of the KCF in the Cleveland Basin (Yorkshire, UK), covering an interval of approximately 800 kyr. The new data are discussed in the context of depositional processes, sediment source and supply, transport and dispersal mechanisms, water column redox conditions, and basin restriction.

Armstrong et al. (2016) recently postulated that an expanded Hadley Cell, with an intensified but alternating hydrological cycle, heavily influenced sedimentation and total organic carbon (TOC) enrichment, through promoting the primary productivity and organic matter burial, in the UK sectors of the Boreal Seaway. Consistent with such climate boundary conditions, petrographic observations, total organic carbon and carbonate contents, and major and trace element data presented here indicate that the KCF of the Cleveland Basin was deposited in the distal part of the Laurasian Seaway. Depositional conditions alternated between three states that produced a distinct cyclicity in the lithological and geochemical records: lower variability mudstone intervals (LVMIs) which comprise of clay-rich mudstone, TOC-rich sedimentation, and carbonate-rich sedimentation. The lower variability mudstone intervals dominate the studied interval but are punctuated by three ~2-4 m thick intervals of alternating TOC-rich and carbonate-rich sedimentation (here termed higher variability mudstone intervals, HVMIs). During the lower variability mudstone intervals, conditions were quiescent with oxic to sub-oxic bottom water conditions. During the higher variability mudstone intervals, highly dynamic conditions resulted in repeated switching of the redox system in a way similar to the modern deep basins of the Baltic Sea. During carbonate-rich sedimentation, oxic conditions prevailed, most likely due to elevated depositional energies at the seafloor by current/wave action. During TOC-rich sedimentation, anoxic-euxinic conditions led to an enrichment of redox sensitive/sulphide forming trace metals at the seafloor and a preservation of organic matter, and an active Mn-Fe particulate shuttle delivered redox sensitive/sulphide forming trace metals to the seafloor. In addition, based on TOC-S-Fe relationships, organic matter sulphurisation appears to have increased organic material preservation in about half of the analysed samples throughout the core, while the remaining samples were either dominated by excess Fe input into the system or experienced pyrite oxidation and sulphur loss during oxygenation events. New Hg/TOC data do not provide evidence of increased volcanism during this time, consistent with previous work. Set in the context of recent climate modelling, our study provides a comprehensive example of the dynamic climate-driven depositional and redox conditions that can control TOC and metal accumulations in the distal part of a shallow epicontinental sea, and is therefore key to understanding the formation of similar deposits throughout Earth's history.

5.2 Introduction

It is widely accepted that fine-grained marine sedimentary rocks preserve the most complete record of Earth's history (but see Trabuco-Alexandre (2015a) and references therein for discussion). As such, understanding their formation is fundamental to investigating changes in climate, weathering regime, biogeochemical cycles, sedimentation, land-ocean linkages, and environmental change throughout geological time. Organic carbon-enriched mudstones are particularly pertinent to this as they represent dramatic perturbations in the carbon cycle, and might therefore be of value in predicting future environmental dynamics. Such mudstones also represent some of the most important global energy resources: petroleum source rocks. Understanding their formation is therefore of economic as well as environmental and broader scientific interest.

The Phanerozoic sedimentary record is punctuated by several instances of increased organic carbon burial, for example, the oceanic anoxic events during the early Toarcian, early Aptian, and early Albian (Jenkyns, 2010). The deposition of organic carbon-rich mudstones results from an interplay between the production and preservation of organic material as well as dilution by total organic carbon-poor sediment (e.g. Sageman et al. (2003)). Sediment source and supply, primary production, biogeochemical cycling, water column redox conditions, and ocean connectivity have major implications for the formation of organic carbon-rich mudstones. However, the relative role of each of these processes is widely debated (Demailson and Moore, 1980b, Pedersen and Calvert, 1990b, Tyson, 2001, Katz, 2005, Tyson, 2005b, Demailson et al., 1991). The chemical makeup of a sedimentary succession can be used to assess these processes and reveal much about the depositional system, palaeoclimate, and basin history during deposition (e.g. Brumsack (2006)). When combined with petrographic observations, such analysis is a powerful tool with which environmental change can be determined over geological time.

A conceptual model developed for the Cretaceous (Hofmann and Wagner, 2011, Wagner et al., 2013) and further expanded to the Late Jurassic (Armstrong et al., 2016) linked the deposition of the total organic carbon-rich Kimmeridge Clay Formation (KCF) to atmospheric dynamics, specifically the shift and expansion of the orbitally modulated subtropical-tropical Hadley Cell, and associated changes in precipitation. Based on data from the type successions in Dorset, UK, Armstrong et al. (2016) proposed that organic carbon-lean mudstones in the Kimmeridge Clay Formation were deposited during drier intervals, characterised by mixed-layer oxygenated conditions, whereas organic carbon-rich intervals were deposited under monsoonal conditions similar to those seen in the present-day tropics. During such intervals, enhanced fresh water and nutrient input from continental runoff produced stratified basins across the Boreal Seaway (Armstrong et al. 2016). The chronostratigraphic framework

indicated that major fluctuations between wet and dry conditions occurred on a short eccentricity (100 kyr) timescale (Huang et al., 2010, Armstrong et al., 2016).

Here we present total organic carbon (TOC), total sulphur (TS), carbonate, major and trace element contents, and carbon isotope data, together with petrographic observations, in order to investigate the primary controls on Late Jurassic sedimentation and TOC enrichment in the Cleveland Basin, Yorkshire, UK, and to further refine the hypotheses proposed by Armstrong et al. (2016).

5.3 Geological setting

Deposited during the Kimmeridgian and Tithonian stages of the Late Jurassic, the Kimmeridge Clay Formation (KCF) is up to 620 m thick and is biostratigraphically and geochemically correlated across Northwest Europe. In the Late Jurassic, atmospheric carbon dioxide concentrations were more than four times greater than those of the present day (Sellwood and Valdes, 2008). Much of Northwest Europe was submerged by a shallow epicontinental sea, the Lurasian Seaway. The Lurasian Seaway comprised a series of interconnected basins, one of which was the Cleveland Basin, formed as a result of differential subsidence that started in the Triassic and continued through the Jurassic and Cretaceous (Rawson et al., 2000). The seaway connected the Boreal Sea to the Tethys Ocean through the Viking Corridor, situated between ~ 35 and $\sim 40^\circ$ N palaeo-latitude (Korte et al., 2015) (Figure 5.1). Recent palaeoclimate modelling, with geochemistry and sedimentology from the Dorset and Yorkshire Basins, indicates that the Lurasian Seaway was affected by a hot, humid climate comparable to present-day tropical monsoon regions (Armstrong et al., 2016). Deposition under these conditions was posited to have been strongly influenced by an intensified hydrological cycle and associated storm events. This would have promoted organic carbon enrichment through enhanced nutrient supply from increased precipitation and continental runoff, ocean overturn, salinity/temperature stratification, and redox conditions. However, water depth reconstructions for the Lurasian Seaway are contentious and depend upon the preferred depositional model (Bradshaw et al., 1992b). A water depth of tens of metres has been proposed by some authors (e.g. Hallam (1975), Aigner (1980) and Oschmann (1988)) while others (e.g. Gallois (1976), Haq et al. (1988) and Herbin et al. (1991)) have suggested a major Late Jurassic transgression that led to water depths of hundreds of metres.

The KCF type section is exceptionally exposed along the coast around Kimmeridge Bay, Dorset, UK (Figure 5.1) and was cored as part of a high-resolution analysis project (see e.g. Morgans-Bell et al. (2001)). It has been extensively studied by sedimentologists (Macquaker and Gawthorpe, 1993, Macquaker et al., 2010b), stratigraphers (Morgans-Bell et al., 2001), palaeontologists (Lees et al., 2004), geochemists (Pearce et al., 2010), and

palaeoclimatologists (Hesselbo et al., 2009), all trying to unravel the processes responsible for its deposition.

Owing to a lack of coastal outcrops, however, study of laterally equivalent deposits in the Cleveland Basin (Yorkshire, UK) has been limited to four cores drilled in the 1980s (Herbin et al., 1991, Herbin and Geyssant, 1993, Herbin et al., 1993, Herbin et al., 1995, Boussafir et al., 1995, Boussafir and Lallier-Vergès, 1997, Lallier-Vergès et al., 1997, Tribovillard et al., 1994, Tribovillard et al., 2004). These four cores (Marton 87, Flixton 87, Ebberston 87, and Reighton 87)(Figure 5.1) have been correlated to the type section in Dorset using the so-called 'Organic Rich Intervals' (ORIs) (See Fig. 6 in Armstrong et al., 2016) defined by Herbin and Geyssant (1993).

The focus of the present study is the Ebberston 87 Core (Herbin et al., 1991), which is thermally immature (average T_{max} = 425 degrees C; Herbin et al. (1993)), and contains type II and III kerogens (Herbin et al., 1993, Scotchman, 1991). The interval of detailed analysis spans the *Pectinatites wheatleyensis* to *Pectinatites pectinatus* ammonite biozones and is equivalent to the ORIs 4 and 5 of Herbin and Geyssant (1993) (Figure 5.1).

5.4 Materials and methods

A detailed methodology is presented in chapter 2. For this study, a total of 116 samples were collected from the Ebberston 87 Core, in the IFP Energies Nouvelles (IFPEN) facilities, Chartres, France. Samples were analysed for $\delta^{13}C_{org}$ values and for major and trace elements by XRF. A subset of 49 samples were analysed for select trace elements (Mo, Cd, U, V, Re, Tl, As, and Sb) and Hg contents by Quadrupole Inductively Coupled Plasma Mass Spectrometry and a direct mercury analyser (DMA80, Milestone), respectively. A total of 47 samples were prepared as thin sections and examined under optical light and a Scanning Electron Microscope (SEM).

Major and trace element contents were normalised to Al to allow for assessment of relative changes irrespective of dilution by organic matter or carbonate. Aluminium was chosen as representative of the siliciclastic fine-grained sediment fraction due to its generally high contents in the samples and its limited involvement in biological, redox and diagenetic processes (Tribovillard et al., 2006). Element/Al ratios are expressed as wt%/wt%, ppm/wt%, or ppb/% as appropriate. Trace element enrichment factors (EFs; Brumsack, 2006) were calculated relative to element/Al ratio of Upper Continental Crust (UCC; Rudnick and Gao, 2003).

On geological timescales, mercury is released in large volumes during volcanism (Percival et al., 2015). A relatively long atmospheric residence time (1-2 years) means it can be globally distributed prior to deposition in the sedimentary record. Mercury enters the ocean primarily

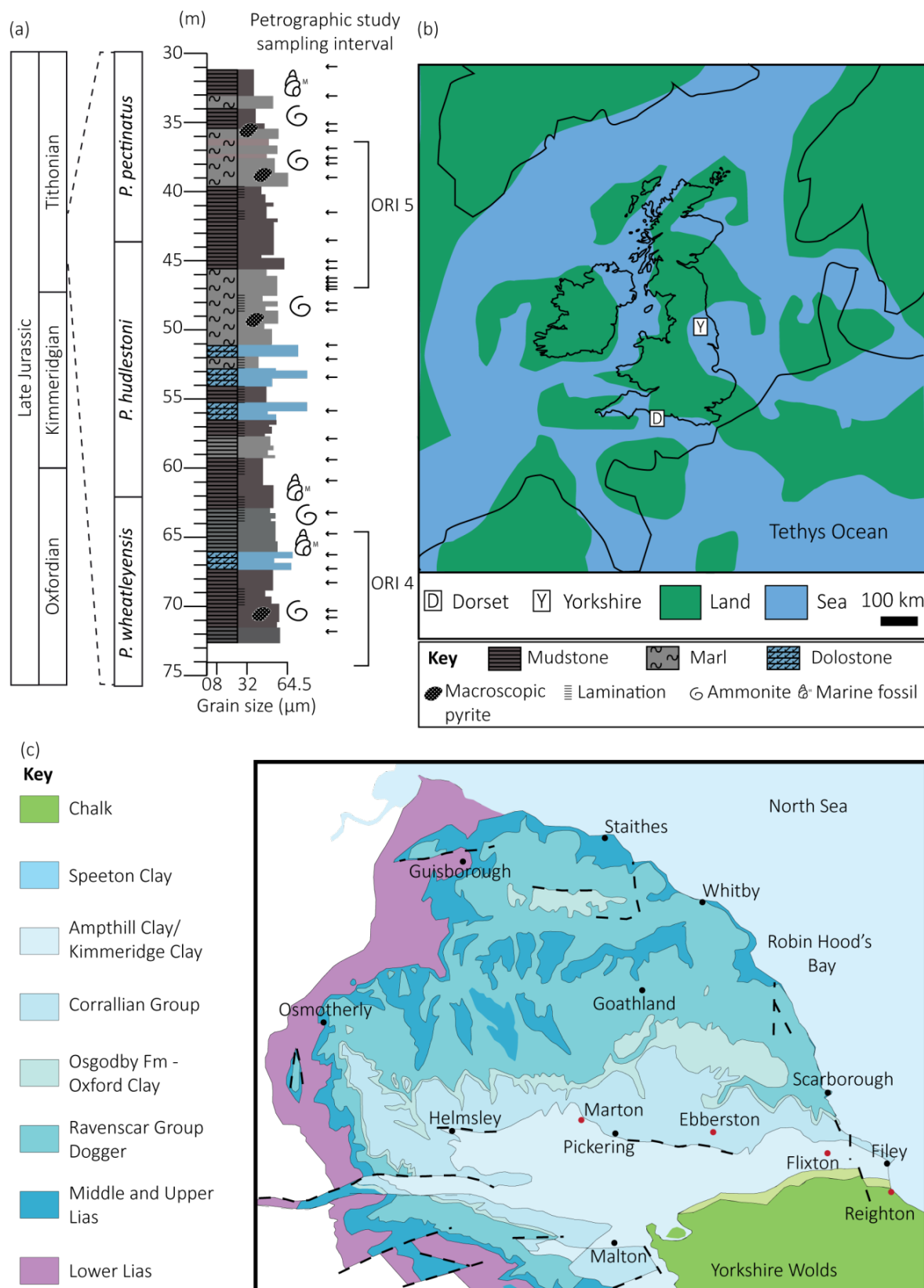


Figure 5.1 (a) Graphic log showing lithological variation of the studied section against geological time. See key for details. Horizontal arrows point to the petrographic study sample positions. Organic rich intervals (ORIs) 4 and 5 as defined by Herbin et al. (1991) noted for reference. (b) Palaeogeographical map (after Powell, 2010). Solid black lines depict location of modern day landmasses. (c) Modern day geological map of the Cleveland Basin (after Powell, 2010). Red dots mark the location of the Marton 87, Ebberston 87, Flixton 87, and Reighton 87 boreholes.

Through meteoric precipitation, and once in the ocean it is preferentially adsorbed on to organic matter. Assuming the Hg is adsorbed to the organic material, assessment of Hg/TOC ratios can indicate an increased/reduced supply of Hg in the system (Percival et al., 2015), hence it can be utilised as a proxy for volcanism. However, caution must be taken when interpreting records of Hg enrichments in sedimentary rocks because Hg can accumulate as a result of several other processes (e.g. Them et al. (2019)).

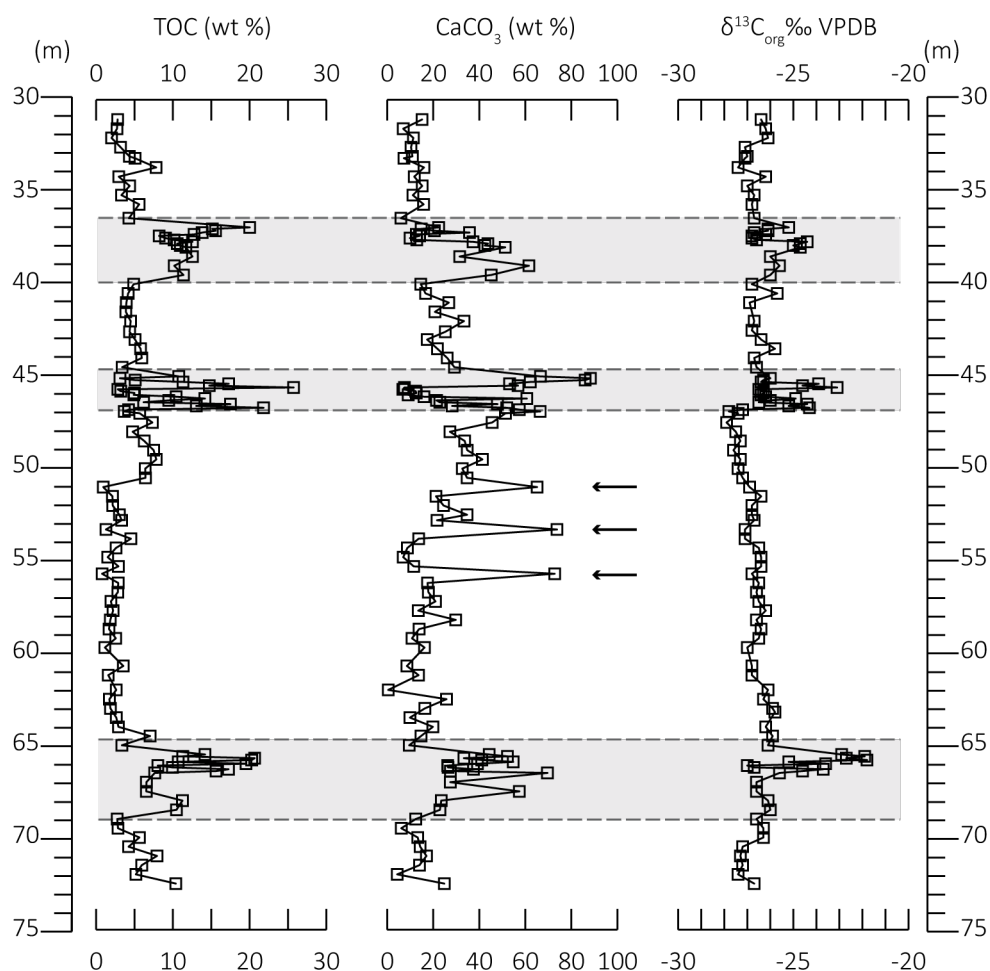


Figure 5.2 Depth plots of total organic carbon (TOC) contents (wt %), calcium carbonate (CaCO_3) contents (wt %), and organic carbon isotope values (‰ VPDB). Grey panels depict the higher variability intervals (HVMI) defined in this study. Black horizontal arrows indicate samples with obvious diagenetic overprint.

5.5 Results

Based on integrated geochemical data and petrographic observations, the studied section is divided into four lower variability mudstone intervals (LVMI) and three distinct higher variability mudstone intervals (HVMI) at 37-40 m, 45-47 m, and 65-69 m core depth (Figure 5.2). The HVMI are defined by distinct alternating facies along with repeated extreme enrichments of total organic carbon contents and trace elements.

5.5.1 Petrographic characterization

We defined six lithofacies based on compositional and textural observations (Table 5.1): 1) clastic detritus-rich medium-grained mudstone, 2) organic material and calcareous pellet-rich laminated medium to coarse-grained mudstone, 3) coccolith-dominated medium mudstone, 4) agglutinated foraminifera-bearing, medium to coarse-grained carbonaceous mudstone, 5) biogenic detritus-dominated fine to medium-grained mudstone, and 6) carbonate-cemented coarse-grained mudstone. The lower variability mudstone intervals are comprised of facies 1 and 6, while the higher variability mudstone intervals are dominated by facies 2, 3, 4, and 5. Facies 4 is very similar to Facies 1 but contains sand-sized quartz and is dominated by disarticulated calcitic shells, some of which are wholly or partially replaced by pyrite (Table 5.1).

5.5.2 Lower variability mudstone interval (LVMI) petrography

Facies 1 comprises an argillaceous matrix containing medium to coarse mud-sized grains (Table 5.1). The coarsest grain fraction is fine to coarse mud-sized, unrounded quartz grains, occasional medium mud-sized chlorite grains, fine mud-sized titanium oxide grains, and very occasional phosphatic clasts. Equant pieces of organic matter (2–5 μm in diameter) and framboidal pyrite are finely disseminated throughout the matrix. Occasional organo-mineral aggregates, comprised of wispy orange organic material (OM) and clay material, are found within the matrix. Calcitic microfossils, predominantly foraminifera tests and disarticulated shell fragments, are present, and commonly infilled with authigenic kaolinite. These mudstones have a churned texture so most of the primary sedimentary structures have been destroyed; however, some samples contain infilled burrows indicating the sediment was bioturbated. Physical mixing processes, indicated by occasional erosional surfaces, probably contributed to the homogenisation of the sediment.

Facies 6 is a medium to coarse mud-sized, angular, diagenetic carbonate grain-dominated sedimentary rock with an argillaceous matrix. Carbonate grains are microcrystalline, zoned, non-ferroan calcite and non-ferroan dolomite crystals. Relicts of the primary matrix, comprised of coccolith debris, organic matter, illitic clay and fine quartz grains, can be seen between the diagenetic components. The three samples representing this facies type (Figure 5.2) are not included in the palaeoenvironmental interpretation as their primary sedimentary and geochemical signature appears to be strongly overprinted by diagenesis.

5.5.3 Higher variability mudstone interval (HVMI) petrography

Facies 2 comprises sub-mm length, discontinuous, wavy lamina organized into normally graded centimetre scale beds with erosional bases. The facies is dominated by amorphous algal marine-derived organic material aligning with and wrapped around the other

sedimentary components, including the clay matrix, quartz grains, microfossils, lithic clasts, coccoliths and framboidal pyrite. The amorphous algal material commonly occurs as organo-mineral aggregates, and extensive 'network' structures that are 500 μm thick and up to 2mm in length point towards algal mat deposition. Coccoliths commonly occur within faecal pellets but also in the matrix. Facies 3 comprises normally graded, sub-mm laminae with erosional bases. The predominant sedimentary components are coccolith-rich faecal pellets that range in size from 30–3000 μm .

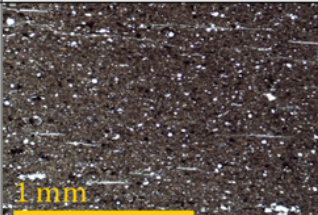
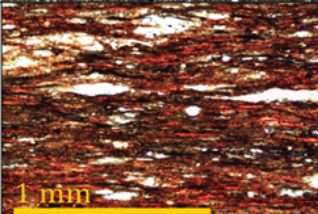
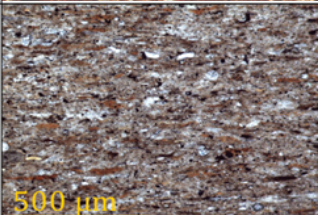
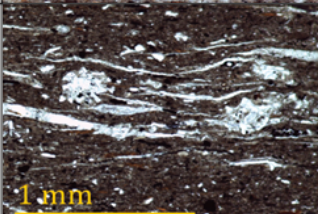
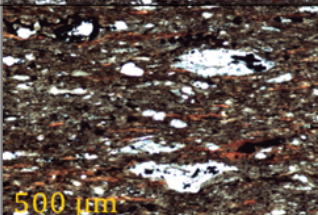
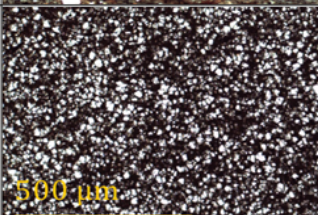
Name	Description	Interpretation	Optical light image
1. Clastic detritus-rich medium-grained mudstone	Well churned, argillaceous matrix. Abundant medium detrital grains and calcareous nanofossils which are commonly filled with authigenic kaolinite. Equant organic material grains sit within the matrix.	Deposited in a distal setting with a constant detrital input. Bioturbation indicates well oxygenated conditions with a moderate sedimentation rate allowing for extensive faunal colonisation. Organic material is commonly type III.	
2. Organic material and calcareous pellet-rich, laminated mudstone	Discontinuous wavy laminae are organised in to normally graded beds with erosional bases. Comprised of organo-mineralic aggregates, detrital material and calcareous faecal pellets.	Organic material was deposited as algal mats that were occasionally disturbed and locally reworked. Supply of detrital material was continuous. This facies represents the highest levels of primary productivity.	
3. Coccolith-dominated medium-grained mudstone	Fine to medium normally graded calcareous mudstone beds. Dominated by coccolith plates and coccolith-rich faecal pellets in a coccolith, clay mineral and quartz rich matrix.	This facies represents times of peak carbonate productivity. Continuous supply of detrital material that was diluted by coccolith material. Material was locally reworked in to graded beds.	
4. Biogenic detritus-dominated, fine to medium-grained mudstone	Disarticulated shell fragments dominate this facies. Shells and abundant fine to coarse mud-sized quartz grains sit within an argillaceous matrix. Diagenetic calcite stringers overprint.	Deposited when depositional energy was relatively high. Shells and framework grains brought in by unusual storm activity. Calcitic stringers were formed during early diagenesis.	
5. Agglutinated foraminifera bearing, medium to coarse-grained, carbonaceous mudstone	Well churned, argillaceous and algal material matrix. Detrital grains, abundant agglutinated foraminifera, and lithic clasts sit within the matrix.	This facies represent a finely balanced system between a well mixed water productive column indicated by the foraminifera and faunal colonisation, and the production and preservation of the algal material.	
6. Carbonate cemented, coarse-grained mudstone	Medium to coarse, angular, diagenetic carbonate grain-dominated sediment with an argillaceous matrix.	Dolomite rhombs formed during early diagenesis resulting from microbial sulphate reduction. These samples are discounted from paleoenvironmental interpretation.	

Table 5.1. Summary table describing the six lithofacies identified in the petrographic study. Key descriptions and interpretations are noted for each facies along with a representative micrograph. All images are under plain polarised light. For further description see text.

The matrix is predominately pristine coccoliths and coccospheres but also contains clay minerals, equant lumps of organic material, and wispy algal macerals, calcispheres, chlorite grains, coarse mud-sized sub-rounded quartz grains, pyrite framboids, euhedral pyrite crystals, and occasional agglutinated foraminifera. Facies 5 is similar to facies 2 in that it has a carbonaceous, calcareous, and argillaceous matrix with medium to coarse mud-size grains. However, abundant agglutinated foraminifera, composed of quartz grains, clay minerals, and pyrite crystals, are observed in this facies. It is homogenised due to a combination of extensive bioturbation indicated by burrows and physical mixing suggested by occasional relict lamina.

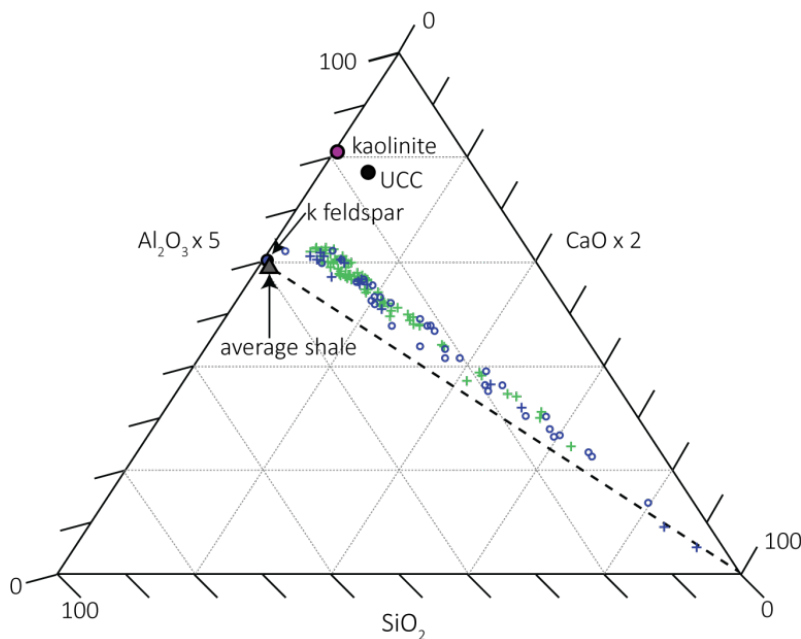


Figure 5.3 Ternary diagram (Brumsack, 1989) displaying the relative contributions of clay (Al_2O_3), quartz (SiO_2), and carbonate (CaO) within all samples. Lower variability mudstone interval (LVMI) samples are indicated by green crosses and higher variability mudstone interval (HVMI) samples are marked by blue symbols, TOC-rich samples ($\text{TOC} > 10 \text{ wt } \%$) are indicated by blue circles and TOC-lean samples ($\text{TOC} < 10 \text{ wt } \%$) are indicated by blue crosses. Axes are scaled to improve display of the data. Average shale (Wedepohl, 1991), upper continental crust (UCC; Rudnick and Gao, 2003), k-feldspar and kaolinite are plotted for reference. Dashed line shows the average shale-carbonate mixing line.

5.5.4 Geochemistry

Figure 5.3 shows a ternary diagram with the main inorganic lithogenic components represented by key proxy elements (Brumsack, 1989): clay is denoted by Al_2O_3 , quartz by SiO_2 , and carbonate by CaO . All samples fall on or very close to a mixing line between the calcium carbonate end member and a quartz-clay mixture that is more clay-rich than average shale (Wedepohl, 1971, Wedepohl, 1991) but less clay-rich than Upper Continental Crust (Rudnick and Gao, 2003). Across the studied core section, total organic carbon (TOC)

contents range from 0.8 wt % to 21.8 wt % with a mean of 6.6 wt %. Equivalent CaCO_3 contents range between 0.5 wt % and 73.8 wt % with a mean value of 28.5 wt % (Figure 5.2). The CaCO_3 contents of three samples (51.0 m, 53.3 m, and 57.0 m; indicated by arrows in Figure 5.2) are likely to be erroneous given the abundance of dolomite identified in the petrographic analysis (Table 5.1). However, petrographic and geochemical characteristics indicate strong overprinting by later-stage diagenesis (Facies 6; Table 5.1) so these samples are discounted from palaeoenvironmental interpretation.

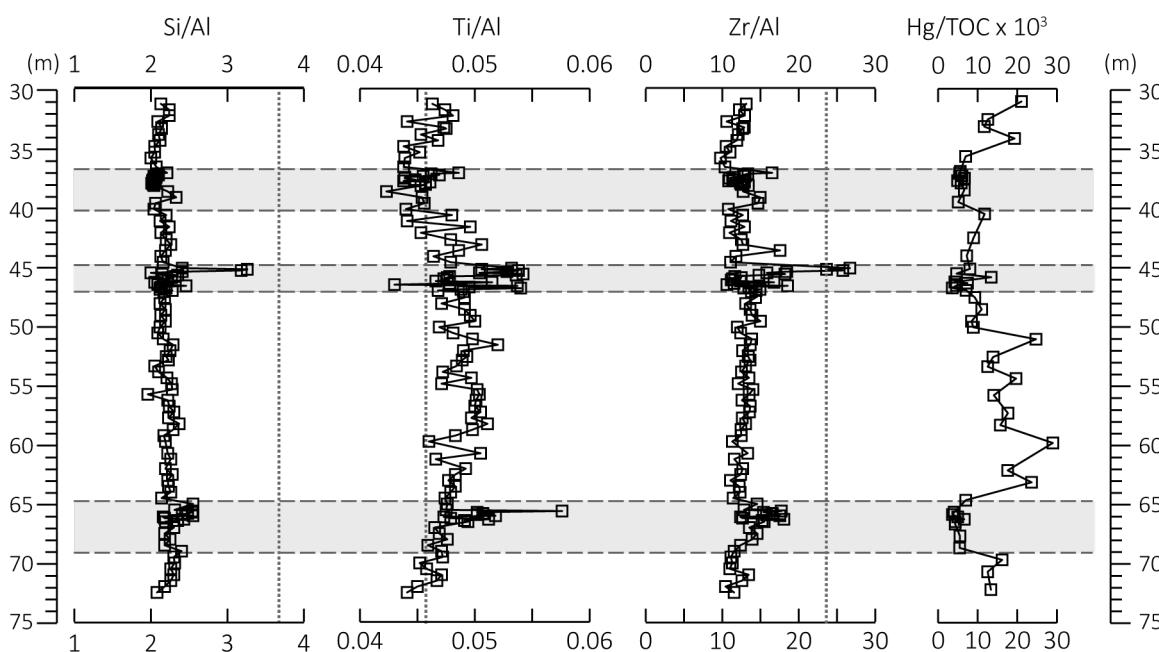


Figure 5.4 Depth plots of element/aluminium ratios and Hg/TOC. Si/Al (%/%), Ti/Al (%/%), Zr/Al (ppm/%), Hg/TOC (ppm/%). Grey panels depict the higher variability mudstone intervals (HVMIs) defined in this study. Vertical dashed lines represent upper continental crust (UCC) reference ratios.

5.5.4.1 Lower variability mudstone interval (LVMI) geochemistry

The lower variability mudstone intervals are characterised by TOC contents ranging from 0.8 wt % to 10.4 wt % (Figure 5.2) with a mean of 4.0 wt %. Marine organic matter (OM) has a higher $\delta^{13}\text{C}_{\text{org}}$ than terrestrial OM. $\delta^{13}\text{C}_{\text{org}}$ ranges from -25.7‰ to -27.9‰ with a mean of -26.7‰ (Figure 5.2). Fluctuations in $\delta^{13}\text{C}_{\text{org}}$ correspond to the changes in dominant OM source (marine versus terrestrial) as demonstrated in the petrography; therefore we use $\delta^{13}\text{C}_{\text{org}}$ as a proxy for OM source.

Silicon and Al range between 6.1 and 22.2 wt %, and between 3.1 and 10.4 wt %, respectively. The Al-normalised ratios of Si, Ti, and Zr (indicative of coarse grain sizes and/or heavy minerals; (Dellwig et al., 2000)) range from 2.0 to 2.6, 0.04 to 0.05, and 9.8 to 17.6, respectively (Figure 5.4). All redox sensitive/sulphide forming trace metals (Mo, U, V, Re, Tl,

As, Sb, Hg, Fe, and Mn; Figure 5.5, Cu, Zn, Cd; Figure 5.6) are consistently lower in the LVMIIs compared to the HVMIIs. Enrichment factors (Figure 5.7) calculated to UCC for Mo, Re, Tl, As, Sb, Hg, Cu, Zn, and Cd are generally around 1 for the LVMIIs. Uranium and V are slightly greater than 1 indicating a slight enrichment relative to UCC.

5.5.4.2 Higher variability mudstone intervals (HVMIIs) geochemistry

In the three higher variability mudstone intervals (HVMIIs), TOC ranges from 2.8 wt % to 25.7 wt % with a mean of 11.7 wt %. Calcium carbonate contents range from 6.8 wt % to 88.3 wt %, and a mean of 36.0 wt %. $\delta^{13}\text{C}_{\text{org}}$ ranges from -21.8 ‰ to -27.0 ‰, and the average of -25.3 ‰ is higher than in the lower variability mudstone intervals (Figure 5.2). The records of Si and Al exhibit larger ranges in the HVMIIs than in the LVMIIs and range from 1.9 to 23.9 wt %, and from 0.59 to 10.3 wt %, respectively. The coarse grain size/heavy mineral bound elements are slightly higher than in the LVMIIs. Si/Al, Ti/Al, and Zr/Al range from 2.0 to 3.3, 0.04 to 0.06, and 10.6 to 26.7, respectively (Figure 5.4).

Silica is positively correlated with Al ($R^2 = 0.98$), which suggests that the Si is strongly associated with the clay fraction rather than biogenic, volcanogenic or diagenetic silica in the sediment, consistent with petrographic observations. We can therefore use Si/Al in conjunction with Ti/Al and Zr/Al ratios as proxies for variations in grain size, and thus depositional energy (Tribovillard et al., 2006). The grain size indicators presented here (Figure 5.4) suggest the HVMIIs are slightly coarser-grained and more variable than the LVMIIs. However, for samples with Al value close to 0, this could partly be an artefact of normalisation to Al, as some values in the HVMIIs are low in Al contents compared to the LVMIIs, probably due to the increased dilution of background terrigenous input by organic material and biogenic carbonate (Figure 5.4). Therefore, normalisation to Al in these intervals may produce spuriously high grain size proxy results and should be regarded with caution (see Van der Weijden (2002) for further discussion).

All redox-sensitive/sulphide-forming trace metals (Mo, U, V, Re, Tl, As, Sb, Hg, Fe, and Mn; Figure 5.5, Cu, Zn, Cd; Figure 5.6) are variable and enriched relative to the LVMIIs. Notably, Mn/Al correlates with CaCO_3 content for the HVMIIs. Enrichment factors (Figure 5.7) calculated to UCC for Mo, U, V, Re, Tl, As, Sb, Cu, Zn, and Cd are variable but generally > 1 in the HVMIIs, indicating their enrichment relative to UCC.

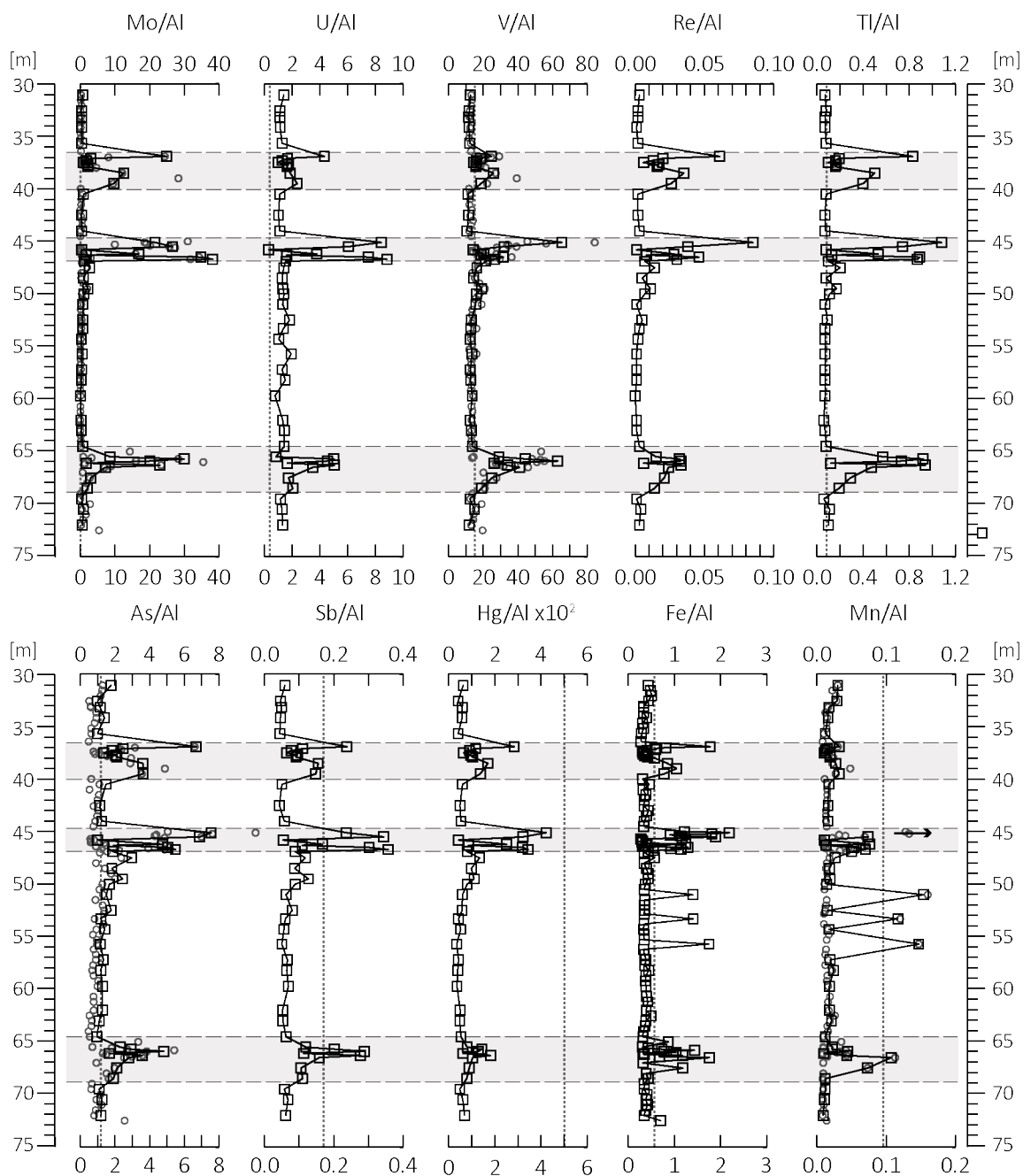


Figure 5.5. Depth plots of elemental ratios used as palaeoredox indicators. Mo/Al (ppm/wt %), U/Al (ppm/wt %), V/Al (ppm/wt %), Re/Al (ppm/wt %), Ti/Al (ppm/wt %), As/Al (ppm/wt %), Sb/Al (ppm/wt %), Hg/Al $\times 10^2$ (ppm/wt %), Fe/Al (wt %/wt %), and Mn/Al (ppm/wt %). Grey panels depict the higher variability mudstone intervals (HVMIs) defined in this study. Where grey and black circles are seen on the same plot, grey circles mark the XRF data and black circles mark the ICP-MS data.

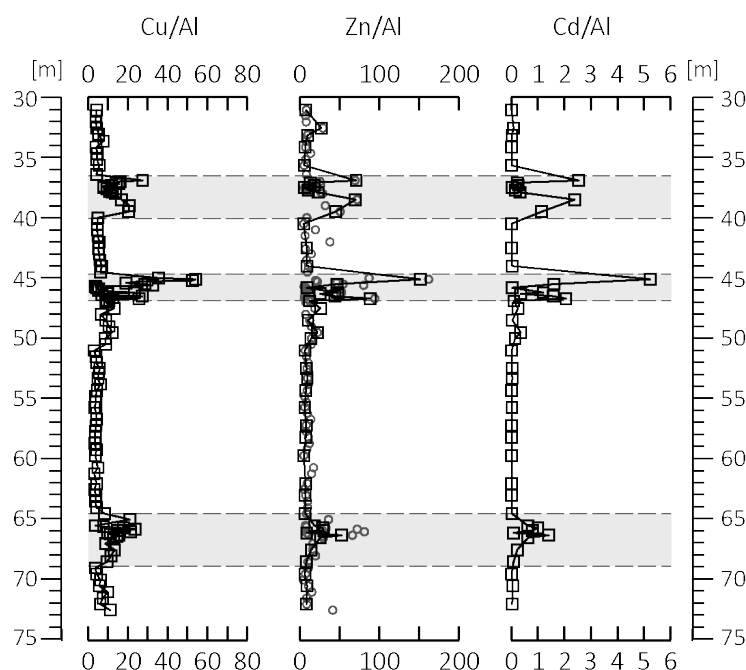


Figure 5.6. Depth log plots of Cu/Al, Zn/Al, and Cd/Al for the Ebberston 87 Core. Grey panels depict the higher variability mudstone intervals (HVMIs).

5.6 Discussion

5.6.1 Depositional environment: sediment source, depositional energy, dispersal mechanisms, and climatic context

The studied succession is a three-component system, comprising clay-dominated, organic carbon-dominated, and carbonate-dominated facies (Figure 5.3). The clay fraction of the mudstones is probably derived from detrital inputs to the basin, through the weathering of nearby emergent landmasses. Possible sources include Cornubia, or the Welsh, Irish, or London-Brabant landmasses (Figure 5.1), as discussed by Hesselbo et al. (2009). Terrestrial organic matter (OM) was likely washed into the basin along with detrital clays, while carbonate and marine OM formed in the water column. A volcanogenic sediment source is ruled out using Hg/TOC as a proxy (Scaife et al., 2017) (Figure 5.4), which agrees with other studies of the KCF (Percival et al., 2015), and petrographic evidence (conchoidally fractured quartz grains without Fe oxide rims) rules out an aeolian source, which is also supported by the palaeogeographical position of this basin in the outer palaeo-subtropics (Armstrong et al., 2016).

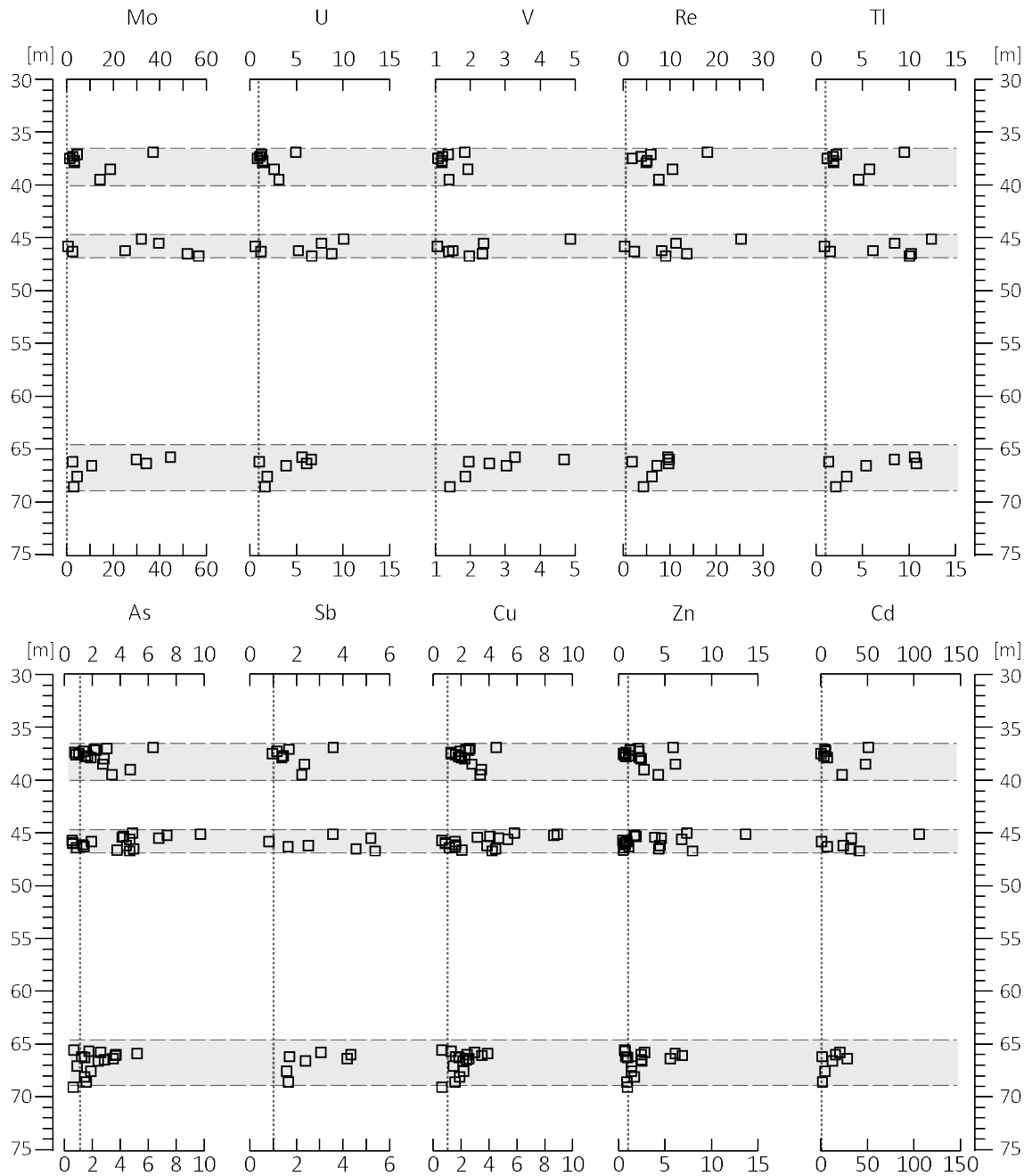


Figure 5.7. Enrichment factors for the studied section calculated relative upper continental crust (UCC: Rudnick and Gao (2003)).

The SiO_2 , Al_2O_3 , and CaCO_3 ternary diagram (Figure 5.3) suggests the studied mudstones have an overall finer grain size than average shale. This may result from either the presence of more clay material or a higher contribution of Al-rich clay minerals (e.g., kaolinite), however petrographic results show a predominance of illite (K-Al rich clay mineral) in the matrix suggesting it is more clay-rich than average shale. The fine-grained nature of the sedimentary rock may indicate a siliciclastic starvation process. In this, the coarse-grained clastic fraction of the sediment was trapped in nearshore proximal settings, with only fine-grained material being transported to more distal settings within the Cleveland Basin. Alternatively, the fine-grained nature of the sediment may result from the weathering of fine-grained source

material on the hinterland or the deposition of palimpsest sediment that was deposited and remobilised on the ocean.

Depth plots of geochemical grain size proxies (Figure 5.4) indicate generally quiescent conditions in the LVMI, with slightly more variable energy in the HVMI. Petrographic observations support the geochemical grain size proxies, showing a lower proportion of clay material and a dominance of alternating organic carbon- and carbonate-rich sediment in the HVMI (particularly in facies 2 and 3). In addition to the compositional variations, the occurrence of normally graded beds with erosional bases in TOC-rich sections of the HVMI indicates an energetically dynamic setting. Occasional higher energy conditions affected sediment deposition and dispersal at the seafloor and led to winnowing of the finest grain sizes. Significant quantities of terrestrial OM (identified by $\delta^{13}\text{C}_{\text{org}}$ and petrography), coupled with its overall fine-grained nature, suggest that the sediments accumulated in a distal depositional setting where hydrodynamic processes sorted the sediment based on particle size and density.

Owing to the shallow gradients and vast extent of epicontinental seaways, sediment dispersal in the LVMI, which are dominated by terrigenous mud, is likely to have been controlled by wind- and tide-induced bottom currents (Schieber, 2016b). In contrast, the HVMI contain marine organic material and carbonate-rich faecal pellets. The occurrence of organo-mineral aggregates and algal OM (20 μm thick and 200 μm long; Table 5.1) demonstrate marine snow and algal mat settling as key mechanisms for the delivery of OM to the seafloor (Macquaker et al., 2010). Filter-feeding organisms strip nutrients and fine grained sediment out of the water column and excrete them as faecal pellets (Ittekkot et al., 1992). This biological mediation of the sediment is a key process in the export of OM, sediment, and nutrients from the water column to the sediment. Ittekkot et al. (1992) demonstrated a link between enhanced sediment and nutrient flux to the ocean during wet phases of the monsoonal cycle. They showed also that there was an increase in biotic-abiotic pellet production, and thus an enhanced OM and mineral flux to the seafloor, in response to enhanced continental runoff and weathering associated with the monsoonal wet phases.

The occurrence of faecal pellets, increases in grain size, TOC, and CaCO_3 observed in the HVMI studied here points towards enhanced productivity, which is likely to be a regional phenomenon. If this was not limited to the Cleveland Basin, it may explain a coeval organic enrichment across the Laurasian Seaway. The causal mechanism behind the increase in productivity cannot be constrained with the present dataset. However, slight increases in depositional energy may result from intermittent storm mixing or changes in bottom water currents, which could both increase primary productivity.

Armstrong et al. (2016) attributed alternations in TOC enrichment to orbitally forced changes in humidity-aridity occurring over a short eccentricity timescale (100 kyr). Based on the

chronostratigraphic time frame for the Yorkshire and Dorset sections (Armstrong et al., 2016, Huang et al., 2010) and assuming a linear sedimentation rate, the changes between the HVMI and LVMI equate with short eccentricity cycles. Thus our observations match with the prediction of Armstrong et al. (2016) that enhanced TOC burial occurred during wet periods through enhanced continental weathering, nutrient supply to the ocean, and primary productivity.

5.6.2 Productivity and organic matter composition

Biological components (coccolithophores, foraminiferans, and organic carbon) occur in differing proportions throughout the section (Figure 5.2). Our petrographic observations (Table 5.1) and organic carbon isotope data (Figure 5.2) indicate a mixed OM type II-III component, in agreement with the literature (Herbin et al., 1993, Scotchman, 1991). Type III OM, with typical carbon isotopes values of -26 to -28 ‰ VPDB, is ubiquitous in the LVMI (Figure 5.2 and Table 5.1). The OM was produced on adjacent land masses and was transported into the marine environment along with other detrital components, such as quartz and clay minerals. The largely very fine-grained nature of the LVMI suggests that organic material, together with clay-sized siliciclastic detritus, was preferentially deposited in the distal location represented by the Ebberston 87 Core. Furthermore, Type III organic material is more resistant to oxidative degradation and hydrodynamic disaggregation due to its structure and chemistry, which explains how organic material enrichment in the LVMI (average TOC = 4.0 wt %) is possible in an environment that had an active benthic ecosystem indicative of oxic-suboxic bottom water conditions. In addition to abundant terrestrial organic material, there are occasional algal macerals in the LVMI.

In contrast, the TOC-rich intervals of the HVMI (average TOC = 12.3 wt %) are dominated by Type II OM. Wispy lamina, algal maceral material (Table 5.1), and algal mats are the main source of OM in these intervals, although Type III OM remains ubiquitous and coincides with the occurrence of detrital material, i.e. quartz grains, lithic clasts, and clay minerals in the samples. In the TOC-rich parts of the HVMI, large amounts of type II algal derived material deposited at the seafloor acted to dilute the detrital sediment and type III OM.

Production of algal macerals in the oceans is affected by the availability of light and nutrients (Pedersen and Calvert, 1990). Water depth is not likely to have exceeded a few hundreds of meters in the distal Cleveland Basin (Bradshaw et al., 1992b), suggesting that the euphotic zone could have reached the seafloor and light did not limit primary productivity. We therefore propose that nutrient availability was the likely driver of changes in productivity. Nutrients are supplied to the euphotic zone through continental weathering or upwelling/overturning of nutrient rich waters. Given the palaeogeographic setting of the Cleveland Basin in an epicontinental seaway, it is likely that changes in precipitation on the surrounding landmasses were a key driver of changes in productivity. The wet-dry cycles

proposed by recent climate modelling (Armstrong et al., 2016) may therefore be the key driver behind oscillations in the production and preservation of TOC, i.e. the switching between the LVMI and HVMI.

Carbonate productivity, mainly in the form of coccoliths, varies throughout the studied KCF section and is at its maximum within the carbonate-rich sections of the HVMI. High nutrient availability in the photic zone of the water column, indicated by high OM productivity, also influences the rate of carbonate productivity (Lees et al., 2006). Within the HVMI's, alternations between TOC-rich deposition likely occurred during high nutrient availability, and carbonate-rich deposition is more likely under less nutrient-rich conditions. This alternation may result from ecological switching driven by oceanographic or climate processes that subtly altered the nutrient levels during these intervals. The organisation of the coccoliths into faecal pellets in both the TOC-rich and carbonate-rich intervals of the HVMI indicates a high abundance of higher trophic organisms to graze on a plentiful supply of food further supporting an elevated nutrient level during these intervals. For the Dorset section, Macquaker et al. (2010) suggested that zooplankton were the main grazers and producers of faecal pellets. Our petrographic study of the Ebberston 87 Core reveals strong similarities with the type section in Dorset, so we tentatively suggest that zooplankton were also the main grazers in the Cleveland Basin at the time of deposition.

5.6.3 Redox conditions

5.6.3.1 Redox conditions in the lower variability mudstone intervals (LVMI)

In the lower variability mudstone intervals, petrographic results demonstrate extensive bioturbation, most likely resulting from widespread faunal colonisation of the sediment surface due to well oxygenated bottom waters. However, enrichment factors of redox sensitive trace elements (Mo and U; Figure 5.5) (Brumsack, 2006; Tribovillard et al., 2006; Piper and Calvert, 2009) indicate that during the deposition of the LVMI, the sediment pore water was suboxic to anoxic. This interpretation is further supported by the low Mn/Al and high (TOC=0.8–10.4 wt %; Figure 5.2) TOC contents.

It is difficult to reconcile the high TOC contents, which is considered extremely TOC-rich and qualifies as a potential hydrocarbon source rock, with oxygenated bottom waters. We explain this apparent conundrum by the presence of terrestrial OM in the LVMI as demonstrated by lower $\delta^{13}\text{C}_{\text{org}}$ (Figure 5.2), petrography (Table 5.1) from this study, and from published Rock Eval data (Herbin et al., 1993). In comparison to its marine counterpart, terrestrial organic matter often has a higher preservation potential because its chemical structure can make it less susceptible to oxidative degradation and because sulphate reducing bacteria have a lower affinity for terrestrial OM (Dellwig et al., 2001). Similarly, marine algal macerals have a greater chance of being preserved when incorporated into organo-mineral aggregates that

are observed in the HVMI, because physical and chemical attractions between the aggregate components can form a protective barrier to oxidative destruction of the algal macerals (Macquaker et al., 2010).

5.6.3.2 Redox conditions in the higher variability mudstone intervals (HVMI)

The TOC-rich parts of the HVMI are dominated by algal macerals (Table 5.1) which account for the elevated TOC concentrations of up to 25.7 wt % (Figure 5.2). Enrichments in redox sensitive/sulphide forming elements (Mo, U, V, Zn, Cd, Re, As, Sb, Hg, and Fe; Figure 5.5; Zn and Cd; Figure 5.6) clearly support the notion of periodically anoxic to euxinic pore and bottom waters at the study site (Brumsack, 2006; Tribovillard et al., 2006), which enhanced preservation of OM during these intervals. However, the presence of agglutinated foraminifera within the TOC-rich parts of the HVMI, as well as enrichments of Mn relative to the LVMI (Figure 5.5), argue that oxygen must have been present at the seafloor, at least episodically (Macquaker et al., 2010b, Dellwig et al., 2018). A positive correlation between Mn/Al and CaCO₃ in the HVMI is further evidence that during favourable conditions for CaCO₃ formation, Mn was sequestered into the sediment thus implying repeated oxygenation events (but see Herndon et al. (2018) for alternative discussion). But note that the enrichment factor of Mn in the HVMI is on a much lower level than for sediments of the Baltic Sea deeps (Figure 5.10). Nevertheless, this scenario has similarities to the modern Baltic Sea deeps (Landsort Deep, Gotland Basin) that display dramatic shifts between euxinic conditions during stagnation and oxic conditions during North Sea water incursions, leading to the sequestration of large amounts of Mn carbonate into the sediments (Scholz et al., 2018, Dellwig et al., 2018, Häusler et al., 2018).

5.6.3.3 Fe enrichment and sulphide formation

The significant enrichments of Fe in the TOC-rich intervals of the HVMI are related to microbial sulphate reduction and pyrite formation, following dissolution of Fe (oxyhydr)oxides at the seafloor. The formation of pyrite (FeS₂) depends on the redox conditions of the sediment pore and overlying water column, so it can be used to reconstruct palaeoenvironmental conditions beyond the redox state (Hetzl et al., 2011). Figure 5.8 shows a Fe_x-TOC-S ternary diagram for the studied interval. Reactive iron is calculated as $Fe_x = Fe - 0.25 \cdot Al$ to account for the fraction of Fe that is bound in the silicate fraction and unavailable for redox reactions (Brumsack, 1988, Dellwig et al., 1999). A fully quantified measurement of reactive iron in a sample must be determined experimentally, owing to an absence of this, we discuss samples only in a relative way. For the samples plotting above the TOC-pyrite mixing line, pyrite formation was limited by the availability of sulphur (in the form of H₂S generated by bacterial sulphate reduction) and excess, less-pyritised reactive iron was preserved in the sediments (potentially as oxides or carbonates). Both in the LVMI

and the HVMI, there are samples with an excess of reactive Fe relative to S. Limited availability of reactive OM to support bacterial sulphate reduction (i.e. limited H_2S generation) may be the reason for the observed excess iron. Alternatively, it might either be related to the re-oxidation of pyrite during oxygenation events (removing S but not Fe from the sediment), or a strong input of Fe into the system via a particulate shuttle mechanism (discussed in section 0).

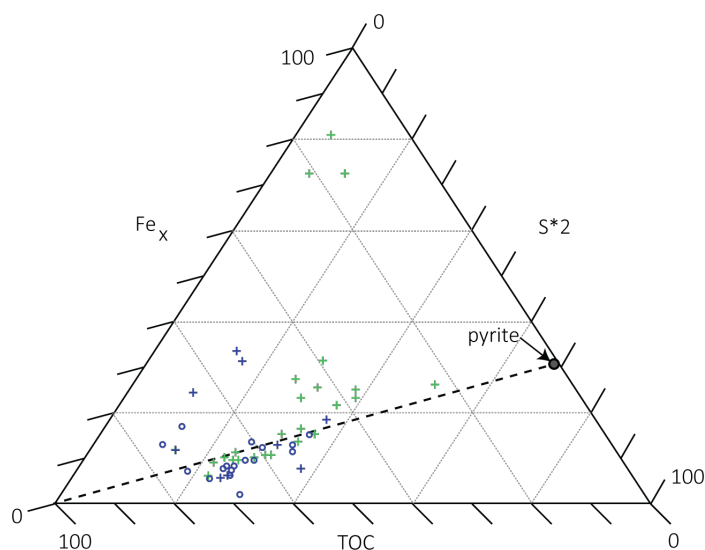


Figure 5.8 Fe_x -TOC-S Ternary diagram (after Dellwig et al., (1999); Hetzel et al., (2011)). See text for comments on Fe_x calculation. Dashed line represents TOC-pyrite mixing line. Lower variability mudstone interval (LVMI) samples are indicated by green crosses (three samples nearest to the Fe_x corner represent the diagenetically overprinted samples that were excluded from the interpretation). Higher variability mudstone interval (HVMI) samples are marked by blue symbols, TOC-rich samples ($\text{TOC} > 10 \text{ wt } \%$) are indicated by blue circles and TOC-lean samples ($\text{TOC} < 10 \text{ wt } \%$) are indicated by blue crosses.

The samples that plot near the TOC-pyrite mixing line in Figure 5.8 are assumed to represent an availability of reactive Fe and S in the system that matches the stoichiometry of pyrite, hence they have a higher degree of pyritisation. Depth plots of As/Al and Sb/Al (Figure 5.5), trace elements that are known to accumulate strongly in pyrite, support these conditions (Tribovillard et al., 2004). In samples that plot below the TOC-pyrite mixing line in Figure 5.8, pyrite formation is limited by the availability of reactive iron, meaning the degree of pyritisation was high but there also was an excess of sulphide available in the system. Under these conditions, sulphide was able to react with OM through sulphurisation (or natural vulcanisation). Our results are consistent with Tribovillard et al. (2004) who concluded that pyrite formation prior to OM sulphurisation may increase the sequestration of Mo into the sediment. This highlights the need of caution when using Mo as a single diagnostic proxy in palaeoenvironmental reconstruction. Tribovillard et al. (2004) further demonstrated a linear relationship between the quantity of 'orange algal macerals' and Mo concentrations in the

Ebberston 87 Core, supporting the presence of sulphurised OM. The resulting sulphurised OM is less vulnerable to oxidative degradation and thus has a greater preservation potential during burial. We suggest that this mechanism is partly the reason we observe high TOC concentrations in intervals that underwent first sustained periods of pore or bottom water euxinia and later periods of reoxygenation. Studying Jurassic sediments of the Marton 87 core (Figure 5.1), drilled 4 km away from the Ebberston 87 Core, Boussafir et al. (1995) and Lallier-Vergès et al. (1997) also conclude that sulphurisation/natural vulcanisation of Type II OM enhanced organic material preservation potential.

5.6.3.4 Evidence for a Fe-Mn shuttle and ocean restriction

In the context of pyrite formation versus OM sulphurisation, and the enrichment of trace metals at the seafloor, the delivery of Fe and Mn (oxyhydr)oxides via a so-called particulate shuttle may play an important role. The particulate shuttle effect describes the cycling of Mn and Fe through the redoxcline, which is an ocean layer characterised by steep geochemical gradients and the point at which solubility of certain mineral phases increases or diminishes, in particular Mn, Fe, and P phases (Dellwig et al., 2010). Dissolved Mn^{2+} diffuses from anoxic waters beneath the redoxcline to the oxygenated surface layer where it is oxidised to form MnO_2 particles. These particles react with Fe^{2+} to form mixed Mn/Fe (oxyhydr)oxide phases which are highly efficient adsorbents of dissolved trace metals in the ocean (Goldberg, 1954). If these phases sink and reach deeper sulphidic waters, the (oxyhydr)oxides are reduced, and Mn^{2+} diffuses back into the overlying waters, while Fe^{2+} reacts with H_2S to form Fe sulphides that incorporate part of the released trace metals (Canfield et al., 1992, Dellwig et al., 2010, Neretin et al., 2004, Huckriede and Meischner, 1996, Tribovillard et al., 2015). This particulate shuttle plays a key role in the transfer of trace elements from the water column to the sediment (Goldberg, 1954, Tribovillard et al., 2015). Of particular relevance to this study is the transfer of Mo, As, and Sb to the sediment, elements that Tribovillard et al. (2015) used as proxy for the presence of a Mn-Fe shuttle in ancient anoxic-euxinic ocean basins. In the present study, Fe/Al (Figure 5.5) and Mo/U (Figure 5.9) co-variations point towards a Mn-Fe shuttle operating during deposition of TOC-rich sediment in the HVMIs. Manganese is repeatedly recycled through the shuttle so the observed concentrations are easily accounted for. Peaks in Fe/Al coincide with peaks in pyrite associated trace metals (As/Al, Sb/Al; Figure 5.5) and increased abundance of pyrite in thin sections (Table 5.1). We propose that a suboxic shuttle that remobilised Fe from shelf sediments (Dellwig et al., 2010, Eckert et al., 2013, Severmann et al., 2008, Wijsman et al., 2001) was active during deposition of the TOC-rich parts of the HVMIs in the Ebberston 87 Core, and enriched reactive Fe in the sediments to levels significantly above UCC. Episodically high inputs of reactive Fe via a suboxic shuttle also prevented the accumulation of H_2S in the pore waters, thereby limiting OM sulphurisation.

During ventilation events (as suggested by benthic foraminifera and Mn enrichments), some of the pyrite was reoxidised, and sulphate diffused from the pore water to the water column while reactive Fe was retained in the sediment by precipitation of Fe (oxyhydr)oxides. Thus, samples that appear to be deposited under S limited conditions in Figure 5.8 may still contain organic sulphur. We conclude that the hyper-accumulation of TOC in this setting was controlled by high primary productivity, increased OM production, the balance of H_2S generation, and the supply of reactive Fe via a suboxic shuttle.

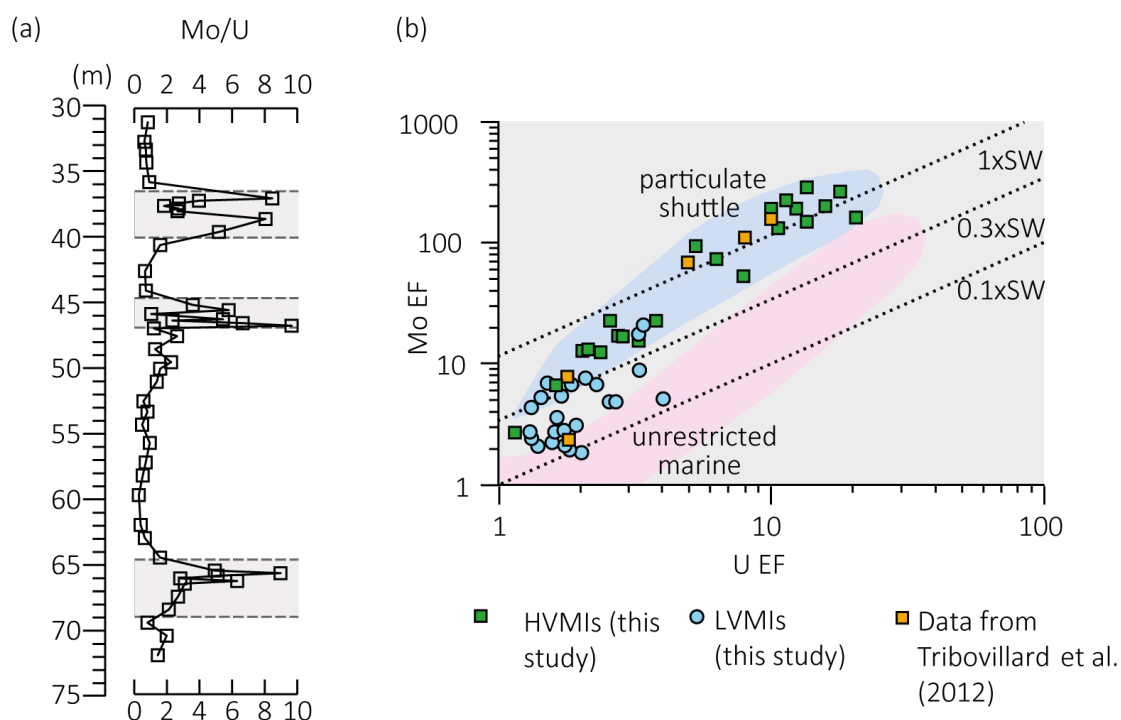


Figure 5.9 a) Depth plot Mo/U (ppm/ppm) (after Algeo and Tribovillard (2009)). Grey panels depict the higher variability mudstone intervals (HVMIs) defined in this study, b) scatter plot of Mo EF versus U EF calculated relative to Post Archean Average Shale (PAAS; Taylor and McLennan (2001)(after Tribovillard et al., 2012). Lower variability mudstone interval (LVMI) samples are indicated by blue circles, HVMIs are indicated by green squares. Data from the Ebberston 87 Core by Tribovillard et al., (2005) are represented by orange squares. Dashed lines are modern day seawater, 0.3 x modern day seawater and 0.1 x modern day seawater values shown for reference. The particulate shuttle is mapped in blue and unrestricted marine setting is mapped in pink. Axes are logarithmic.

In the context of developing an anoxic/euxinic water column in the Cleveland Basin with associated enrichments of redox sensitive/sulphide forming trace metals (Figure 5.5), not only primary productivity but also basin restriction has to be considered as a contributing factor. A key element for the reconstruction of hydrographic basin restriction is Mo (Algeo and Lyons, 2006), as its removal from the water column and sequestration into the sediments

changes dramatically under different redox conditions, more so than is the case for other redox sensitive/sulphide forming trace metals (Helz et al., 1996).

Due to the specific biogeochemical behaviour of Mo, the ratio of Mo/U enrichment factors can give insights into the degree of restriction of a basin (Algeo and Lyons, 2006). Both elements tend to be enriched in sediments deposited under oxygen-depleted bottom water conditions, but to varying degrees. Under suboxic conditions, U enrichment is likely to exceed Mo enrichment owing to the trapping of U at the Fe(II)/Fe(III) redox boundary (Algeo and Tribovillard, 2009). As oxygenation of the water mass decreases further, and sulphidic conditions develop in pore and bottom waters, Mo enrichment increases relative to that of U, and the Mo/U ratio approaches or surpasses that of seawater due to the presence of sufficient H_2S to convert the conservative molybdate ion to the highly particle-reactive thiomolybdate (Algeo and Tribovillard, 2009, Erickson and Helz, 2000). Mo/U ratios for the LVMI in this study are similar to that of average shale (Figure 5.9), pointing towards a detrital, rather than authigenic, source of the Mo and U in these samples. Therefore, these samples cannot be used to investigate the presence of a Mn-Fe shuttle. In contrast, the HVMI display repeated peaks in the Mo/U ratio, indicative of strong Mo enrichments under euxinic conditions, facilitated by the activity of a Mn-Fe shuttle preferentially transferring Mo from the water column to the sediment (Algeo and Tribovillard, 2009).

We compare our new results with existing data from Tribovillard et al. (2004), who analysed trace elements (Figure 5.9a) in several samples from the Ebberston 87 Core, with cycle 3 in their study being equivalent to the stratigraphically oldest (*Pectinatites wheatleyensis*) HVMI in our study. The authors concluded that TOC enrichment in the Cleveland Basin occurred during times of transgression due to clastic sediment starvation, high primary productivity, and water column stratification. Our higher resolution sampled data agree with this conclusion in that on a Mo-U enrichment factor plot (Figure 5.9b), the TOC-rich intervals plot clearly within the particulate shuttle field, which is good agreement with our Fe/Al and Mn/Al data discussed above. Samples from the LVMI plot outside of this field, which confirms that during deposition of these samples the suboxic conditions were limited to the sediment. Pearce et al. (2010) concluded that the deposition of the KCF occurred in an unrestricted basin. Tribovillard et al. (2012) compared their results to those presented by Pearce et al. (2010) and agreed that it is unlikely that either the Cleveland or Wessex Basins were restricted for a prolonged period, if at all. In combination with our geochemical and petrographic data, we can confirm that the repeated development of anoxic/euxinic conditions in the distal Cleveland Basin was most likely due to high primary productivity, and possibly salinity stratification due to high amounts of freshwater runoff, but it is unlikely that the Cleveland Basin experienced prolonged restriction.

5.6.3.5 Comparison to modern organic carbon-rich sediments

Comparing our data with those from different TOC-rich deposits enables us to better understand common processes involved in TOC enrichment in different palaeoenvironmental/depositional settings (Brumsack, 2006) and draw wider conclusions for the present study. Figure 9 shows average enrichment factors (calculated with respect to average shale for select trace metals (Mn, As, Cd, Co, Cu, Mo, Re, Sb, U, V, and Zn) for the carbonate-rich and TOC-rich sections of the HVMI in the present study and other well-studied deposits. Depositional environments, in which TOC and trace elements are enriched, can fall on a scale between two end members; coastal upwelling systems (e.g. Gulf of California, Peru coastal margin) and anoxic basin type settings (e.g. Mediterranean Sapropels, Black Sea, Baltic Sea deeps). The former are characterised by seasonally high primary productivity and extensive oxygen minimum zones (OMZ) that are fuelled by wind-driven upwelling of high nutrient and trace metal waters, while the latter are characterised by permanent salinity stratification and water mass restriction (Brumsack, 2006).

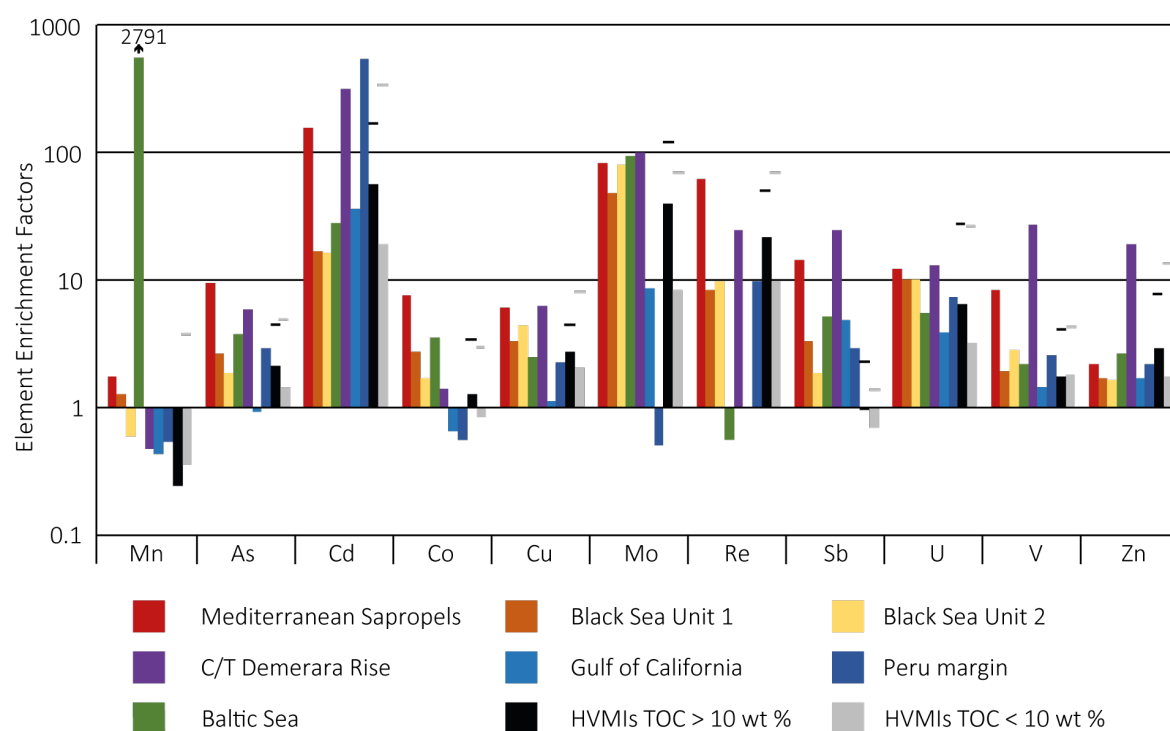


Figure 5.10 Bar chart illustrating enrichment factors (EF) for Mn, As, Cd, Co, Mo, Ni, Re, Sb, U, V, and Zn relative to average shale (Wedepohl, 1991) for Mediterranean Sapropels, Black Sea Units 1 and 2, C/T Demerara Rise, Gulf of California, Peru margin (Brumsack, 2006), Baltic Sea (Dellwig, Unpublished data), and higher variability mudstone intervals (HVMI) from the present study. Maximum EFs in this study are marked by black and grey lines.

The HVMI in the present study bears similarities to the Gulf of California in that they exhibit similarities in Cd enrichment and Mn depletion, indicating high productivity and suboxic conditions in the water column. Cd enrichments suggest that parts of the HVMI experienced upwelling-like processes, which may have resulted in high productivity. However, sulphidic

conditions in the water column are rarely observed in upwelling settings (Brumsack, 2006); this differs from the studied Cleveland Basin and is reflected in the sulphide indicators (As and Mo; Figure 5.5). This indicates that the method of trace metal sequestration is different in modern upwelling settings and the studied section, meaning they are a poor analogue for the present study.

The anoxic basin type settings exhibit strong enrichments in sulphide forming trace metals (Brumsack, 2006). However, the enrichment factors for the Mediterranean Sapropels and Units 1 and 2 from the Black Sea exhibit different patterns (Figure 5.10), owing to the pronounced depletion of trace elements in the water column of the Black Sea. The studied HVMIs are most similar to Black Sea Unit 2 in that redox sensitive (As, Cu, Mo, Re, U, V, and Zn) and productivity (Cd) elements are on the same order of magnitude. From this, we may infer similarities operating in the two intervals of deposition. However, the modern Black Sea is permanently stratified and is governed by its unique hydrological setting. This is in stark contrast to the HVMIs in the Cleveland Basin, which exhibit rapid oscillations and were deposited in a shallow epicontinental seaway. It may be that the Late Jurassic Laurasian Seaway fluctuated between a setting close to an anoxic basin-type setting or a setting more analogous to a coastal upwelling zone.

5.6.3.6 Evidence for Baltic Sea characteristics

While the studied interval shares similarities and differences with both upwelling and anoxic basin type settings, we are still lacking an appropriate modern analogue. Palaeogeography exerts a fundamental control on sedimentation, in particular, TOC enrichment, but there is no modern-day example of a shallow epicontinental seaway. If at all, the Baltic Sea comprises a series of small basins that are interconnected by narrow sills and channels. It receives saline water input from the North Sea and fresh water from riverine input resulting in permanent stratification of the water column (Dellwig et al., 2018; Häusler et al., 2018). Coupled restriction of water mass exchange in the deeper sub-basins of the Baltic Sea leads to appearance of water column anoxia/euxinia. However, large (and infrequent) inputs of saline and oxic water from the North Sea promote overturning and reoxygenation of the Baltic Sea deeps, causing extensive Mn carbonate formation in the sediments (Dellwig et al., 2018; Häusler et al., 2018). While the mechanism of Mn carbonate formation is still debated, the Mn carbonate deposits are generally associated with intervals of prolonged reoxygenation (Häusler et al., 2018). The Baltic Sea deeps represent an extreme example of Mn shuttling, where Mo is highly enriched as it adsorbed to Mn, but U and Re are much less enriched. Enrichment factors calculated relative to average shale (Wedepohl, 1971, Wedepohl, 1991) for the Landsorp Deep in the Baltic Sea is plotted on Figure 5.10. Data was generated from the 36GC-4 core (see (Häusler et al., 2017, Häusler et al., 2018) for Landsorp Deep core and site description) and is presented in the data repository.

This geographical setting bears resemblance to the Late Jurassic Laurasian Seaway in that it was comprised of a series of interconnected shallow basins. Therefore, we propose that redox dynamics in the Cleveland Basin during the Late Jurassic shared similarities to those in the modern-day Baltic Sea in that they both exhibit signs of complex redox dynamics and trace metal sequestration. The enrichment factors in Figure 5.10 are averaged across the HVMI, indicating Mn depletion across these zones. However, there are several samples that are enriched in Mn within the HVMI (Figure 5.5), which point towards prolonged reoxygenation events during episodes of organic enrichment in the Kimmeridge Clay Formation.

5.7 Conclusions and conceptual model

This study provides an insight into the sedimentation in the distal parts of an epicontinental seaway during a greenhouse world. Examining sediment away from strong detrital dilution and overprint allows us to unpick the global controls on sedimentation and gives us further insight into the key processes in this palaeogeographic setting. Far away from detrital inputs, this distal location provides an excellent data set for examining changes in water column processes.

The studied interval of the Kimmeridge Clay Formation in the distal part of the Cleveland Basin was deposited in a highly dynamic environment that fluctuated from LVMI deposition to HVMI (Figure 5.11). During LVMI sedimentation (Figure 5.11a), the water column was oxic and was able to sustain life to a degree that the sediment was extensively bioturbated. However, the sediment pore waters were suboxic to anoxic which facilitated the enrichment of TOC. During each HVMI, the depositional environment experienced episodic and drastic changes. Trace element data indicate redox conditions of the bottom waters alternating between fully oxic and euxinic. During oxic conditions, organic matter (OM) and carbonate production proliferated (Figure 5.11a, b). High primary productivity led to an increase in higher trophic feeders that produced masses of faecal pellets, in turn resulting in an increase in OM flux rate that aided the preservation of carbon and diluted the detrital material. At the same time, Mn and Fe (oxyhydr)oxides were deposited at the seafloor, together with adsorbed trace metals (Figure 5.11b). Detrital element proxies indicate that the oxygenation events were accompanied by elevated depositional energies at the seafloor, most likely related to the downward supply of oxic water by either currents or waves.

Once these higher energetic conditions ended, the supply of oxygen to the seafloor could not keep up with the oxygen demand of organic matter degradation, and the deeper waters became anoxic/euxinic. During these intervals, sedimentation was predominated by algal macerals delivered to the sediment as organo-mineral aggregates and marine snow under quiescent conditions. The production of sulphide minerals (e.g. pyrite) and the accumulation of related sulphide forming trace metals was enhanced under these conditions, with the Fe being resupplied by a suboxic Fe shuttle that remobilised Fe through the chemocline. At times

when Fe was not supplied, OM became sulphurised, which enhanced its preservation potential. Trace element enrichment was facilitated by a Mn/Fe particulate shuttle.

Comparisons of trace element geochemistry show the studied section exhibits patterns similar to upwelling- and anoxic basin-type deposits. However, we observe that the studied section bears similarity to the Landsort Deep of the present-day Baltic Sea.

In the context of the published chronostratigraphic framework, alternations between LVMI and HVMI occur on a short eccentricity (100 kyr) timescale. This is in line with the predictions presented by Armstrong et al. (2016), whereby an orbitally modulated expansion of the Late Jurassic Hadley Cell led to alternations between humid and arid climate conditions. We propose that the highly dynamic conditions in the studied intervals are representative of wet and humid conditions during which changes in continental weathering enhanced primary productivity and led to TOC enrichment. Conversely, the LVMI were deposited under arid conditions.

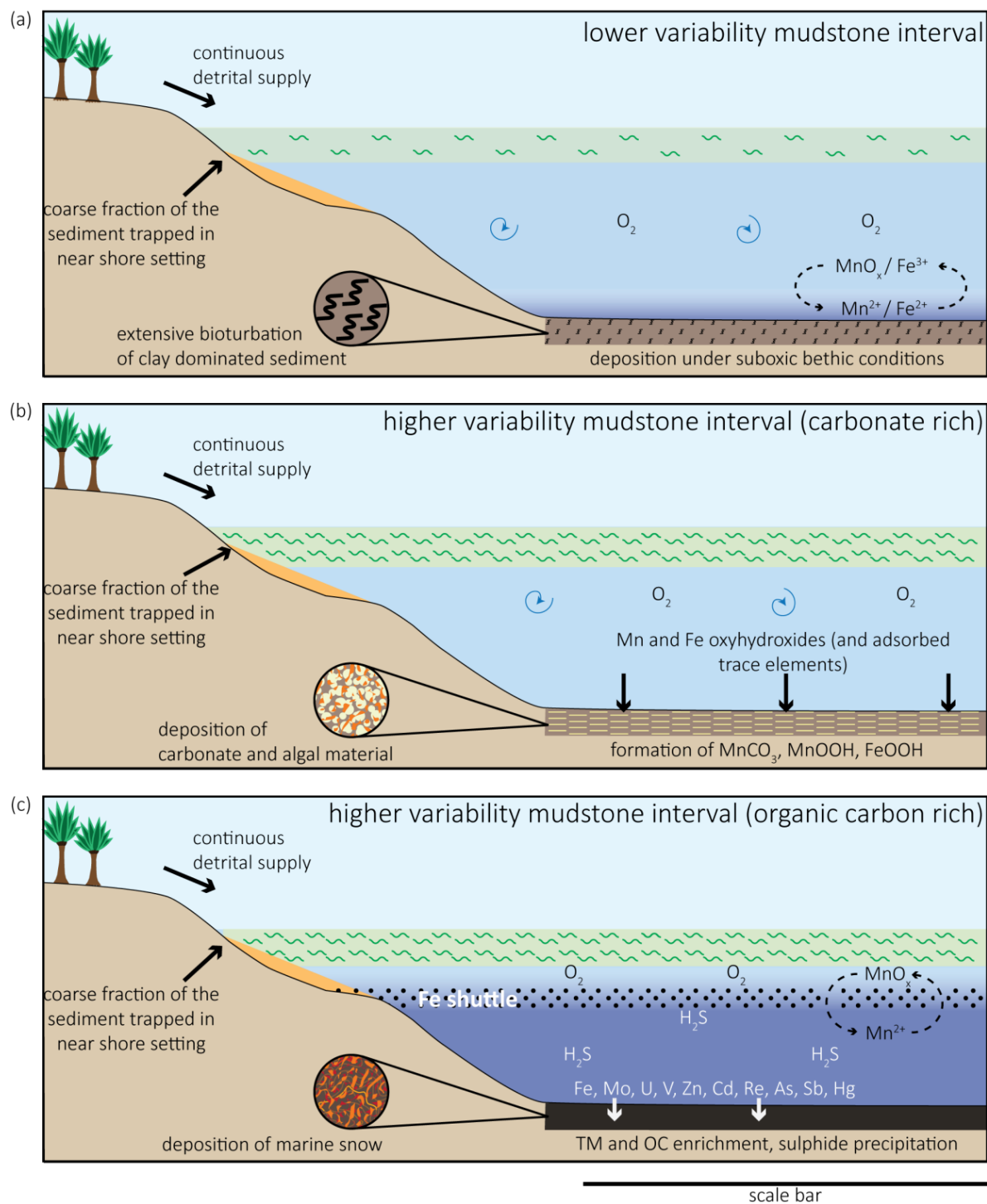


Figure 5.11 Schematic diagram illustrating depositional conditions during the different intervals of sedimentation. a) Lower variability mudstone interval, b) Periods of carbonate-rich sedimentation in the higher variability mudstone intervals, c) Periods of organic carbon-rich sedimentation during the higher variability mudstone intervals. Scale bar represents bathymetric lows, generally considered to be 10–100's km across.

6 | Local to global controls on the deposition of organic-rich muds across the Late Jurassic Lurasian Seaway

This chapter is based on a manuscript that is under review in the *Journal of the Geological Society* at the time of submission:

Atar, E., März, C., Wagner, T., and Aplin, A., submitted. Local to global controls on the deposition of organic-rich muds across the Late Jurassic Lurasian Seaway.

6.1 Abstract

Muds deposited in large-scale epicontinental seaways provide deep insights into palaeoclimates, biogeochemical cycles, sedimentation processes, and organic carbon burial during exceptionally warm periods throughout the Phanerozoic. Temporal changes can be explored at single locations but the key, larger-scale oceanographical and related biogeochemical processes are likely to be more clearly revealed by comparisons between individual sub-basins within seaways. Here, we compare inorganic geochemical records from the Jurassic (upper *wheatleyensis* to lower *pectinatus* ammonite zones) of the Swanworth Quarry 1 Core from the Wessex Basin (Dorset, UK) to time-equivalent records from the Ebberston 87 Core in the Cleveland Basin (Yorkshire, UK), 400 km apart. Our synthesis shows that while the Dorset sediments were deposited in an energetically more dynamic setting than the Yorkshire sediments, the overarching climatic and oceanographical processes responsible for variations in organic carbon enrichment and sedimentation, were similar. Intervals of coeval organic carbon-rich sedimentation occurred in both basins, and a particulate shuttle was intermittently active in both basins. Consistent with recent climate simulations, we conclude that tropical climate conditions, associated with enhanced nutrient supply, were key drivers of sedimentation between the Jurassic Wessex and Cleveland Basins.

6.2 Introduction

Deposition of organic carbon-rich muds has occurred in epicontinental seaways intermittently since at least the onset of the Palaeozoic (Schieber, 2016b, Negri et al., 2009). These seaways, often termed continental interior or epeiric seas, are vast, shallow (< 100 m), partially enclosed seaways that form as a result of high sea level flooding low lying, flat continental areas (Schieber, 2016b, Kemp et al., 2018, Shaw, 1964). Much of what is known about deposition in epicontinental seaways is derived from rock records due to a lack of an appropriate modern day analogue (Arthur and Sageman, 1994). Many of the world's hydrocarbon reserves were deposited in these settings making them of economic importance. This, along with their 'completeness of record', has sparked a strong interest in the correlation of these deposits across vast distances, and in the processes responsible for their formation (Schieber, 2016b).

Flooding of low lying continental areas occurs when global sea level is high during periods when the Earth is under greenhouse conditions and there are no or only small polar ice caps. However, maximum water depths are not thought to have exceeded 100 metres across most epicontinental seaways (Schieber, 2016b). Another consequence of greenhouse conditions is an enhanced hydrological cycle (Sellwood and Valdes, 2008), where precipitation and consequently weathering and erosion are intense. This can lead to the delivery of high amounts of freshwater to the oceans from the surrounding land masses. Given the positioning of epicontinental seaways in intracontinental settings, nutrient supply from land is abundant

and supports particularly high primary productivity. In addition, the development of salinity stratification due to the formation of a surface freshwater layer can limit vertical exchange processes in the water column. This combination of shallow, stratified, warm seas and plentiful nutrient supply provides ideal conditions for the production of organic material and its export to the seafloor. High primary productivity, coupled with sluggish ocean circulation and limited vertical mixing, leads to oxygen depletion in the bottom waters and creates favourable conditions for the preservation of organic material.

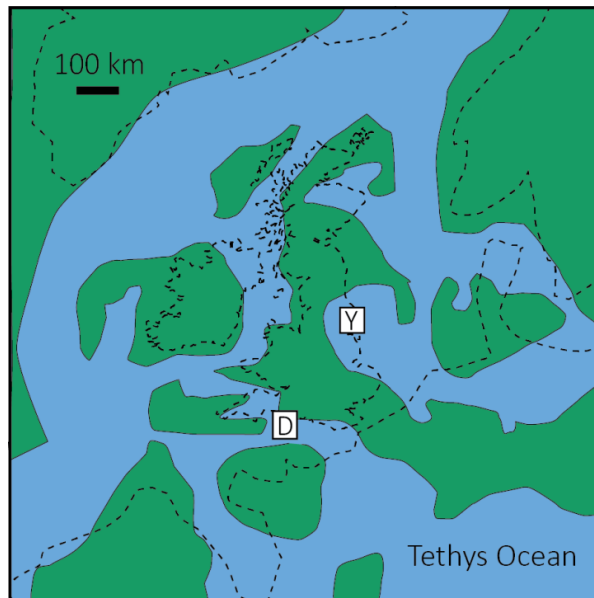


Figure 6.1 Palaeogeographical map of the UK after Miller (1990). The solid black lines mark the outline of the modern day UK. The black dashed lines mark other modern day landmasses.

Deposited across the Laurasian Seaway (Figure 6.1) during the Kimmeridgian-Tithonian stages of the Late Jurassic, the Kimmeridge Clay Formation (KCF) is a laterally extensive succession stretching from northern France up to the Arctic sector, mainly comprising intercalated mudstones and siltstones (Armstrong et al., 2016). The KCF exhibits multiscale cyclicity ranging from micron-scale heterogeneity, interpreted to represent annual seasonality in coccolith productivity (Lees et al., 2004), to metre- and decimetre-scale cyclicity interpreted to represent orbitally forced shifts in water column stability and nutrient supply through continental precipitation (Waterhouse, 1999, Weedon et al., 2004, Morgans-Bell et al., 2001). The KCF has been correlated using ammonite biostratigraphy between the Wessex (Dorset, UK) and Cleveland (Yorkshire, UK) Basins (Cox and Gallois, 1981, Herbin et al., 1995, Herbin et al., 1993, Gallois, 1979). Organic enrichment occurs in five distinct intervals that are termed organic rich belts (ORBs) by Cox and Gallois (1981). (Armstrong et al., 2016) paired geochemical and sedimentological data with global climate modelling and suggested that the ORBs of the Kimmeridge Clay Formation were deposited under the influence of an expanded Hadley Cell with orbitally modulated northwards shifts of the Intertropical Convergence Zone (ITCZ), which promoted enhanced organic carbon production and preservation in the UK sector of the KFC through elevated continental precipitation and runoff rates.

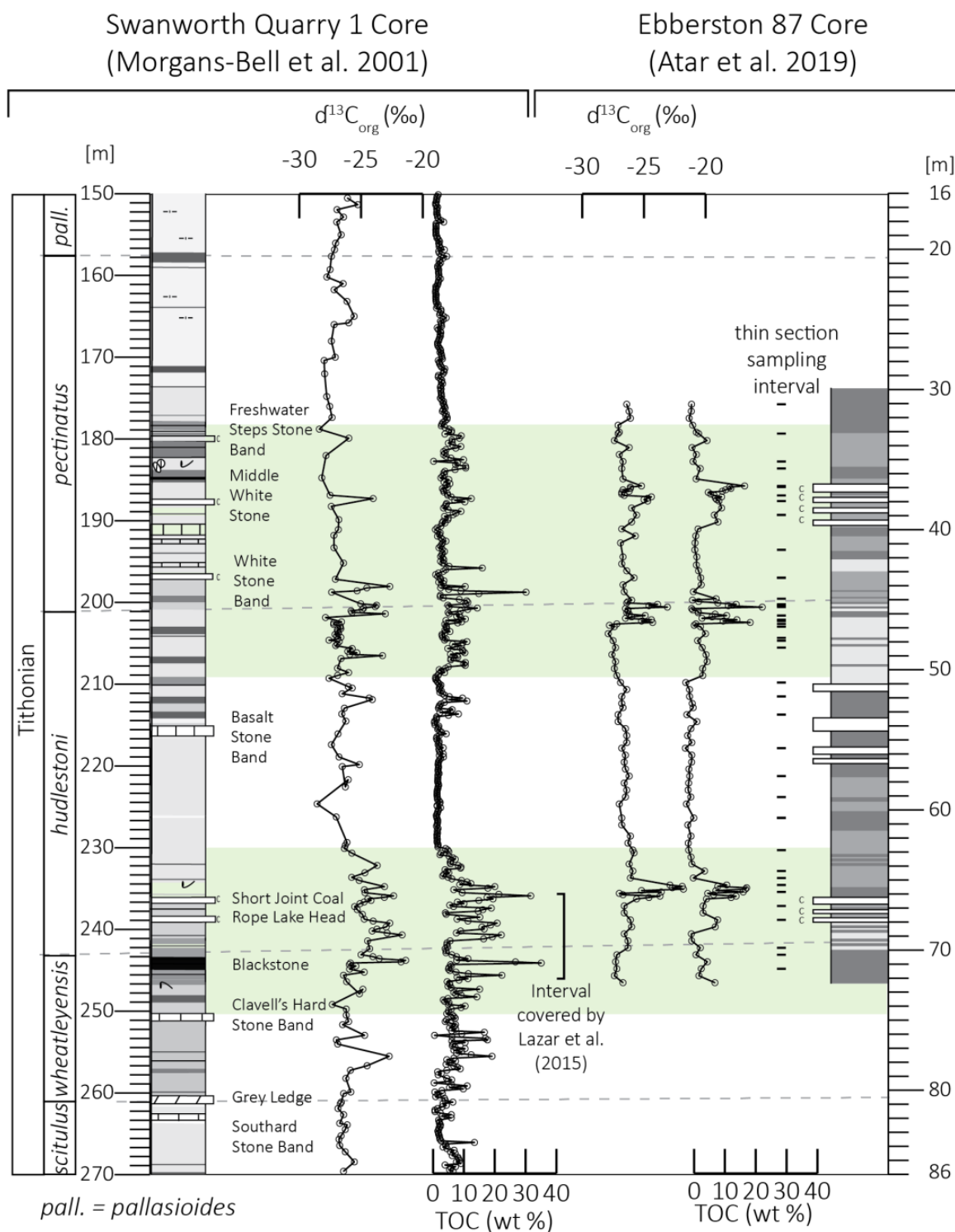


Figure 6.2. Correlation panel between the Swanworth Quarry 1 (SQ1) core from the Wessex Basin (Dorset, UK) and Ebberston 87 Core from the Cleveland Basin (Yorkshire, UK). Depths are metres below surface. Graphic log and total organic carbon (TOC) and organic carbon isotope ($\delta^{13}\text{C}_{\text{org}}$) data for the SQ1 Core are from Morgans-Bell et al. (2001). Lithology is with Munsell Colour. Graphic log for the EB87 Core is from IFPEN archives, and total organic carbon (TOC) and organic carbon isotope ($\delta^{13}\text{C}_{\text{org}}$) data is from Atar et al. (2019). Colour is based on drilling descriptions. Horizontal dashed lines mark biostratigraphical zonation ties. Green panels depict 'Organic Rich Bands' 4 (lowermost) and 5 (uppermost) defined by Cox and Gallois (1981). Interval over which detailed petrographical study was conducted in Lazar et al. (2015b) is marked on the SQ1 depth scale. Chronostratigraphic divisions after Gradstein et al. (2012).

Here we present new major and trace element records for ORBs 4 and 5 from the Swanworth Quarry 1 Core drilled in the Wessex Basin (Dorset, UK). We compare these data to a recently published equivalent dataset for the coeval succession in the Ebberston 87 Core (Atar et al., 2019) drilled in the Cleveland Basin (Yorkshire, UK). We also compare petrographic analyses for ORB 4 from the coastal outcrop in the Wessex Basin (Macquaker and Gawthorpe, 1993, Lazar et al., 2015b, Macquaker et al., 2010b) to the Ebberston 87 Core (Atar et al., 2019). We look beyond the traditional total organic carbon (TOC) and biostratigraphic correlation to explore the extent to which large-scale environmental processes influenced sedimentation generally, and organic matter preservation specifically, across the UK sector of the Lurasian Seaway in the Late Jurassic.

6.3 Material and methods

A detailed methodology is presented in Chapter 2. For this study, 172 samples were collected at 50 cm intervals across a *c.* 79 m interval (181.42–260.05 metres below surface) from the Swanworth Quarry 1 (SQ1) Core, drilled in the Wessex Basin (Figure 6.1).

Total organic carbon contents were measured at Newcastle University. Wavelength-Dispersive X-Ray Fluorescence (XRF) analyses were conducted at the ICBM (University of Oldenburg) to determine the contents of selected major (Si, Al, Ti, and Fe) and trace (Mn, As, Co, Cr, Cu, Mo, V, U, Zn, and Zr) elements, reported as wt % and ppm, respectively. Major and trace element contents were normalised to Al to allow for assessment of relative changes irrespective of lithogenesis (Tribovillard et al., 2006). Mo and U enrichment factors (EFs; Brumsack, 2006) were calculated relative to Post Archean Average Shale (PAAS; Taylor and McLennan (2001)), after (Algeo and Tribovillard, 2009).

6.4 Results

Geochemical results are discussed with reference to the ‘organic rich belts’ first described by Cox and Gallois (1981). Based on the established chronostratigraphic framework, in the SQ1 Core, ORB 4 is 20.5 m thick and spans 230.00–250.50 metres below surface (mbs) and ORB 5 is 30.5 m thick and spans 178.5–209.00 mbs (Figure 6.2). The EB87 Core is a more condensed section relative to the SQ1 Core. In the EB87 Core, ORB 4 is 11.5 metres thick and spans 63.00–74.50 mbs and ORB 5 is 18 metres thick and spans 32.5–50.50 mbs (Figure 6.2). Note that in the SQ1, not the entire section of ORB 4 and 5 is analysed due to sampling.

In the SQ1 Core, TOC contents in ORB 4 range from 1.3–38.2 wt %, with a mean of 5.2 wt % (Figure 6.3). In ORB 5, TOC contents range from 2.9–42.6 wt %, with a mean of 10.3 wt % (Figure 6.3) and between ORBs 4 and 5, TOC is markedly lower, ranging from 0.2–5.7 wt %, with a mean of 1.9 wt % (Figure 6.3). In the EB87 Core, TOC ranges from 2.8–20.7, with a mean of 9.5 wt % in ORB 4. In ORB 5 of the EB87 Core, TOC ranges from 2.8–25.7 wt %, with a mean of 8.8 wt %. In between ORBs 4 and 5, TOC ranges from 0.8–6.4 wt %, with a mean of

2.4 wt % (Figure 6.3). Figure 6.4 shows contents of Al_2O_3 , CaO , and SiO_2 in all analysed samples, representing the main sediment components clay, carbonate, and quartz or biogenic silica, respectively. Samples from the SQ1 Core plot along a mixing line between carbonate and average shale (Wedepohl, 1991) end-members, whereas samples from the EB87 Core plot on a mixing line between carbonate and a detrital end-member that is more Al-rich than average shale (Figure 6.4). Al-normalised values of Si, Ti, and Zr can be used as grain size indicators and Al-normalised K and Rb can be used as weathering and sediment provenance indicators. Aluminium-normalised Si, Ti, Zr, K, and Rb range from 2.0–3.8, 0.04–0.07, 8.2–33.2, 0.2–0.3, and 16.5–24.0 in ORB 4, respectively (Figure 6.5). In ORB 5, they range from

2.0–4.1, 0.05–0.07, 12.2–34.7, 0.2–0.3, and 13.2–20.0, respectively (Figure 6.5).

However, in between the ORBs, they are less variable, ranging from 2.2–2.8, 0.05–0.06, 11.1–19.4, 0.3–0.4, and 18.6–20.1, respectively (Figure 6.5). In ORB 4 of the EB87 Core, Al-normalised Si, Ti, Zr, K, and Rb range from 2.1–2.6, 0.05–0.06, 10.4–18.0, 0.2–0.3, and 10.1–17.0, respectively. In ORB 5, Al-normalised Si, Ti, Zr, K, and Rb range from 2.0–3.3, 0.04–0.05, 9.8–26.7, 0.1–0.3, and 8.6–17.6, respectively. As in the SQ1 Core, in between ORBs 4 and 5 the Al-normalised Si, Ti, Zr, K, and Rb are lower and much less variable, ranging from 2.0–2.4, 0.05–0.05, 11.0–14.0, 0.2–0.3, and 12.0–17.0, respectively. In ORB5, Ti/Al , Zr/Al , and Rb/Al are generally the same or exceed average

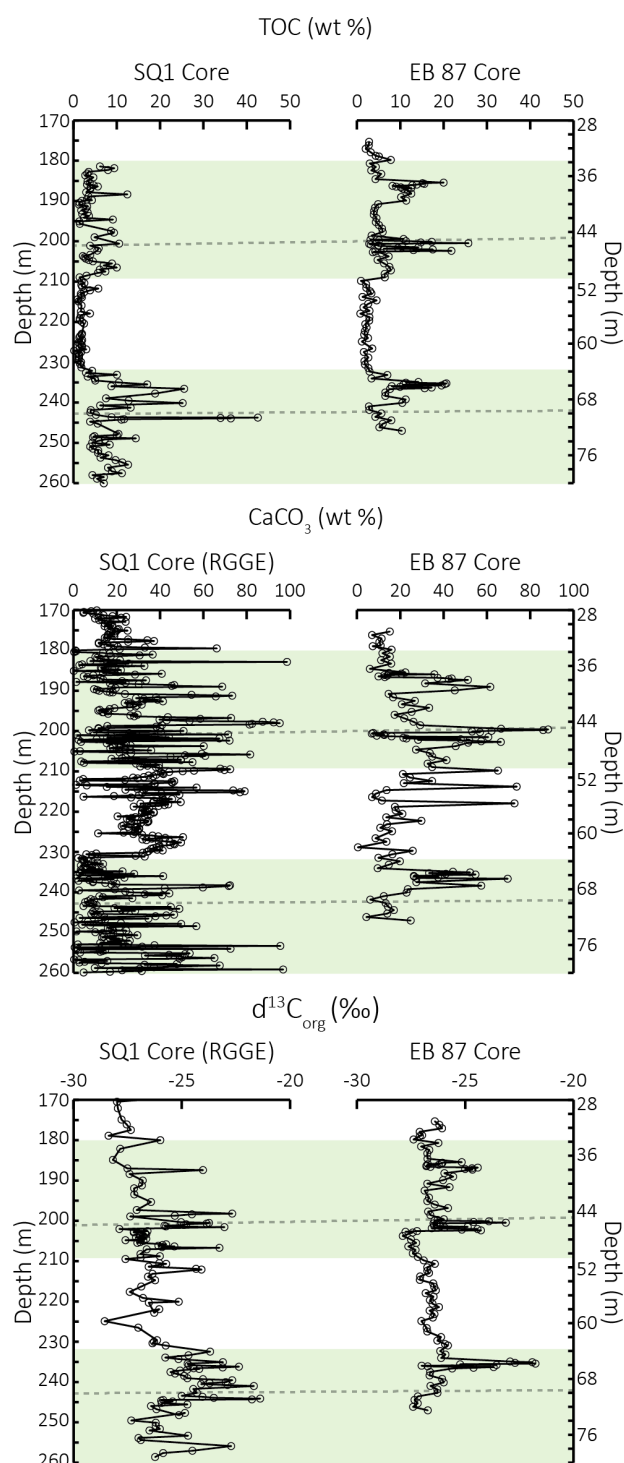


Figure 6.3. Total organic carbon (TOC), calcium carbonate (CaCO_3), and organic carbon isotopes ($\delta^{13}\text{C}_{\text{org}}$) for the Swanworth Quarry 1 (SQ1) and Ebberston 87 (EB87) cores. Depths are in metres below surface. Horizontal dashed lines mark biostratigraphical zonation ties. Green panels depict 'Organic Rich Bands' 4 (lowermost) and 5 (uppermost) defined by Cox and Gallois (1981). CaCO_3 and $\delta^{13}\text{C}_{\text{org}}$ for the SQ1 Core is from Morgans-Bell et al. (2001). TOC, CaCO_3 , and $\delta^{13}\text{C}_{\text{org}}$ data from the EB87 Core is from Atar et al. (2019).

shale values in the SQ1 Core, but the values are below average in the EB87 Core (Figure 6.5). Si/Al and K/Al are generally below average shale values for both cores in ORB 5 (Figure 6.5). For ORB 4, values of Si/Al, Ti/Al, Zr/Al, and K/Al are generally less than average shale in both cores (Figure 6.5). In ORB4, Rb/Al is higher than average shale in the SQ1 Core but lower in the EB87 Core (Figure 6.5). Generally, Al-normalised Si, Ti, Zr, and K are about the same or lower than average shale between ORBs 4 and 5 in both cores (Figure 6.5). Conversely, Rb/Al is higher than average shale in SQ1 and around average shale in EB 87 in between ROBs 4 and 5 (Figure 6.5).

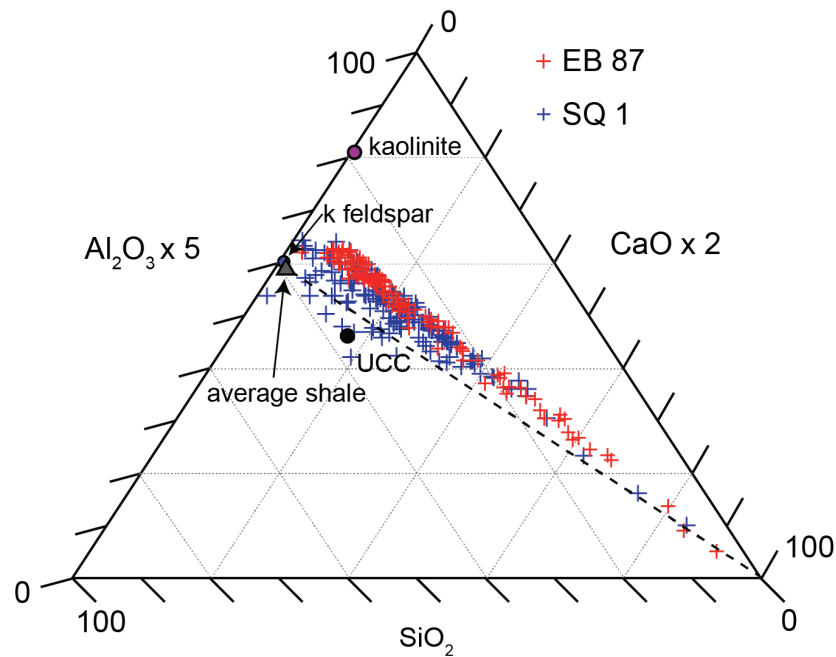


Figure 6.4. Ternary diagram (Brumsack, 1989) displaying the relative contributions of clay (Al_2O_3), quartz/biogenic silica (SiO_2), and carbonate (CaO) of all samples. Blue and red crosses depict the SQ1 and EB87 data, respectively. Axes are scaled to improve display of the data. Average shale (Wedepohl, 1991), upper continental crust (UCC; Rudnick and Gao (2003)), K-feldspar and kaolinite are plotted for reference. Dashed line shows the average shale–carbonate mixing line. Blue and red crosses depict the SQ1 and EB87 data, respectively.

Each trace element has a unique sensitivity to ambient redox conditions and affinity to organic matter or hydrogen sulphide, and application of these trace metal proxies enables us to reconstruct palaeo-redox conditions. In the present study, we are specifically concerned with the application of these proxies but we refer to (Calvert and Pedersen, 2007, Tribouvillard et al., 2006, Brumsack, 2006) for further details and discussion on trace element sequestration. In both the SQ1 and the EB87 Cores, the Al-normalised ratios of the redox-sensitive elements (Fe, Mn, As, Cu, Mo, U, V, and Zn) are generally higher and more variable within ORBs 4 and 5 but are generally lower and markedly more uniform in between the ORBs (Figure 6.6). However, the baseline values in EB87 are slightly higher than in the SQ1 Core. See appendices for data tables.

Linear sedimentation rates (LSRs) were calculated for the *wheatleyensis*, *hudlestoni*, and *pectinatus* biozones for both cores. For the SQ1 Core, the LSRs were 10.1, 9.0, and 7.3 cm/ky,

respectively. For the EB87 Core, the LSRs were 6.6, 5.1, and 4.1 cm/ky for each biozone, respectively.

6.5 Discussion

6.5.1 Depositional controls in the UK Wessex and Cleveland Basins

In the Cleveland and Wessex Basins, ORB 4 comprises a mixture of detrital material, carbonate, and organic material. The detrital fraction constitutes sub-rounded quartz, feldspar, and titanium oxide grains, the clay minerals kaolinite and illite, and terrestrial Type III organic material (Macquaker and Gawthorpe, 1993, Lazar et al., 2015b, Atar et al., 2019). Authigenic kaolinite infills foraminifer tests in both sections (Atar et al., 2019, Macquaker and Gawthorpe, 1993). Carbonate is present as pristinely preserved coccoliths, foraminifera, calcispheres, and rhombohedral dolomite (Atar et al., 2019, Macquaker and Gawthorpe, 1993, Lazar et al., 2015b). The former three carbonate components are biological and formed in the ocean whereas the dolomite crystals are post-depositional and therefore do not reflect primary depositional conditions. The geochemical characterisation of the main constituents of the SQ1 and EB87 Core is illustrated by the SiO_2 , Al_2O_3 , and CaO ternary plot (Figure 6.4), where SiO_2 represents quartz and/or biogenic silica, Al_2O_3 denotes clay, and CaO indicates carbonate (after Brumsack, 1989). The higher degree of scatter for the SQ1 Core samples indicates an overall more heterogeneous lithology than in the EB87 Core (Figure 6.4). Samples that plot above the line towards higher Al_2O_3 fractions may indicate either a higher degree of chemical weathering or a higher clay to quartz (or biogenic silica) ratio.

Petrographic observations of wispy algal macerals and high $\delta^{13}\text{C}_{\text{org}}$ values (Figure 6.3) in the EB78 core indicate that the dominant source of carbon in ORBs 4 and 5 is Type II marine organic material. In between the ORBs, the organic material occurs as equant lumps and lower $\delta^{13}\text{C}_{\text{org}}$ indicate a more dominant Type III terrestrial organic matter source. The isotope trends in the SQ1 are similar to that of the EB87 Core, in that they are more positive in the ORBs than in the intervals between. We interpret this to indicate shifts in the dominant sources of organic carbon between the ORBs and intercalated sediments in the SQ1 Core. The changes in organic material type throughout both sections (Figure 6.3) suggest higher primary productivity during deposition of the ORBs, which may have resulted from mixing of the water column associated with higher depositional energies, higher nutrient supply from enhanced continental weathering, or both. Another option is stratification of the water column resulting in a more anoxic/euxinic lower water column which enhances the preservation of OC at the sediment/water interface.

As expected, the terrigenous components in both cores decrease as the biogenic components increase (Figure 6.5). The terrigenous components may be diluted by the biological components at times of high productivity. Alternatively, the lower detrital contents in the ORBs may represent times where the supply of detrital material dwindled. However, distance

from the terrigenous sediment source is difficult to constrain in an epicontinental seaway due to low bathymetric gradients, imprecise estimations of water depths, palaeogeographical reconstructions (Schieber, 2016b) and only weakly constrained fluctuations of bulk sedimentation and compound accumulation rates. Based on these limitations we conclude that it is not possible to confidently discern these control mechanisms with the present dataset.

Depth plots of geochemical indicators at both sites for coarser grain sizes/higher amounts of heavy minerals (Figure 6.5; Al-normalised Si, Ti, and Zr; (Schnetger et al., 2000) are generally lower than average shale. However, the site of deposition of SQ1 in the Wessex Basin experienced overall higher but also more variable energetic conditions during the deposition of the ORBs. Quartz (Si) and heavy mineral enrichment (zircon, Ti-minerals) can occur either by a winnowing effect due to a higher depositional energy as a result of stronger ocean currents or by a preferential transport of these minerals due to a higher wind strength on the continent. The same indicators are lower in the sediment deposited in between the ORBs, consistent with deposition of finer-grained sediment under more quiescent conditions. In contrast, depositional energy indicators are consistently lower in EB87 than in SQ1 (Figure 6.5), supporting the interpretation of the ternary diagram where all samples are richer in Al and poorer in Si in EB87 than in SQ1 (Figure 6.5). Relative enrichments of Al-normalised Si, Ti, and Zr ratios within the ORBs (Figure 6.5) suggest that depositional energies were elevated and variable during deposition of these intervals in both the Cleveland and Wessex Basins, which is further supported by petrographic evidence of normally-graded erosional beds of ORB 4. The higher energy and coarser grain sizes in the Wessex Basin may result from winnowing of the sediment by bottom currents and/or wave activity reaching the seafloor.

In contrast to the coarse grain size-/heavy mineral-bound elements Si, Ti and Zr, the abundance of K and Rb in marine sedimentary rocks is related to sediment provenance and/or weathering rates on the adjacent sediment because they are (like Al) commonly associated with fine-grained/lower-density terrigenous minerals like K-feldspar and clay minerals (Calvert and Pedersen, 2007, Grygar et al., 2019). Sediment routing systems and weathering rates are both affected by climate-driven processes, so K/Al and Rb/Al ratios can be used to infer changes in climatic conditions and processes on landmasses adjacent to depositional basins. The similarity between these ratios in both cores (Figure 6.5) therefore indicates the same overarching processes being responsible for their down-core patterns in both the Wessex and the Cleveland Basins. While the elements/proxies discussed so far behave biogeochemically conservatively and are mainly affected by physical processes in the depositional environment (with the exception of K and Rb), selected trace elements behave differently under different redox conditions. In general, most redox-sensitive/sulphide-forming trace elements (e.g. As, Mo, U, V, Cu, and Zn) are enriched under anoxic (oxygen-free) to euxinic (anoxic and sulphidic) sediment pore and bottom water conditions; this is due to

several mechanisms, including association of the trace elements to organic material and formation of sulphide minerals (Calvert and Pedersen, 2007, Tribovillard et al., 2006, Brumsack, 2006). Generally, during low oxygen depositional conditions Mn is depleted whereas under oxic conditions Mn/Al in ocean sediments is close to average shale or above (Brumsack, 2006). Relatively low values of Mn/Al (Figure 6.6) indicate sediment pore waters were suboxic for most of the deposition of both successions.

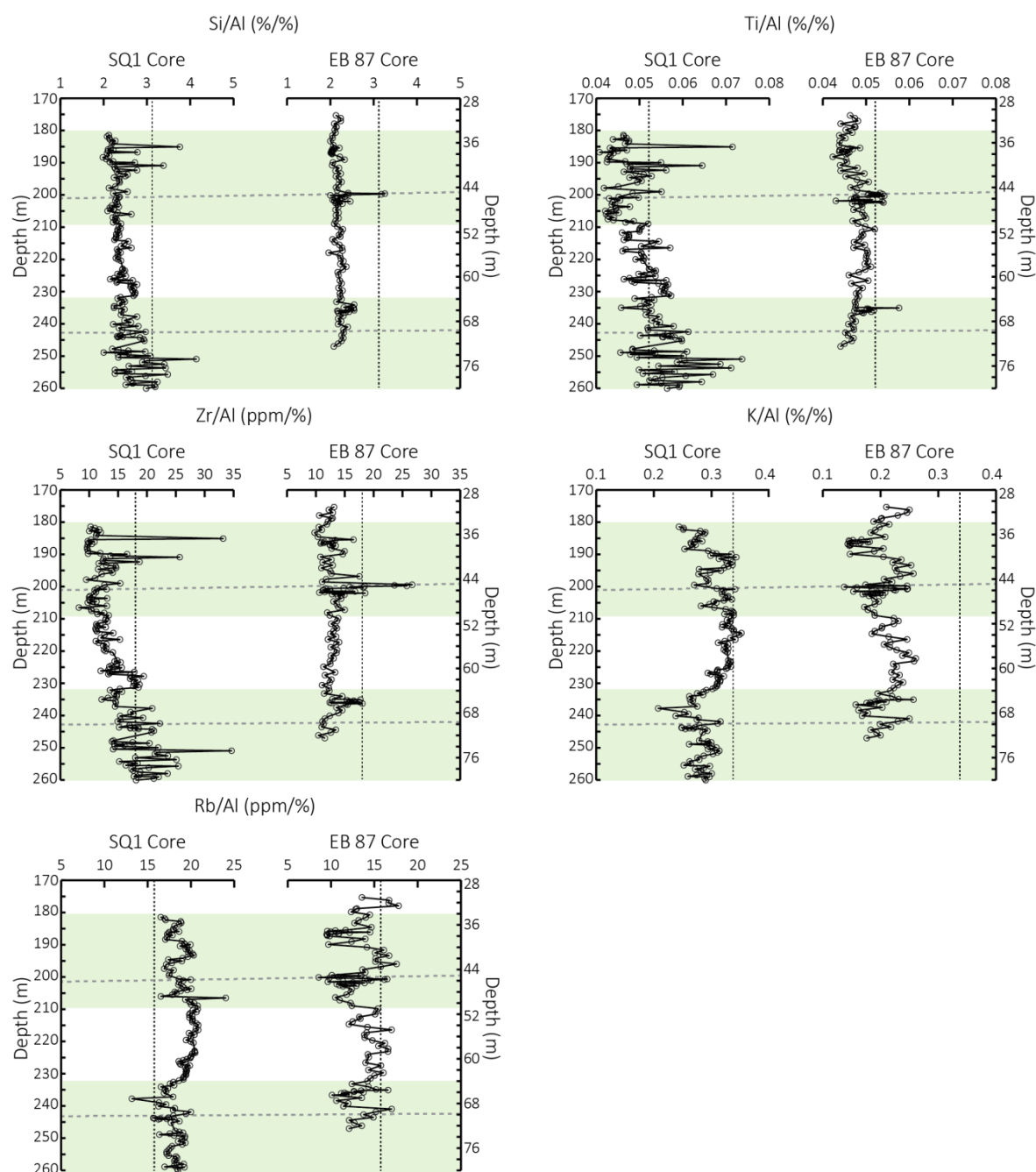


Figure 6.5. Depth plots of depositional energy and continental weathering indicators (Al-normalised Si, Ti, Zr, K, and Rb) for the Swanworth Quarry 1 and Ebberston 87 Cores. Vertical dashed lines indicate average shale values (Wedepohl, 1991). Depths are in metres below surface. Horizontal dashed lines mark biostratigraphical zonation ties. Green panels depict 'Organic Rich Bands' 4 (lowermost) and 5 (uppermost) defined by Cox and Gallois (1981). Data for the Ebberston 87 Core is from Atar et al. (2019).

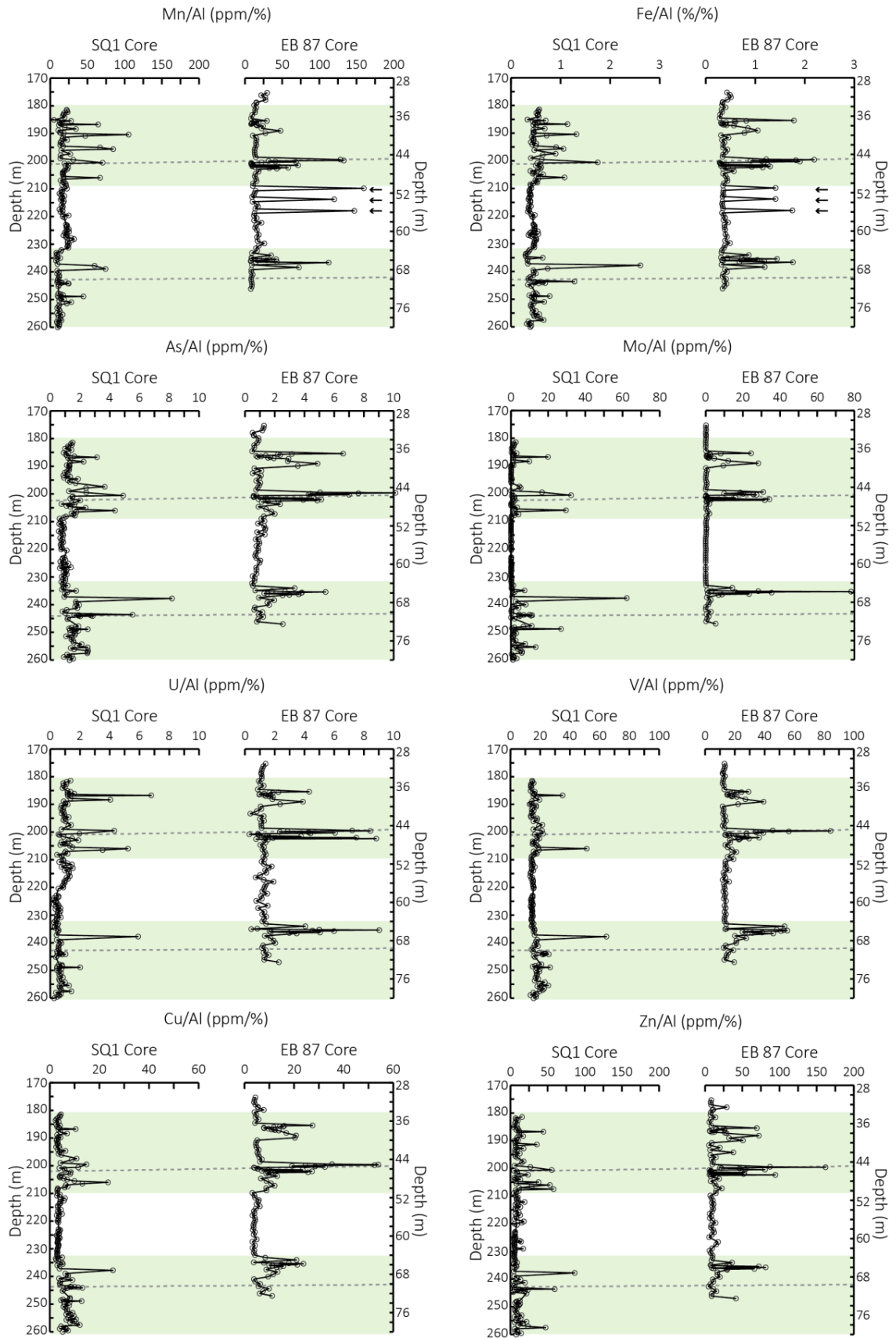


Figure 6.6. Depth plots of redox indicators (Al-normalised Mn, Fe, As, Mo, U, V, Cu, and Zn) for the Swanworth Quarry 1 and Ebberston 87 Cores. Depths are in metres below surface. Horizontal dashed lines mark biostratigraphical zonation ties. Vertical dashed lines indicate average shale values (Wedepohl, 1991). Green panels depict 'Organic Rich Bands' 4 (lowermost) and 5 (uppermost) defined by Cox and Gallois (1981). Data for the Ebberston 87 Core is from Atar et al. (2019).

Repeated enrichments compared the average shale level of redox-sensitive/sulphide-forming trace elements (As, Mo, U, V, Cu, and Zn: Figure 6.6) in line with a depletion in Mn within the ORBs demonstrate that pore and bottom water conditions were anoxic to euxinic, at least episodically, in both the Wessex and Cleveland Basins. This is supported by organic carbon enrichments because its preservation is enhanced by an absence of oxygen and the presence of hydrogen sulphide at the seafloor. However, values approaching average shale for the Mn/Al ratio within the ORBs in both sections and parallel low element/Al ratios of redox-sensitive/sulphide-forming trace elements (As, Mo, U, V, Cu, and Zn) indicate repeated phases of oxic bottom water conditions (Figure 6.8). In EB87, such oxic incursions are supported by petrographic evidence that reveals co-occurrence between relatively elevated Mn contents, agglutinated foraminifera, and pristinely preserved carbonate (coccolith) material (Atar et al., 2019). Repeated fluctuations between oxic and anoxic/euxinic redox conditions may result from storm activity mixing and ventilating the water column as evidenced by normally-graded beds with erosional bases within the ORBs, which point towards the remobilisation and lateral transport of sediment (Lazar et al., 2015b). In the interval between ORBs 4 and 5, both cores exhibit much less variation, representing overall more stable redox conditions. The low concentrations of redox sensitive/sulphide-forming trace elements (Figure 6.6) and TOC (Figure 6.3), along with slightly elevated Mn/Al values (Figure 6.6), support that the bottom waters of the Wessex Basin were suboxic during this interval. In contrast, in the correlative interval in EB87, As and U are slightly enriched and Mn is low (Figure 6.6), suggesting that pore waters were suboxic-anoxic in the Cleveland Basin (Figure 6.8).

Active bottom water currents/wave action, as previously indicated by Si/Al, Ti/Al and Zr/Al ratios, would have increased bottom water ventilation, which may account for the suboxic bottom water conditions observed in the Wessex Basin between the ORBs. The particulate shuttle is significant in the transfer of trace metals from the water column to the sediment in some depositional settings (Algeo and Tribovillard, 2009, Goldberg, 1954, Tribovillard et al., 2015). Tribovillard et al. (2015) use Mo, As, and Sb as proxies for the presence of an Fe-Mn particulate shuttle, which involves the oxidation of Mn^{2+} in the surface waters, the reaction with Fe^{2+} to form (oxyhydr)oxides, adsorption of trace elements to the (oxyhydr)oxides, and the subsequent sinking of them. In anoxic-euxinic settings, the (oxyhydr)oxides are reduced, the Mn^{2+} diffuses back to the surface waters, and the Fe^{2+} reacts to form Fe sulphide minerals (e.g. pyrite) (Canfield et al., 1992, Dellwig et al., 2010, Huckriede and Meischner, 1996, Neretin et al., 2004). Atar et al. (2019) concluded that a Mn-Fe particulate shuttle was intermittently active in the Cleveland Basin during the deposition of the ORBs (Figure 6.7). The SQ1 data (Figure 6.7) show that a particulate shuttle was also active intermittently during deposition of the ORBS but that suboxic conditions were likely limited to the sediment pore waters during deposition in between the ORBs in the Wessex Basin.

Pertinent to assessing interconnectivity of sub-basins within an epicontinental seaway is the relative degree of water-mass restriction within each of these sub-basins. Trace element ratios, specifically Mo and U, can be used to assess hydrographic restriction of a basin because of their respective redox behaviours (Algeo and Tribovillard, 2009)(Figure 6.7). Molybdenum is quantitatively removed from the water column under moderately to strongly euxinic conditions, much more so than U. Conversely, under suboxic conditions, U is likely to be enriched as it becomes trapped at the Fe(II)/Fe(III) redox boundary (Algeo and Tribovillard, 2009, Tribovillard et al., 2012). Atar et al. (2019) concluded the Cleveland Basin was unlikely to have been restricted for prolonged periods of time, if at all. This agreed with previous studies that concluded prolonged restriction of the Wessex Basin was also unlikely (Tribovillard et al., 2012, Pearce et al., 2010). Data from the present study (Figure 6.7) also align with this; high enrichments of Mo relative to U indicate intermittently strongly euxinic conditions during the deposition of the ORBs in the Wessex Basin. Such enrichments would have required a connected water mass to resupply the Mo, which is indicated by values around three times that of seawater (Figure 6.7).

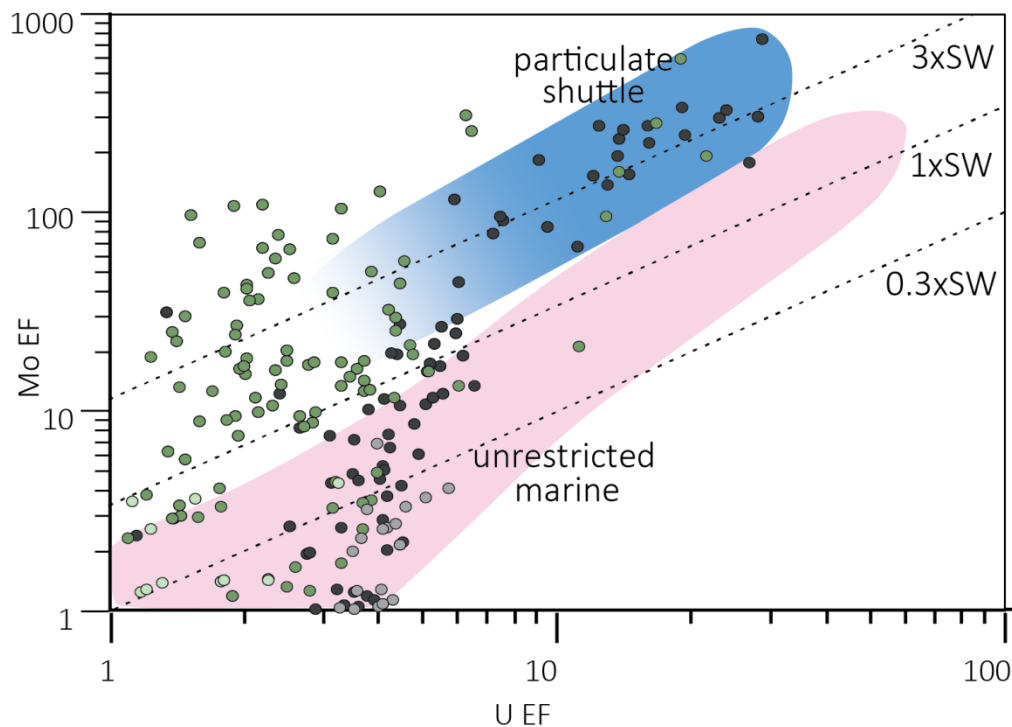


Figure 6.7. Plot of Mo EF against U EF calculated relative to Post Archean Average Shale (PAAS; Taylor and McLennan (2001)(after Tribovillard et al., 2012). Samples from Organic Rich Bands (ORBs) 4 and 5 from the SQ1 and EB87 Cores are indicated by dark green circles and dark grey circles, respectively. Samples in between the ORBs in the SQ1 and EB87 Cores are depicted by pale green circles and pale grey circles, respectively. Dashed lines are modern day seawater, 0.3 x modern day seawater and 0.1 x modern day seawater values shown for reference. The particulate shuttle is mapped in blue and unrestricted marine setting is mapped in pink. Axes are logarithmic.

Overall, our observations align with the hypothesis that sediment deposition in the Laurasian Seaway took place under the influence of tropical conditions that resulted from an expanded or migrated Intertropical Convergence Zone (Armstrong et al., 2016). We suggest that during the deposition of ORBs 4 and 5, elevated production and preservation of organic carbon was promoted by an enhanced nutrient supply through continental weathering and water column mixing during storm events, which resulted from tropical-like climate conditions. Regional sea level has been reconstructed through the application of sequence stratigraphy to the coastal section in Boulonnais (France). Biostratigraphic correlation of the Wessex and Cleveland Basin deposits to the Boulonnais section reveals that ORBs 1–5 do not correlate to fluctuations in sea level, so this cannot be the primary driver of coeval organic carbon variability across the seaway (Herbin et al., 1995). Herbin et al. (1995) instead concluded that sea level worked in conjunction with overarching climate conditions to facilitate the repeated organic carbon enrichments.

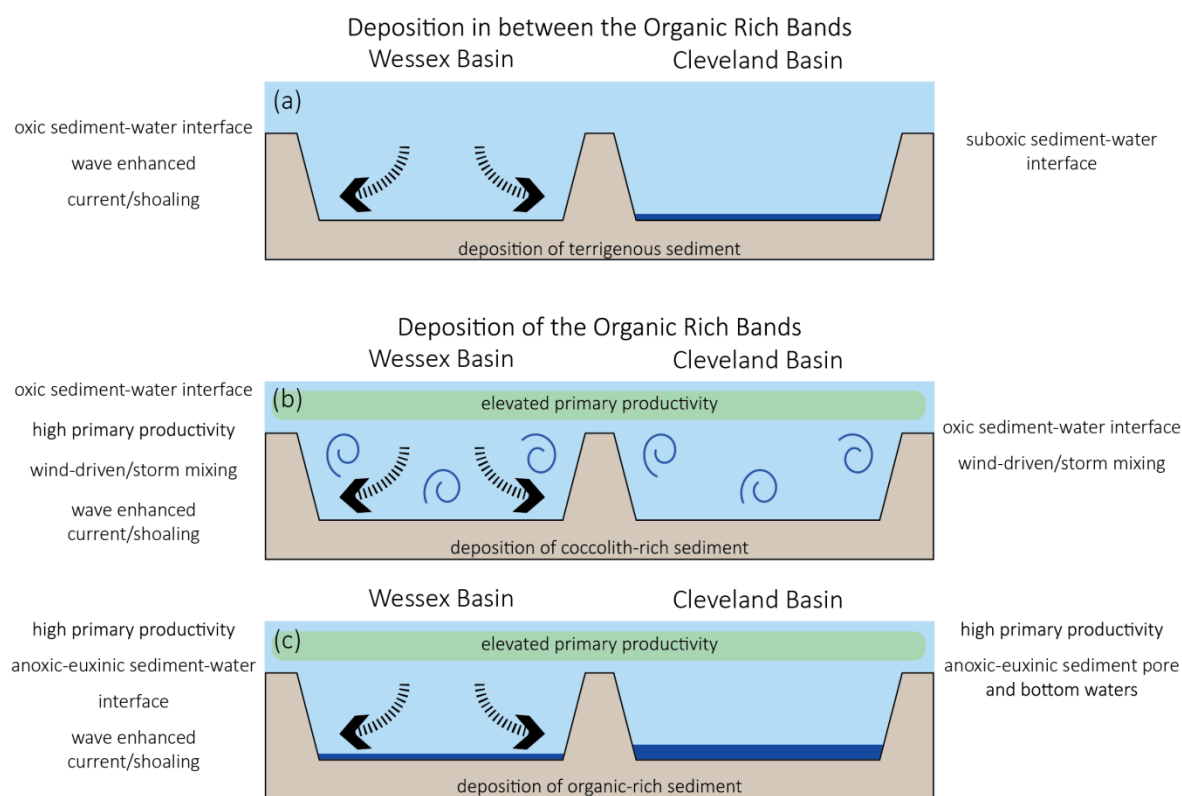


Figure 6.8. Schematic diagram showing the differences between the Wessex and Cleveland Basins during the deposition of the Organic Rich Bands and the interval in between. Black dashed arrows denote the presence of bottom currents/shoaling.

6.5.2 Chemostratigraphic cross-seaway correlation

The use of ammonite biostratigraphy in the correlation of Jurassic deposits across Northwest Europe is a well-established method (Jenkyne, 2003, Cope, 2009). It is generally more successful when conducted on well-exposed outcrops where the chance of finding specimens is maximised through following laterally extensive beds. This is not the case for drill wells, thus the chances of finding a relevant specimen in a five-centimetre drill core is markedly less

compared to extensive outcrops. This poses a challenge when conducting high resolution correlations between two biostratigraphically constrained cores, as in the present study.

The biostratigraphic ties between the SQ1 and EB87 Cores are marked by grey dashed lines on relevant figures. As discussed, the geochemical indicators bare a remarkable similarity to one another. However, when considering the geochemical plots relative to the biostratigraphical boundaries, there is a slight offset between the two cores around the *huddlestoni* and *pectinatus* ammonite zone boundary. This may result from a difference in thickness of the sediment deposited in the two basins, where the EB87 Core may exhibit a more condensed section relative to the SQ1 Core due to a difference in sedimentation rates and processes. Alternatively, the slight offset in geochemical profiles between the two cores may result from diachronous sedimentary processes which would be driven by variations in climate and/or sea level. Further, the fauna used to date these sediments may have migrated temporally, which could lead to an offset between the biostratigraphic ages in the two cores. Finally, the SQ1 Core has been extensively studied so sampling depths of the core may have been disrupted during storage over the past ten years. It is difficult to determine whether or not the observed offset is due to erroneous biostratigraphy through either lack of appropriate specimens or temporal migration of fauna, or whether it records a true offset between environmental conditions, with the present dataset. However, given the slight nature of the offset, and considering the age of the studied sedimentary rocks, the apparent anomaly is not significant enough to discredit the comparison between the two sections.

In an attempt to correlate sections at greater resolution, biostratigraphy was paired with TOC data to correlate five broad bands of organic carbon enrichment across the Wessex and Cleveland Basins; these ORBs occur on a metre to decimetre scale (Gallois, 1979). However, TOC data cannot be used to correlate the sections at a higher resolution, i.e. centimetre scale, owing to the labile nature of organic material (Jenkyns et al., 2002). Organic material is highly susceptible to degradation in the presence of oxidants, therefore very specific local conditions are required to preserve significant amounts of it. Furthermore, TOC contents are affected by sedimentation rate and primary productivity, both of which are influenced by a range of factors such as nutrient supply and ocean circulation. To mitigate this challenge, ratios of elements with biogeochemically and hydrodynamically conservative behaviour must be used instead. Potassium and rubidium are strong candidates for this as changes in the Al ratios of both of these elements is dependent upon weathering on adjacent hinterlands (Grygar et al., 2019).

Similarities between the Wessex and Cleveland Basins are clear; both settings underwent intervals of enhanced primary productivity and organic matter preservation. In both sections, these intervals were highly dynamic and oscillated between fully oxic to euxinic sediment pore and bottom waters during periods of enhanced depositional energies. However, the

grain size indicators (Figure 6.5) demonstrate that deposition in the Wessex Basin occurred under much higher energy conditions relative to the Cleveland Basin. Despite this, overarching climate processes are still recognisable in the K/Al and Rb/Al trends of both cores, implying that we can in principle use inorganic geochemical data sets to unpick large-scale climate controls, such as precipitation over adjacent land, across seaways.

Provenance/weathering indicators, specifically K/Al and Rb/Al, are uniform across the UK sector of the Laurasian Seaway and are controlled by the same, large-scale climate factors in both basins. Consequently, the expected/assumed synchronicity between the K/Al and Rb/Al profiles can be used to improve the age model proposed from biostratigraphy. In this instance, chemostratigraphy should complement biostratigraphy, which has been shown to be particularly useful when working with core material (e.g. Turner et al., 2016). Furthermore, this provides a robust tool when sedimentation rates are known to differ between depositional settings, and when the application of cyclostratigraphy to the studied sections is not statistically robust due to a limited number of sampled cycles.

6.6 Conclusions and implications

- The depositional environment in the Wessex and Cleveland Basins, 400 km apart, were remarkably similar during the Late Jurassic.
- Geochemical and petrographic data agree that depositional energy was more variable and slightly higher in the Wessex Basin than in the Cleveland Basin in ORB 4.
- Redox conditions during deposition of the two sediment intervals were similar in that during the ORBs, both sub-basins experienced fluctuations between oxic and euxinic conditions. However, in the Wessex Basin, the anoxic-euxinic periods were shorter and less sustained than in the Cleveland Basin. The interval between ORBs 4 and 5 was predominantly suboxic in both the Wessex and Cleveland Basins.
- Overarching warm and wet tropical climate conditions were likely responsible for sedimentation across the UK sector of the Laurasian Seaway in the Late Jurassic.
- Varying element/Al ratios, in this particular study K/Al and Rb/Al ratios, are valuable chemostratigraphic correlation tools in environments with differing depositional energies, in particular when studying drill cores.

This study demonstrates the value of studying time-equivalent but geographically distant sediment cores when investigating large scale depositional processes, particularly in settings such as epicontinental seaways that exhibit high resolution records.

7 | Organic carbon enrichments in the northern Lurasian Seaway (Svalbard) during the Late Jurassic

Chapter Summary

Petrographic observations and geochemical data are presented for the upper Oppdalsåta and lower Slottsmøya Members of the Agardhfjellet Formation. This interval is contemporaneous to the interval discussed in the preceding chapters. Organic carbon (OC) is predominantly terrestrial Type III and sedimentation occurred in a deltaic depositional environment so OC enrichment is the product of continental weathering and transport of OC from land to the ocean. Carbon isotopes reflect a global signal that is identified in other sites around the world, ruling out an OC type control on carbon isotopes (as discussed in the previous two chapters).

7.1 Introduction

Through Earth history, climate, sea level, and tectonics exert fundamental controls on the deposition of sediments in marine basins, and their combined effects often translate into the sedimentary record. Investigating the nature and chemical composition of sediment can unravel the underlying environmental processes and mechanisms, and can therefore give unique insight into the local and global scale factors influencing sedimentation (Tribovillard et al., 2016, Brumsack, 2006). Sedimentary rocks are invaluable archives of these variable and coupled Earth system processes so studying them is a window into the past.

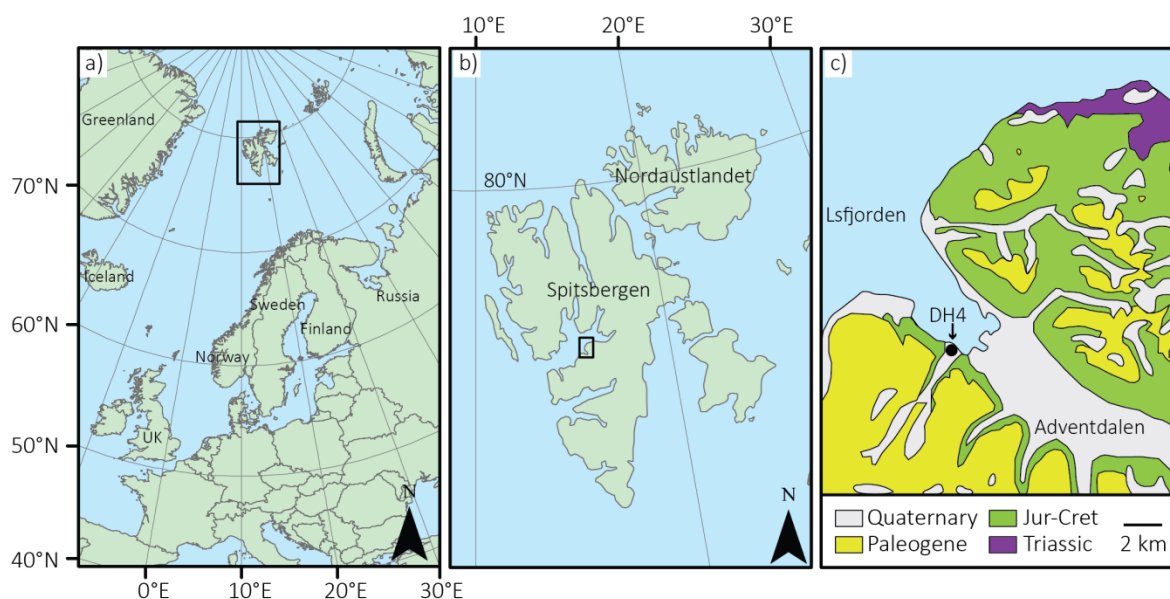


Figure 7.1. a) Map showing the position of the Svalbard Archipelago (black box) in the Arctic Circle. b) Location of the Adventdalen (black box) on Spitsbergen Island. c) Location of the DH4 well on an Adventdalen geological map. Redrawn after Koevoets et al. (2016).

High latitude regions are known to be particularly sensitive to subtle changes in climate, e.g., changes in atmospheric temperature or moisture, so constraining the effects that past intervals of higher than present atmospheric CO₂ levels had on high latitude ocean basins is pertinent to improving future climate predictions. Moreover, a large proportion of Jurassic sedimentary rocks deposited at palaeo-high latitudes is enriched in organic carbon, e.g. Bazhenoc and Ringnes Formations (Leith et al., 1993). Understanding the processes behind past organic carbon enrichments in environments that are oligotrophic and well-ventilated in the modern-day gives insights into the global carbon cycle and can be used in hydrocarbon exploration therefore is of both scientific and economic interest. Deposits of past high latitude oceans are particularly well preserved on the Arctic archipelago of Svalbard, which is where the studied sediment successions were recovered. The Agardhfjellet Formation is an organic-rich succession dominated by mudstone, which was deposited in the northernmost part of the Laurasian Seaway during the Late Jurassic-Early Cretaceous (Koevoets et al., 2016, Koevoets et al., 2018, Dypvik, 1984, Dypvik, 1978, Dypvik, 1980, Hvoslef et al., 1986). Inorganic geochemical data and petrographic observations are presented for the middle two

members of the Agardhfjellet Formation: the Oppdalsåta and Slottsmøya Members. These members are time equivalent to the sedimentary rocks discussed in the chapters 4, 5, and 6, in which petrographic and geochemical data point towards an overarching climate process controlling OC-enrichment and sedimentation across the southern Lurasian Seaway at mid-latitudes. This chapter looks at controls on sedimentation at the northern end of the Lurasian Seaway and the data are used to establish the local and global scale controls on sedimentation of these at high latitude deposits.

7.2 Geological setting

The studied core was drilled near Longyearbyen, Spitsbergen, on the Svalbard Archipelago located between 76–80° N and 10–30° E, on the western margin of the Barents Sea (Figure 7.1). Svalbard has a complex geological history; the crystalline basement comprises Precambrian and Early Palaeozoic metamorphic rocks and is overlain by Devonian to Quaternary sedimentary strata (Braathen et al., 2012, Bergh et al., 1997). This study is concerned with the Upper Jurassic rocks that were deposited during a major marine transgression in the Late Jurassic to Early Cretaceous. On Svalbard, this event is represented by a siliciclastic succession organised into the Adventdalen Group.

Depth (mbs)	lithostratigraphic unit		Petrographic Description	
	Formation	Member	Facies	notes
504.52	Agardhfjellet	Slottsmøya	mSs	
504.75	Agardhfjellet	Slottsmøya	mSs	parallel lamination, erosional surface
507.00	Agardhfjellet	Slottsmøya	mSs	lenticular fabric (mud and sand lenses)
512.25	Agardhfjellet	Slottsmøya	sMs	peloidal lithic clasts
514.00	Agardhfjellet	Slottsmøya	sMs	
515.25	Agardhfjellet	Slottsmøya	mSs	
516.24	Agardhfjellet	Slottsmøya	sMs	
518.50	Agardhfjellet	Slottsmøya	mSs	lenticular fabric (mud and sand lenses)
519.25	Agardhfjellet	Slottsmøya	mSs	discontinuous wavy non parallel lamina
522.75	Agardhfjellet	Slottsmøya		wavy continuous parallel lamina
523.25	Agardhfjellet	Slottsmøya	mSs	
526.25	Agardhfjellet	Slottsmøya		
529.50	Agardhfjellet	Slottsmøya	mSs	lenticular fabric (mud lenses)
530.50	Agardhfjellet	Slottsmøya	mSs	parallel lamination
531.00	Agardhfjellet	Slottsmøya	mSs	discontinuous, wavy, non-parallel lamina
535.75	Agardhfjellet	Slottsmøya	mSs	

Table 7.1. Summary table of the petrographic study conducted on the Slottsmøya Member of the Agardhfjellet Formation. mSs = muddy sandstone, sMs = sandy mudstone.

The lower part of the Adventdalen Group is called the Janusfjellet Subgroup, which is further divided into the older Agardhfjellet and younger Rurikfjellet Formations. The Agardhfjellet Formation is subdivided into the Oppdalen, Lardyfjellet, Oppdalsåta, and Slottsmøya Members (Koevoets et al., 2016, Braathen et al., 2012). The Agardhfjellet Formation is broadly coeval to the prolific source rocks found across Europe; namely the Kimmeridge Clay Formation (UK sector), Draupne and Heather Formations (Norwegian Sea), Mandal and Farsund Formations (Danish sector), and Hekkingen Formation (Barents Sea).

Depth (mbs)	lithostratigraphic unit		Petrographic Description	
	Formation	Member	Facies	notes
540.26	Agardhfjellet	Oppdalsåta	mSs	
540.50	Agardhfjellet	Oppdalsåta	mSs	
541.00	Agardhfjellet	Oppdalsåta	cMs	small calcite veins
542.75	Agardhfjellet	Oppdalsåta	cMs	occasional silt lenses
547.50	Agardhfjellet	Oppdalsåta	Ss	
548.25	Agardhfjellet	Oppdalsåta	mSs	discontinuous, wavy, non-parallel lamina
551.50	Agardhfjellet	Oppdalsåta	mSs	discontinuous, wavy, non-parallel lamina
552.00	Agardhfjellet	Oppdalsåta	mSs	occasional mud lenses
552.75	Agardhfjellet	Oppdalsåta	mSs	lenticular fabric (mud lenses)
553.24	Agardhfjellet	Oppdalsåta	mSs	
553.75	Agardhfjellet	Oppdalsåta	mSs	lamination
555.75	Agardhfjellet	Oppdalsåta	mSs	lenticular fabric (silt lenses)
556.75	Agardhfjellet	Oppdalsåta	Ss	discontinuous, wavy, non-parallel lamina
558.50	Agardhfjellet	Oppdalsåta	mSs	
559.75	Agardhfjellet	Oppdalsåta	Ss	mud lenses
561.05	Agardhfjellet	Oppdalsåta	mSs	mud lenses
562.00	Agardhfjellet	Oppdalsåta	mSs	discontinuous, wavy, non-parallel lamina
563.25	Agardhfjellet	Oppdalsåta	mSs	discontinuous, wavy, non-parallel lamina

Table5.1. Summary table of the petrographic study conducted on the Oppdalsåta Member of the Agardhfjellet Formation. mSs = muddy sandstone, sMs = sandy mudstone. Ss = sandstone, cMs = coarse mudstone

The studied core, DH4, is one of four cores (DH1-4) drilled as part of the CO₂ sequestration project, which aimed to assess the capabilities of the regional geology of Longyearbyen as a potential CO₂ subsurface storage site (Braathen et al., 2012). The DH4 Core was drilled in Adventdalen, in c. 40 m distance from the DH5R core discussed by Koevoets et al. (2018). The biostratigraphic framework of the DH2 and DH5 cores is discussed by Koevoets et al. (2016). We sampled the upper Oppdalsåta and lower Slottsmøya Members of the Aghardfjellet Formation from the DH4 Core. We define the top of the Oppdalsåta member in the DH4 log, which is characterised by a sandstone unit in the DH5R core (Koevoets et al., 2016), at 534 m in the DH4 well based on the change in gamma-ray log response for the well (Braathen et al., 2012). The Oppdalsåta Member is organised into several cycles comprised basal mud and siltstones that grade upwards over ca. 10 m into very fine-grained burrowed sandstone (Koevoets et al., 2016). The overlying Slottsmøya Member comprises black and grey mudstones and siltstones with intercalated siderite and dolomite beds (Collignon and Hammer, 2012, Koevoets et al., 2016).

7.3 Methods and materials

A detailed methodology is presented in Chapter 2. 195 samples were collected from the DH4 Core, drilled in Adventdalen (Svalbard). Samples were analysed for total organic carbon (TOC) contents, and XRF for major and trace elements. Major and trace elements are expressed as wt % and ppm, respectively. See appendix F for geochemical data tables, appendix G for petrography, and appendices H and I for SEM images. 33 samples were selected analysed under optical light using a Leica DM750P microscope and a Hitachi SE-70 High Resolution Analytical Scanning Electron Microscope.

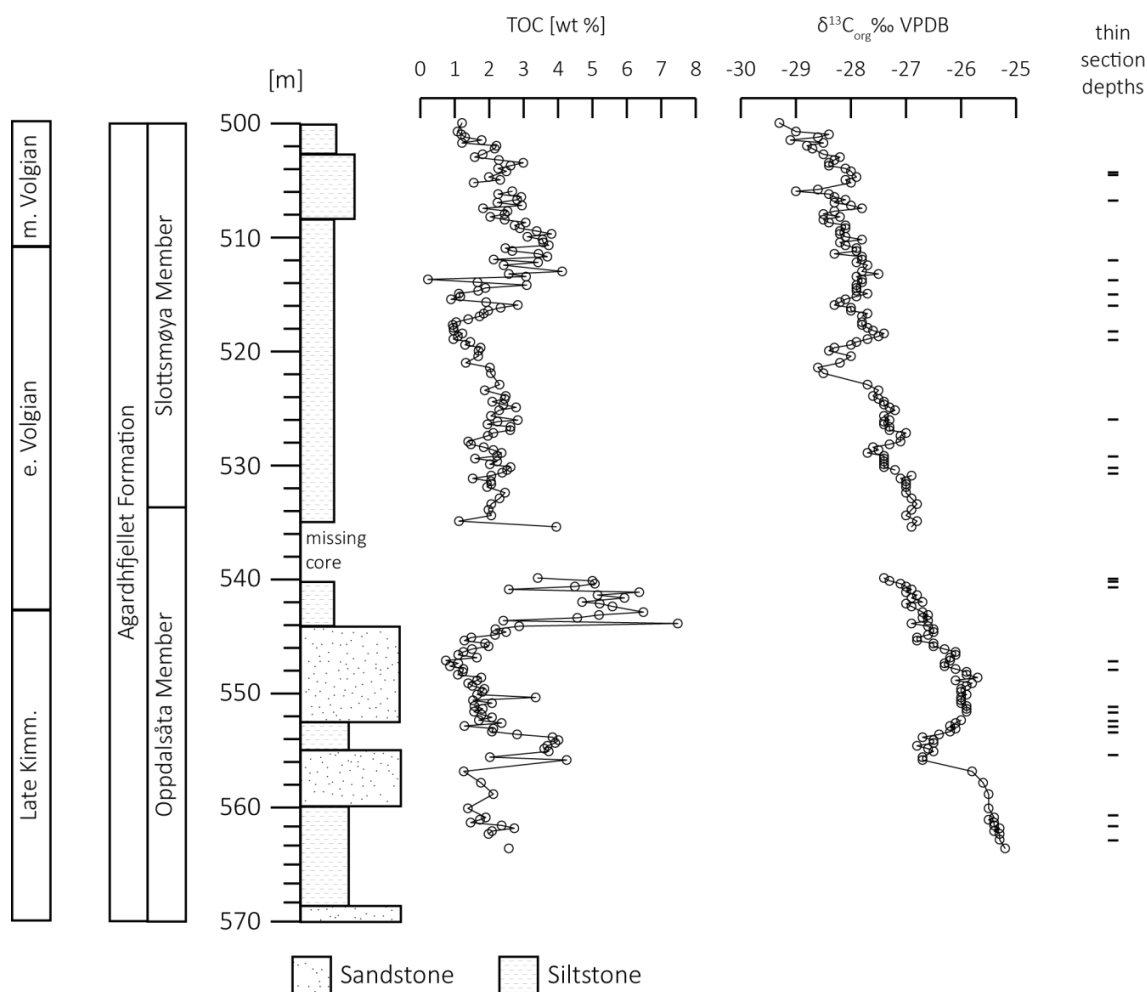


Figure 7.2. Lithological column of the studied section of the DH4 Core, with a depth plot for the total organic carbon (TOC) content and organic carbon isotope values ($\delta^{13}\text{C}_{\text{org}}$) generated in this study, and locations of samples prepared as thin sections intervals. Chronostratigraphic divisions after Koevoets et al. (2016).

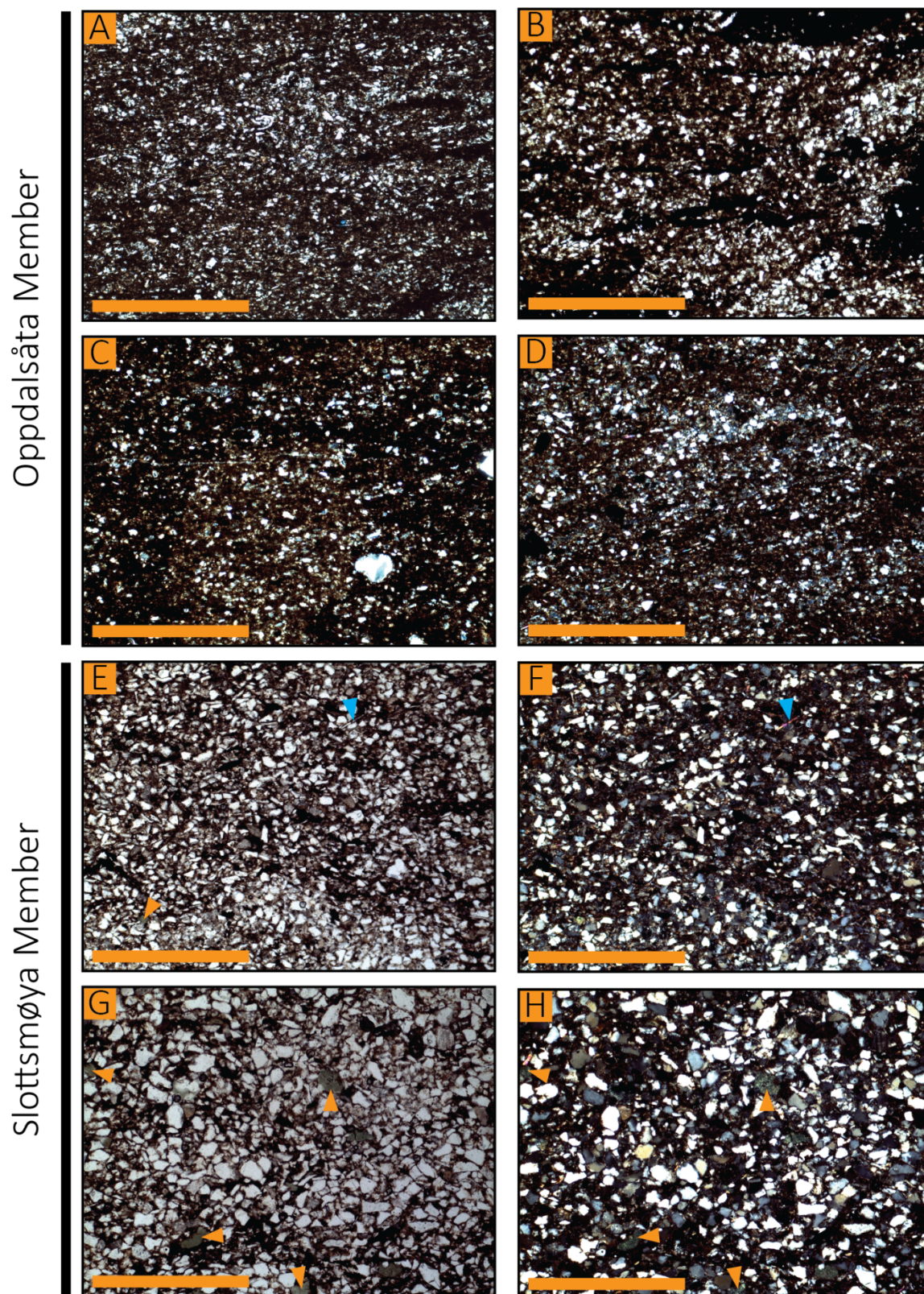
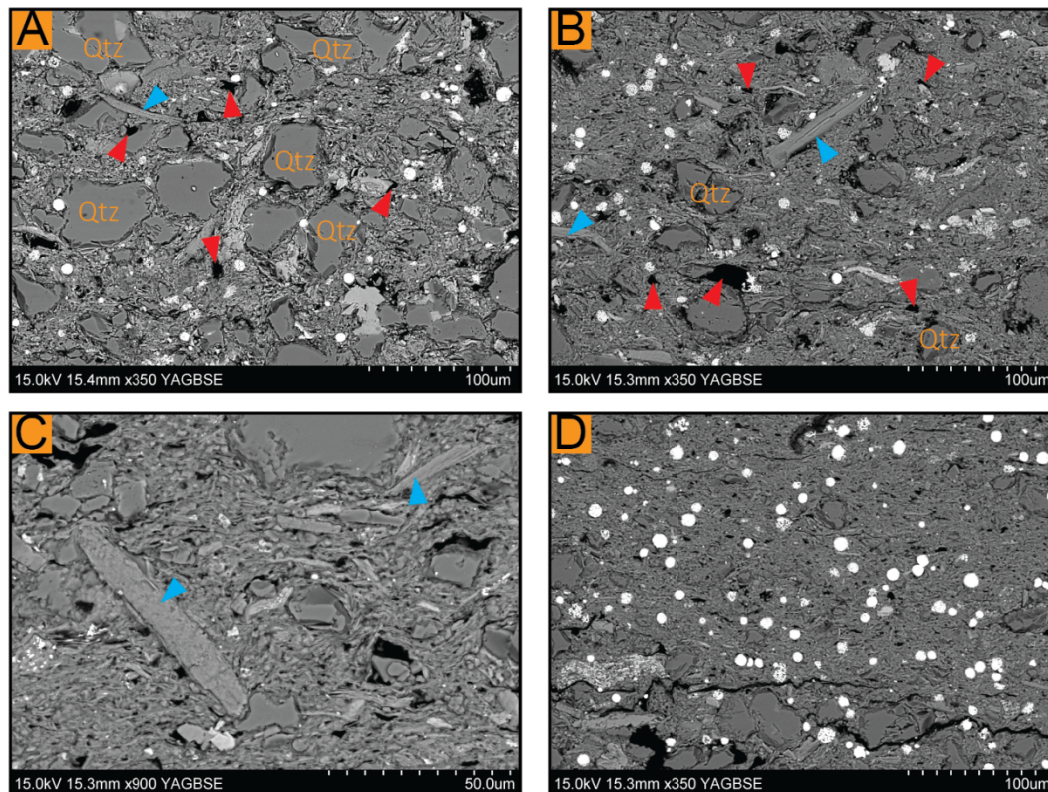


Figure 7.3 Optical micrographs of Oppdalsåta and Slottsmøya Members of the Agardhfjellet Formation. All scale bars = 1 mm. A) Sample 507.00 m, Oppdalsåta Member, plane-polarised light. B) Sample 515.25 m, Oppdalsåta Member, plane-polarised light. C) Sample 516.24 m, Oppdalsåta Member, cross-polarised light. D) Sample 526.25 m, Oppdalsåta Member, cross-polarised light. Note the fine grain size of the quartz in a mud-rich matrix in the Oppdalsåta Member samples. E) Sample 548.25 m, Slottsmøya Member, plane-polarised light. F) Same sample as E, cross-polarised light. G) Sample 556.75 m, Slottsmøya Member, plane-polarised light. H) Same sample as G, cross-polarised light. Note coarse grain size of the quartz grains. Yellow arrows point to glauconite grains, blue arrows point to muscovite grains.

Oppdalsåta Member



Slottsmøya Member

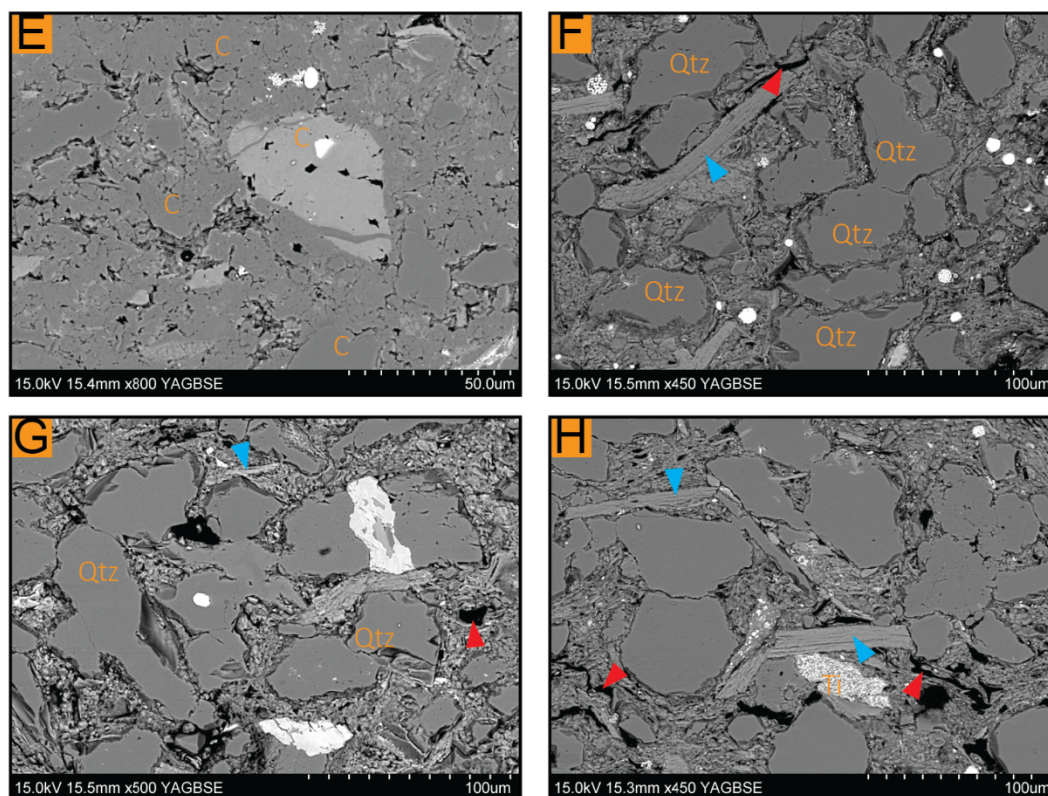


Figure 7.4. Backscattered scanning electron microscope images of the Oppdalsåta and Slottsmøya Members of the Agardhfjellet Formation. Red triangles point to equant organic matter, blue arrows point to muscovite grains, bright white objects are pyrite. Qtz = quartz. Ti – titanium oxide. C = carbonate. A) Sample 504.52 m, Slottsmøya Member. Angular grains float within an argillaceous matrix. B) Sample 507.00 m, Slottsmøya Member. C) Sample 512.25 m, Slottsmøya Member. D) Sample 526.25, Slottsmøya Member. E) Sample 541.00 m, Oppdalsåta Member. F) Sample 548.25, Oppdalsåta Member. G) Sample 551.00 m, Oppdalsåta Member. H) Sample 562.00 m, Oppdalsåta Member.

7.4 Results

7.4.1 Petrography

The studied interval is compositionally heterogeneous. The samples are comprised of varying proportions of a detrital clay mineral matrix and coarser detrital grains (Figure 7.5). The most abundant grains are quartz; they range from medium mud to sand size, are angular and exhibit low sphericity (Figure 7.3). Coarse mud-sized, subrounded alkali feldspar grains and lath-shaped muscovite grains (*ca.* 100 μm in length) are common throughout all samples but are most abundant in the coarser grained Slottsmøya Member

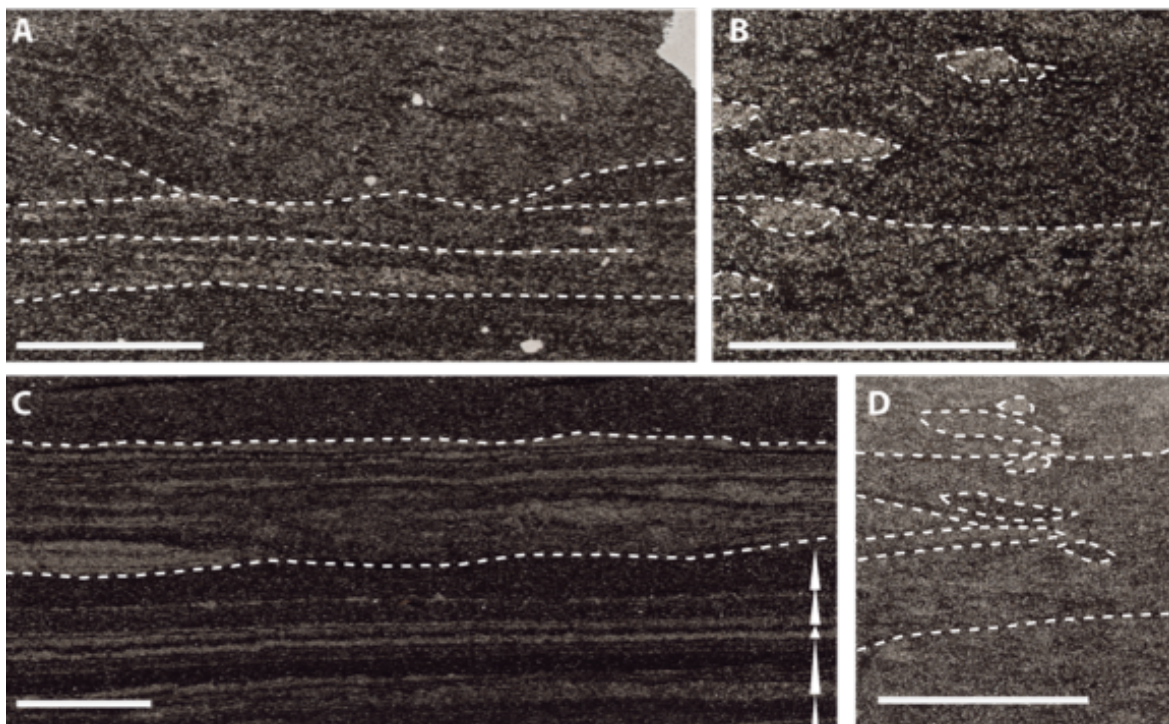


Figure 7.5. Optical light photography of thin sections. Scale bars = 5 mm. a) = Sample 504.75 m, Slottsmøya Member. Normally graded bed separate by erosional surfaces (marked by dashed lines). B) Sample 553.24 m, Oppdalsåta Member. Horizontal dashed white line marked erosional surface. Pale brown burrows are outlined by dashed white lines. C) sample 535.75 m, Oppdalsåta Member. Normally graded beds (white triangles) with erosional bases overlain by a discontinuous laminated bed. D) Sample 552.00 m, Oppdalsåta Member. Bioturbated muddy sandstone.

Occasional coarse, mud-sized, angular glauconite grains and coarse, mud-sized, angular siderite grains are observed throughout the studied interval. Medium, mud-sized titanium oxide grains (Figure 7.5) are dispersed throughout the interval, and pyrite occurs as framboids of up to 10 μm in diameter and locally as a replacement mineral. Dolomitic overprinting and cementation occurs throughout the samples. Organic carbon (OC) is finely disseminated throughout the interval and occurs as equant lumps (Figure 7.5).

The studied upper Oppdalsåta and lower Slottsmøya Members exhibit variable textural organisation with samples ranging between coarse mudstone, sandy mudstone, and muddy sandstone (Tables 5.1 and 5.2). This textural classification reflects the heterogeneity in

composition described above. All of the samples are matrix-supported, poorly sorted, and have angular grains. The sediment is organised into packages of normally graded beds, some of which have erosional bases, parallel lamination, and/or bioturbation.

7.4.2 Geochemistry

Figure 7.6 shows a ternary diagram displaying the main sedimentary components of the studied interval; Al_2O_3 represents the clay mineral fraction, SiO_2 represents the quartz fraction, and CaO represents the carbonate component of the succession. Samples from the Oppdalsåta Member are spread along a two-component mixing line between quartz and clay mineral end members. A few exceptions are slightly richer in carbonate and are possibly overprinted by later-stage diagenesis. SiO_2 , Al_2O_3 , and CaO contents range from 31.2 to 79.4 wt %, 7.0 to 17.2 wt %, and 0.4 to 14.7 wt %, respectively. Slottsmøya member samples are slightly clustered but are still on a mixing line between quartz and clay. SiO_2 , Al_2O_3 , and CaO contents range from 31.0 to 70.3 wt %, 7.6 to 17.7 wt %, and 0.3 to 12.7 wt %, respectively.

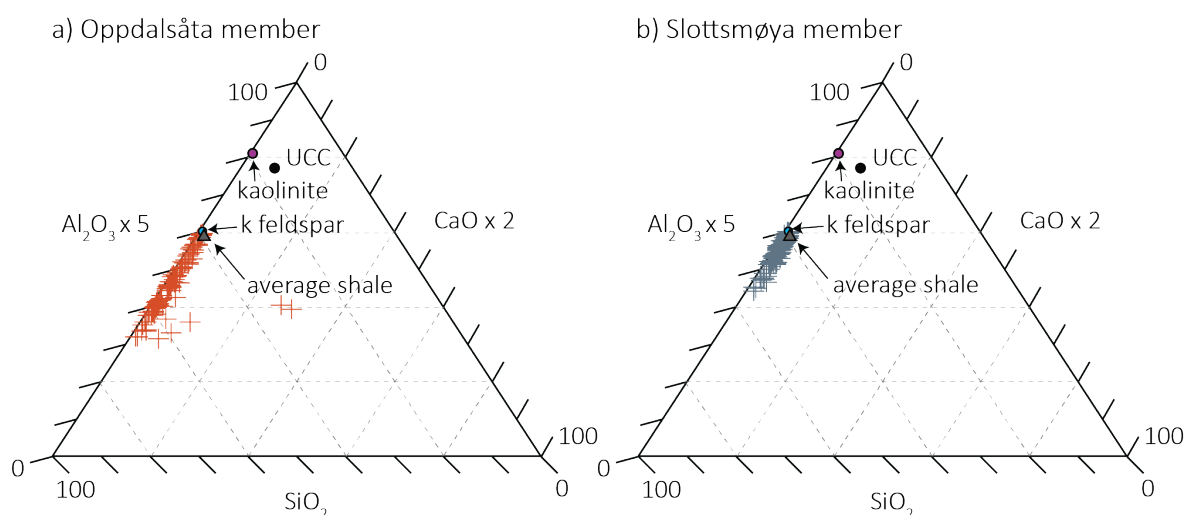


Figure 7.6. SiO_2 , Al_2O_3 , and CaO ternary diagrams showing the distribution of samples in the a) Oppdalsåta Member and b) Slottsmøya Member. Kaolinite, Upper Continental Crust (UCC) (Rudnick and Gao, 2003), average shale, and potassium feldspar are plotted for reference.

Total organic carbon (TOC) contents are variable throughout the section and range from 0.7 to 7.5 wt %, and from 0.2 to 8.4 wt %, in the Oppdalsåta and Slottsmøya members, respectively (Figure 7.2). $\delta^{13}\text{C}_{\text{org}}$ values decrease almost linearly from -25.2 ‰ at the bottom of the Oppdalsåta member to -29.5 ‰ at the top of the Slottsmøya member with slight negative excursions at c. 557 and c. 521 m depth (Figure 7.2). TOC and $\delta^{13}\text{C}_{\text{org}}$ values show no correlation with each other ($R^2 = 0.0003$). Silica in sediments can be detrital, biogenic, or diagenetic in origin but a strong negative linear correlation with Al (Figure 7.7a), and supporting petrographic results, indicate that fine- and coarser-grained siliciclastic material

(clay minerals and quartz, respectively) dilute each other. Therefore, Si is predominantly associated with coarse-grained detrital quartz, and Si patterns over sediment depth can be used as a grain size indicator (Figure 7.7). Not unlike Si that is associated with coarse-grained quartz, Zr is associated with the heavy mineral fraction of the sediment, so the changes in contents of this element can be used as an indicator of the energy of the depositional environment. The potassium content of mudstones is related to weathering of the source area and sediment routing systems, so K/Al trends can be used to investigate climate conditions and sediment provenance. Detrital and depositional energy indicators are generally more variable in the Oppdalsåta member with Si/Al, Ti/Al, Zr/Al, and K/Al values ranging from 2.9 to 5.5, 0.056 to 0.091, 17.5 to 70.5, and 0.3 to 0.4, respectively (Figure 7.7). The overlying Slottsmøya member is characterised by slightly more homogenous profiles with Al-normalised Si, Ti, Zr, and K values ranging from 2.9 to 9.3, 0.055 to 0.063, 17.5 to 41.2, and 0.3 to 0.4, respectively (Figure 7.7).

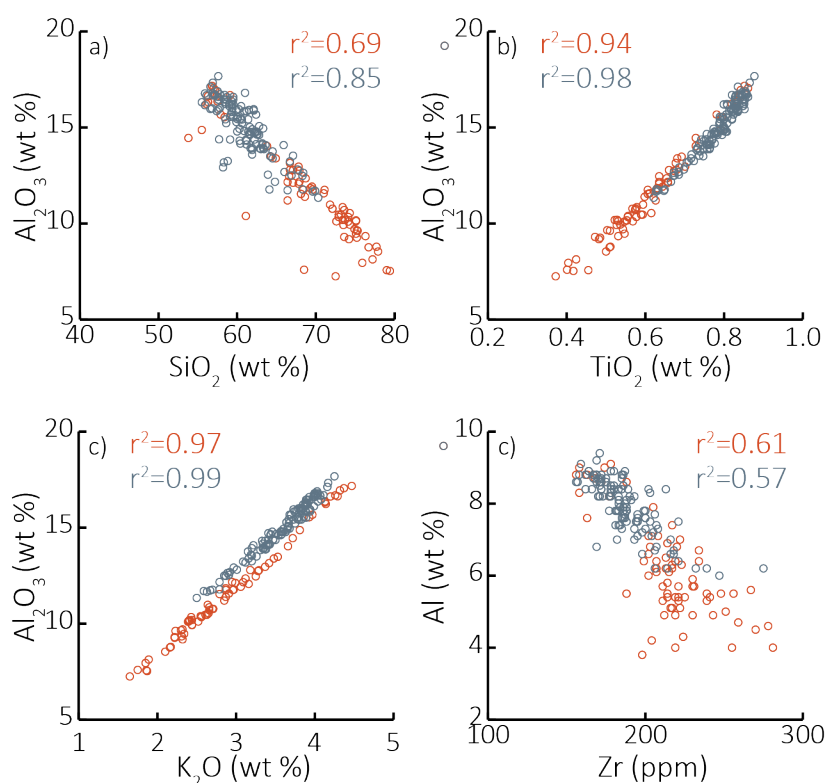


Figure 7.7. Plots of Al_2O_3 against SiO_2 , TiO_2 , and K_2O . The Oppdalsåta and Slottsmøya Members are represented by orange and grey circles, respectively.

Palaeo-redox conditions can be reconstructed by looking at the relative concentrations of selected trace elements in the sediment. The fixation of trace elements into sediment occurs through several well-studied pathways, including microbial mediation (Kiran et al., 2017), coprecipitation with sulphide (Little et al., 2015), and scavenging through a particulate shuttle (Dellwig et al., 2010); see Brumsack (2006) and Tribovillard et al. (2006) for detailed reviews. In general, As, Fe, P, S, Co, Cu, Mo, Ni, V, U, and Zn are enriched in sediment that was

deposited under anoxic to euxinic waters, whereas as Mn is enriched under oxic conditions. Figure 7.9 and Figure 7.10 show the depth plots for these elements in the studied section. Generally, all of the redox-sensitive trace elements have relatively flat profiles with no significant changes, but Al normalised ratios for As, P, S, Cu, Mo, Ni, V, and Zn have slightly higher values at the top of the Oppdalsåta member (c. 540 – 543 m)

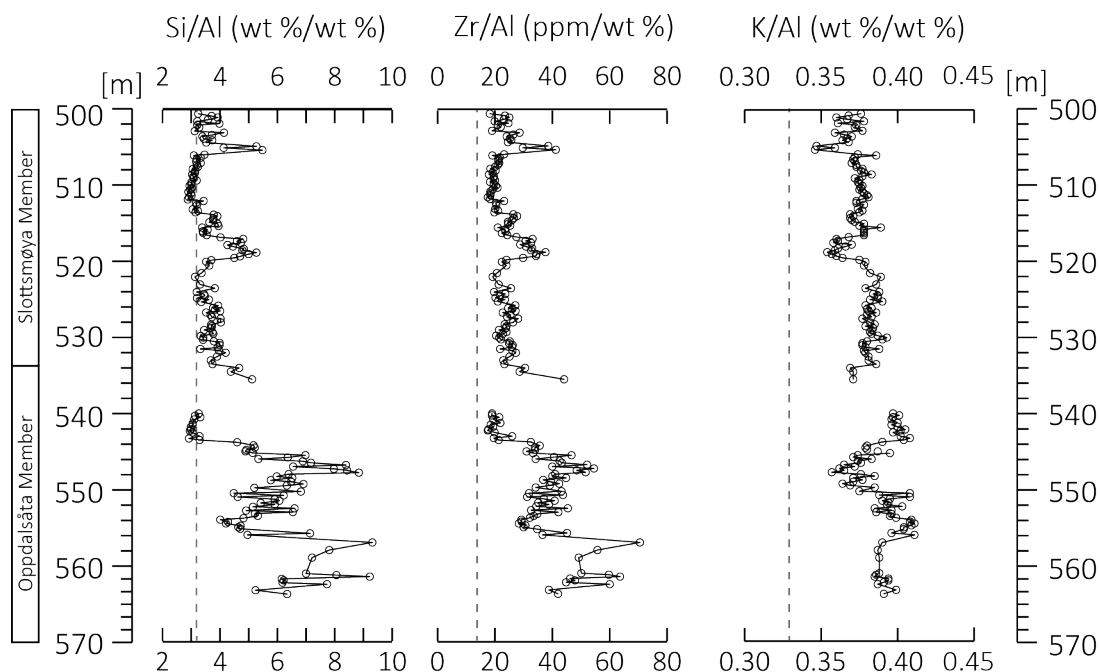


Figure 7.8. Proxies for depositional energy: Si/Al (wt %/ wt %), Zr/Al (ppm/ wt %), and K/Al (wt %/ wt %). Vertical dashed lines denote average shale values.

7.5 Discussion

Constraining the local scale influences on sedimentation of a particular succession is necessary before larger scale processes and wider context can be explored. Here, I discuss the depositional environment of the studied section as evidenced by petrography and geochemistry, and how it relates and compares to the wider literature.

7.5.1 Depositional environment

The Oppdalsåta Member is a compositionally heterogeneous succession comprising detrital grains (quartz, feldspars, titanium oxide, and clay minerals; Figure 7.4 and Figure 7.5). The $\text{SiO}_2\text{-Al}_2\text{O}_3\text{-CaO}$ ternary plot (Figure 7.6) indicates that it is consistently more silica-rich than average shale but proportions of silt (SiO_2) and clay (Al_2O_3) vary within this member. The texturally immature nature of the sediment is demonstrated by petrographic observations of heterolithic, poorly sorted, sand-sized, angular grains in a muddy matrix. Proxies for grain size and depositional energy (Al normalised Si, Ti, and Zr plots; Figure 7.8) support the petrography in that they indicate an energetic depositional environment. The Slottsmøya Member is slightly more compositionally uniform shown by a lesser degree of scatter on the $\text{SiO}_2\text{-Al}_2\text{O}_3\text{-CaO}$ ternary plot (Figure 7.6). Petrographic results (Figure 7.3, Figure 7.4, and

Figure 7.5) indicate a finer-grained, muddier lithology suggesting a quieter depositional setting than for the underlying Oppdalsåta Member, but slight increases in grain size proxies (around 518 m; Figure 7.7) indicate that hydrodynamic energy varied during the deposition of this formation.

The compositional and textural heterogeneity in both the Oppdalsåta and Slottsmøya Members suggest deposition took place in a more proximal setting that experienced a higher depositional energy than the Ebberston 87 and Swanworth Quarry cores. Coarsening upwards cycles, inferred from the grain size proxies, align well with the lower resolution data presented for the nearby DH5R (Koevoets et al., 2018). The data presented here agree with the conclusions made by Koevoets et al. (2018) whereby the coarsening upwards cycles are a response to shifting coastline in either a distal delta-front or middle shore face deposit. However, the cyclicity may be attributed to fluctuations in sea level associated with the possible waxing and waning of ice sheets in the Late Jurassic (Sellwood et al., 2000) and the two possible mechanisms cannot be distinguished with the present dataset.

Figures 1.7 and 1.8c show there is a distinct difference in the K contents and K/Al ratios of the two members. This suggests that there is a difference in either climate conditions affecting the hinterland, and/or changes in the source of the sediment between the two members. Given that regional mapping of the Agardhfjellet Formation indicates a deltaic environment (Koevoets et al., 2018), it is possible that the river shifted course at the end of the Oppdalsåta Member deposition and sediment was sourced from a K-poorer lithology.

The top of the Oppdalsåta Member is the most organic carbon rich of the studied section (TOC up to 8 wt %; Figure 7.2). Rock Eval data, which give an indication of organic matter type and thermal maturity (Espitalie et al., 1977), from the DH5R core indicate that Type III organic material is the predominant organic carbon source in the Agardhfjellet Formation (Koevoets et al., 2016). This is similar for the other DH cores and outcrops across Spitsbergen (Abay et al., 2014), and is supported by petrographic evidence of equant organic material observed in the present study. However, the data indicate that kerogen in the studied section experienced extensive thermal degradation (Koevoets et al., 2016), with peak paleo-temperatures of 150-180 °C (Price, 1983). High burial temperatures raises doubt over the interpretation of geochemical data when determining the source of OC, however, under predominantly oxic conditions, it is unlikely that the OC would be Type II; this is supported by the petrography.

The redox proxies (Figure 7.9 and Figure 7.10) indicate that during the deposition of the Oppdalsåta Member the sediment pore waters were suboxic. This is likely to have been driven by the supply of terrestrial OC, which would have used up oxygen during oxidation. Fully anoxic conditions prevailed when TOC enrichment was at its maximum which is supported by petrographic evidence of equant organic material. The presence of glauconite indicates Fe reduction and the presence of pyrite indicated sulphidic conditions. However,

the framboidal pyrite has a diameter $>5\ \mu\text{m}$ suggesting it formed beneath the sediment water interface and formation of it increased slightly during peak burial of organic carbon (Figure 7.9) indicating it was driven by OC degradation. Peaks in Fe and Mn (Figure 7.9) are likely to relate to diagenetic carbonate deposits, indicated by coeval peaks in Mg/Al and Ca/Al (Figure 7.9) so are excluded from palaeo-environmental interpretation.

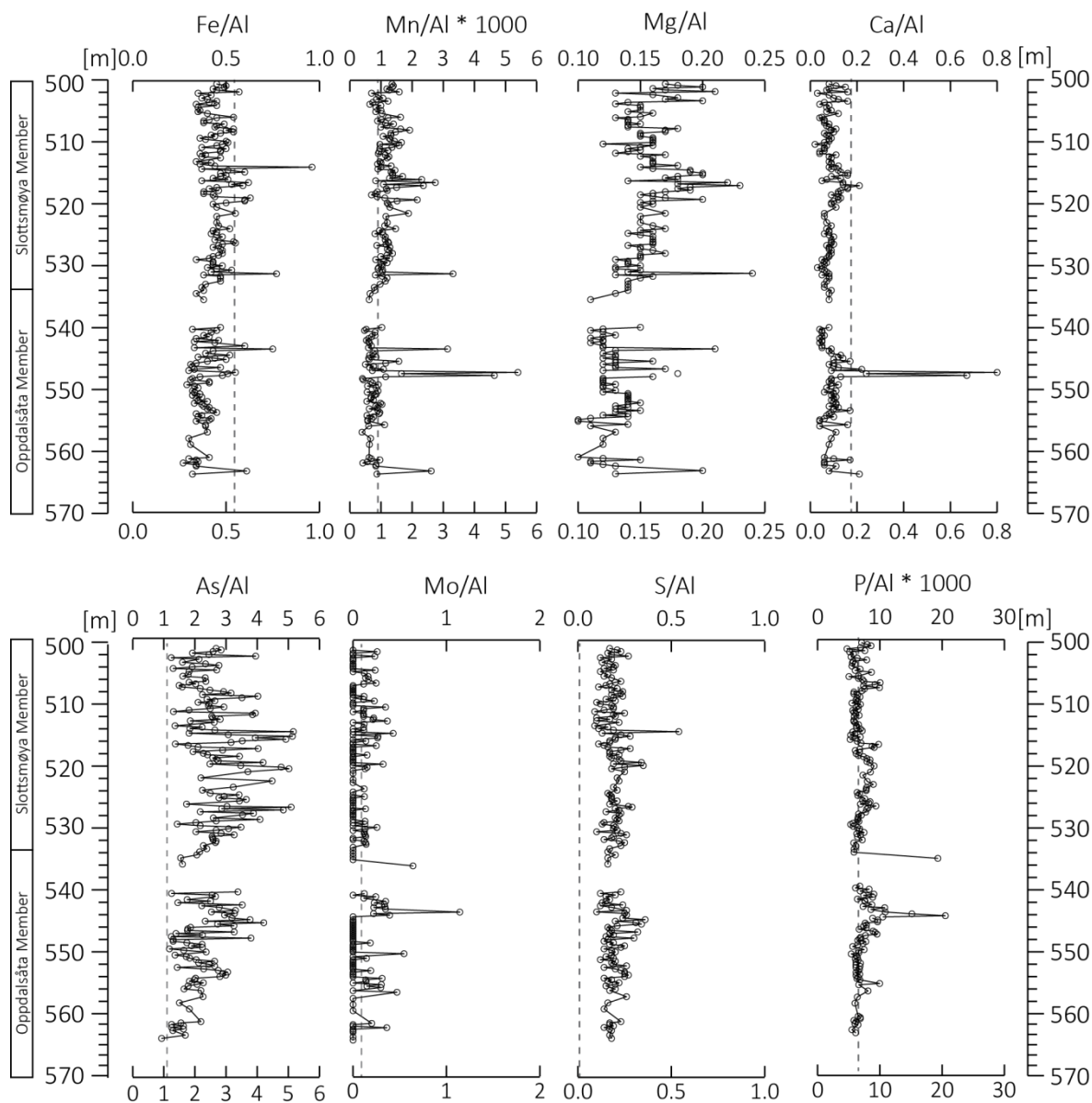


Figure 7.9. Redox indicators: Al-normalised depth plots of Fe, Mn, Mg, Ca, As, Mo, S, and P. Vertical dashed lines indicate average shale values for the respective ratios.

7.5.2 Carbon isotopes

The carbon isotopic composition of organic matter reflects organic matter type, the relative importance of terrestrial versus marine OC sources, and the C isotopic composition of the atmosphere, so can provide an insight in to these processes (Kump and Arthur, 1999). When coupled with inorganic carbon isotopes, they can be used to investigate perturbations in the

global carbon cycle and atmospheric CO₂ levels (Kump and Arthur, 1999); hence they are a valuable tool when reconstructing palaeo-environments. The remarkably continuous, almost linear trend towards heavier isotopes (Figure 7.2) in the present study may result from any one of the aforementioned processes. Petrographic observations of consistently-shaped, ubiquitous Type III organic material, supported by published Rock Eval data (Koevoets et al., 2016), rule out changes in organic matter source as a causal mechanism. Instead, it is likely to

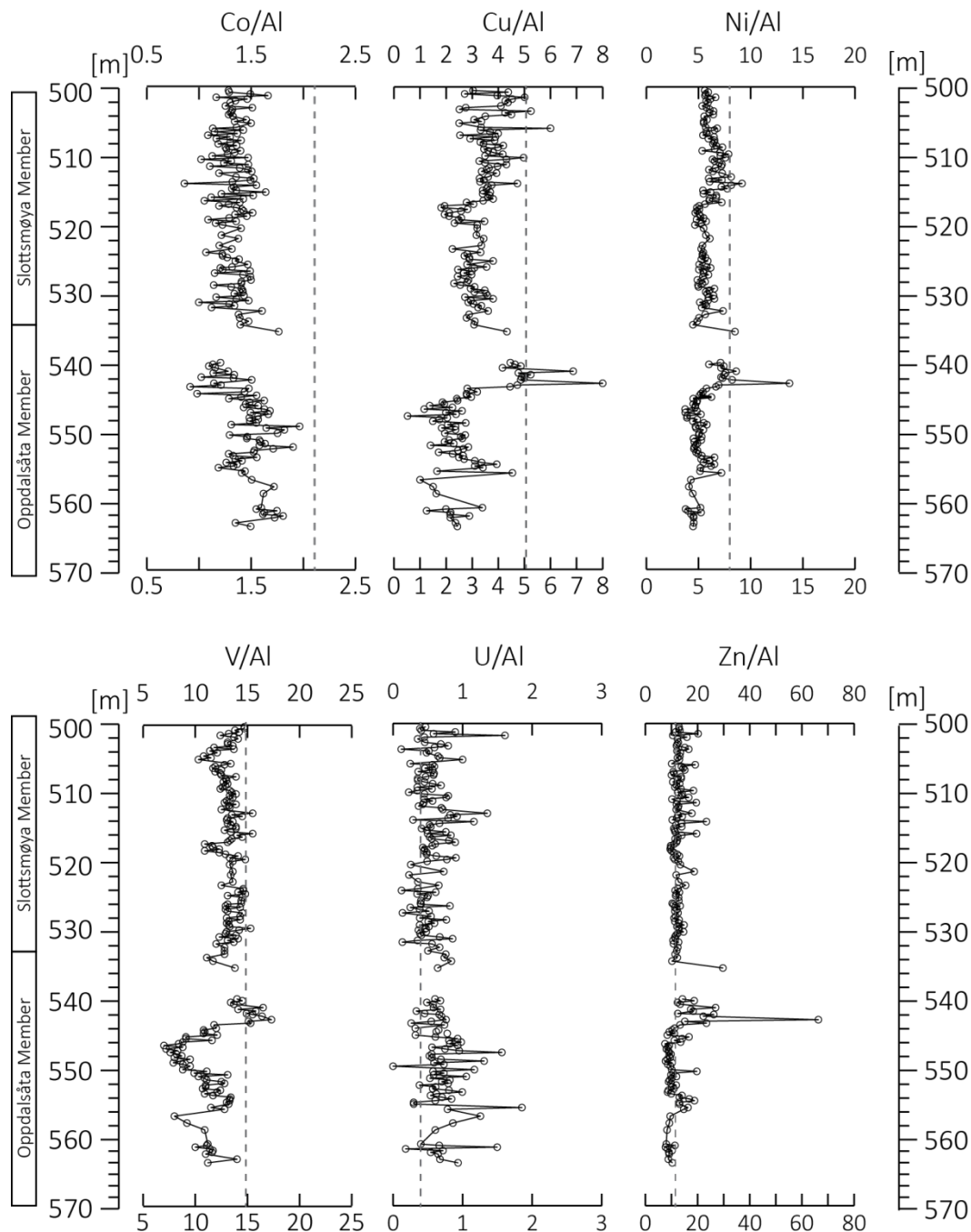


Figure 7.10. Redox indicators: Al-normalised depth plots of Co, Cu, Mo, Ni, V, U, and Zn. Vertical dashed lines indicate average shale values for the respective ratios.

relate to a larger scale process such as volcanism, changes in continental weathering, and/or primary productivity. Volcanism affects carbon isotopes through the outgassing of isotopically light carbon in to the atmosphere and extensive continental weathering alters carbon isotopes by enhancing primary productivity through nutrient supply (Raymo and

Ruddiman, 1992). However, this cannot be determined with a single section alone and is beyond the scope of this project. Carbon isotope curves are routinely used to correlate geographically distant sections; see Koevoets et al. (2016) for discussion of the application of chemostratigraphy with particular attention to coupled carbonate and organic carbon isotopes in the Late Jurassic.

The steady, almost linear upwards decreasing $\delta^{13}\text{C}_{\text{org}}$ trend that is present in the DH4 Core (Figure 7.2) is also observed in the adjacent DH2 and DH5R cores (Koevoets et al., 2016), other places in Svalbard (Hammer et al., 2012), Siberia (Zakharov et al., 2014), and Scotland (Nunn et al., 2009). Using a compilation of $\delta^{13}\text{C}_{\text{carb}}$ from the northern and southern hemispheres, Gröcke et al. (2003) concluded that the persistent negative carbon isotope excursion represents changes in the global carbon cycle, as opposed to a local signal. They went on to postulate that the trend may result from an increase in continental weathering and associated lowering of atmospheric CO_2 levels. However, the authors point out that this is somewhat paradoxical owing to the fact that increased continental weathering should ultimately lead to a positive isotope excursion through enhanced nutrient supply and productivity.

7.6 Conclusions

- The Oppdalsåta and Slottsmøya Members of the Agardhfjellet Formation are immature, compositional and textural heterogeneous, and are predominantly composed of detrital material.
- Geochemical indicators show that depositional energy was moderate but variable throughout the studied interval. The Oppdalsåta member was deposited during more energetic condition than the overlying Slottsmøya Member.
- Potassium contents indicate that either a change in climate dynamics on adjacent landmasses or in sediment source occurred between the two members.
- Sedimentological and geochemical evidence align well with the published literature that attribute the observed cyclicity to changes in the coastline in either a distal delta-front or middle shore face deposit. However, sea level may also exert a strong influence on sedimentation but this cannot be confirmed with the present dataset.
- Organic material is predominantly Type III source and its preservation was likely enhanced by suboxic-anoxic sediment pore waters and a relatively high sedimentation rate relative to the successions discussed in chapter 4, 5, and 6.
- Organic carbon isotope trends align well with data from elsewhere on Svalbard and further afield. This, along with a poor correlation between TOC, Rock Eval parameters, and the isotope data, rules out the organic matter type as a key control on carbon isotopes. Instead, the carbon isotopes are likely to reflect changes in the global carbon

cycle, which may relate increased continental weathering and related atmospheric CO₂ levels.

8 | Synthesis, conclusions, and further work

8.1 Synthesis

This thesis has used an integrated approach to explore controls on sedimentation and organic carbon (OC)-enrichment in a shallow, epicontinental seaway under past Mesozoic greenhouse conditions. Specifically, laterally-equivalent sections from the northern and southern limits of the Late Jurassic Laurasian Seaway have been characterised using inorganic geochemistry and petrography, then synthesised into a refined depositional model for the upper Kimmeridge Clay Formation (KCF). These data have been used to test two hypotheses derived from independent modelling experiments. Chapters 3–7 are written as standalone pieces of work, so this final chapter aims to link the preceding five chapters and synthesise the results in the context of the research questions posed in chapter 1.

In chapter 3, two independent Kimmeridgian/Tithonian climate model experiments were presented. The HadCM3L simulation, provided by Bristol University, utilised a Getech palaeogeography and an atmospheric $p\text{CO}_2$ of 1200 ppm, while the Fast Ocean Atmosphere Model, provided by Equinor ASA, used a modified version of the Merlin+ palaeogeography and an atmospheric $p\text{CO}_2$ of 2400 ppm. These simulations yielded two depositional scenarios that can be tested with and validated against geological data. HadCM3L positioned the intertropical convergence zone (ITCZ) directly over the southern Laurasian Seaway. In this scenario, tropical, monsoon-like conditions would have promoted marine OC enrichment, through enhanced continental weathering and subsequent nutrient supply to the ocean (Armstrong et al., 2016), deposition of detrital sediment, and water column stratification that resulted from fresh water input. The position of the ITCZ moves on several timescales; it migrates seasonally which would translate through to the sedimentary record as annual wet/dry cycles. It is also orbitally forced, and strongly affected by precession modulated short-eccentricity, which would be recorded through cyclicity in the sediment. In contrast, FOAM positioned the outer limb of the Hadley Cell over the southern Laurasian Seaway placing it under the subtropical-temperate climate boundary. Under these conditions, OC enrichment is likely to have been promoted by wind-driven upwelling of nutrient-rich oceanic waters (Wagner et al., 2013) and potentially resulted in biogenous sedimentation. Seasonality is likely to be recorded as alternations in sediment composition and longer cycles are likely to exhibit strong obliquity cyclicity. The two scenarios should be discernible in the rock record by looking at geochemistry and sedimentological data (Wagner et al., 2013). OC enrichment occurs in both settings so it cannot be used to distinguish the two scenarios. Petrographic observations and geochemical proxies can be used to explore the controls on sedimentation but it is affected not only by nutrient supply but also through water column stratification (temperature, nutrient, and/or salinity/density), water mass restriction, relative sedimentation rate, and palaeogeography (Katz, 2005, Tyson, 2005b), so unravelling these processes can prove difficult.

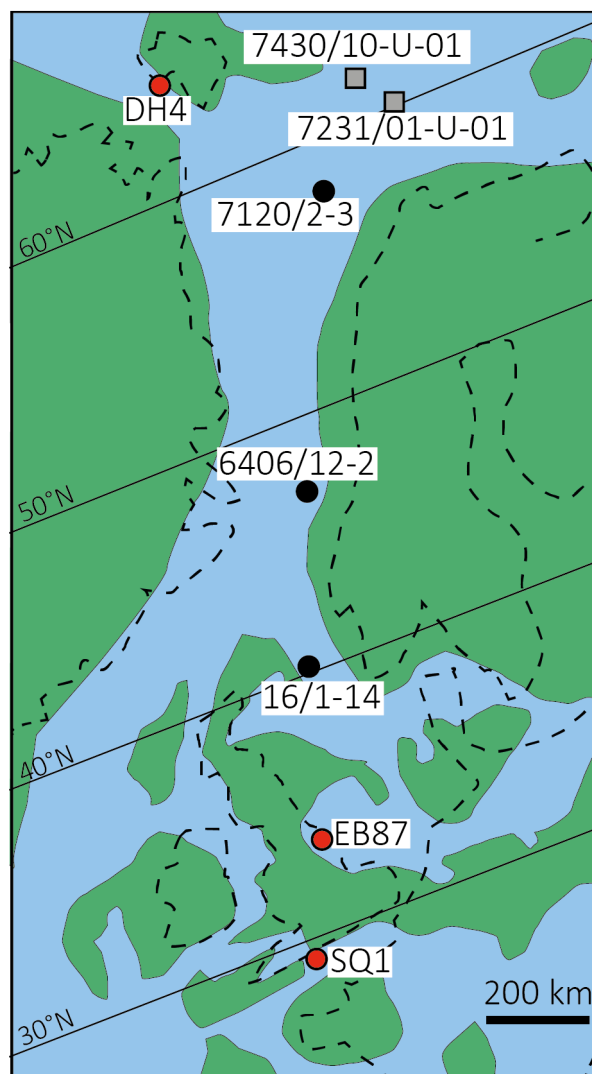


Figure 8.1. Palaeogeographic map of northwest Europe in the Late Jurassic after Miller (1990) and Turner et al. (2019). Red circles denote core locations used in the present study, black circles denote core locations used by Turner et al. (2019), and grey squares denote core locations used by Mutterlose et al. (2003)

Synthesis of geochemical and petrographic data from the Cleveland Basin (Yorkshire, UK), presented in chapters 4 and 5, resulted in a depositional model comprising three modes of sedimentation; detrital-rich, OC-rich, and carbonate-rich sedimentation. In chapter 6, inorganic geochemistry is combined with published petrography (Macquaker and Gawthorpe, 1993, Lazar et al., 2015b) for a coeval section from the Swanworth Quarry 1 Core, drilled in the Wessex Basin (Dorset, UK)(Morgans-Bell et al., 2001). Within the well-established biostratigraphic framework that correlates the Cleveland and Wessex Basin successions, OC-rich bands (ORBS; Cox and Gallois, 1981) are recognised across a distance of 400 km (Herbin and Geyssant, 1993, Herbin et al., 1991). While these ORBs cannot be used for high resolution correlation owing to a complex interplay of factors affecting OC production and burial, remarkable similarities between the chemostratigraphic proxies (K/Al and Rb/Al) means they can be used for correlation (Jenkyns et al., 2002). These

geochemical index proxies point towards an overarching climate control on the deposition in the Cleveland and Wessex Basin, and thus a similar climate control. In both basins, a large proportion of the studied successions comprise detrital sediment and type III terrestrial OC; which indicates climate over the adjacent landmasses was wet, supporting the HadCM3L hypothesis. This is also true for the DH4 Core from Svalbard (1500 km north of the Cleveland Basin) supporting the hypothesis that overall wet and tropical conditions extended, at least periodically, to the northern limit of the seaway. Sedimentation is intrinsically connected to local/regional climate, which in turn is controlled by global scale orbital cycles (Meyers and Malinverno, 2018). In a study of the SQ1 Core in the Wessex Basin, Huang et al. (2010) identify long- and short-eccentricity, obliquity, and precession cyclicity, indicating that deposition of the KCF is strongly influenced by global climate fluctuations. The authors

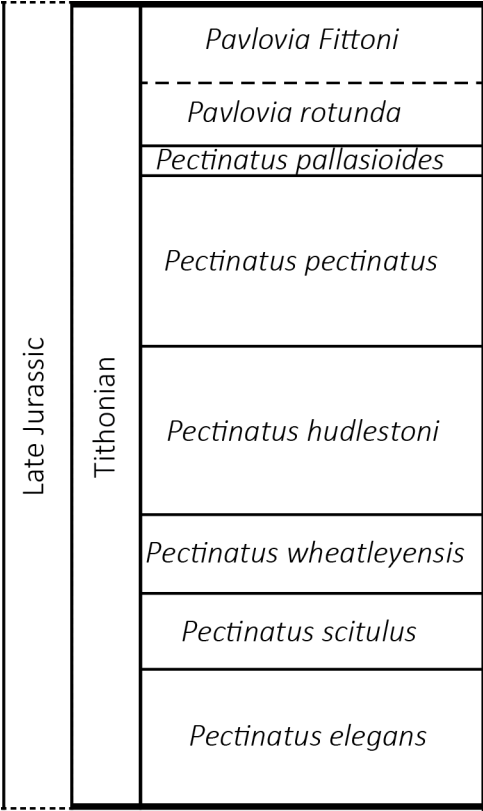


Figure 8.2. Chronostratigraphy for the UK sector of the North Sea (including the Wessex and Cleveland Basins) in the Late Jurassic. After Morgans-Bell et al. (2001).

conclude that short-eccentricity, strongly forced by the precession index, is the dominant effect on KCF cyclicity, resulting in metre-scale OC fluctuations (Huang et al., 2010, Armstrong et al., 2016). This pattern corresponds well to other Kimmeridgian sequences in Tethyan carbonates (Colombié and Strasser, 2005). Precise correlation between the Dorset and Yorkshire therefore enables us to infer sedimentation in the Cleveland Basin using the well-established astronchronology in the Wessex Basin section (Huang et al., 2010, Weedon et al., 2004). Fluctuations between different modes of sedimentation is postulated to be modulated by short-eccentricity and precession, however, higher resolution sampling is required to confirm this. In

that context it is important to note that Mutterlose et al. (2003) also report distinct precession cyclicity time-equivalent cores from the Norwegian shelf (Figure 8.1), which again point towards a low latitude influence of sedimentation comparable to the mid-

latitude seaway (Armstrong et al., 2016). This observation is relevant to testing the hypotheses relating to the climate conditions across the Laurasian Seaway (discussed in chapter 3) because tropical climate conditions are likely to be modulated on a precessional timescale owing to low latitude solar insolation influence; therefore, precession-paced sedimentation across the Laurasian Seaway lends more support to the HadCM3L prediction than the FOAM prediction. Accurate choronostratigraphic successions are imperative for the assessment of coeval climate processes (Mutterlose et al., 2014). Another challenge associated with investigation of palaeoclimate change across wide latitudinal extents (thousands of km) is the absence or lack of robust correlation markers, particularly between the Late Jurassic Boreal and Tethyan regions, where fauna assemblages markedly differ between the two ocean basins (Dzyuba et al., 2013). Chemostratigraphy for these regions is an ongoing area of research (e.g. Dzyuba et al., 2013, Žák et al., 2011, Zakharov and Rogov, 2008, Koevoets et al., 2016, Koevoets et al., 2018). Recent correlation to other sites in the Laurasian Seaway (Figure 8.1) and new clay mineralogical data (Turner et al., 2019) support the occurrence of the postulated mid-Huddlestoni arid event (Wignall and Ruffell, 1990, Hesselbo et al., 2009). Turner et al. (2019) identify diagenetic kaolinite in their core (Figure 8.1), which has also been recognised in coeval section in the Wessex Basin (Lazar et al.,

2015b), but they conclude that similarities in clay mineral trends between high latitude (c. 72 °N) and Dorset (~35°N) sections support a dry-arid-dry transition through the Tithonian. As discussed in chapters 4 and 5, authigenic kaolinite is observed in the Cleveland Basin section, based on this diagenetic overprint and possible alteration/loss of primary signal, I am sceptical about the mid-Hudlestoni event and conclude that further work is needed to explore this proposed climate event.

In an effort to improve global correlation of Late Jurassic–Early Cretaceous successions, Gröcke et al. (2003) generated $^{87}\text{Sr}/^{86}\text{Sr}$, $\delta^{18}\text{O}_{\text{carb}}$, and $\delta^{13}\text{C}_{\text{carb}}$ isotope curves using belemnites from the Volga Basin (Russia) and Kawhia Harbour (New Zealand), which they combined with published data from elsewhere. Oxygen isotope data were used as a proxy for sea surface temperature (SST); an updated compilation is shown in Figure 8.3. The data indicate much warmer global SSTs than present day but, when compared to the model simulations presented in chapter 3, both the HadCM3L and FOAM models appear to over predict global SST. It is important to reconcile model predictions with geological data so this needs to be explored further but is beyond the scope of this study. It should be noted, however, that oxygen isotope data from belemnite shells is affected by factors such as diagenesis, habitat differences, and unknown vital fractionation effects (Voigt et al., 2003).

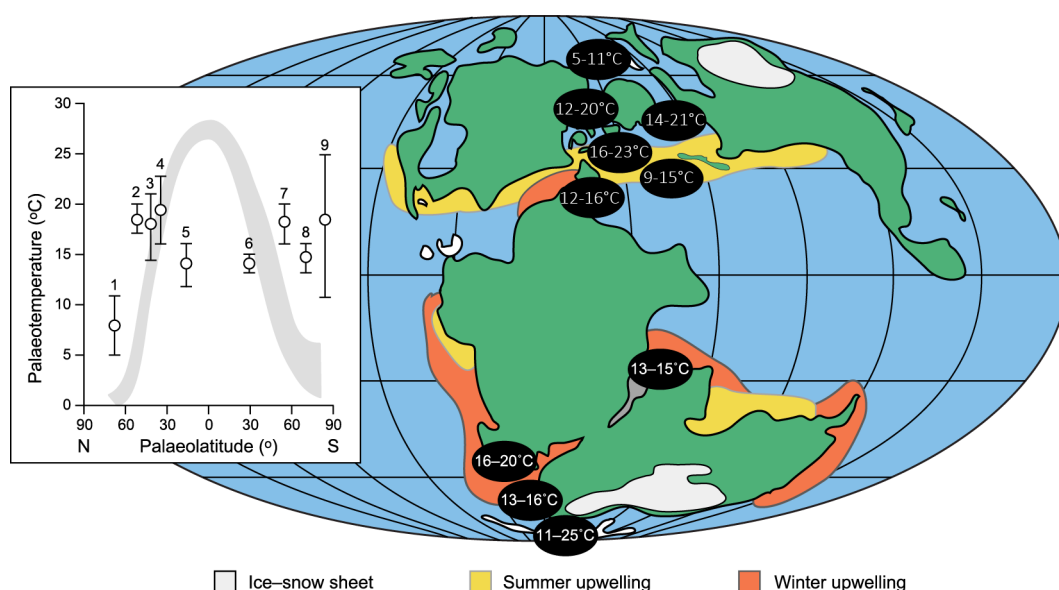


Figure 8.3. Palaeogeographic map (after Smith et al., 2004) showing a compilation of belemnite-derived Kimmeridgian–Tithonian sea surface temperatures (SST) modified after Gröcke et al. (2003). Data sources: (Gröcke et al., 2003, Price and Sellwood, 1994, Price and Sellwood, 1997, Bowen, 1961, Bowen, 1966, Ditchfield, 1997, Ditchfield et al., 1994, Nunn and Price, 2010, Arabas, 2016, Brigaud et al., 2008). The inset graph shows a modern-day pole-to-pole SST profile after Smith (1996). Upwelling zones are from (Parrish and Curtis, 1982) and (Price et al., 1995) and ice/snow sheets are from Sellwood et al. (2000).

Chapters 4–6 highlight the importance that palaeogeography exerts upon sedimentation, OC enrichment, and the translation of climatic signals into the sedimentary rock record. Away from the influence of a coarse-grained, clastic supply, sedimentation in the Cleveland Basin

captured the nuances of climate conditions on the adjacent hinterland, acting as a 'pristine record' of depositional processes at that time. This record then provided a reference point for the interpretation of the Wessex Basin, which had higher depositional energies and flux of detrital sediment that possibly masked the climate signals. The application of a sequence stratigraphical framework to the laterally-equivalent Boulonnais succession (north France) demonstrated that OC enrichment does not correlate with regional sea level fluctuations (Herbin et al., 1995). Herbin et al. (1995) concluded that sedimentation across the southern Lurasian Seaway was controlled by climatic processes but that sea level acted to facilitate the expression of this. Results discussed in chapters 4–6 support this conclusion; deposition in the southern sector of the Lurasian Seaway was very finely balanced and the slightest changes in continental weathering and/or water depth exerted a large influence on marine sedimentation, perhaps owing to the shallow gradients, relatively shallow water depths, and unique tectonic setting of an epicontinental seaway (Schieber, 2016b).

The effect of depositional environment and palaeogeography on the preservation of climate signals is also demonstrated by the synthesis of the northernmost section from Svalbard. In stark contrast to open marine sedimentation in the Wessex and Cleveland Basins, the Svalbard section was deposited in a delta front. This complicates interpretation of climate signals owing to the coarse grain size and large volume of clastic material. The Svalbard section shares similarities with the 'background' EB87 Core sediment in that the OC component is dominated by Type III terrestrial material and is dominated by detrital (opposed to biogenic) sediment. Furthermore, the remarkably consistent negatively decreasing carbon isotope trend observed in Svalbard core can be seen in the stratigraphic intervals with lower OC, i.e. the 'background' sediment of the EB87 Core. Synthesis of geochemistry, specifically redox proxies, and petrography indicates that this too is a very finely balanced system in which OC is preserved under predominantly suboxic conditions.

As discussed in chapter 3, orography exerts a fundamental control on climate model simulations, so geological information can be used to assess model inputs, i.e. the palaeogeography. Large deltaic systems, such as the one mapped across Svalbard and discussed in Chapter 6, imply a large catchment area in the hinterland. Both the Getech and Merlin+ palaeogeographies have large landmasses adjacent to the palaeo-depocentre so this cannot be used to select a preferred model simulation. However, deltas also require wet conditions so the presence of an extensive delta at the northern end of the Lurasian Seaway is more reminiscent of the wetter HadCM3L prediction.

8.2 Conclusions

- Climate modelling using two independent models resulted in two distinctly different climate scenarios for the Late Jurassic Lurasian Seaway. Three time-equivalent sections were analysed to constrain depositional controls on the southern and northern areas of the Lurasian Seaway, thereby validating the model outcomes.
- The HadCM3L model, utilising a Getech paleogeography, predicted an expanded Hadley Cell and northerly migrated intertropical convergence zone influence on marine sedimentation across the Lurasian Seaway, whereas the FOAM simulations instead indicated sub-tropical/temperate conditions prevailed.
- Petrographic examination of the EB87 Core, from the Cleveland Basin (Yorkshire, UK), shows compositionally heterogeneous material, favouring highly dynamic depositional conditions.
- Comparison of time-equivalent records from the SQ1 Core, from the Wessex Basin (Dorset, UK), demonstrates that sedimentation in both basins was remarkably similar, despite subtle differences in depositional energy. These similarities point towards an overarching climate control on sedimentation, at least for the UK sector.
- Deposition in the northern area of the seaway (Svalbard) took place in a deltaic system, which would require extensive precipitation to maintain sediment supply to the ocean thus favouring tropical/wet sedimentation over dry/temperate.
- Geochemistry and sedimentology support the hypothesis that overall wet and tropical conditions extended, at least periodically, to the northern limit of the Lurasian Seaway.
- This study, when integrated with work on other cores from the Lurasian Seaway, overall supports the tropical-subtropical modelling results.
- This study demonstrates the potential for constraining climate dynamics through time and space and the resulting controls on sedimentation in the geological past, through the integration of climate modelling, geochemical, and sedimentological analyses. This approach can be applied to other time intervals and geological events to investigate how the atmosphere, hydrosphere, and biosphere respond to environmental change.

8.3 Future work

This thesis has considered climate modelling, bulk rock geochemistry, and sedimentology to look at the processes controlling OC enrichment and sedimentation across the Lurasian Seaway. Future work required to further this research is extensive.

To fully evaluate the model simulations and to account for their difference, detailed sensitivity studies are required to ascertain 1) the control different pCO_2 concentrations has, 2) the effect palaeogeography exerts on the distribution of heat, 3) the effect orography has upon the positioning of the ITCZ, and 4) the inherent differences/biases in HadCM3L and FOAM. The hypothesis development would benefit from further higher resolution modelling to investigate the role that orbital parameters have on atmospheric dynamics and a look in to simulated oceanic factors such as salinity, stratification, temperature, and currents.

The next step in constraining climate controls on sedimentation at higher latitudes in the seaway is to conduct a detailed sedimentological and geochemical study of cores from this region (e.g. those in Figure 8.1). Ideally, the timeframe and resolution would be extended to better capture the temporal trends in the datasets.

In addition to extending the project in terms of time and space, alternative methods could be utilised to further test the models; stable novel isotopes, such as Os and Li could be used to constrain global weathering rates across the studied interval and a more detailed sedimentological study would yield information on transitions between modes of sedimentation.

9 Bibliography

- ABAY, T. B., KARLSEN, D. A. & PEDERSEN, J. H. 2014. Source rocks at Svalbard: an overview of Jurassic and Triassic formations and comparison with offshore Barents Sea time equivalent source rock formations. *AAPG Datapages Search and Discovery Article*, 30372.
- AIGNER, T. 1980. Biofabrics and stratinomy of the Lower Kimmeridge Clay (U. Jurassic, Dorset, England). *Neues Jahrbuch für Geologie und Paläontologie Abhandlungen*, 159, 324-38.
- ALGEO, T. J., HECKEL, P. H., MAYNARD, J. B., BLAKEY, R., ROWE, H., PRATT, B. & HOLMDEN, C. 2008. Modern and ancient epeiric seas and the super-estuarine circulation model of marine anoxia. *Dynamics of Epeiric seas: sedimentological, paleontological and geochemical perspectives. St. John's, Canada: Geological Association of Canada, Special Publication*, 48, 7-38.
- ALGEO, T. J., KUWAHARA, K., SANO, H., BATES, S., LYONS, T., ELSWICK, E., HINNOV, L., ELLWOOD, B., MOSER, J. & MAYNARD, J. B. 2011. Spatial variation in sediment fluxes, redox conditions, and productivity in the Permian-Triassic Panthalassic Ocean. *Palaeogeography, Palaeoclimatology, Palaeoecology*, 308, 65-83.
- ALGEO, T. J. & LYONS, T. W. 2006. Mo-total organic carbon covariation in modern anoxic marine environments: Implications for analysis of paleoredox and paleohydrographic conditions. *Paleoceanography*, 21.
- ALGEO, T. J. & TRIBOVILLARD, N. 2009. Environmental analysis of paleoceanographic systems based on molybdenum-uranium covariation. *Chemical Geology*, 268, 211-225.
- ALLER, R. C. 1994. Bioturbation and remineralization of sedimentary organic matter: effects of redox oscillation. *Chemical Geology*, 114, 331-345.
- APLIN, A. C., FLEET, A. J. & MACQUAKER, J. H. S. 1999. Muds and mudstones: physical and fluid-flow properties. *Geological Society, London, Special Publications*, 158, 1-8.
- APLIN, A. C. & MACQUAKER, J. H. 2011. Mudstone diversity: Origin and implications for source, seal, and reservoir properties in petroleum systems. *AAPG bulletin*, 95, 2031-2059.
- ARABAS, A. 2016. Middle-Upper Jurassic stable isotope records and seawater temperature variations: New palaeoclimate data from marine carbonate and belemnite rostra (Pieniny Klippen Belt, Carpathians). *Palaeogeography, Palaeoclimatology, Palaeoecology*, 446, 284-294.
- ARKELL, W. J. 1933. The Jurassic System in Great Britain.
- ARMSTRONG, H. A., ABBOTT, G. D., TURNER, B. R., MAKHLOUF, I. M., MUHAMMAD, A. B., PEDENTCHOUK, N. & PETERS, H. 2009. Black shale deposition in an Upper Ordovician-Silurian permanently stratified, peri-glacial basin, southern Jordan. *Palaeogeography, Palaeoclimatology, Palaeoecology*, 273, 368-377.
- ARMSTRONG, H. A., WAGNER, T., HERRINGSHAW, L. G., FARNSWORTH, A. J., LUNT, D. J., HARLAND, M., IMBER, J., LOPTSON, C. & ATAR, E. F. 2016. Hadley circulation and precipitation changes controlling black shale deposition in the Late Jurassic Boreal Seaway. *Paleoceanography*, 31, 1041-1053.
- ARTHUR, M. A. & SAGEMAN, B. B. 1994. Marine Black Shales: Depositional Mechanisms and Environments of Ancient Deposits. *Annual Review of Earth and Planetary Sciences*, 22, 499-551.
- ATAR, E., MÄRZ, C., APLIN, A., DELLWIG, O., HERRINGSHAW, L. G., LAMOUREUX-VAR, V., LENG, M. J., SCHNETGER, B. & WAGNER, T. 2019. Dynamic climate-driven controls on the deposition of the Kimmeridge Clay Formation in the Cleveland Basin, Yorkshire, UK *Clim. Past Discuss.*, 1-34.
- BARRON, E. J. & WASHINGTON, W. M. 1982. Atmospheric circulation during warm geologic periods: Is the equator-to-pole surface-temperature gradient the controlling factor? *Geology*, 10, 633-636.

- BERGH, S. G., BRAATHEN, A. & ANDRESEN, A. 1997. Interaction of basement-involved and thin-skinned tectonism in the Tertiary fold-thrust belt of central Spitsbergen, Svalbard. *AAPG bulletin*, 81, 637-661.
- BERRY, G. & REEDER, M. J. 2014. Objective Identification of the Intertropical Convergence Zone: Climatology and Trends from the ERA-Interim. *Journal of Climate*, 27, 1894-1909.
- BERTRAND, P. & LALLIER-VERGES, E. 1993. Past sedimentary organic matter accumulation and degradation controlled by productivity. *Nature*, 364, 786-788.
- BERTRAND, P., LALLIER-VERGES, E. & BOUSSAFIR, M. 1994. Enhancement of accumulation and anoxic degradation of organic matter controlled by cyclic productivity: a model. *Organic Geochemistry*, 22, 511-520.
- BOHACS, K., GRABOWSKI, G., CARROLL, A., MANKIEWICZ, P., MISKELL-GERHARDT, K., SCHWALBACH, J., WEGNER, M. & SIMO, J. 2005. The deposition of organic-carbon-rich sediments: Models, mechanisms, and consequences.
- BOHACS, K. M., LAZAR, O. R. & DEMKO, T. M. 2014. Parasequence types in shelfal mudstone strata—Quantitative observations of lithofacies and stacking patterns, and conceptual link to modern depositional regimes. *Geology*, 42, 131-134.
- BÖNING, P., BRUMSACK, H.-J., BÖTTCHER, M. E., SCHNETGER, B., KRIETE, C., KALLMEYER, J. & BORCHERS, S. L. 2004. Geochemistry of Peruvian near-surface sediments. *Geochimica et Cosmochimica Acta*, 68, 4429-4451.
- BOUSSAFIR, M., GELIN, F., LALLIER-VERGÈS, E., DERENNE, S., BERTRAND, P. & LARGEAU, C. 1995. Electron microscopy and pyrolysis of kerogens from the Kimmeridge Clay Formation, UK: Source organisms, preservation processes, and origin of microcycles. *Geochimica et Cosmochimica Acta*, 59, 3731-3747.
- BOUSSAFIR, M. & LALLIER-VERGÈS, E. 1997. Accumulation of organic matter in the Kimmeridge Clay formation (KCF): an update fossilisation model for marine petroleum source-rocks. *Marine and Petroleum Geology*, 14, 75-83.
- BOWEN, R. 1961. Paleotemperature analyses of Belemnoida and Jurassic paleoclimatology. *The Journal of Geology*, 69, 309-320.
- BOWEN, R. 1966. Oxygen isotopes as climatic indicators. *Earth-Science Reviews*, 2, 199-224.
- BRAATHEN, A., BÆLUM, K., CHRISTIANSEN, H. H., DAHL, T., EIKEN, O., ELVEBAKK, H., HANSEN, F., HANSEN, T. H., JOCHMANN, M. & JOHANSEN, T. A. 2012. The Longyearbyen CO₂ Lab of Svalbard, Norway—initial assessment of the geological conditions for CO₂ sequestration. *Norwegian Journal of Geology/Norsk Geologisk Forening*, 92.
- BRADSHAW, M., COPE, J., CRIPPS, D., DONOVAN, D., HOWARTH, M., RAWSON, P., WEST, I. & WIMBLEDON, W. 1992a. Atlas of palaeogeography and lithofacies. The Geological Society (Geological Society of London, Memoir) London, UK.
- BRADSHAW, M. J., COPE, J. C. W., CRIPPS, D. W., DONOVAN, D. T., HOWARTH, M. K., RAWSON, P. F., WEST, I. M. & WIMBLEDON, W. A. 1992b. Jurassic. *Geological Society, London, Memoirs*, 13, 107-129.
- BRALOWER, T. & THIERSTEIN, H. 1987. Organic carbon and metal accumulation rates in Holocene and mid-Cretaceous sediments: palaeoceanographic significance. *Geological Society, London, Special Publications*, 26, 345-369.
- BRIGAUD, B., PUCÉAT, E., PELLENARD, P., VINCENT, B. & JOACHIMSKI, M. M. 2008. Climatic fluctuations and seasonality during the Late Jurassic (Oxfordian–Early Kimmeridgian) inferred from $\delta^{18}\text{O}$ of Paris Basin oyster shells. *Earth and Planetary Science Letters*, 273, 58-67.
- BRUMSACK, H.-J. 1988. *Rezente, C-org-reiche Sedimente als Schlüssel zum Verständnis fossiler Schwarzschiefer*.
- BRUMSACK, H.-J. 1989. Geochemistry of recent TOC-rich sediments from the Gulf of California and the Black Sea. *Geologische Rundschau*, 78, 851-882.
- BRUMSACK, H.-J. 2006. The trace metal content of recent organic carbon-rich sediments: Implications for Cretaceous black shale formation. *Palaeogeography, Palaeoclimatology, Palaeoecology*, 232, 344-361.
- CALVERT, S. E. & PEDERSEN, T. F. 2007. Chapter Fourteen Elemental Proxies for Palaeoclimatic and Palaeoceanographic Variability in Marine Sediments:

- Interpretation and Application. In: CLAUDE, H. M. & ANNE DE, V. (eds.) *Developments in Marine Geology*. Elsevier.
- CANFIELD, D. E., JØRGENSEN, B. B., FOSSING, H., GLUD, R., GUNDERSEN, J., RAMSING, N. B., THAMDRUP, B., HANSEN, J. W., NIELSEN, L. P. & HALL, P. O. 1993. Pathways of organic carbon oxidation in three continental margin sediments. *Marine Geology*, 113, 27-40.
- CANFIELD, D. E., RAISWELL, R. & BOTTRELL, S. H. 1992. The reactivity of sedimentary iron minerals toward sulfide. *American Journal of Science*, 292, 659-683.
- COHEN, A. S., COE, A. L., HARDING, S. M. & SCHWARK, L. 2004. Osmium isotope evidence for the regulation of atmospheric CO₂ by continental weathering. *Geology*, 32, 157-160.
- COLLIGNON, M. & HAMMER, Ø. 2012. Petrography and sedimentology of the Slottsmøya Member at Janusfjellet, central Spitsbergen. *Norwegian Journal of Geology/Norsk Geologisk Forening*, 92.
- COLOMBIÉ, C. & STRASSER, A. 2005. Facies, cycles, and controls on the evolution of a keep-up carbonate platform (Kimmeridgian, Swiss Jura). *Sedimentology*, 52, 1207-1227.
- COOPER, B. S., BARNARD, P. C. & TELNAES, N. 1995. The Kimmeridge Clay Formation of The North Sea. In: KATZ, B. J. (ed.) *Petroleum Source Rocks*. Berlin, Heidelberg: Springer Berlin Heidelberg.
- COPE, J. C. W. 2009. Correlation problems in the Kimmeridge Clay Formation (Upper Jurassic, UK): lithostratigraphy versus biostratigraphy and chronostratigraphy. *Geological Magazine*, 146, 266-275.
- COPE, J. C. W. 2015. Detailed stratigraphy of the uppermost Kimmeridge Clay Formation (Upper Jurassic) from the Swanworth Boreholes, Dorset, UK. *Proceedings of the Geologists' Association*, 126, 100-106.
- COX, B. M. & GALLOIS, R. W. 1981. *The stratigraphy of the Kimmeridge Clay of the Dorset type area and its correlation with some other Kimmeridgian sequences*, HMSO.
- COX, P. M. 2001. Description of the "TRIFFID" dynamic global vegetation model.
- CROWLEY, T. J. 1996. Remembrance of things past: greenhouse lessons from the geologic record. *Consequences*, 2, 3-12.
- CURIALE, J. A. & GIBLING, M. R. 1994. Productivity control on oil shale formation—Mae Sot Basin, Thailand. *Organic geochemistry*, 21, 67-89.
- DELLWIG, O., LEIPE, T., MÄRZ, C., GLOCKZIN, M., POLLEHNE, F., SCHNETGER, B., YAKUSHEV, E. V., BÖTTCHER, M. E. & BRUMSACK, H.-J. 2010. A new particulate Mn-Fe-P-shuttle at the redoxcline of anoxic basins. *Geochimica et Cosmochimica Acta*, 74, 7100-7115.
- DELLWIG, O., SCHNETGER, B., MEYER, D., POLLEHNE, F., HÄUSLER, K. & ARZ, H. W. 2018. Impact of the Major Baltic Inflow in 2014 on Manganese Cycling in the Gotland Deep (Baltic Sea). *Frontiers in Marine Science*, 5, 248.
- DELLWIG, O., WATERMANN, F., BRUMSACK, H.-J., GERDES, G. & KRUMBEIN, W. 2001. Sulphur and iron geochemistry of Holocene coastal peats (NW Germany): a tool for palaeoenvironmental reconstruction. *Palaeogeography, Palaeoclimatology, Palaeoecology*, 167, 359-379.
- DELLWIG, O., WATERMANN, F., BRUMSACK, H. J. & GERDES, G. 1999. High-resolution Reconstruction of a Holocene Coastal Sequence (NW Germany) Using Inorganic Geochemical Data and Diatom Inventories. *Estuarine, Coastal and Shelf Science*, 48, 617-633.
- DEMAISON, G., PEDERSEN, T. F. & CALVERT, S. E. 1991. Anoxia vs. productivity; what controls the formation of organic-carbon-rich sediments and sedimentary rocks?; discussion and reply. *AAPG Bulletin*, 75, 499-501.
- DEMAISON, G. J. & MOORE, G. T. 1980a. Anoxic environments and oil source bed genesis. *Organic Geochemistry*, 2, 9-31.
- DEMAISON, G. J. & MOORE, G. T. 1980b. Anoxic environments and oil source bed genesis. *Organic Geochemistry*, 2, 9-31.
- DERA, G., BRIGAUD, B., MONNA, F., LAFFONT, R., PUCÉAT, E., DECONINCK, J.-F., PELLENARD, P., JOACHIMSKI, M. M. & DURET, C. 2011. Climatic ups and downs in a disturbed Jurassic world. *Geology*, 39, 215-218.
- DITCHFIELD, P., MARSHALL, J. & PIRRIE, D. 1994. High latitude palaeotemperature variation: new data from the Thithonian to Eocene of James Ross Island, Antarctica. *Palaeogeography, Palaeoclimatology, Palaeoecology*, 107, 79-101.

- DITCHFIELD, P. W. 1997. High northern palaeolatitude Jurassic-Cretaceous palaeotemperature variation: new data from Kong Karls Land, Svalbard. *Palaeogeography, Palaeoclimatology, Palaeoecology*, 130, 163-175.
- DONNADIEU, Y., GODDÉRIIS, Y. & BOUTTES, N. 2009. Exploring the climatic impact of the continental vegetation on the Mesozoic atmospheric CO₂ and climate history. *Clim. Past*, 5, 85-96.
- DONNADIEU, Y., PIERREHUMBERT, R., JACOB, R. & FLUTEAU, F. 2006. Modelling the primary control of paleogeography on Cretaceous climate. *Earth and Planetary Science Letters*, 248, 426-437.
- DYPVIK, H. 1978. Origin of carbonate in marine shales of the Janusfjellet Formation, Svalbard. *Norsk Polarinstitutt Årbok 1977*, 101-110.
- DYPVIK, H. 1980. The sedimentology of the Janusfjellet Formation, central Spitsbergen (Sassenfjorden and Agardhfjellet areas). *Norsk Polarinstitutt Skrifter*, 172, 97-134.
- DYPVIK, H. 1984. Jurassic and Cretaceous black shales of the Janusfjellet Formation, Svalbard, Norway. *Sedimentary Geology*, 41, 235-248.
- DZYUBA, O. S., IZOKH, O. P. & SHURYGIN, B. N. 2013. Carbon isotope excursions in Boreal Jurassic-Cretaceous boundary sections and their correlation potential. *Palaeogeography, Palaeoclimatology, Palaeoecology*, 381-382, 33-46.
- ECKERT, S., BRUMSACK, H.-J., SEVERMANN, S., SCHNETGER, B., MÄRZ, C. & FRÖLLJE, H. 2013. Establishment of euxinic conditions in the Holocene Black Sea. *Geology*, 41, 431-434.
- ERICKSON, B. E. & HELZ, G. R. 2000. Molybdenum(VI) speciation in sulfidic waters: Stability and lability of thiomolybdates. *Geochimica et Cosmochimica Acta*, 64, 1149-1158.
- ESPITALIE, J., MADEC, M., TISSOT, B., MENNIG, J. & LEPLAT, P. Source rock characterization method for petroleum exploration. Offshore Technology Conference, 1977. Offshore Technology Conference.
- FLÖGEL, S., PARKIN, G., POLLARD, D., DULLO, W.-C. & WAGNER, T. 2011. Simulating zonal scale shifts in the partitioning of surface and subsurface freshwater flow in response to increasing pCO₂. *Climate Dynamics*, 37, 1565-1573.
- FLUTEAU, F., RAMSTEIN, G., BESSE, J., GUIRAUD, R. & MASSE, J. 2007. Impacts of palaeogeography and sea level changes on Mid-Cretaceous climate. *Palaeogeography, Palaeoclimatology, Palaeoecology*, 247, 357-381.
- FOX-STRANGWAYS, C. 1892. *The Jurassic Rocks of Britain*, HM Stationery Office.
- FRIERSON, D. M. W. 2007. The Dynamics of Idealized Convection Schemes and Their Effect on the Zonally Averaged Tropical Circulation. *Journal of the Atmospheric Sciences*, 64, 1959-1976.
- GALLOIS, R. 1979. Oil shale resources in Great Britain. *Institute of Geological Sciences, London*, 2.
- GALLOIS, R. 2000. The stratigraphy of the Kimmeridge Clay Formation (Upper Jurassic) in the RGGE Project boreholes at Swanworth Quarry and Metherrills, south Dorset. *Proceedings of the Geologists' Association*, 111, 265-280.
- GALLOIS, R. & ETCHES, S. 2001. The stratigraphy of the youngest part of the Kimmeridge Clay Formation (Upper Jurassic) of the Dorset type area. *Proceedings of the Geologists' Association*, 112, 169-182.
- GALLOIS, R. W. 1976. Coccolith blooms in the Kimmeridge Clay and origin of North Sea Oil. *Nature*, 259, 473-475.
- GALLOIS, R. W. 2004. The Kimmeridge Clay: the most intensively studied formation in Britain. *Open University Geological Journal*, 25.
- GALLOIS, R. W. & MEDD, A. W. 1979. Coccolith-rich marker bands in the English Kimmeridge Clay. *Geological Magazine*, 116, 247-260.
- GHADEER, S. G. & MACQUAKER, J. H. S. 2012. The role of event beds in the preservation of organic carbon in fine-grained sediments: Analyses of the sedimentological processes operating during deposition of the Whitby Mudstone Formation (Toarcian, Lower Jurassic) preserved in northeast England. *Marine and Petroleum Geology*, 35, 309-320.
- GOLDBERG, E. D. 1954. Marine geochemistry 1. Chemical scavengers of the sea. *The Journal of Geology*, 62, 249-265.
- GRADSTEIN, F. M., OGG, J. G., SCHMITZ, M. & OGG, G. 2012. *The geologic time scale 2012*, elsevier.

- GRÖCKE, D. R., PRICE, G. D., RUFFELL, A. H., MUTTERLOSE, J. & BARABOSHKIN, E. 2003. Isotopic evidence for Late Jurassic–Early Cretaceous climate change. *Palaeogeography, Palaeoclimatology, Palaeoecology*, 202, 97-118.
- GRYGAR, T. M., MACH, K. & MARTINEZ, M. 2019. Checklist for the use of potassium concentrations in siliciclastic sediments as paleoenvironmental archives. *Sedimentary Geology*, 382, 75-84.
- HALLAM, A. 1975. *Jurassic environments*, Cambridge University Press.
- HALLAM, A. 1985. A review of Mesozoic climates. *Journal of the Geological Society*, 142, 433-445.
- HALLAM, A. & BRADSHAW, M. 1979. Bituminous shales and oolitic ironstones as indicators of transgressions and regressions. *Journal of the Geological Society*, 136, 157-164.
- HAMMER, Ø., COLLIGNON, M. & NAKREM, H. A. 2012. Organic carbon isotope chemostratigraphy and cyclostratigraphy in the Volgian of Svalbard. *Norwegian Journal of Geology*, 92, 103-112.
- HAQ, B. U., HARDENBOL, J. & VAIL, P. R. 1988. Mesozoic and Cenozoic chronostratigraphy and cycles of sea-level change.
- HASTENRATH, S. 1991. *Climate dynamics of the tropics*, Kluwer Academic Publishers.
- HÄUSLER, K., DELLWIG, O., SCHNETGER, B., FELDENS, P., LEIPE, T., MOROS, M., POLLEHNE, F., SCHÖNKE, M., WEGWERTH, A. & ARZ, H. W. 2018. Massive Mn carbonate formation in the Landsort Deep (Baltic Sea): Hydrographic conditions, temporal succession, and Mn budget calculations. *Marine Geology*, 395, 260-270.
- HÄUSLER, K., MOROS, M., WACKER, L., HAMMERSCHMIDT, L., DELLWIG, O., LEIPE, T., KOTILAINEN, A. & ARZ, H. W. 2017. Mid - to late Holocene environmental separation of the northern and central Baltic Sea basins in response to differential land uplift. *Boreas*, 46, 111-128.
- HAY, W. W. 1995. Paleooceanography of marine organic-carbon-rich sediments.
- HELZ, G. R., MILLER, C. V., CHARNOCK, J. M., MOSSELMANS, J. F. W., PATTRICK, R. A. D., GARNER, C. D. & VAUGHAN, D. J. 1996. Mechanism of molybdenum removal from the sea and its concentration in black shales: EXAFS evidence. *Geochimica Et Cosmochimica Acta*, 60, 3631-3642.
- HERBIN, J. P., FERNANDEZ-MARTINEZ, J. L., GEYSSANT, J. R., ALBANI, A. E., DECONINCK, J. F., PROUST, J. N., COLBEAUX, J. P. & VIDIER, J. P. 1995. Sequence stratigraphy of source rocks applied to the study of the Kimmeridgian/Tithonian in the north-west European shelf (Dorset/UK, Yorkshire/UK and Boulonnais/France). *Marine and Petroleum Geology*, 12, 177-194.
- HERBIN, J. P. & GEYSSANT, J. R. 1993. Organic belts during Kimmeridgian/Tithonian in England (Yorkshire, Dorset) and France (Boulonnais) *Comptes Rendus de L'Academie des Sciences Series II*, 317, 1309-1316.
- HERBIN, J. P., MÜLLER, C., GEYSSANT, J., MELIERES, F. & PENN, I. 1991. *Heterogeneity of organic matter distribution in relation to a transgressive systems tract: Kimmeridge Clay (Jurassic), England*, ; None.
- HERBIN, J. P., MÜLLER, C., GEYSSANT, J. R., MÉLIÈRES, F., PENN, I. E. & GROUP, Y. 1993. Variation of the distribution of organic matter within a transgressive system tract: Kimmeridge Clay (Jurassic), England. *Source Rocks in a Sequence Stratigraphic Framework*, 67-100.
- HERNDON, E. M., HAVIG, J. R., SINGER, D. M., MCCORMICK, M. L. & KUMP, L. R. 2018. Manganese and iron geochemistry in sediments underlying the redox-stratified Fayetteville Green Lake. *Geochimica et Cosmochimica Acta*, 231, 50-63.
- HESELBO, S. P., DECONINCK, J. F., HUGGETT, J. M. & MORGANS BELL, H. S. 2009. Late Jurassic palaeoclimatic change from clay mineralogy and gamma-ray spectrometry of the Kimmeridge Clay, Dorset, UK. *Journal of the Geological Society*, 166, 1123-1133.
- HETZEL, A., MÄRZ, C., VOGT, C. & BRUMSACK, H.-J. 2011. Geochemical environment of Cenomanian - Turonian black shale deposition at Wunstorf (northern Germany). *Cretaceous Research*, 32, 480-494.
- HOFMANN, P. & WAGNER, T. 2011. ITCZ controls on Late Cretaceous black shale sedimentation in the tropical Atlantic Ocean. *Paleoceanography*, 26, PA4223.

- HU, Y., TAO, L. & LIU, J. 2013. Poleward expansion of the Hadley circulation in CMIP5 simulations. *Advances in Atmospheric Sciences*, 30, 790-795.
- HUANG, C., HESSELBO, S. P. & HINNOV, L. 2010. Astrochronology of the late Jurassic Kimmeridge Clay (Dorset, England) and implications for Earth system processes. *Earth and Planetary Science Letters*, 289, 242-255.
- HUCKRIEDE, H. & MEISCHNER, D. 1996. Origin and environment of manganese-rich sediments within black-shale basins. *Geochimica et Cosmochimica Acta*, 60, 1399-1413.
- HVOSLEF, S., DYPVIK, H. & SOLLI, H. 1986. A combined sedimentological and organic geochemical study of the Jurassic/Cretaceous Janusfjellet formation (Svalbard), Norway. *Organic Geochemistry*, 10, 101-111.
- IPCC 2014. Impacts, Adaptation, and Vulnerability. Part A: Global and Sectoral Aspects. Contribution of Working Group II to the Fifth Assessment Report of the Intergovernmental Panel on Climate Change. *IPCC*.
- IRWIN, H., CURTIS, C. & COLEMAN, M. 1977. Isotopic evidence for source of diagenetic carbonates formed during burial of organic-rich sediments. *Nature*, 269, 209.
- ITTEKKOT, V., HAAKE, B., BARTSCH, M., NAIR, R. & RAMASWAMY, V. 1992. Organic carbon removal in the sea: the continental connection. *Geological Society, London, Special Publications*, 64, 167-176.
- JACOB, R., SCHAFER, C., FOSTER, I., TOBIS, M. & ANDERSON, J. Computational Design and Performance of the Fast Ocean Atmosphere Model, Version One. In: ALEXANDROV, V. N., DONGARRA, J. J., JULIANO, B. A., RENNER, R. S. & TAN, C. J. K., eds. Computational Science — ICCS 2001, 2001// 2001 Berlin, Heidelberg. Springer Berlin Heidelberg, 175-184.
- JENKINS, D. M., JAGNIECKI, E. A., DEMICCO, R. V. & LOWENSTEIN, T. K. 2015. Eocene atmospheric CO₂ from the nahcolite proxy. *Geology*, 43, 1075-1078.
- JENKINS, H. C. 2003. *Evidence for rapid climate change in the Mesozoic–Palaeogene greenhouse world*.
- JENKINS, H. C. 2010. Geochemistry of oceanic anoxic events. *Geochemistry, Geophysics, Geosystems*, 11, Q03004.
- JENKINS, H. C., HESSELBO, S. P., JONES, C. E., GRÖCKE, D. R. & PARKINSON, D. N. 2002. Chemostratigraphy of the Jurassic System: applications, limitations and implications for palaeoceanography. *Journal of the Geological Society*, 159, 351-378.
- JOCHUM, K. P., NOHL, U., HERWIG, K., LAMMEL, E., STOLL, B. & HOFMANN, A. W. 2005. GeoReM: A New Geochemical Database for Reference Materials and Isotopic Standards. *Geostandards and Geoanalytical Research*, 29, 333-338.
- JOHANSON, C. M. & FU, Q. 2009. Hadley Cell Widening: Model Simulations versus Observations. *Journal of Climate*, 22, 2713-2725.
- KATZ, B. J. 1995. A survey of rift basin source rocks. *Geological Society, London, Special Publications*, 80, 213-240.
- KATZ, B. J. 2005. Controlling factors on source rock development—a review of productivity, preservation, and sedimentation rate.
- KEMP, D. B., FRASER, W. T. & IZUMI, K. 2018. Stratigraphic completeness and resolution in an ancient mudrock succession. *Sedimentology*, 65, 1875-1890.
- KIRAN, M. G., PAKSHIRAJAN, K. & DAS, G. 2017. Heavy metal removal from multicomponent system by sulfate reducing bacteria: Mechanism and cell surface characterization. *Journal of Hazardous Materials*, 324, 62-70.
- KJELLSSON, J. & DÖÖS, K. 2012. Lagrangian decomposition of the Hadley and Ferrel cells. *Geophysical Research Letters*, 39.
- KOEVOETS, M. J., ABAY, T. B., HAMMER, Ø. & OLAUSSEN, S. 2016. High-resolution organic carbon-isotope stratigraphy of the Middle Jurassic–Lower Cretaceous Agardhfjellet Formation of central Spitsbergen, Svalbard. *Palaeogeography, Palaeoclimatology, Palaeoecology*, 449, 266-274.
- KOEVOETS, M. J., HAMMER, Ø., OLAUSSEN, S., SENGGER, K. & SMELROR, M. 2018. Integrating subsurface and outcrop data of the Middle Jurassic to Lower Cretaceous Agardhfjellet Formation in central Spitsbergen. *Norwegian Journal of Geology*, 98, 1-34.

- KORTE, C., HESSELBO, S. P., ULLMANN, C. V., DIETL, G., RUHL, M., SCHWEIGERT, G. & THIBAUT, N. 2015. Jurassic climate mode governed by ocean gateway. *Nature communications*, 6, 10015.
- KRANCK, K. 1975. Sediment deposition from flocculated suspensions. *Sedimentology*, 22, 111-123.
- KUMP, L. R. & ARTHUR, M. A. 1999. Interpreting carbon-isotope excursions: carbonates and organic matter. *Chemical Geology*, 161, 181-198.
- KUMP, L. R., KASTING, J. F. & CRANE, R. G. 2004. *The earth system*, Pearson Prentice Hall Upper Saddle River, NJ.
- LALLIER-VERGÈS, E., HAYES, J. M., BOUSSAFIR, M., ZABACK, D. A., TRIBOVILLARD, N. P., CONNAN, J. & BERTRAND, P. 1997. Productivity-induced sulphur enrichment of hydrocarbon-rich sediments from the Kimmeridge Clay Formation. *Chemical Geology*, 134, 277-288.
- LAUDERDALE, J. M., GARABATO, A. C. N., OLIVER, K. I., FOLLOWS, M. J. & WILLIAMS, R. G. 2013. Wind-driven changes in Southern Ocean residual circulation, ocean carbon reservoirs and atmospheric CO₂. *Climate dynamics*, 41, 2145-2164.
- LAZAR, O. R., BOHACS, K. M., MACQUAKER, J. H., SCHIEBER, J. & DEMKO, T. M. 2015a. Capturing key attributes of fine-grained sedimentary rocks in outcrops, cores, and thin sections: nomenclature and description guidelines. *Journal of Sedimentary Research*, 85, 230-246.
- LAZAR, O. R., BOHACS, K. M., SCHIEBER, J., MACQUAKER, J. H. & DEMKO, T. M. 2015b. *Mudstone Primer: Lithofacies Variations, Diagnostic Criteria, and Sedimentologic-stratigraphic Implications at Lamina to Bedset Scales*, SEPM (Society for Sedimentary Geology).
- LEES, J. A., BOWN, P. R. & YOUNG, J. R. 2006. Photic zone palaeoenvironments of the Kimmeridge Clay Formation (Upper Jurassic, UK) suggested by calcareous nannoplankton palaeoecology. *Palaeogeography, Palaeoclimatology, Palaeoecology*, 235, 110-134.
- LEES, J. A., BOWN, P. R., YOUNG, J. R. & RIDING, J. B. 2004. Evidence for annual records of phytoplankton productivity in the Kimmeridge Clay Formation coccolith stone bands (Upper Jurassic, Dorset, UK). *Marine Micropaleontology*, 52, 29-49.
- LEITH, T. L., WEISS, H. M., MØRK, A., ÅRHUS, N., ELVEBAKK, G., EMBRY, A. F., BROOKS, P. W., STEWART, K. R., PCHELINA, T. M., BRO, E. G., VERBA, M. L., DANYUSHEVSKAYA, A. & BORISOV, A. V. 1993. Mesozoic hydrocarbon source-rocks of the Arctic region. In: VORREN, T. O., BERGSAGER, E., DAHL-STAMNES, Ø. A., HOLTER, E., JOHANSEN, B., LIE, E. & LUND, T. B. (eds.) *Norwegian Petroleum Society Special Publications*. Elsevier.
- LI, Z. & SCHIEBER, J. 2018. Composite Particles in Mudstones: Examples from the Late Cretaceous Tununk Shale Member of the Mancos Shale Formation. *Journal of Sedimentary Research*, 88, 1319-1344.
- LITTLE, S. H., VANCE, D., LYONS, T. W. & MCMANUS, J. 2015. Controls on trace metal authigenic enrichment in reducing sediments: Insights from modern oxygen-deficient settings. *American Journal of Science*, 315, 77-119.
- LOPTSON, C., LUNT, D. & FRANCIS, J. 2014. Investigating vegetation–climate feedbacks during the early Eocene. *Climate of the Past*, 10, 419-436.
- LOUTIT, T. S., HARDENBOL, J., VAIL, P. R. & BAUM, G. R. 1988. Condensed sections: the key to age determination and correlation of continental margin sequences.
- LU, J., VECCHI, G. A. & REICHLER, T. 2007. Expansion of the Hadley cell under global warming. *Geophysical Research Letters*, 34.
- LUNT, D., ELDERFIELD, H., PANCOST, R., RIDGWELL, A., FOSTER, G., HAYWOOD, A., KIEHL, J., SAGOO, N., SHIELDS, C. & STONE, E. 2013. Warm climates of the past—a lesson for the future? : The Royal Society Publishing.
- LUNT, D. J., DUNKLEY JONES, T., HEINEMANN, M., HUBER, M., LEGRANDE, A., WINGUTH, A., LOPTSON, C., MAROTZKE, J., ROBERTS, C. & TINDALL, J. 2012. A model–data comparison for a multi-model ensemble of early Eocene atmosphere–ocean simulations: EoMIP. *Climate of the Past*, 8, 1717-1736.

- LUNT, D. J., FARNSWORTH, A., LOPTSON, C., FOSTER, G. L., MARKWICK, P., O'BRIEN, C. L., PANCOST, R. D., ROBINSON, S. A. & WROBEL, N. 2016. Palaeogeographic controls on climate and proxy interpretation. *Climate of the Past*, 12, 1181-1198.
- LUNT, D. J., HUBER, M., ANAGNOSTOU, E., BAATSEN, M. L., CABALLERO, R., DECONTO, R., DIJKSTRA, H. A., DONNADIEU, Y., EVANS, D. & FENG, R. 2017. The DeepMIP contribution to PMIP4: experimental design for model simulations of the EECO, PETM, and pre-PETM (version 1.0). *Geoscientific Model Development*.
- MACKENZIE, A., LEYTHAEUSER, D., SCHAEFER, R. & BJØRØY, M. 1983. Expulsion of petroleum hydrocarbons from shale source rocks. *Nature*, 301, 506.
- MACQUAKER, J., BENTLEY, S., BOHACS, K., LAZAR, O. & JONK, R. Advective sediment transport on mud-dominated continental shelves: processes and products. 2010a. American Association of Petroleum Geologists, Annual Meeting, New Orleans, LA, Search and Discover Article# 50281.
- MACQUAKER, J. & GAWTHORPE, R. 1993. Mudstone lithofacies in the Kimmeridge Clay Formation, Wessex Basin, southern England: implications for the origin and controls of the distribution of mudstones. *Journal of Sedimentary Research*, 63.
- MACQUAKER, J. H., CURTIS, C. D. & COLEMAN, M. L. 1997. The role of iron in mudstone diagenesis: Comparison of Kimmeridge Clay Formation mudstones from onshore and offshore (UKCS) localities. *Journal of Sedimentary Research*, 67.
- MACQUAKER, J. H. S. 1994. A lithofacies study of the Peterborough Member, Oxford Clay Formation (Jurassic), UK: an example of sediment bypass in a mudstone succession. *Journal of the Geological Society*, 151, 161-172.
- MACQUAKER, J. H. S. & ADAMS, A. E. 2003. Maximizing Information from Fine-Grained Sedimentary Rocks: An Inclusive Nomenclature for Mudstones. *AAPG*, 73, 735-744.
- MACQUAKER, J. H. S. & BOHACS, K. M. 2007. On the Accumulation of Mud. *Science*, 318, 1734-1735.
- MACQUAKER, J. H. S. & HOWELL, J. K. 1999. Small-scale (<5.0 m) vertical heterogeneity in mudstones: implications for high-resolution stratigraphy in siliciclastic mudstone successions. *Journal of the Geological Society*, 156, 105-112.
- MACQUAKER, J. H. S., KELLER, M. A. & DAVIES, S. J. 2010b. Algal blooms and marine snow: mechanisms that enhance preservation of organic carbon in ancient fine-grained sediments. *Journal of Sedimentary Research*, 80, 934-942.
- MACQUAKER, J. H. S., TAYLOR, K. G. & GAWTHORPE, R. L. 2007. High-Resolution Facies Analyses of Mudstones: Implications for Paleoenvironmental and Sequence Stratigraphic Interpretations of Offshore Ancient Mud-Dominated Successions. *Journal of Sedimentary Research*, 77, 324-339.
- MACQUAKER, J. H. S., TAYLOR, K. G., KELLER, M. A. & POLYA, D. 2014. Compositional controls on early diagenetic pathways in fine-grained sedimentary rocks: Implications for predicting unconventional reservoir attributes of mudstones. *Diagenesis of Organic-Rich Mudstones. AAPG Bulletin*, 98, 587-603.
- MARKWICK, P. J. & VALDES, P. J. 2004. Palaeo-digital elevation models for use as boundary conditions in coupled ocean-atmosphere GCM experiments: a Maastrichtian (late Cretaceous) example. *Palaeogeography, Palaeoclimatology, Palaeoecology*, 213, 37-63.
- MARTINEZ-RUIZ, F., KASTNER, M., GALLEGU-TORRES, D., RODRIGO-GÁMIZ, M., NIETO-MORENO, V. & ORTEGA-HUERTAS, M. 2015. Paleoclimate and paleoceanography over the past 20,000 yr in the Mediterranean Sea Basins as indicated by sediment elemental proxies. *Quaternary Science Reviews*, 107, 25-46.
- MÄRZ, C., BECKMANN, B., FRANKE, C., VOGT, C., WAGNER, T. & KASTEN, S. 2009. Geochemical environment of the Coniacian-Santonian western tropical Atlantic at Demerara Rise. *Palaeogeography, Palaeoclimatology, Palaeoecology*, 273, 286-301.
- MÄRZ, C., WAGNER, T., AQLEH, S., AL-ALAWEE, M., VAN DEN BOORN, S., PODLAHA, O. G., KOLONIC, S., POULTON, S. W., SCHNETGER, B. & BRUMSACK, H. J. 2016. Repeated enrichment of trace metals and organic carbon on an Eocene high-energy shelf caused by anoxia and reworking. *Geology*, 44, 1011-1014.
- MEILIJSON, A., ASHCKENAZI-POLIVODA, S., ILLNER, P., SPEIJER, R. P., ALMOGI-LABIN, A., FEINSTEIN, S., PÜTTMANN, W. & ABRAMOVICH, S. 2018. From phytoplankton to oil

- shale reservoirs: A 19-million-year record of the Late Cretaceous Tethyan upwelling regime in the Levant Basin. *Marine and Petroleum Geology*, 95, 188-205.
- MEYER, K. M. & KUMP, L. R. 2008. Oceanic Euxinia in Earth History: Causes and Consequences. *Annual Review of Earth and Planetary Sciences*, 36, 251-288.
- MEYERS, P. A. 2006. Paleooceanographic and paleoclimatic similarities between Mediterranean sapropels and Cretaceous black shales. *Palaeogeography, Palaeoclimatology, Palaeoecology*, 235, 305-320.
- MEYERS, S. R. & MALINVERNO, A. 2018. Proterozoic Milankovitch cycles and the history of the solar system. *Proceedings of the National Academy of Sciences*, 115, 6363-6368.
- MILLER, R. G. 1990. A Paleooceanographic Approach to the Kimmeridge Clay Formation: Chapter 2.
- MOORE, G. T., HAYASHIDA, D. N., ROSS, C. A. & JACOBSON, S. R. 1992a. Paleoclimate of the Kimmeridgian/Tithonian (Late Jurassic) world: I. Results using a general circulation model. *Palaeogeography, Palaeoclimatology, Palaeoecology*, 93, 113-150.
- MOORE, G. T., SLOAN, L. C., HAYASHIDA, D. N. & UMRIGAR, N. P. 1992b. Paleoclimate of the Kimmeridgian/Tithonian (Late Jurassic) world: II. Sensitivity tests comparing three different paleotopographic settings. *Palaeogeography, Palaeoclimatology, Palaeoecology*, 95, 229-252.
- MORGANS-BELL, H. S., COE, A. L., HESSELBO, S. P., JEMKYNS, H. C., WEEDON, G. P., A., M. J. E., TYSON, R. V. & WILLIAMS, C. J. 2001. Integrated stratigraphy of the Kimmeridge Clay Formation (Upper Jurassic) based on exposures and boreholes in south Dorset, UK. *Geological Magazine*, 138, 511-539.
- MUTTERLOSE, J., BODIN, S. & FÄHNRIK, L. 2014. Strontium-isotope stratigraphy of the Early Cretaceous (Valanginian–Barremian): Implications for Boreal–Tethys correlation and paleoclimate. *Cretaceous Research*, 50, 252-263.
- MUTTERLOSE, J., BRUMSACK, H., FLÖGEL, S., HAY, W., KLEIN, C., LANGROCK, U., LIPINSKI, M., RICKEN, W., SÖDING, E. & STEIN, R. 2003. The Greenland - Norwegian Seaway: A key area for understanding Late Jurassic to Early Cretaceous paleoenvironments. *Paleoceanography*, 18.
- NEGRI, A., FERRETTI, A. & WAGNER, T. 2009. Organic-carbon-rich sediments through the Phanerozoic: Processes, progress, and perspectives (SPECIAL ISSUE). *Palaeogeography Palaeoclimatology Palaeoecology*, 213-410.
- NERETIN, L. N., BÖTTCHER, M. E., JØRGENSEN, B. B., VOLKOV, I. I., LÜSCHEN, H. & HILGENFELDT, K. 2004. Pyritization processes and greigite formation in the advancing sulfidization front in the upper Pleistocene sediments of the Black Sea 1. *Geochimica et Cosmochimica Acta*, 68, 2081-2093.
- NEWPORT, S. M., TAYLOR, K. G., JERRETT, R. M., HOUGH, E. & WORDEN, R. H. 2017. Sedimentology and microfacies of a mud-rich slope succession: in the Carboniferous Bowland Basin, NW England (UK). *Journal of the Geological Society*, 175, 247-262.
- NUNN, E. V. & PRICE, G. D. 2010. Late Jurassic (Kimmeridgian–Tithonian) stable isotopes ($\delta^{18}\text{O}$, $\delta^{13}\text{C}$) and Mg/Ca ratios: New palaeoclimate data from Helmsdale, northeast Scotland. *Palaeogeography, Palaeoclimatology, Palaeoecology*, 292, 325-335.
- NUNN, E. V., PRICE, G. D., HART, M. B., PAGE, K. N. & LENG, M. J. 2009. Isotopic signals from Callovian–Kimmeridgian (Middle–Upper Jurassic) belemnites and bulk organic carbon, Staffin Bay, Isle of Skye, Scotland. *Journal of the Geological Society*, 166, 633-641.
- O'BRIEN, N. R. & SLATT, R. M. 2012. *Argillaceous rock atlas*, Springer Science & Business Media.
- OSCHMANN, W. 1988. Kimmeridge clay sedimentation — A new cyclic model. *Palaeogeography, Palaeoclimatology, Palaeoecology*, 65, 217-251.
- PALACAS, J. G. 1870. Characteristics of carbonate source rocks of petroleum. *Petroleum Systems of the United States. United States Geological Survey Bulletin*, 20-25.
- PANCOST, R. D., CRAWFORD, N., MAGNESS, S., TURNER, A., JENKYNS, H. C. & MAXWELL, J. R. 2004. Further evidence for the development of photic-zone euxinic conditions during Mesozoic oceanic anoxic events. *Journal of the Geological Society*, 161, 353-364.
- PARRISH, J. T. 1995. Paleogeography of Corg-rich rocks and the preservation versus production controversy.

- PARRISH, J. T. & CURTIS, R. L. 1982. Atmospheric circulation, upwelling, and organic-rich rocks in the Mesozoic and Cenozoic eras. *Palaeogeography, Palaeoclimatology, Palaeoecology*, 40, 31-66.
- PEARCE, C. R., COE, A. L. & COHEN, A. S. 2010. Seawater redox variations during the deposition of the Kimmeridge Clay Formation, United Kingdom (Upper Jurassic): Evidence from molybdenum isotopes and trace metal ratios. *Paleoceanography*, 25.
- PEARCE, C. R., COHEN, A. S., COE, A. L. & BURTON, K. W. 2008. Molybdenum isotope evidence for global ocean anoxia coupled with perturbations to the carbon cycle during the Early Jurassic. *Geology*, 36, 231-234.
- PEARSON, S. J. 2000. *High-resolution environmental change in the late Jurassic Kimmeridge clay formation*. University of Southampton.
- PEDERSEN, T. F. & CALVERT, S. E. 1990a. Anoxia vs. Productivity: What Controls the Formation of Organic-Carbon-Rich Sediments and Sedimentary Rocks?(1). *AAPG Bulletin*, 74, 454-466.
- PEDERSEN, T. F. & CALVERT, S. E. 1990b. Anoxia vs. Productivity: What Controls the Formation of Organic-Carbon-Rich Sediments and Sedimentary Rocks?(1). *AAPG Bulletin*, 74, 454-466.
- PERCIVAL, L. M. E., WITT, M. L. I., MATHER, T. A., HERMOSO, M., JENKYNS, H. C., HESSELBO, S. P., AL-SUWAIDI, A. H., STORM, M. S., XU, W. & RUHL, M. 2015. Globally enhanced mercury deposition during the end-Pliensbachian extinction and Toarcian OAE: A link to the Karoo-Ferrar Large Igneous Province. *Earth and Planetary Science Letters*, 428, 267-280.
- PICARD, M. D. 1971. Classification of fine-grained sedimentary rocks. *Journal of Sedimentary Research*, 41, 179-195.
- PIETRAS, J. T. & SPIEGEL, E. B. 2018. Xrf-based Chemostratigraphy Between and Across Two Disconformities in the Ordovician Trenton Group and Utica Shale of Central New York, U.s.a. *Journal of Sedimentary Research*, 88, 365-384.
- POTTER, P. E., MAYNARD, J. B. & DEPETRIS, P. J. 2005. *Mud and mudstones: Introduction and overview*, Springer Science & Business Media.
- POULSEN, C. J., GENDASZEK, A. S. & JACOB, R. L. 2003. Did the rifting of the Atlantic Ocean cause the Cretaceous thermal maximum? *Geology*, 31, 115-118.
- POULSEN, C. J., JACOB, R. L., PIERREHUMBERT, R. T. & HUYNH, T. T. 2002. Testing paleogeographic controls on a Neoproterozoic snowball Earth. *Geophysical Research Letters*, 29, 10-1-10-4.
- POULSEN, C. J., PIERREHUMBERT, R. T. & JACOB, R. L. 2001. Impact of ocean dynamics on the simulation of the Neoproterozoic "snowball Earth". *Geophysical research letters*, 28, 1575-1578.
- POWELL, J. 2010. Jurassic sedimentation in the Cleveland Basin: a review. *Proceedings of the Yorkshire Geological Society*, 58, 21-72.
- PRICE, G. & SELLWOOD, B. 1994. Palaeotemperatures indicated by Upper Jurassic (Kimmeridgian-Tithonian) fossils from Mallorca determined by oxygen isotope composition. *Palaeogeography, Palaeoclimatology, Palaeoecology*, 110, 1-10.
- PRICE, G. & SELLWOOD, B. 1997. "Warm" palaeotemperatures from high Late Jurassic palaeolatitudes (Falkland Plateau): ecological, environmental or diagenetic controls? *Palaeogeography, Palaeoclimatology, Palaeoecology*, 129, 315-327.
- PRICE, G. D., SELLWOOD, B. W. & VALDES, P. J. 1995. Sedimentological evaluation of general circulation model simulations for the "greenhouse" Earth: Cretaceous and Jurassic case studies. *Sedimentary Geology*, 100, 159-180.
- PRICE, G. D., VALDES, P. J. & SELLWOOD, B. W. 1997. Quantitative palaeoclimate GCM validation: Late Jurassic and mid-Cretaceous case studies. *Journal of the Geological Society*, 154, 769-772.
- PRICE, L. C. 1983. Geologic Time as a Parameter in Organic Metamorphism and Vitrinite Reflectance as an Absolute Palaeogeothermometer. *Journal of Petroleum Geology*, 6, 5-37.
- PROUST, J. N., DECONINCK, J. F., GEYSSANT, J. R., HERBIN, J. P. & VIDIER, J. P. 1995. Sequence analytical approach to the upper Kimmeridgian-lower tithonian storm-dominated

- ramp deposits of the Boulonnais (Northern France). A landward time-equivalent to offshore marine source rocks. *Geologische Rundschau*, 84, 255-271.
- RAISWELL, R., NEWTON, R. & WIGNALL, P. 2001. An indicator of water-column anoxia: resolution of biofacies variations in the Kimmeridge Clay (Upper Jurassic, UK). *Journal of Sedimentary Research*, 71, 286-294.
- RAWSON, P. F., WRIGHT, J. K., STARMER, I., WHITHAM, F., HEMINGWAY, J. & GREENSMITH, J. T. 2000. *The Yorkshire Coast*, Geologists' Association.
- RAYMO, M. E. & RUDDIMAN, W. F. 1992. Tectonic forcing of late Cenozoic climate. *Nature*, 359, 117-122.
- REES, P., ZIEGLER, A. M., VALDES, P. J., HUBER, B., MACLEOD, K. & WING, S. 2000. Jurassic phytogeography and climates: new data and model comparisons. *Warm climates in earth history*, 297-318.
- REES, P. M., NOTO, CHRISTOPHER R., PARRISH, J. M. & PARRISH, JUDITH T. 2004. Late Jurassic Climates, Vegetation, and Dinosaur Distributions. *The Journal of Geology*, 112, 643-653.
- RUDNICK, R. L. & GAO, S. 2003. Composition of the continental crust. *Treatise on geochemistry*, 3, 659.
- SAGEMAN, B. B., LYONS, T. & JOO, Y. J. 2013. Geochemistry of fine-grained, organic carbon-rich facies. *Treatise on Geochemistry: Second Edition*. Elsevier Inc.
- SAGEMAN, B. B., MURPHY, A. E., WERNE, J. P., VER STRAETEN, C. A., HOLLANDER, D. J. & LYONS, T. W. 2003. A tale of shales: the relative roles of production, decomposition, and dilution in the accumulation of organic-rich strata, Middle–Upper Devonian, Appalachian basin. *Chemical Geology*, 195, 229-273.
- SCAIFE, J. D., RUHL, M., DICKSON, A. J., MATHER, T. A., JENKYN, H. C., PERCIVAL, L. M. E., HESSELBO, S. P., CARTWRIGHT, J., ELDRETT, J. S., BERGMAN, S. C. & MINISINI, D. 2017. Sedimentary Mercury Enrichments as a Marker for Submarine Large Igneous Province Volcanism? Evidence From the Mid - Cenomanian Event and Oceanic Anoxic Event 2 (Late Cretaceous). *Geochemistry, Geophysics, Geosystems*, 18, 4253-4275.
- SCHIEBER, J. 1989. Facies and origin of shales from the mid-Proterozoic Newland Formation, Belt Basin, Montana, USA. *Sedimentology*, 36, 203-219.
- SCHIEBER, J. 1999. Microbial mats in terrigenous clastics; the challenge of identification in the rock record. *PALAIOS*, 14, 3-12.
- SCHIEBER, J. 2011. Reverse engineering mother nature — Shale sedimentology from an experimental perspective. *Sedimentary Geology*, 238, 1-22.
- SCHIEBER, J. 2016a. Experimental testing of the transport-durability of shale lithics and its implications for interpreting the rock record. *Sedimentary Geology*, 331, 162-169.
- SCHIEBER, J. 2016b. Mud re-distribution in epicontinental basins – Exploring likely processes. *Marine and Petroleum Geology*, 71, 119-133.
- SCHIEBER, J., SOUTHARD, J. & THAISEN, K. 2007. Accretion of Mudstone Beds from Migrating Floccule Ripples. *Science*, 318, 1760-1763.
- SCHIEBER, J., SOUTHARD, J. B., KISSLING, P., ROSSMAN, B. & GINSBURG, R. 2013. Experimental deposition of carbonate mud from moving suspensions: importance of flocculation and implications for modern and ancient carbonate mud deposition. *Journal of Sedimentary Research*, 83, 1025-1031.
- SCHNEIDER, T., BISCHOFF, T. & HAUG, G. H. 2014a. Migrations and dynamics of the intertropical convergence zone. *Nature*, 513, 45.
- SCHNEIDER, T., BISCHOFF, T. & HAUG, G. H. 2014b. Migrations and dynamics of the intertropical convergence zone. *Nature*, 513, 45.
- SCHNETGER, B., BRUMSACK, H. J., SCHALE, H., HINRICHS, J. & DITTERT, L. 2000. Geochemical characteristics of deep-sea sediments from the Arabian Sea: a high-resolution study. *Deep Sea Research Part II: Topical Studies in Oceanography*, 47, 2735-2768.
- SCHOLZ, F., BAUM, M., SIEBERT, C., EROGLU, S., DALE, A. W., NAUMANN, M. & SOMMER, S. 2018. Sedimentary molybdenum cycling in the aftermath of seawater inflow to the intermittently euxinic Gotland Deep, Central Baltic Sea. *Chemical Geology*, 491, 27-38.
- SCHWARZKOPF, T. A. 1992. Source rock potential (TOC + hydrogen index) evaluation by integrating well log and geochemical data. *Organic Geochemistry*, 19, 545-555.

- SCOTCHMAN, I. C. 1991. Kerogen facies and maturity of the Kimmeridge Clay Formation in southern and eastern England. *Marine and Petroleum Geology*, 8, 278-295.
- SELLWOOD, B. W. & VALDES, P. J. 2006. Mesozoic climates: General circulation models and the rock record. *Sedimentary Geology*, 190, 269-287.
- SELLWOOD, B. W. & VALDES, P. J. 2008. Jurassic climates. *Proceedings of the Geologists' Association*, 119, 5-17.
- SELLWOOD, B. W., VALDES, P. J. & PRICE, G. D. 2000. Geological evaluation of multiple general circulation model simulations of Late Jurassic palaeoclimate. *Palaeogeography, Palaeoclimatology, Palaeoecology*, 156, 147-160.
- SEVERMANN, S., LYONS, T. W., ANBAR, A., MCMANUS, J. & GORDON, G. 2008. Modern iron isotope perspective on the benthic iron shuttle and the redox evolution of ancient oceans. *Geology*, 36, 487-490.
- SHAW, A. B. 1964. Time in stratigraphy.
- SMITH, A. G., SMITH, D. G. & FUNNELL, B. M. 2004. *Atlas of Mesozoic and Cenozoic coastlines*, Cambridge University Press.
- SMITH, E. 1996. Satellite - derived sea surface temperature data available on - line. *Eos, Transactions American Geophysical Union*, 77, 135-135.
- STEIN, R., RULLKÖTTER, J. & WELTE, D. H. 1986. Accumulation of organic-carbon-rich sediments in the Late Jurassic and Cretaceous Atlantic Ocean — A synthesis. *Chemical Geology*, 56, 1-32.
- STOW, D. A. 1981. Fine-grained sediments: Terminology. *Quarterly Journal of Engineering Geology and Hydrogeology*, 14, 243-244.
- TABOR, C. R., POULSEN, C. J., LUNT, D. J., ROSENBLOOM, N. A., OTTO-BLIESNER, B. L., MARKWICK, P. J., BRADY, E. C., FARNSWORTH, A. & FENG, R. 2016. The cause of Late Cretaceous cooling: A multimodel-proxy comparison. *Geology*, 44, 963-966.
- TAYLOR, K. G. 1998. Spatial and temporal variations in early diagenetic organic matter oxidation pathways in Lower Jurassic mudstones of eastern England. *Chemical Geology*, 145, 47-60.
- TAYLOR, S. R. & MCLENNAN, S. M. 2001. Chemical composition and element distribution in the Earth's crust. *Encyclopedia of Physical Science and Technology*.
- THEM, T. R., JAGOE, C. H., CARUTHERS, A. H., GILL, B. C., GRASBY, S. E., GRÖCKE, D. R., YIN, R. & OWENS, J. D. 2019. Terrestrial sources as the primary delivery mechanism of mercury to the oceans across the Toarcian Oceanic Anoxic Event (Early Jurassic). *Earth and Planetary Science Letters*, 507, 62-72.
- TRABUCHO-ALEXANDRE, J. 2015a. More gaps than shale: erosion of mud and its effect on preserved geochemical and palaeobiological signals. *Strata and Time: Probing the Gaps in Our Understanding: Geological Society, London, Special Publications*, 404, 251-270.
- TRABUCHO-ALEXANDRE, J. 2015b. Organic Matter-Rich Shale Depositional Environments. *Fundamentals of Gas Shale Reservoirs*. John Wiley & Sons, Inc.
- TRABUCHO-ALEXANDRE, J., DIRKX, R., VELD, H., KLAVER, G. & DE BOER, P. L. 2012. Toarcian Black Shales In the Dutch Central Graben: Record of Energetic, Variable Depositional Conditions During An Oceanic Anoxic Event. *Journal of Sedimentary Research*, 82, 104-120.
- TRABUCHO-ALEXANDRE, J., VAN GILST, R. I., RODRÍGUEZ-LÓPEZ, J. P. & DE BOER, P. L. 2011. The sedimentary expression of oceanic anoxic event 1b in the North Atlantic. *Sedimentology*, 58, 1217-1246.
- TRIBOVILLARD, N.-P., CAULET, J.-P., VERGNAUD-GRAZZINI, C., MOUREAU, N. & TREMBLAY, P. 1996. Lack of organic matter accumulation on the upwelling-influenced Somalia margin in a glacial-interglacial transition. *Marine Geology*, 133, 157-182.
- TRIBOVILLARD, N.-P., DESPRAIRIES, A., LALLIER-VERGÈS, E., BERTRAND, P., MOUREAU, N., RAMDANI, A. & RAMANAMPISOA, L. 1994. Geochemical study of organic-matter rich cycles from the Kimmeridge Clay Formation of Yorkshire (UK): productivity versus anoxia. *Palaeogeography, Palaeoclimatology, Palaeoecology*, 108, 165-181.
- TRIBOVILLARD, N., ALGEO, T. J., BAUDIN, F. & RIBOULLEAU, A. 2012. Analysis of marine environmental conditions based on molybdenum-uranium covariation—Applications to Mesozoic paleoceanography. *Chemical Geology*, 324-325, 46-58.

- TRIBOVILLARD, N., ALGEO, T. J., LYONS, T. & RIBOULLEAU, A. 2006. Trace metals as paleoredox and paleoproductivity proxies: An update. *Chemical Geology*, 232, 12-32.
- TRIBOVILLARD, N., HATEM, E., AVERBUCH, O., BARBECOT, F., BOUT-ROUMAZEILLES, V. & TRENTESAUX, A. 2015. Iron availability as a dominant control on the primary composition and diagenetic overprint of organic-matter-rich rocks. *Chemical Geology*, 401, 67-82.
- TRIBOVILLARD, N., TRENTESAUX, A., RAMDANI, A., BAUDINET, F. & RIBOULLEAU, A. 2004. Controls on organic accumulation in late Jurassic shales of northwestern Europe as inferred from trace-metal geochemistry. *Bulletin de la Societe Geologique de France*, 175, 491-506.
- TURNER, B. W., TRÉANTON, J. A. & SLATT, R. M. 2016. The use of chemostratigraphy to refine ambiguous sequence stratigraphic correlations in marine mudrocks. An example from the Woodford Shale, Oklahoma, USA. *Journal of the Geological Society*, jgs2015-125.
- TURNER, H. E., BATENBURG, S., GALE, A. S. & GRADSTEIN, F. M. 2019. The Kimmeridge Clay Formation (Upper Jurassic-Lower Cretaceous) of the Norwegian Continental Shelf and Dorset, UK: a chemostratigraphic correlation. *Newsletters on Stratigraphy*, 52/1.
- TURNER, J. T. 2015. Zooplankton fecal pellets, marine snow, phytodetritus and the ocean's biological pump. *Progress in Oceanography*, 130, 205-248.
- TYSON, R. 2005a. The "productivity versus preservation" controversy: cause, flaws, and resolution. *Special Publication-SEPM*, 82, 17.
- TYSON, R. V. 2001. Sedimentation rate, dilution, preservation and total organic carbon: some results of a modelling study. *Organic Geochemistry*, 32, 333-339.
- TYSON, R. V. 2005b. The "Productivity versus Preservation" controversy: Cause, Flaws and Resolution. *Sedimentary Geology*.
- TYSON, R. V., WILSON, R. C. L. & DOWNIE, C. 1979. A stratified water column environmental model for the type Kimmeridge Clay. *Nature*, 277, 377-380.
- VALDES, P., SPICER, R., SELLWOOD, B. & PALMER, D. 1999. Understanding Past Climates: Modelling Ancient Weather (CD ROM). Gordon and Breach Publ., Reading.
- VALDES, P. J., ARMSTRONG, E., BADGER, M. P., BRADSHAW, C. D., BRAGG, F., DAVIES-BARNARD, T., DAY, J. J., FARNSWORTH, A., HOPCROFT, P. O. & KENNEDY, A. T. 2017. The BRIDGE HadCM3 family of climate models: HadCM3@ Bristol v1. 0. *Geoscientific Model Development*, 10, 3715-3743.
- VALDES, P. J. & SELLWOOD, B. W. 1992. A palaeoclimate model for the Kimmeridgian. *Palaeogeography, Palaeoclimatology, Palaeoecology*, 95, 47-72.
- VALDES, P. J., SELLWOOD, B. W. & PRICE, G. D. 1995. Modelling Late Jurassic Milankovitch climate variations. *Geological Society, London, Special Publications*, 85, 115-132.
- VAN DER WEIJDEN, C. H. 2002. Pitfalls of normalization of marine geochemical data using a common divisor. *Marine Geology*, 184, 167-187.
- VAN LITH, Y., WARTHMANN, R., VASCONCELOS, C. & MCKENZIE, J. A. 2003. Sulphate-reducing bacteria induce low-temperature Ca-dolomite and high Mg-calcite formation. *Geobiology*, 1, 71-79.
- VASCONCELOS, C., MCKENZIE, J. A., BERNASCONI, S., GRUJIC, D. & TIENS, A. J. 1995. Microbial mediation as a possible mechanism for natural dolomite formation at low temperatures. *Nature*, 377, 220.
- VOIGT, S., WILMSEN, M., MORTIMORE, R. N. & VOIGT, T. 2003. Cenomanian palaeotemperatures derived from the oxygen isotopic composition of brachiopods and belemnites: evaluation of Cretaceous palaeotemperature proxies. *International Journal of Earth Sciences*, 92, 285-299.
- WAGNER, T., HOFMANN, P. & FLÖGEL, S. 2013. Marine black shale deposition and Hadley Cell dynamics: A conceptual framework for the Cretaceous Atlantic Ocean. *Marine and Petroleum Geology*, 43, 222-238.
- WALISER, D. E., SHI, Z., LANZANTE, J. R. & OORT, A. H. 1999. The Hadley circulation: assessing NCEP/NCAR reanalysis and sparse in-situ estimates. *Climate Dynamics*, 15, 719-735.
- WANG, W., XIE, P., YOO, S.-H., XUE, Y., KUMAR, A. & WU, X. 2011. An assessment of the surface climate in the NCEP climate forecast system reanalysis. *Climate dynamics*, 37, 1601-1620.

- WAPLES, D. W. 1983. Reappraisal of anoxia and organic richness, with emphasis on Cretaceous of North Atlantic. *AAPG bulletin*, 67, 963-978.
- WATERHOUSE, H. K. 1999. Orbital forcing of palynofacies in the Jurassic of France and the United Kingdom. *Geology*, 27, 511-514.
- WEDEPOHL, K. 1971. Environmental influences on the chemical composition of shales and clays. *Physics and Chemistry of the Earth*, 8, 307-333.
- WEDEPOHL, K. H. 1991. Chemical composition and fractionation of the continental crust. *Geologische Rundschau*, 80, 207-223.
- WEEDON, G. P., COE, A. L. & GALLOIS, R. W. 2004. Cyclostratigraphy, orbital tuning and inferred productivity for the type Kimmeridge Clay (Late Jurassic), Southern England. *Journal of the Geological Society*, 161, 655-666.
- WIGNALL, P. B. 1989. Sedimentary dynamics of the Kimmeridge Clay: tempests and earthquakes. *Journal of the Geological Society*, 146, 273-284.
- WIGNALL, P. B. 1991. Model for transgressive black shales? *Geology*, 19, 167-170.
- WIGNALL, P. B. & HALLAM, A. 1991. Biofacies, stratigraphic distribution and depositional models of British onshore Jurassic black shales. *Geological Society, London, Special Publications*, 58, 291-309.
- WIGNALL, P. B. & RUFFELL, A. 1990. The influence of a sudden climatic change on marine deposition in the Kimmeridgian of northwest Europe. *Journal of the Geological Society*, 147, 365-371.
- WIJSMAN, J. W., MIDDELBURG, J. J. & HEIP, C. H. 2001. Reactive iron in Black Sea sediments: implications for iron cycling. *Marine Geology*, 172, 167-180.
- WILSON, R. D. & SCHIEBER, J. 2014. Muddy prodeltaic hyperpycnites in the Lower Genesee Group of central New York, USA: implications for mud transport in epicontinental seas. *Journal of Sedimentary Research*, 84, 866-874.
- YIN, J. H. 2005. A consistent poleward shift of the storm tracks in simulations of 21st century climate. *Geophysical Research Letters*, 32.
- ŽÁK, K., KOŠTÁK, M., MAN, O., ZAKHAROV, V. A., ROGOV, M. A., PRUNER, P., ROHOVEC, J., DZYUBA, O. S. & MAZUCH, M. 2011. Comparison of carbonate C and O stable isotope records across the Jurassic/Cretaceous boundary in the Tethyan and Boreal Realms. *Palaeogeography, Palaeoclimatology, Palaeoecology*, 299, 83-96.
- ZAKHAROV, V. A. & ROGOV, M. A. 2008. Let the Volgian stage stay in the Jurassic. *Russian Geology and Geophysics*, 49, 408-412.
- ZAKHAROV, V. A., ROGOV, M. A., DZYUBA, O. S., ŽÁK, K., KOŠTÁK, M., PRUNER, P., SKUPIEN, P., CHADIMA, M., MAZUCH, M. & NIKITENKO, B. L. 2014. Palaeoenvironments and palaeoceanography changes across the Jurassic/Cretaceous boundary in the Arctic realm: case study of the Nordvik section (north Siberia, Russia). *Polar Research*, 33, 197-214.
- ZHANG, S., WANG, X., HAMMARLUND, E. U., WANG, H., COSTA, M. M., BJERRUM, C. J., CONNELLY, J. N., ZHANG, B., BIAN, L. & CANFIELD, D. E. 2015. Orbital forcing of climate 1.4 billion years ago. *Proceedings of the National Academy of Sciences*, 112, E1406-E1413.
- ZHOU, J., POULSEN, C. J., ROSENBLOOM, N., SHIELDS, C. & BRIEGLEB, B. 2012. Vegetation-climate interactions in the warm mid-Cretaceous. *Clim. Past*, 8, 565-576.

10 Appendix A - Climate modelling figures

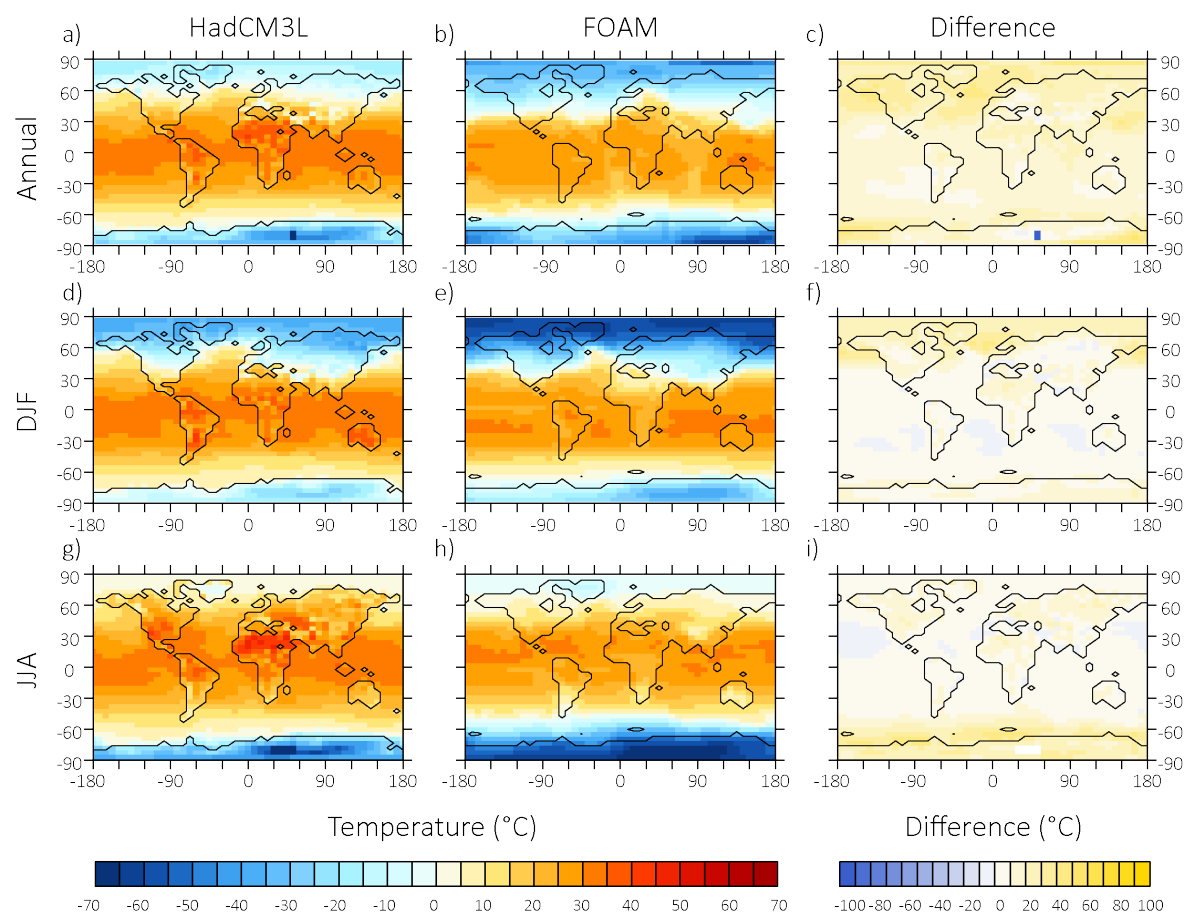


Figure A1. Preindustrial simulation surface temperature maps. (a, d, and g) Annual, winter (DJF), and summer (JJA) surface temperature maps from HadCM3L. (b, e, h) Annual, winter (DJF), and summer (JJA) surface temperature maps from FOAM. (c, f, and i) Annual, winter (DJF), and summer (JJA) temperature differences between HadCM3L and FOAM, calculated as HadCM3L minus FOAM.

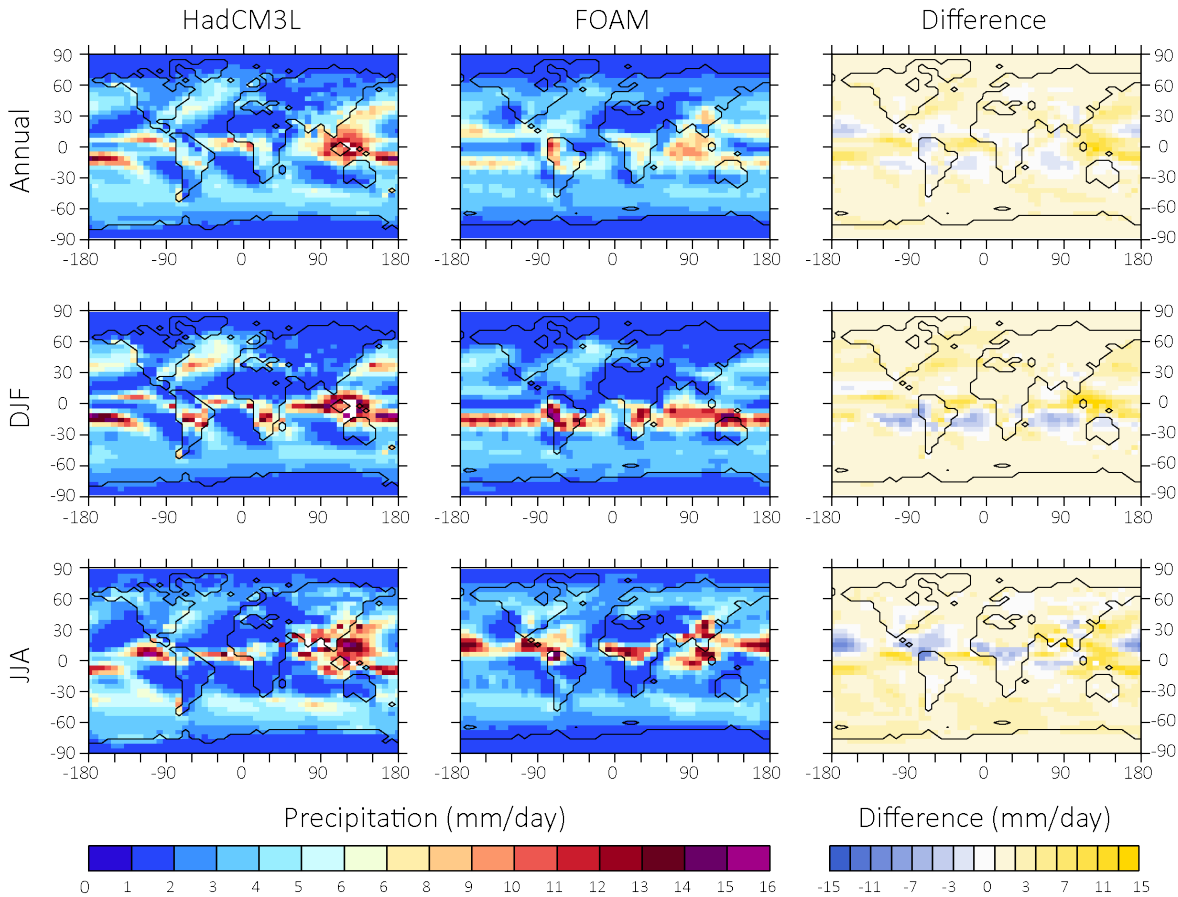


Figure A2. Preindustrial simulation precipitation maps. (a, d, and g) Annual, winter (DJF), and summer (JJA) precipitation from HadCM3L. (b, e, h) Annual, winter (DJF), and summer (JJA) precipitation from FOAM. (c, f, and i) Annual, winter (DJF), and summer (JJA) precipitation differences between HadCM3L and FOAM, calculated as HadCM3L minus FOAM.

Near Surface temperature (°C)	HadCM3L	FOAM	HadCM3L/FOAM Difference
Annual	14.6	7.3	7.3
DJF	12.3	5.1	7.2
JJA	16.5	8.8	7.7

Table A1. Preindustrial annual, winter (DJF), and summer (JJA) global mean surface temperatures for the HadCM3L and FOAM and the difference between the two models.

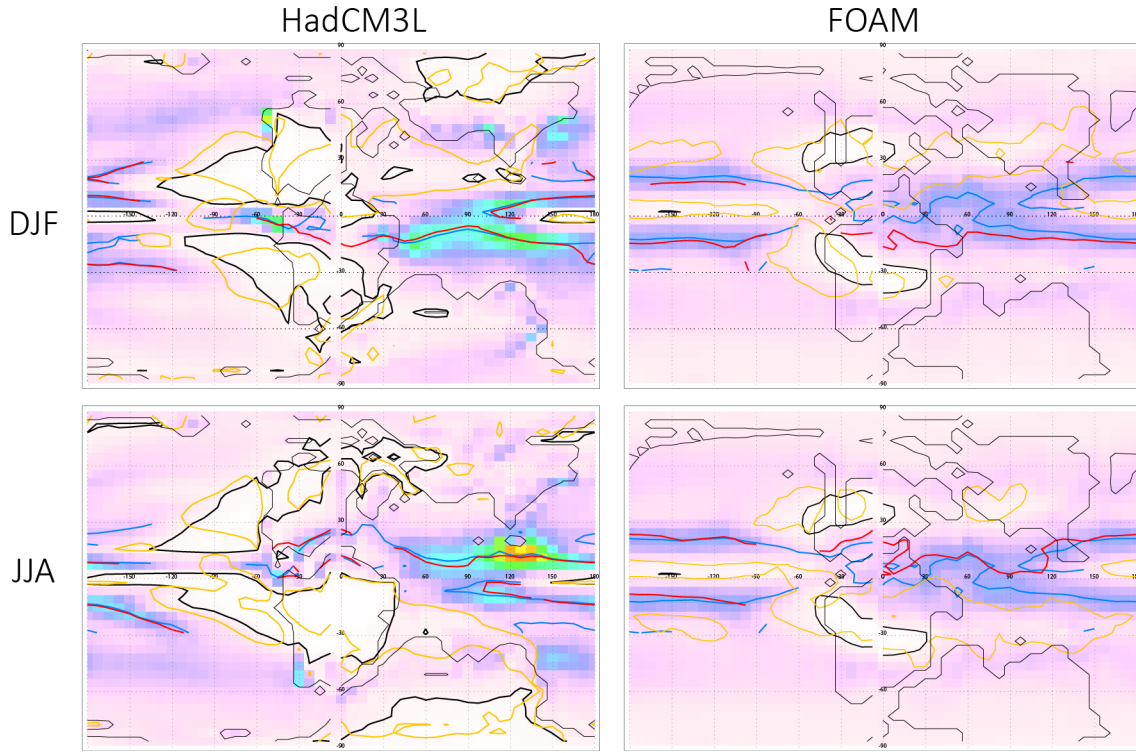


Figure A3. Boreal summer (JJA) and winter (DJF) mean precipitation (mm/s) from HadCM3L (left) and FOAM (right). Overlain, the red lines show the local maximum in vertical atmospheric ascent velocity (w) at a height of 500 mbar, for regions equator-wards of 30 degrees N/S, with 500 mbar temperature of greater than 260 K, and $w > 0.005$ m/s. The blue lines show the local maximum in precipitation (p), for regions equator-wards of 30 degrees N/S, with 500 mbar temperature of greater than 260K, and $p > 0.00003$ mm/s. Thick black line encompasses dry regions where the precipitation rate is less than $1 \cdot 10^{-5}$ mm/s. The orange line encompasses regions of mid-atmospheric descent where the vertical velocity at 500 mbar is towards the surface and greater than 0.02 is m/s. After Armstrong et al., (2016).

11 Appendix B – EB87 Core petrographic images

Please see the USB stick attached to the hard copy for this dataset.

12 Appendix C – EB87 Core SEM images

Please see the USB stick attached to the hard copy for this dataset.

13 Appendix D – EB 87 SEM-EDX

Please see the USB stick attached to the hard copy for this dataset.

14 Appendix E – EB87 Core geochemical data

Please see the USB stick attached to the hard copy for this dataset.

15 Appendix F – SQ1 Core geochemical data

Please see the USB stick attached to the hard copy for this dataset.

16 Appendix G – DH4 Core petrographic images

Please see the USB stick attached to the hard copy for this dataset.

17 Appendix H – DH4 Core SEM images

Please see the USB stick attached to the hard copy for this dataset.

18 Appendix I – DH4 SEM-EDX

Please see the USB stick attached to the hard copy for this dataset.

19 Appendix J – DH4 Core geochemical data

Please see the USB stick attached to the hard copy for this dataset.

